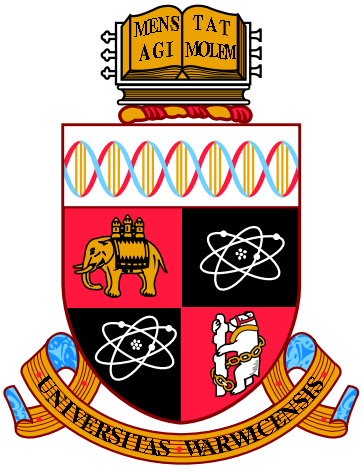

Regulation of Agonist-induced Ca^{2+} Oscillations by Intraluminal Ca^{2+}: an Experimental and Theoretical Study

by

Benjamin Francis Hamilton

Thesis

Submitted to the University of Warwick

for the degree of

Doctor of Philosophy

Systems Biology

September 2013

THE UNIVERSITY OF WARWICK

Abstract

The ubiquity of Ca^{2+} signalling makes understanding its underlying processes vitally important. This thesis probes one part of that system, the regulation of agonist-induced Ca^{2+} oscillations, using both theoretical and experimental approaches. *CHO–hOT* cells transfected with human oxytocin receptors are used as the vehicle to assess the mechanisms underlying oxytocin-induced Ca^{2+} oscillations. The methodologies used to interrogate these oscillations are

1. varying the plasmalemmal Ca^{2+} entry and removal;
2. manipulating Ca^{2+} buffering within the endoplasmic reticulum (ER) and Ca^{2+} uptake into the ER lumen; and
3. constructing a mathematical model that replicates the experimentally observed phenomena.

To Dr Kat Rock, without whom this would have been impossible.

Acknowledgements

Thank you to everyone who has contributed both directly and indirectly to my ability to produce this work.

I would like to express my special appreciation and thanks to my supervisor Dr. Anatoly Shmygol, who is a tremendous mentor. His constant attention to and encouragement of my research whilst allowing me to grow as a research scientist has been incredible. His 'first-principles' approach to problems, both large and small, has been an inspiration and I have tried to adopt it here. I would further like to thank my special appreciation and thanks to my supervisor Dr. Yulia Timofeeva. Her patience and determination to understand the biology of my problem explained, often inexpertly, by myself so that we could formulate a sound mathematical approach has been priceless. I would also like to thank my advisory committee members, Dr. Till Bretschneider, Dr. Magnus Richardson and Dr. Mark Wall for serving as my committee members even in hardship.

I particularly want to express my gratitude to Dr Anne Green and Dr Oleg Gerasimenko for taking the time to so thoroughly familiarise themselves with my work and in so doing for making my viva an enjoyable moment; and for your brilliant comments and suggestions, thanks to you. Thank you to BBSRC for funding my this work. I would also like to thank all of the staff of Systems Biology, especially Professor Vicky Buchanan-Wollaston for enduring my viva as examination advisor. Thank you to all those at University Hospital Coventry and Warwickshire's Clinical Sciences Research Institute who aided a poor mathematician lost in a jungle of pipettes, chemicals and microscopes – especially those who made me laugh!

I would also like to thank all of my friends and family – especially my Mum, my Dad, Felicity Green, Dr Alex Jironkin, Chipo Mashayamombe and Dr Kat Rock – who both supported me in writing and incented me to strive towards my goal.

Contents

List of Figures

Part A

Introduction

Chapter 0

Outline and Aims

0.1 Aims

Several indirect methods for manipulating intraluminal calcium concentration, $\left[Ca^{2+}\right]_{ER}$, have been presented in the literature [119, 118, 24, 130]. The aim of this project was investigate the regulatory role of $\left[Ca^{2+}\right]_{ER}$ on oxytocin-induced Ca^{2+} oscillations by using the aforementioned methods for $\left[Ca^{2+}\right]_{ER}$ manipulation. Namely:

1. varying the plasmalemmal Ca^{2+} entry and removal;
2. manipulating Ca^{2+} buffering within the endoplasmic reticulum (ER) and Ca^{2+} uptake into the ER lumen; and then by
3. constructing a mathematical model that would replicate the experimentally observed phenomena.

0.2 Outline

Cell signalling orchestrates everything from 'birth' of cells during cell proliferation, to their differentiation into specific cell types of specific function, and, eventually, to their 'death' through a process such as apoptosis. Specific processes within adult cells, including contraction, secretion, metabolism, proliferation, information processing and sensory perception, are all controlled by these same signalling systems.

Chapter 1 first presents a survey of cell-signalling mechanisms in §1.1 and then goes on, in §1.2, to introduce the importance and the roles of Ca^{2+} signalling in cell behaviour. In particular, this section introduces the concept of 'ON' and 'OFF'

mechanisms and reactions: that is, a cell's ability to finely control the temporal dynamics of a Ca^{2+} transient during oscillatory behaviour. These include an ability to regulate its precise amplitude, duration or morphology.

Having established the importance of Ca^{2+} oscillations in cell signalling, as well as the current understanding of the role of the G_q signalling pathway in establishing them, §1.3 introduces the hormone oxytocin (*OT*). *OT* is used here to stimulate this pathway and is known to result in *OT*-induced Ca^{2+} oscillations in different cell types which are introduced and discussed in §2.1. Finally, §1.4 introduces the role that mathematical modelling can play in increasing understanding of a biological system by bridging the gap between what is biologically known from first principles, and what can be observed without, or even without the possibility of, a first-principles explanation.

This understanding forms the framework on which *OT*-induced Ca^{2+} oscillations are then investigated in *CHO–hOT* cells. Chapter 3 confirms that *CHO–hOT* cells oscillate in a predictable manner in response to *OT*. Further, it establishes that these oscillations are not dose-dependent, an important consideration since several cell-types have been known to show dose independent oscillatory behaviour. This chapter goes on to establish that Ca^{2+}_{EC} is required for *OT*-induced Ca^{2+} oscillations to occur. This discovery leads to the work in Chapters 4 and 5 which details experimental approaches that have been used to investigate the impact of the concentration of extracellular Ca^{2+}, $\left[Ca^{2+}\right]_{EC}$, and intraluminal Ca^{2+}, $\left[Ca^{2+}\right]_{ER}$, respectively, upon *OT*-induced Ca^{2+} oscillations.

Chapter 6 introduces a mathematical framework for modelling Ca^{2+}-oscillations by considering the approaches taken by two previous models. It goes on to investigate the possible behaviours of these systems, their stability and dynamic behaviours, as well as the assumptions and simplifications that their authors used to make them useful in understanding their systems. Chapter 7 then goes on to extend their work to account for the results established in the experimental chapters of this thesis (Chapters 3–5). Chapter 8 then introduces a complete model for the system and analyses its ability to replicate the established experimental results.

The discussion in Chapter 9.1 then attempts to tie these two streams of work together before Chapter 9.2 provides concluding remarks as well as a view of possible future extensions of this work.

Chapter 1

Background

1.1 Cell signalling mechanisms

Cells within our bodies use a repertoire of electrical and chemical signals to remain in constant communication with one another.

Electrical signals are utilised in excitable systems where very fast communication, via gap junctions for instance, is required. A gap junction is a channel composed of two hemichannels, or connexons, which are in turn formed primarily of homo- or hetero-hexamers of connexin proteins (see Figure 1.1). The channels span across the intercellular space, directly connecting the cytoplasm of two cells. As well as allowing propagation of electrical signals, the pore of a gap junction is large enough to allow low-molecular-mass molecules, such as metabolites or secondary messengers (including Ca^{2+} and $InsP_3$) to diffuse from one cell to the other [11].

In general, however, communication through chemical signals is by far the most widespread method of information-transfer between cells. In this type of cell communication, one cell releases a chemical stimulus, such as a hormone, growth factor or neurotransmitter, to a target cell. Receiving the incoming signal is a non-trivial problem for the target cell since it has a lipophilic plasma membrane through which only hydrophobic hormones can cross with ease to their cytosolic or nuclear protein receptors.

Hence, a more complex mechanism is required for the target cell to receive, interpret, and relay to downstream sensors and/or effectors any water-soluble signals received and thus induce a change in cellular activity. It is this mechanism that makes up the cell signalling pathway which in turn is made up of 'ON' and 'OFF' mechanisms.

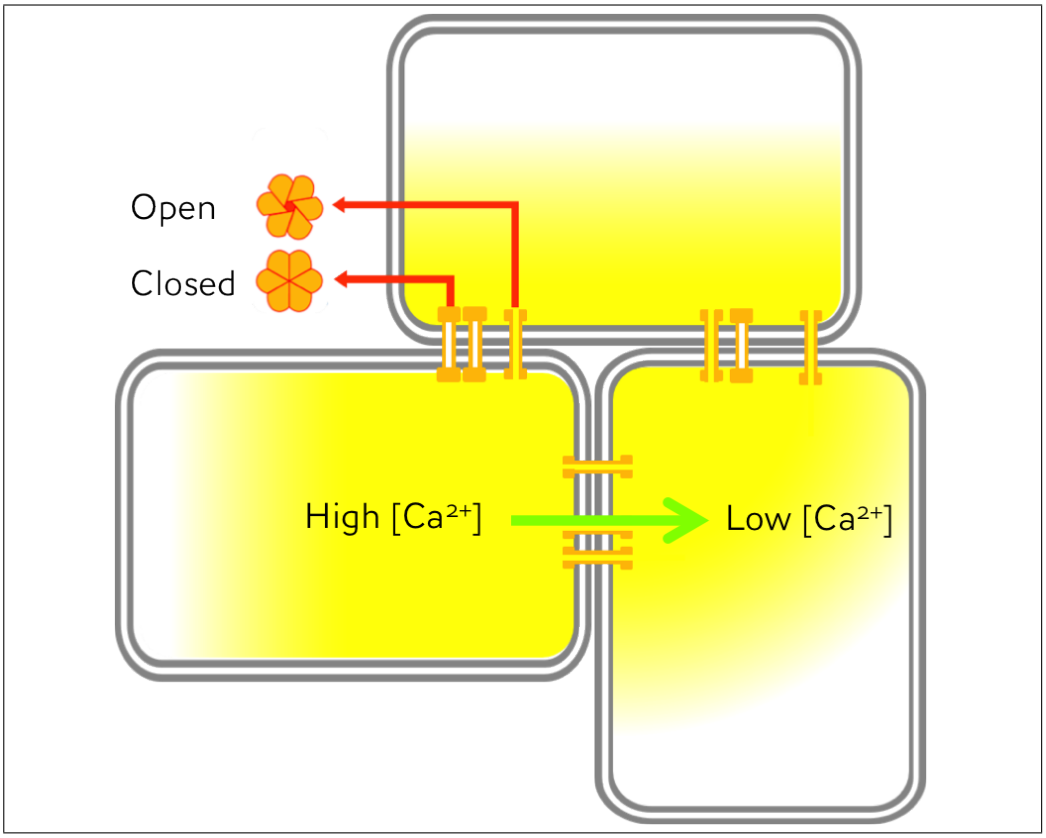

Figure 1.1 *A schematic of three cells connected by gap junctions. These hydrophilic channels, made up of two hemichannels which are in turn made up of six connexin monomers, connect the cytoplasm of neighbouring cells. They appear in either an open of closed conformation. In the open conformation, low-molecular-mass molecules such as metabolites or secondary messengers can passively diffuse from a cell of higher concentration to one of lower concentration. A path of such a passive diffusion is shown here in green.*

1.1.1 'ON' and 'OFF' Mechanisms

'ON' mechanisms are processes in a cell signalling pathway which are responsible for the onset of cellular response to external stimuli (green arrows in Figure 1.2). These 'ON' mechanisms are counteracted by 'OFF' mechanisms (red arrows in Figure 1.2) which switch off the flow of information upon the removal of external stimuli. An important and related 'OFF' mechanism is receptor desensitisation whereby receptors lose their sensitivity to external stimuli. For example, receptor desensitisation is often seen during prolonged labour when increased application of *OT* doesn't result in increased contractile force.

The process of controlling a signalling cascade through 'ON' and 'OFF' mechanisms is a dynamic one, described in very general terms in Figure 1.2. In this process cell stimuli are received by receptors, at or on the cell periphery, that function as 'antennae' embedded in the plasma membrane. These receptors then transfer information to a variety of transducers and amplifiers which produce

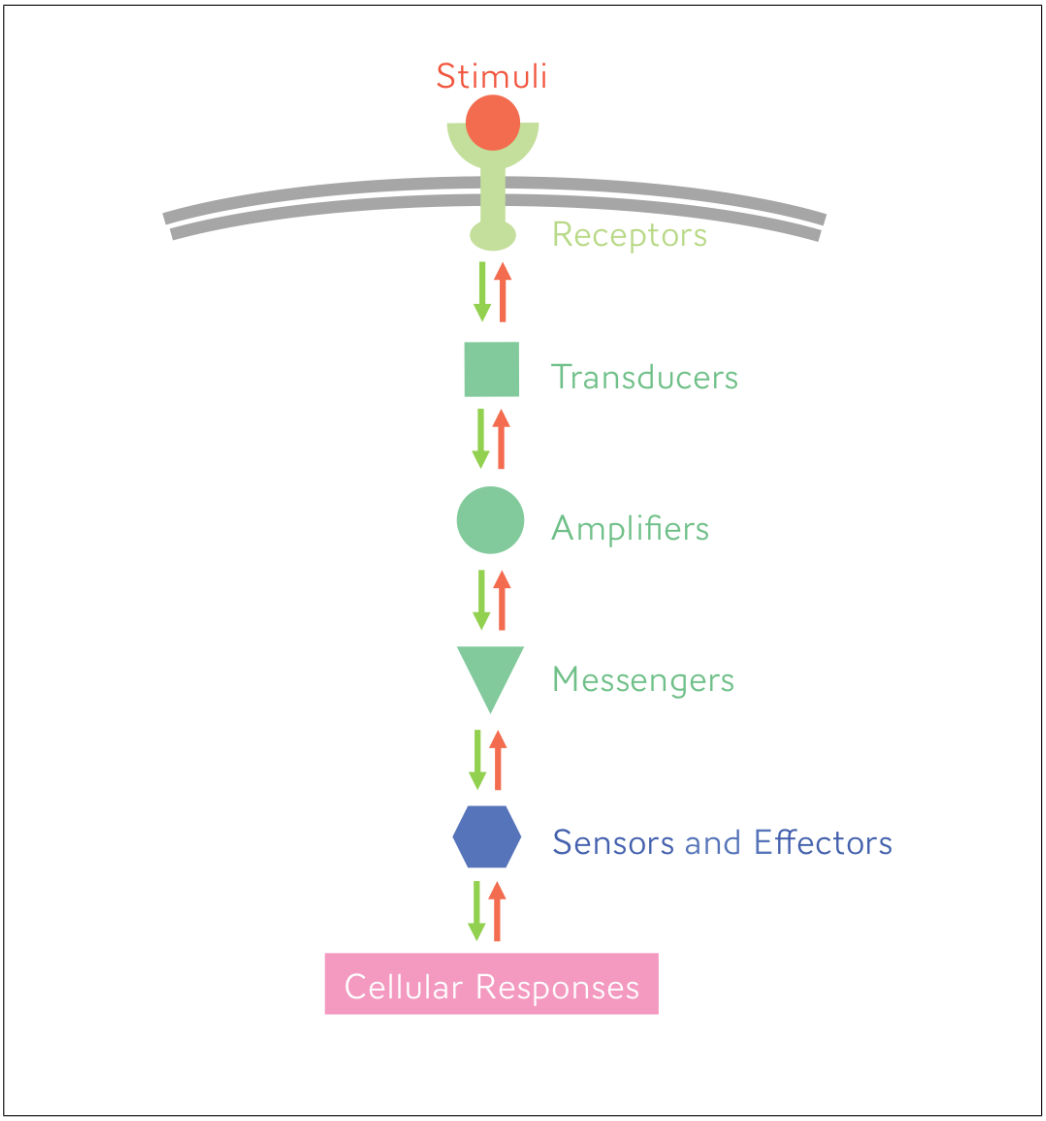

Figure 1.2 *A generalised cell signalling pathway: Stimuli acting on cell-surface receptors relay information to induce cellular responses via a cell signalling pathway. This pathway usually begins with activation of transducers which use amplifiers to generate internal messengers which, in turn, engage sensors that are coupled to the effectors responsible for inducing the cellular response. As demonstrated later (§1.2) this process is a dynamic one, consisting of a delicate balance of both 'ON' and 'OFF' reactions which are responsible for information flow down (green arrows) and up (red arrows) the signalling pathway, respectively [100].*

intracellular messengers. In turn, these messengers stimulate the sensors and effectors which are responsible for activating cellular responses [52].

1.1.2 The transfer of information

Cell signalling pathways have a number of ways to transfer this information, for example by diffusion, direct protein-protein interactions or by covalent modifications such as protein phosphorylation, acetylation and nitrosylation. All of these events are affected by spatial and temporal aspects of signalling pathways.

Each cell-type has a unique repertoire of cell signalling components: its cell-type-specific signalsome [12]. This signalsome is needed to control that cell-type's particular functions. Indeed, the cell's repertoire of signals relies upon cross-talk between different signalling pathways. Further, the signalsome is very adaptable and is constantly remodelling itself to cope with the constantly changing cell-environment.

These highly integrated signalling mechanisms then act through different effectors (e.g. muscle proteins, secretory vesicles, transcription factors, ion channels and metabolic pathways) to control the activity of cellular processes such as development, proliferation, neural signalling, stress responses and apoptosis [104].

1.1.3 Signalling through G-protein-coupled cell-surface receptors (GPCRs) and small intracellular messengers

G-protein-coupled cell-surface receptors (GPCRs), the largest family of cell-surface receptors with over 700 identified in humans, are used by all eucaryotes in cell signalling. They mediate most responses to signals from both the external world (sight, taste, smell) and from other cells (hormones, neurotransmitters, growth factors and local mediators). The signalling molecules that act on GPCRs are as diverse in structure as they are in function. Examples of stimuli of GPCRs vary from photons of light to everything we can see or taste and include proteins, small peptides, amino acid and fatty acid derivatives.

Despite the chemical and functional diversity of their signal molecules, the members of the GPCR superfamily all have a similar structure. Their characteristic orientation consists of a single polypeptide chain that threads back and forth across the plasma membrane seven times (Figure 1.3) and they all use G-proteins to relay the received signal into the cell's interior.

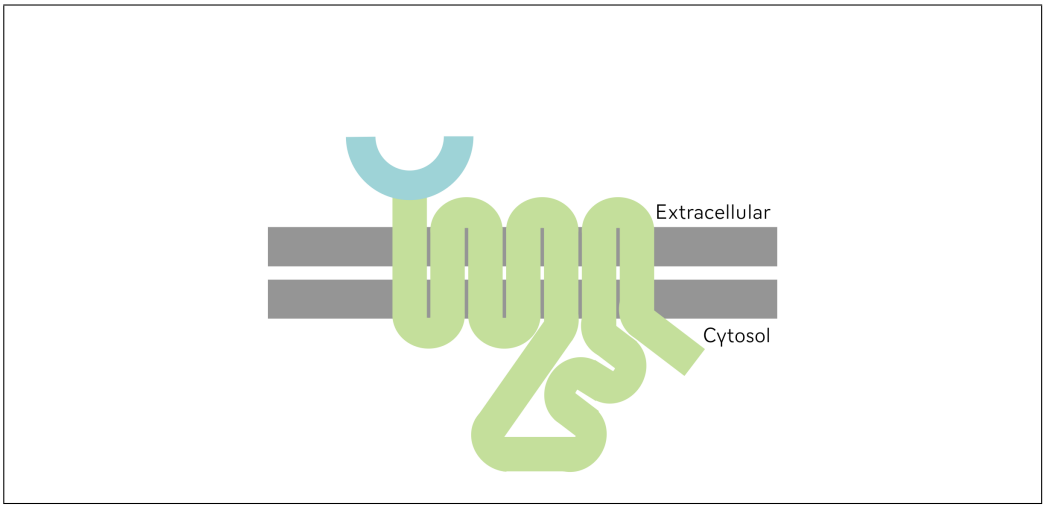

Figure 1.3 *G-protein-coupled cell-surface receptor (GPCR): Showing the characteristic structure of a GPCR with its seven crossings of the plasma membrane. Both the depth of ligand-binding and the size of the extracellular part of the polypeptide chain (shown in light-blue) varies with the ligand that binds it.*

1.1.4 Trimeric GTP binding protein (G-protein) Relay Signals from GPCRs

Upon binding of an extracellular signal molecule to a GPCR, the receptor undergoes a conformational change which enables it to activate a trimeric GTP binding protein (G-protein). There are a large range of G-proteins with different functions and modes of action; all G-proteins, however, are composed of the same basic structure: an α, β and γ protein subunit, attached to the cytoplasmic side of the plasma membrane (Figure 1.4).

When a GPCR is stimulated, upon binding of a signal molecule, it induces the α subunit to release its bound GDP allowing the abundant GTP to bind in its place in a process not dissimilar to a guanine nucleotide exchange factors (GEFs) (Figure 1.5).

The resultant conformational change in the G-protein activates it. The traditional view is that this causes the trimer to dissociate into an α subunit and an $\beta\gamma$-complex. Recent evidence suggests, however, that in some cases at least, the conformational change exposes previously sheltered faces between the α subunit and an $\beta\gamma$-complex (Figure 1.7). This allows them to interact with their enzyme or ion channel targets in the plasma membrane, to relay the signal down the signalling pathway without dissociating.

Indeed, GPCRs can trigger a large number of different intracellular signalling pathways, including some also activated by enzyme-coupled receptors. However, here we focus on those that use the small intracellular mediators inositol phos-

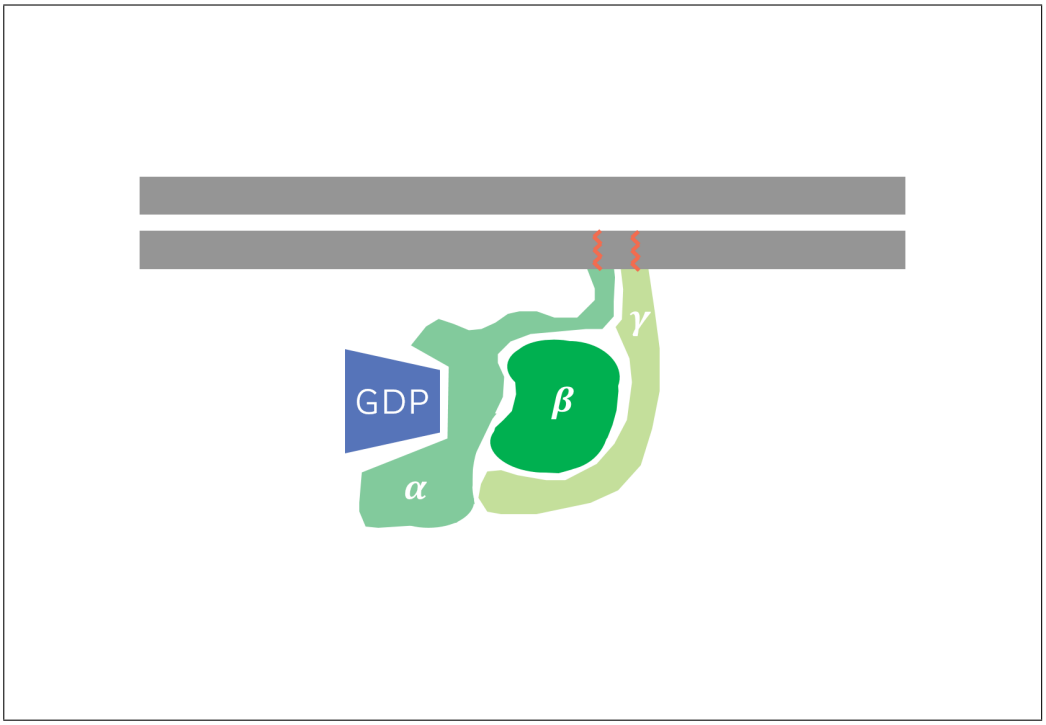

Figure 1.4 *The structure of an inactive G-protein showing the GDP molecule bound to the α subunit and the covalent attachments between the α and γ subunits and the plasma membrane (red).*

pholipids [88, 14].

1.1.5 G-protein Activation of An Inositol Phospholipid Signalling Pathway

Many GPCRs exert their effects mainly via G-proteins that activate the plasma-membrane-bound enzyme phospholipase-Cβ (PLCβ). The phospholipase acts on a phosphorylated inositol phospholipid (a phosphoinositide) called phosphatidylinositol 4,5-bisphosphate (PIP2) ($PI(4,5)P_2$ or PIP_2) which is found bound in small quantity to the inner half of the plasma membrane lipid bilayer (Figure 1.6). In much the same way as the G-protein G_s cascade activates the adenylyl cascade, the inositol phospholipid signalling pathway is mainly triggered by receptors that operate via the G-protein G_q which activates phospholipase C-β.

As shown in Figure 1.6 (a), the phosphorylation of phosphatidylinositol and $PI(4)P$ produce the phosphoinositides $PI(4)P$ and $PI(4,5)P_2$ (PIP_2), respectively. Whilst all three phospholipids can be broken down in a signalling response, it is the breakdown of the least abundant $PI(4,5)P_2$, making up just 10% of the total phospholipids and about 1% of the lipids in the plasma membrane, that predominates. Once activated, the phospholipase cleaves PIP_2 to generate

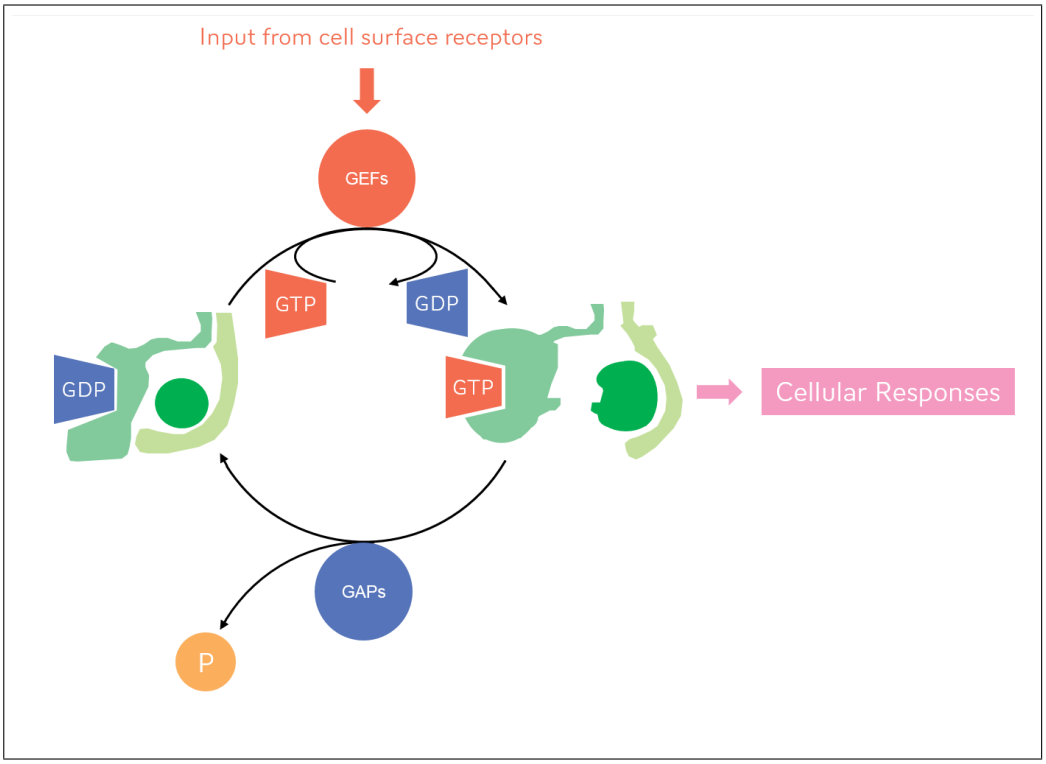

Figure 1.5 *All GTP-binding proteins (G-proteins) function through a binary switching mechanism that is driven by the binding of GTP. When GDP-bound, the G protein is inactive. Upon the exchange of GDP for GTP, the G-protein becomes activated and can stimulate any number of different signalling responses. This switching to the active state is rapid and facilitated by guanine nucleotide exchange factors (GEFs) which receive information from the receptors on the cell surface. GTPase-activating proteins (GAPs) on the other hand accelerate the OFF reaction by enhancing the hydrolysis into GDP of GTP.*

- inositol 1,4,5-triphosphate ($InsP_3$) and
- diacylglycerol.

in the way demonstrated in Figure 1.6. inositol 1,4,5-triphosphate (InsP3) then diffuses through the cytosol and releases Ca^{2+} from the endoplasmic reticulum, while diacylglycerol, which remains bound to the membrane, helps to activate the enzyme protein kinase C (PKC).

The activated GPCR stimulates plasma-membrane-bound phospholipase PLCβ via its G_q protein by the $\beta\gamma$ subunit of another G protein or by both. When $PI(4,5)P_2$ is hydrolysed by activated PLCβ, $InsP_3$ and diacylglycerol are produced as described in Figure 1.6 (b). $InsP_3$ diffuses through the cytosol, releasing Ca^{2+} from the cell's Ca^{2+} store, the endoplasmic reticulum (ER), by binding to and opening $InsP_3Rs$. Ca^{2+} escapes the ER when the $InsP_3Rs$ are open because of the massive electrochemical gradient (since $\left[Ca^{2+}\right]_{ER} \gg \left[Ca^{2+}\right]_i$). Diacylglycerol remains in the plasma membrane and, with phosphatidylserine and Ca^{2+}, activates protein kinase C (PKC) which is recruited to the cytosolic face of the

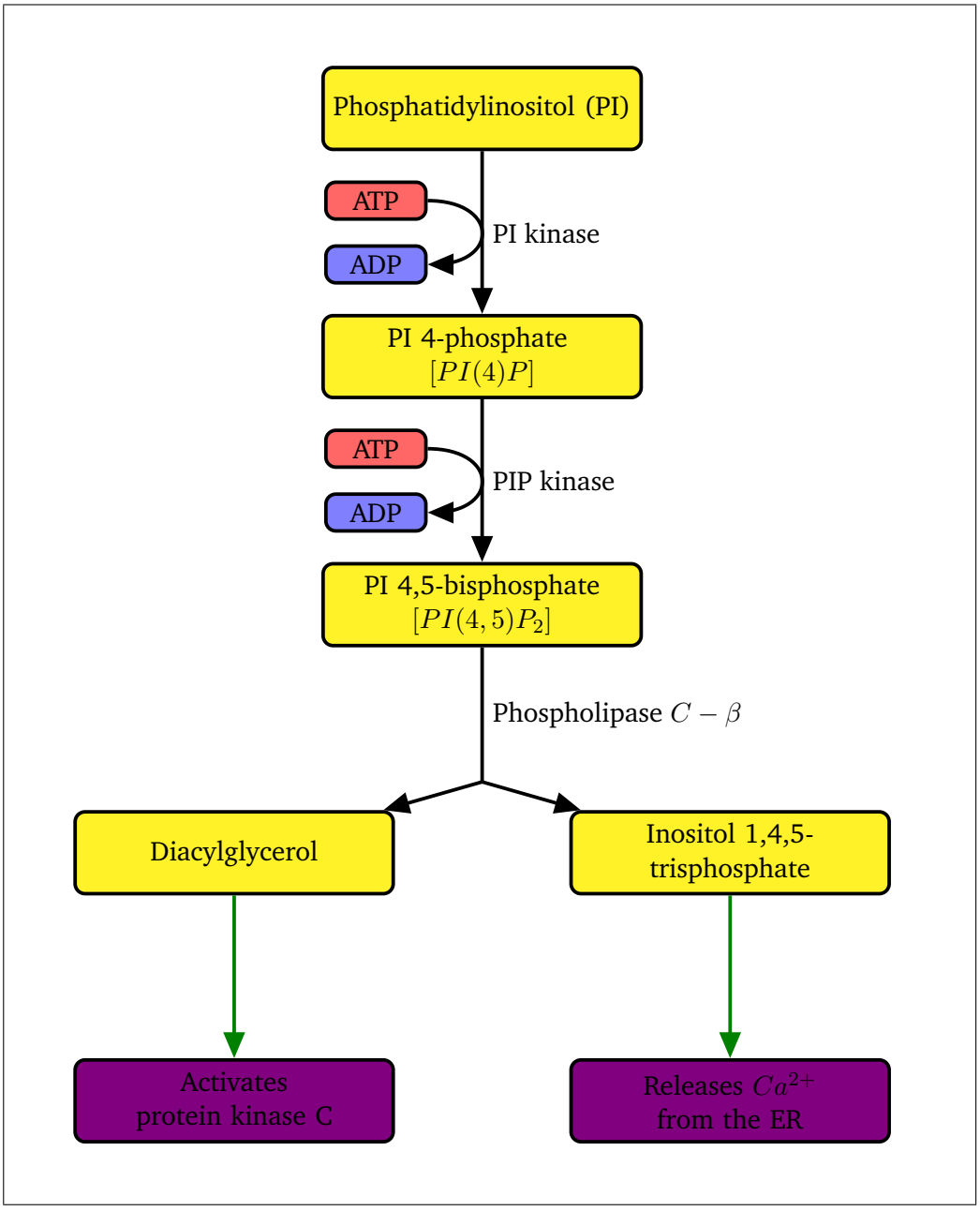

Figure 1.6 *The hydrolysis and phosphorylation of phosphoinsoitides*

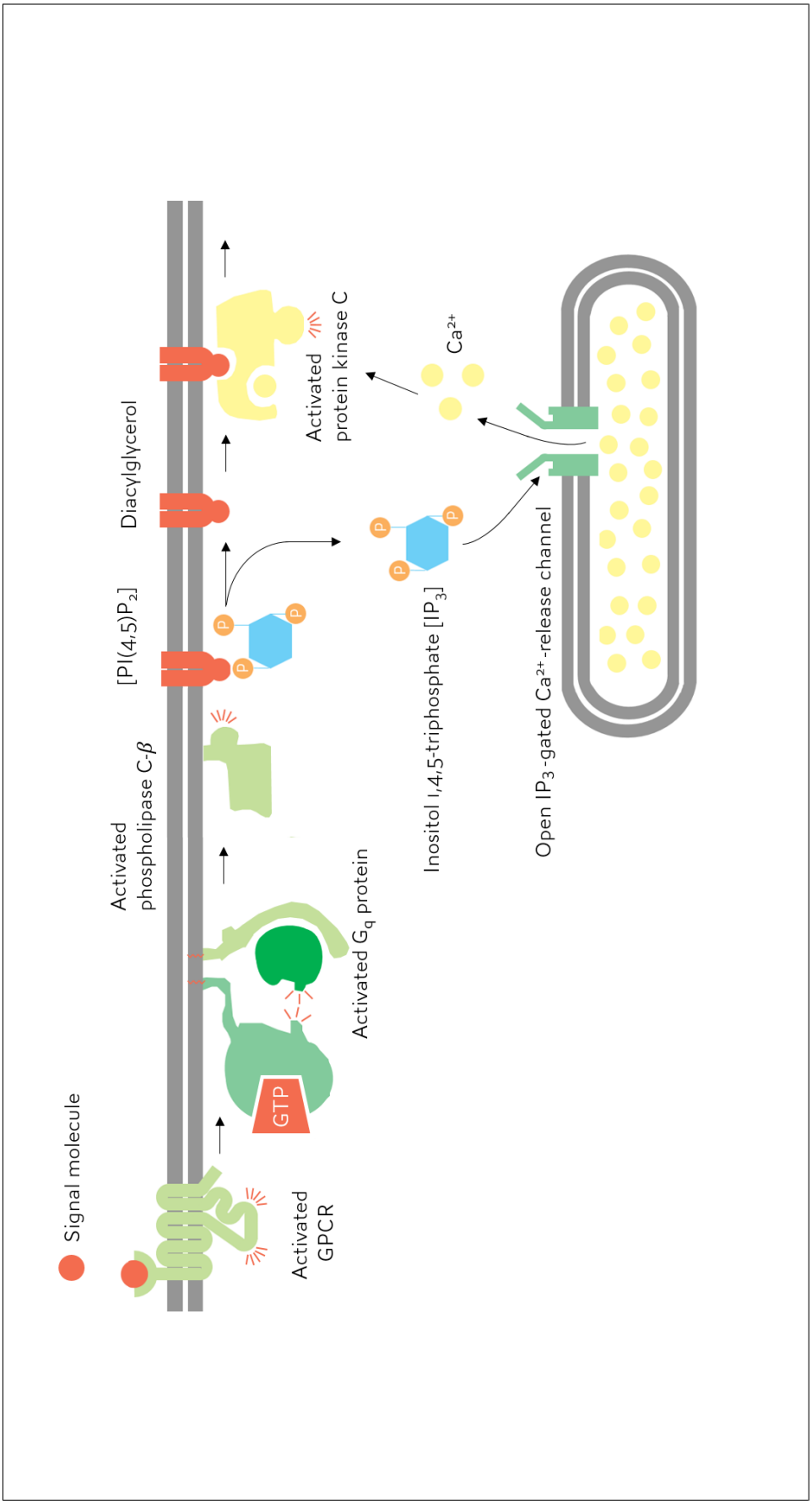

Figure 1.7 *The G_q signalling cascade*

plasma membrane from the cytosol [111, 12].

1.2 Ca^{2+} Signalling

Ca^{2+} signalling is one of the major signalling systems in cells and is ubiquitous, being found in organisms from bacteria to mammals. Ca^{2+} triggers new life at fertilisation and stimulates parturition. It controls many developmental processes and, post-differentiation, governs most cellular processes, determining how we metabolise, secrete, move and think. Larger than normal elevations of Ca^{2+} are also known to cause cell death, either by triggering controlled cell-death via apoptosis, or the catastrophic necrotic changes seen during a stroke or cardiac ischaemia.

Most intracellular signalling molecules are produced by ON mechanisms in the cell, have an effect on the cell and then are destroyed by OFF mechanisms, e.g. as described in the case of the cAMP pathway, cAMP is produced (ON), it activates a kinase, and then is destroyed by a phosphodiesterase (OFF).

However, in the case of Ca^{2+} signalling, it is changes in the cytosolic concentration of Ca^{2+} ions, $\left[Ca^{2+}\right]_i$ experienced by the effector molecule where it acts, rather than the production or destruction of Ca^{2+}, that controls the many metabolic processes within the cell.

At rest, cells maintain a low intracellular Ca^{2+} concentration with $\left[Ca^{2+}\right]_i \sim 100\ nM$ but this can increase into the micro-molar range upon stimulation. Ca^{2+} signalling uses this seemingly simple mechanism to trigger a vast range of events over differing time scales. These range from the microsecond control of exocytosis to fertilisation which occurs over a number of hours (Figure 1.8). A cell's ability to control this increase depends on its cell-specific Ca^{2+} signalling signalsome and the repertoire of elements from the Ca^{2+} toolkit it is able to express [18].

Several pathways controlling cellular Ca^{2+} are listed below and then addressed individually in §6.1.

- Ca^{2+} *entry channels* which control the entry of Ca^{2+} from the extracellular space
- Ca^{2+} *release channels* which control the release of Ca^{2+} from internal stores
- Ca^{2+} *buffers* which ensure the concentration of Ca^{2+} remains within its operational range and does not rise to levels that induce cell death

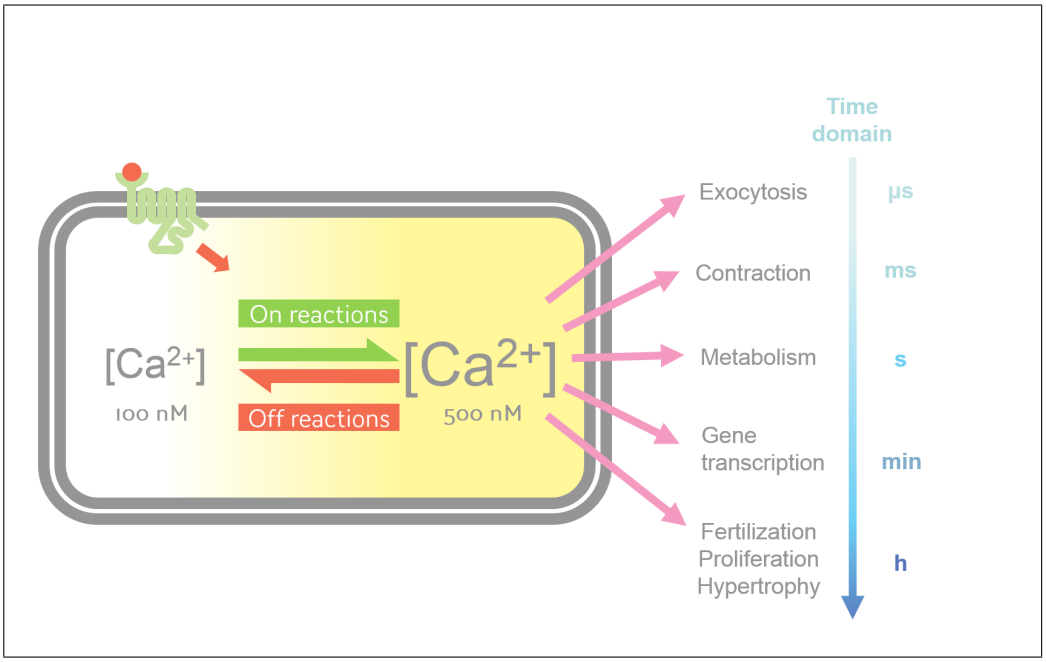

Figure 1.8 *Ca^{2+} is a signalling molecule capable of activating many different cellular processes operating over a very wide time — and spatial — domain. Cytosolic Ca^{2+} rests at approximately 100 nM, but this increases to 500 nM or more immediately following a stimulus that activates the Ca^{2+} ON reactions. When the stimulus is removed, the Ca^{2+} OFF reactions work to return the concentration of Ca^{2+} to the resting level [18].*

- *Ca^{2+} pumps and exchangers* to remove it from the cytoplasm of the cell by either extrusion from the cell or re-uptake into internal stores
- *Ca^{2+} sensors and effectors* are responsible for translating Ca^{2+} signals into a change in cellular activity

1.2.1 Ca^{2+} ON mechanisms: Ca^{2+} entry and release channels

External stimuli cause the cell to use its repertoire of both Ca^{2+} entry and Ca^{2+} release channels to allow Ca^{2+} to flow into the cytoplasm and bring about the commensurate elevation in $\left[Ca^{2+}\right]_i$ responsible for cell activation. The cell signalsome has a repertoire of entry and release channels, named to indicate how the channels are opened. These have very different spatial and temporal properties which allow the variety of types of signals described in Figure 1.9:

- Ca^{2+} entry channels
  - Voltage-operated channels (VOCs)
  - Receptor-operated channels (ROCs)
  - Store-operated channels (SOCs)

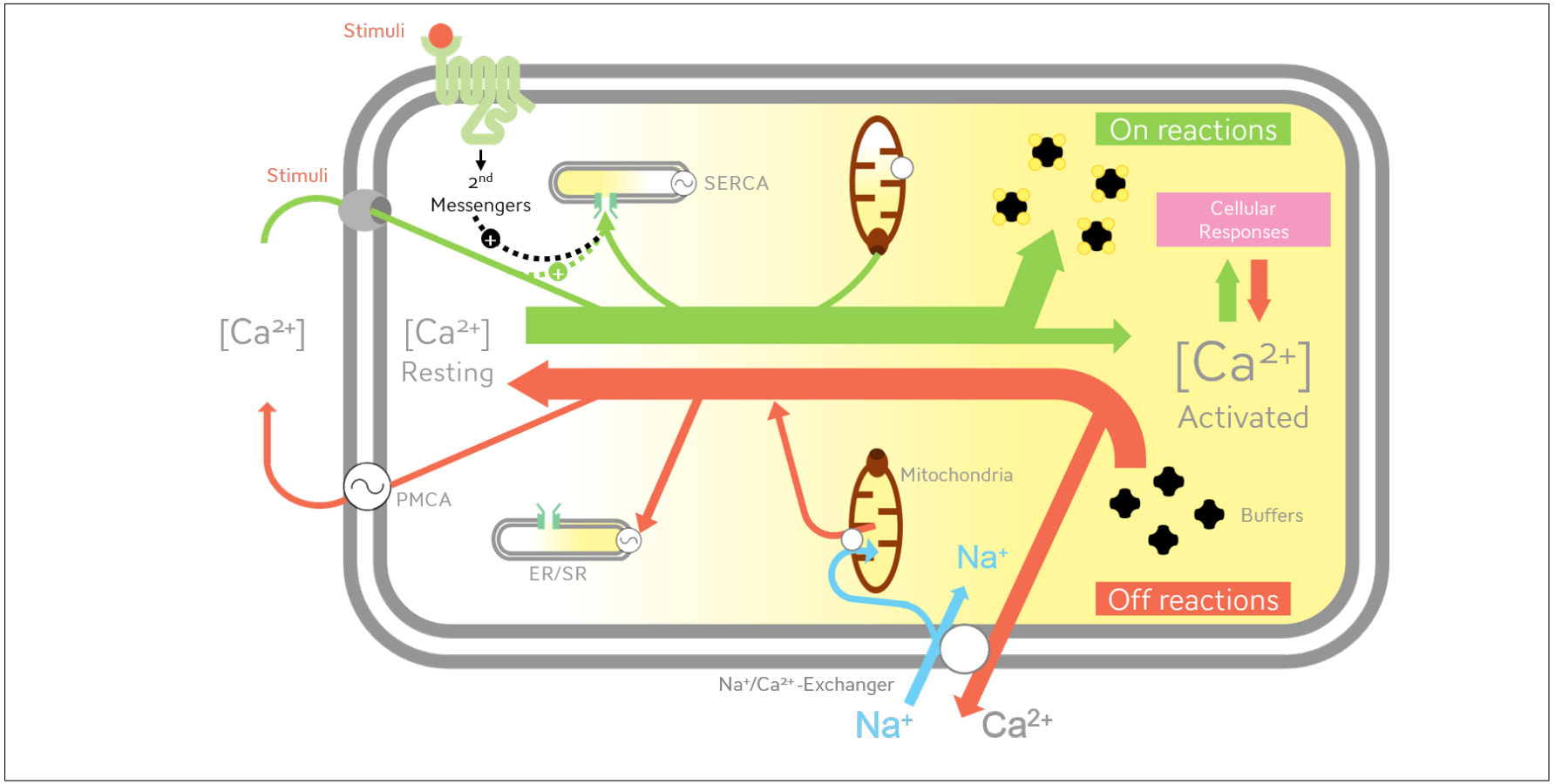

Figure 1.9 *Ca^{2+} signalling dynamics are governed by the interplay between ON and OFF reactions which moderate the fluxes of Ca^{2+} across both the plasma membrane and the internal stores such as the sarco-endoplasmic reticulum and mitochondria.*
ON reactions introduce Ca^{2+} into the cytoplasm through either channels in the plasma membrane or from internal stores such as the ER and are triggered by external stimuli. Most cells make use of both sources, but there are examples of cells using either external or internal sources to control specific processes. Most of the Ca2+ that enters the cytoplasm is adsorbed on to buffers, while a much smaller proportion activates the effectors to stimulate cellular processes. The OFF reactions remove Ca2+ from the cytoplasm using a combination of mitochondria and different pumping mechanisms. When cells are at rest, these OFF reactions keep the concentration low, but these are temporarily overwhelmed when external stimuli activate the ON reactions. Sequential activation of the ON and OFF reactions gives rise to the Ca2+ transients , which are such a characteristic feature of Ca2+ signalling systems. PMCA, plasma membrane Ca2+-ATPase; SERCA, sarco/endo-plasmic reticulum Ca2+-ATPase [18].

- Ca^{2+} release channels
  - Ryanodine Receptors (RYR s)
  - $InsP_3$ receptors ($InsP_3Rs$)
  - NAADP control of Ca^{2+} release

1.2.2 Ca^{2+} OFF mechanisms: Ca^{2+} buffers, pumps and exchangers

A cell has a variety of OFF mechanisms it can use for the removal of Ca^{2+} from the cytosol. This is vital for ensuring termination of Ca^{2+} signals. The recovery process thus relies on a complex interplay between the ON reactions and the following OFF reactions:

- Cytosolic Ca^{2+} buffers
- Mitochondria
- Ca^{2+} pumps and exchangers
  - Plasma membrane calcium-ATPase (PMCA)
  - Sarco/endo-plasmic reticulum calcium-ATPase (SERCA)
  - $Na^{+}/Ca^{2+}-$exchanger

Hence, it is important to see the ON and OFF mechanisms not necessarily as a switch but as 'rate limiting'. Different OFF reactions act at different times and rates during the recovery phase of a typical Ca^{2+} spike.

Initially, much of the Ca^{2+} that enters the cell during the ON reactions is rapidly bound to cytoplasmic buffers or taken up into the mitochondria. As the $\left[Ca^{2+}\right]_i$ returns to the resting level, Ca^{2+} leaves the buffers and mitochondria and is returned to the ER or is pumped out of the cell by the pumps or exchangers. These, in turn, operate at different times to shape the resultant Ca^{2+} transient. As introduced in §1.1, the first step in this process is triggered by an extracellular signalling molecule. For the purposes of this thesis *OT* and its receptors are used to allow *OT*-induced Ca^{2+} oscillations to be studied.

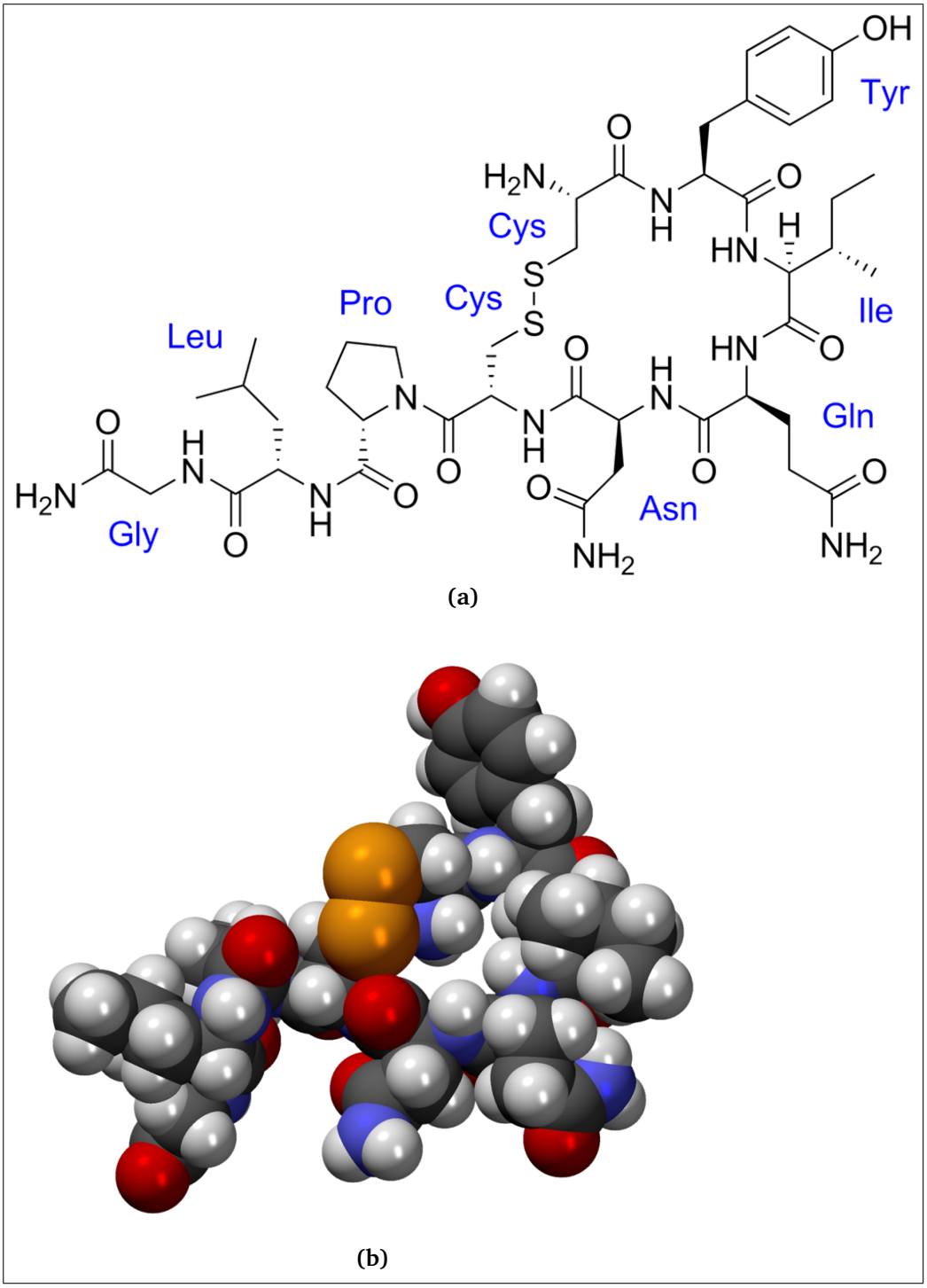

Figure 1.10 *Two graphical representations of the structure of Oxytocin whose systematic name is cysteine-tyrosine-isoleucine-glutamine-asparagine-cysteine-proline-leucine-glycine-amine* ($cys-tyr-ile-gln-asn-cys-pro-leu-gly-NH_2$, *or* $CYIQNCPLG-NH_2$)

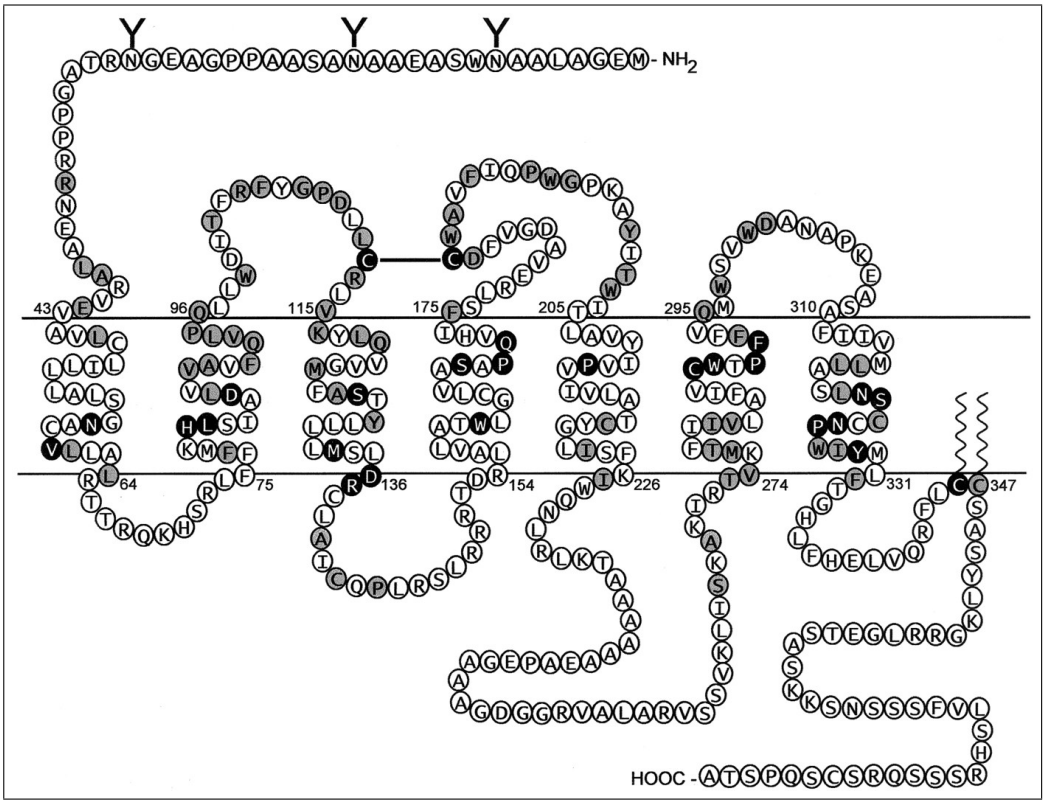

Figure 1.11 *A schematic model of the human oxytocin receptor indicating the amino acid residues that are putatively involved in ligand-binding and associated signal transduction events [60].*

1.3 Use of Oxytocin and its receptor to improve parturition and reduce birth deaths

1.3.1 Oxytocin and its receptor

The label for the polypeptide hormone oxytocin was derived from the Greek words for quick (*oxys*) and birth (*tokos*). Its uterine-contracting properties leading to a so called 'quick-birth', were discovered in 1906 by British pharmacologist Sir Henry Hallett Dale [36].

Oxytocin's ability to induce or augment labour led to it being one of the first polypeptide hormones to be sequenced and synthesised [45]. Whilst the mechanistic role of oxytocin in the initiation of labour is still debated today, it is used here because of its importance during pregnancy and parturition and its ability to induce Ca^{2+}-oscillations by binding to the G_q-linked oxytocin receptor (a GPCR) and thus initiating the $InsP_3$ pathway and resultant Ca^{2+} release described in §1.1.

1.3.2 The Structure, Synthesis and Transport of Oxytocin

Oxytocin (OT) is a nonapeptide and its nine amino acid sequence was determined by Vincent du Vigneaud et al. and by Tuppy in 1953 [46] and synthesised biochemically soon after by du Vigneaud et al. in 1953 [44, 45]. Oxytocin has a molecular mass of 1007 daltons and one international unit (IU) of oxytocin is the equivalent of about 2 micrograms of pure peptide.

In the human body, oxytocin is synthesised in the paraventricular and supraoptic nucleus of the hypothalamus as a large precursor molecule which is quickly broken down to the active hormone and its neurophysin before it is packaged into neurosecretory granules. These granules are distributed throughout the perikarya[1] and along the neurons whose axons pass through the median eminence into the posterior pituitary gland at a rate of 1-3 $mm/hour$ [116]. Once the granules reach the neurohypophysis they are released by exocytosis and thus oxytocin and its neurophysin appear simultaneously in the blood. As a result of this transcriptional and post-translational processing, there are several different molecular forms of circulating oxytocin each with different biological properties [23].

1.3.3 The Oxytocin Receptor

In humans, the oxytocin receptor (OTR) is encoded by the OXTR gene [37, 89], which has been localised to chromosome 3p25 [36]. The human oxytocin receptor, at about 43 kDa, is a polypeptide of 388 amino acids and has seven transmembrane domains typical of G-protein-coupled receptors [76]. It has been determined to belong to the G_q subset of that family [91] meaning that it triggers the cascade described in §1.1. A topographic model of the *OT* receptor is depicted in Figure 1.11 which has similar structure to Figure 1.4.

1.3.4 Oxytocin-induced Uterine Contractions

Oxytocin stimulates uterine contraction by the activation of the receptor-operated calcium mechanism and consequent release of Ca^{2+} from the endoplasmic reticulum described in §1.1.

After binding to its receptors, the action of *OT* is mediated by the secondary messengers $InsP_3$ and diacylglycerol (DAG). Influx of extracellular Ca^{2+}, through voltage and/or hormonally controlled receptor-mediated Ca^{2+} channels in the cell membrane of the myometrium, is needed to accomplish oxytocin-mediated

[1] The cell body of a neurone

contractions [10, 30]. *OT* then increases hydrolysis of phosphoinositides, which leads to release of $InsP_3$ [30, 90, 112]. $InsP_3$ acts to mobilise and release stored intracellular Ca^{2+} from the ER.

OT also induces an inward current through receptor-activated, nonselective cation channels [117] which could depolarize the cell membrane and trigger action potential, leading to contraction of the muscle. However, also in [117], this oxytocin-induced voltage-dependent Ca^{2+} current may be inhibited by the resulting release of intracellular calcium. Besides slow Ca^{2+} channels, fast Na^{+} channels, which become more numerous towards term [122], are also needed for Myometrial contractions but *OT* does not affect Na^{+} currents [66]. Ca^{2+}-dependent phosphorylation of myosin then triggers the interaction of actin and myosin, leading to contractions in a process known as excitation-contraction coupling [115].

1.4 Mathematical modelling

There are multiple reasons why a mathematical model of a system can be advantageous in the study of that system. Many argue that it is in the interplay between such a mathematical model and experimental observations that is the key to gaining a full understanding of the system under study. This juxtaposition of modelling and experiment is the essence of a Systems Biology approach.

When observations are made experimentally of a system, they are often a snapshot of understanding of a complex system in a particular conformation. It is often not possible to elucidate the underlying processes from first principles and to find an exact biological explanation for the observed results. Even if the biochemistry of the system is well understood, for instance in the case of enzyme-catalyzed reactions, the biochemistry of the individual molecules is often unknown, and there can be huge variations between cell type, organ or species. Experiments result in a biological hypothesis, a biological model, about individual components in a system, but it is often unclear how several hypotheses can be combined into a coherent picture of a system's global behaviour. For instance, in the case of Ca^{2+} signalling, it is possible to know the exact rate of Ca^{2+} flux of all the elements in a system under a particular set of circumstance (the 'ON' and 'OFF' reactions). You can also understand their exact physiological mechanism. However, this does not tell one anything about how these elements combine into a global release of Ca^{2+} within the cell.

Mathematical models can help to bridge the gap between what is understood and what is observed biologically as well as investigating the possible dynamics of the

system in order to arrive at predictions, for instance, about their development over time or in different biological conditions.

1.4.1 What is a mathematical model?

The word, model, is ultimately derived from the latin *modulus* meaning 'small measure' and the word is used to describe everything from Cara Delevingne to a miniature 1:50 aeroplane. Thus a model can be seen as an

> *'idealised representation of objects or processes that explains features of these objects or processes.'* [78]

Mathematical modelling embodies these principles and can be defined as

> *'the description of an experimentally delineated phenomenon by means of mathematics, with a view to capturing the salient aspects of the phenomenon at hand.'* [131]

Modelling is a subjective and selective procedure and thus some caution is needed in applying this definition. A model is modest as it only aims at 'capturing salient aspects' and a modeller must be cautious by understanding that it only captures specific aspects of reality. If done properly, however, these are not unduly limiting and, rather, can allow a specific question to be addressed when no answer would be available if a less selective, cautious approach were taken.

1.4.2 Dynamical systems theory and ordinary differential equations

The nature of the best 'means of mathematics' to employ in the construction of a model is often a subtle question. One option is to keep the mathematical approach as simple as possible. The aim of this being to allow for ease of implementation, simplicity and/or comprehensibility of results. Another approach is to model the system as realistically as the known material will allow, making the model more complex but more 'realistic'.

In this thesis, dynamical systems theory, and in particular, the theory of ordinary differential equations (ODEs), is the 'means of mathematics' that is employed for constructing our models. The theory of dynamical systems pervades the analysis of biological processes. The motivation for using ordinary differential equations is straightforward: they provide a mathematically simple way of describing the rate of change in the state variables of a system as time progresses. ODEs depend on one independent variable (most often time), otherwise they are called partial differential equations (PDEs).

The system state is a snapshot of the system at a given time (for instance its initial conditions) and contained within this snapshot is enough information to predict the behaviour of the system for all future times: the system is deterministic. The state of the system is described by the set of variables, the x_i. The set of all possible states is the state space and the number, n, of independent variables defines the dimension of that state space.

The behaviour of a biological system can thus be described by the system of equations:

$$\frac{dx_i}{dt} = f_i(x_1, \ldots, x_n, t; p_1, \ldots, p_m), \text{ for } i = 1, \ldots, n, \tag{1.4.1}$$

where x_i is one of the n state variables of the system (e.g. the concentrations in each compartment), p_j ($j = 1, \ldots, m$) is one of the m parameters (e.g. the number of pumps or their activity) and t is time.

A particular solution of the ODE system 1.4.1 is determined from a general solution by specifying each of the parameters, p_j, and initial conditions at $t = t_0$:

$$x_i(t_0) = x_i^0 \quad \in \mathbb{R}, \tag{1.4.2}$$

for each $i = 1, \ldots, n$. Such a solution describes a path through the state space called a trajectory.

Using the notation $dx_i/dt = \dot{x}$ and $\mathbf{x} = (x_1, x_2, \ldots, x_n)$, the steady states of Equation (1.4.1) are the points, , in the phase plane, where the condition

$$\frac{d\mathbf{x}}{dt} = 0. \tag{1.4.3}$$

That is, those points, $\bar{\mathbf{x}} = (\bar{x}_1, \bar{x}_2, \ldots, \bar{x}_n)$ where $dx_i/dt = 0$ for all $i = 1, \ldots, n$ simultaneously.

At a steady state, the system of n differential equations is represented by a system of n algebraic equations in n variables. Thus, the steady state equation, $\dot{\mathbf{x}} = 0$, can have multiple solutions which refer to multiple steady states of the system. The change of number or stability of steady states upon the change of parameter values $\mathbf{p} = (p_1, p_2, \ldots, p_m)$ is called a bifurcation and can be represented in a bifurcation diagram. Such a diagram plots the value of the steady state of a variable, x_i as a parameter, p_j is changed. The bifurcation diagrams presented in this thesis are accompanied by a numerically computed plot of the minimum and maximum amplitude of any oscillations that exist along with their frequency.

The behaviour of a system close to the steady state is of interest and may enable the study of the long term behaviour of the system. Considering a deviation from

steady state, $\bar{\mathbf{x}}$, linear stability analysis can be performed using the perturbation from the steady state, $\mathbf{x}(t) = \bar{\mathbf{x}} + \hat{\mathbf{x}}(t)$ and, thus:

$$\dot{\mathbf{x}} = f(\bar{\mathbf{x}} + \hat{\mathbf{x}}(t)) = \frac{d}{dt}(\bar{\mathbf{x}} + \hat{\mathbf{x}}(t)) = \frac{d}{dt}\hat{\mathbf{x}}(t). \tag{1.4.4}$$

Taylor expanding with regard to time of the deviation, $\frac{d}{dt}\hat{x_i} = f_i(x_1 + \hat{x}_1, \ldots, \bar{x}_n + \hat{x}_n)$, gives n equations of the form:

$$\frac{d}{dt}\hat{x}_i = f_i(\bar{\mathbf{x}}, t; \mathbf{p}) + \sum_{j=1}^{n} \frac{\partial f_i}{\partial x_j}\bigg|_{\bar{\mathbf{x}}} \hat{x}_j + \frac{1}{2}\sum_{j=1}^{n}\sum_{k=1}^{n} \frac{\partial^2 f_i}{\partial x_j \partial x_k}\bigg|_{\bar{\mathbf{x}}} \hat{x}_j \hat{x}_k + \ldots. \tag{1.4.5}$$

Since the system is considered at steady state, it holds that $f_i(\bar{\mathbf{x}}, t; \mathbf{p}) = 0$. Thus, if higher order terms are neglected,

$$\frac{d}{dt}\hat{x}_i = \sum_{j=1}^{n} \frac{\partial f_i}{\partial x_j}\bigg|_{\bar{\mathbf{x}}} \hat{x}_j = \sum_{j=1}^{n} a_{ij}\hat{x}_j, \tag{1.4.6}$$

where the coefficients, $a_{ij} = \partial f_i / \partial x_j|_{\bar{\mathbf{x}}}$, are constant since they are calculated at steady state. They form the so-called Jacobian matrix of the system (1.4.1):

$$J = \begin{pmatrix} \frac{\partial f_1}{\partial x_1} & \frac{\partial f_1}{\partial x_2} & \cdots & \frac{\partial f_1}{\partial x_n} \\ \frac{\partial f_2}{\partial x_1} & \frac{\partial f_2}{\partial x_2} & \cdots & \frac{\partial f_2}{\partial x_n} \\ \vdots & \vdots & \ddots & \vdots \\ \frac{\partial f_n}{\partial x_1} & \frac{\partial f_n}{\partial x_2} & \cdots & \frac{\partial f_n}{\partial x_n} \end{pmatrix}\Bigg|_{\bar{\mathbf{x}}}. \tag{1.4.7}$$

When this Jacobian matrix is evaluated at a steady state, its eigenvalues tell us something about the stability of the system. The system is stable if the real parts of the eigenvalues are all strictly negative. That is, a small perturbation away from the steady state will eventually return to this original equilibrium. The behaviour when one or more of the eigenvalues is non-negative requires more calculation and will be investigated as necessary within the main text [78].

1.4.3 A model as a bridge

In short, a model can provide a bridge between

- what has been observed,
- what can be observed and

- what is (currently) understood (or hypothesised) about the individual components or processes in a system, and
- what can be observed about the system: its (experimental) 'output.'

The statistician George Box once said

> *'essentially, all models are wrong, but some are useful'* [20].

In reality none of the above approaches to modelling is either 'right' or 'wrong', since, excepting technical errors, there is only 'appropriately' and 'inappropriately' modelled. The strength of the bridge created by a model between first principles and system observations, very much depends upon its foundations: that is, the assumptions, simplifications and mathematical tools that are used in constructing it.

Chapter 2

Methods

This chapter introduces the various experimental and mathematical methods used to generate the results in this thesis. It begins by introducing the cellular model used to collect the data, the *CHO–hOT* cell-line. It then addresses the instrumentation used both to collect the data and model the system before introducing the experimental procedures used to generate the data. Before finally assessing the limitations of the methodology, the method of data analysis is introduced.

2.1 Chinese Hamsters: Source of a Cellular Model

Since their first use in research in 1919, Chinese hamsters (Cricetulus griseus, Figure 2.1) which originate from the deserts of northern China and Mongolia have proven to be useful in several areas of research. Initially used as a replacement for mice in the typing of pneumococci, the Chinese hamster was identified as highly-successful carrier for the transmission of visceral leishmaniasis in 1948 which facilitated research in epidemiology [69].

Chinese hamsters were brought to the United States of American for breeding in research laboratories in 1948. Thereafter the Chinese hamster has became noteworthy for the cell lines that were derived from its tissues. This is especially true since its chromosome number, which is very low for a mammal at $2n = 22$, makes the Chinese hamster ideal for tissue culture [1].

Indeed, it was this fact that caused Theodore T. Puck to obtain a female Chinese hamster from Dr. George Yerganian's laboratory at the Boston Cancer Research Foundation in 1957. He then used it to derive the original Chinese Hamster Ovary (CHO) cell line. CHO cells have become the mammalian cell-line equivalent of

Figure 2.1 *A wild-type Chinese hamster [2]*

E. coli in research and biotechnology because of their rapid growth, high protein production and long-term, stable gene expression.

2.1.1 *CHO–hOT* Cell-line

Our biological model Chinese Hamster Ovary human oxytocin receptor (CHO-hOT) cells were given to this project as a donation from Glaxo-Smith-Klein and were cultured as per Protocol 1. The model CHO-hOT cells were generated from Chinese Hamster Ovary cells stably transfected with human oxytocin receptor (CHO-OT1).

Unlike transient transfection, where the DNA introduced only remains in cells for several days, DNA introduced by stable transfection remains in the cells long-term. Further, stably transfected cells pass on the introduced DNA to their progeny, usually because the transfected DNA has been fully incorporated into the genome. Stable expression of the protein is achieved by the integration of the gene of interest into the target cell's chromosome. Figure 2.2 provides as schematic of this process: the gene of interest is introduced into the cell (A), sequently the nucleus (B) and finally it is integrated into chromosomal DNA (C).

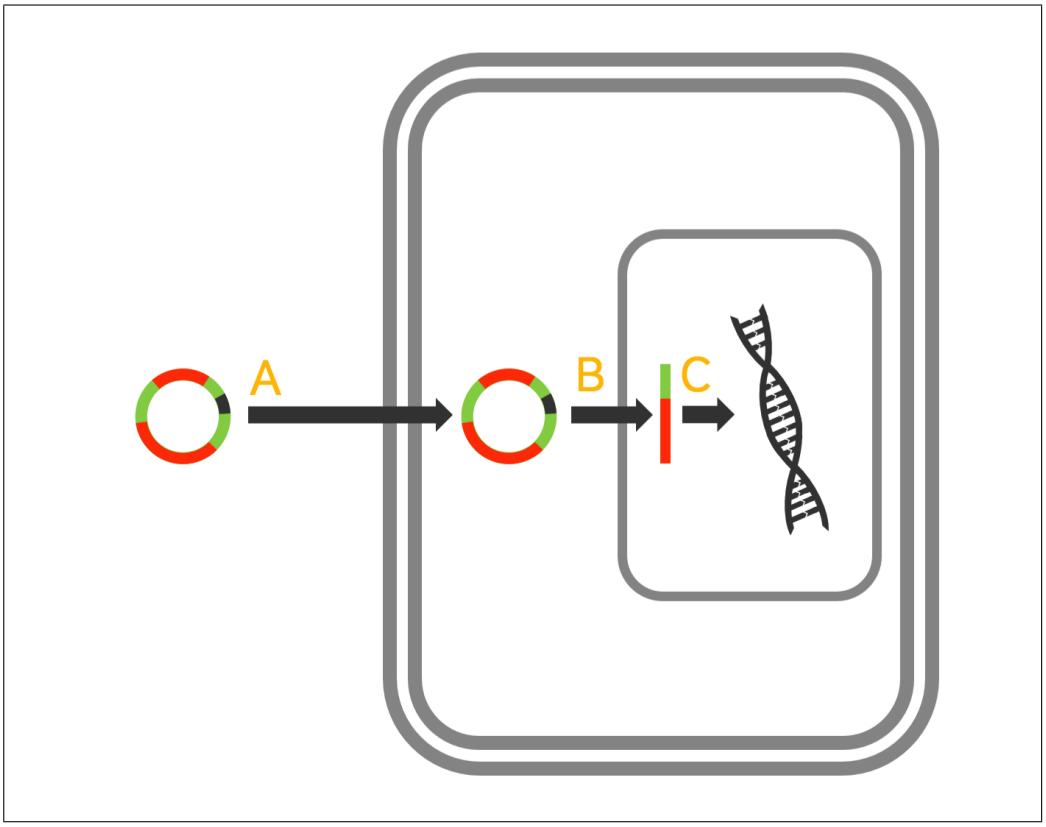

Figure 2.2 *Stable expression is achieved by integration of the gene of interest into the target cell's chromosome: Initially the gene of interest has to be introduced into the cell (A), subsequently into the nucleus (B) and finally it has to be integrated into chromosomal DNA (C).*

2.2 Instrumentation

2.2.1 Summary

The reason a simple divalent ion such as Ca^{2+} can regulate a vast array of cellular activities is that it acts as a very versatile messenger: different cells use a multitude of Ca^{2+} signals varying in amplitude, kinetics, frequency, duration and spatial dimension. This incredible variety means it is not possible to use just one technique to visualise Ca^{2+} in the cell and so a number of different situation-specific techniques must be employed. This section focusses on methods to use fluorescence to visualise Ca^{2+} within the cell.

2.2.2 Fluorescence Microscopy

Sir George G. Stokes was the first to describe fluorescence in 1852 when he noted that the mineral fluorspar emits red light when illuminated by ultraviolet light.

Early investigations showed that many specimens (including butter!) fluoresce when illuminated by ultraviolet light. It was not until the 1930s, however, that the discovery of several fluorophores, which were highly specific to particular tissue components, bacteria, and other pathogens, led to the development of the fluorescence microscope.

This technique has become an essential tool in biology, enhancing the information available from traditional optical microscopy alone. For instance, through the use of multiple labelling where different probes can simultaneously identify several target molecules. Further, whilst fluorescence microscopy cannot provide spatial resolution below the diffraction limit, it can be used to detect fluorescing molecules below that limit.

Whilst some specimens exhibit autofluorescence, of far greater value for the study of Ca^{2+} are added fluorophores. These are excited by specific wavelengths of irradiating light and emit light of defined, detectable intensity. Fluorophores are often highly specific in their attachment targeting, and in general have a significant quantum yield (the ratio, photon absorption:emission). The widespread growth in the utilisation of fluorescence microscopy in Ca^{2+} signalling has been caused by the development of new synthetic and naturally occurring fluorophores with known intensity profiles of excitation and emission, with a variety of known affinities for Ca^{2+}.

Fundamentals of Excitation and Emission

An epifluorescence microscope, a schematic of which is illustrated in Figure 2.3 is designed to irradiate a specimen with a specific band of wavelengths, and then to separate out the emitted fluorescence from that excitation light. The aim is to ensure only the emission light, often a million times dimmer than the excitation light, reaches the detector. This allows one to maintain high contrast between the fluorescent material and the background. It is the darkness of this background, or rather the ability of the microscope to separate the excitation and emission light, that determines the detection limit of the microscope.

A monochromator is used to filter white light to give a specific range of wavelengths known to excite the Ca^{2+}-bound fluorophore. Excitatory light is passed through the objective lens and then on to the specimen. The fluorophore emits light of a different wavelength from the excitatory light when (and, in theory, only when) bound to Ca^{2+}. This emitted light, and the reflected excitatory light, is reflected back through the objective. The excitatory light is filtered using an emission filter to a camera for recording.

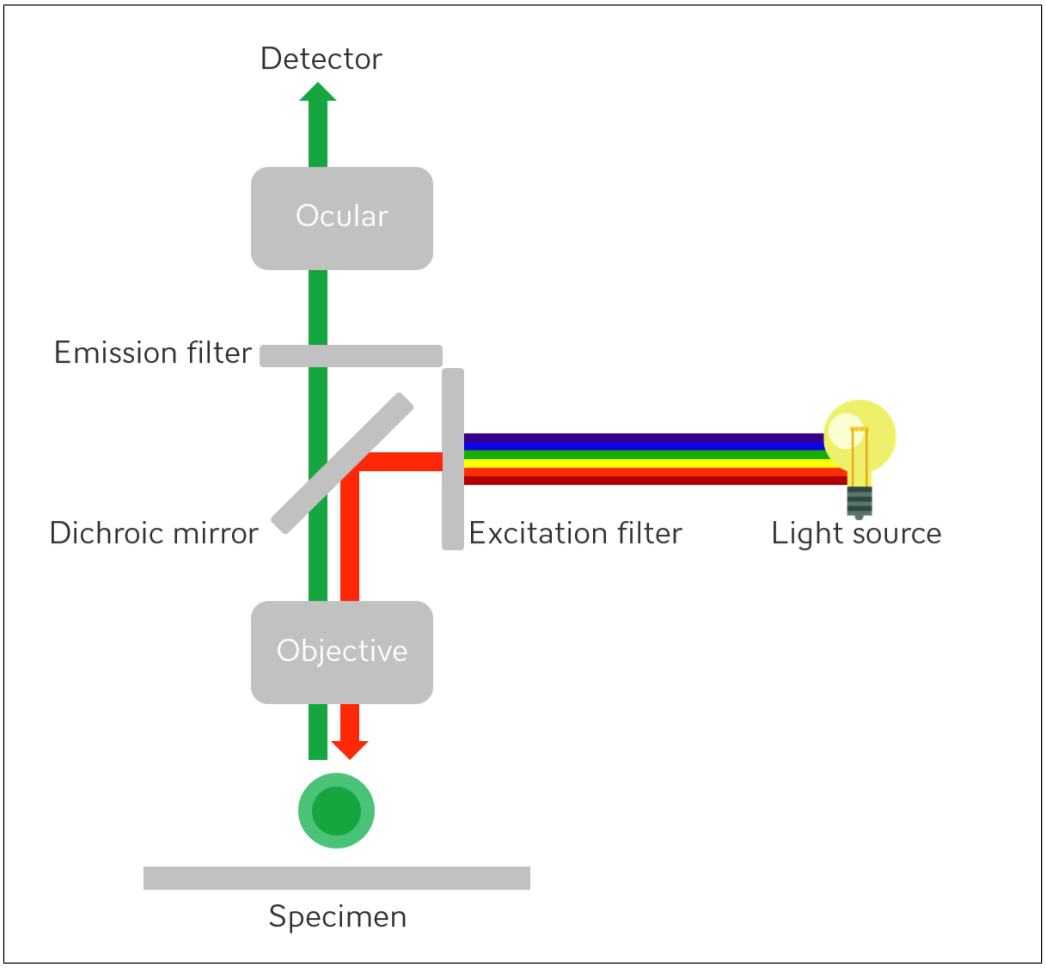

Figure 2.3 *Schematic of a Fluorescence Microscope*

Stokes' Shift

Vibrational energy is lost when electrons relax from an excited state to their ground state. The result of this energy loss is that the emission spectrum of an excited fluorophore is usually shifted to longer wavelengths when compared to the absorption or excitation spectrum. This phenomenon is known as Stokes' Law or Stokes' shift owing to the fact it was Stokes who first noted that fluorescence emission always occurred at a longer wavelength than that of the excitation light. As Stokes' shift values increase, it becomes easier to separate excitation from emission light through the use of fluorescence filter combinations.

The fluorophore emission intensity peak is much lower than the excitation peak, and the emission spectral profile (curve) is often a mirror image (or nearly so) of the excitation curve, but shifted to longer wavelengths. This is illustrated in Figure 2.4 for Fluo-4 and Fura-2, the two probes most often used in this research In order to achieve maximum fluorescence intensity, a fluorophore (often termed a dye) is usually excited at wavelengths near or at the peak of the excitation

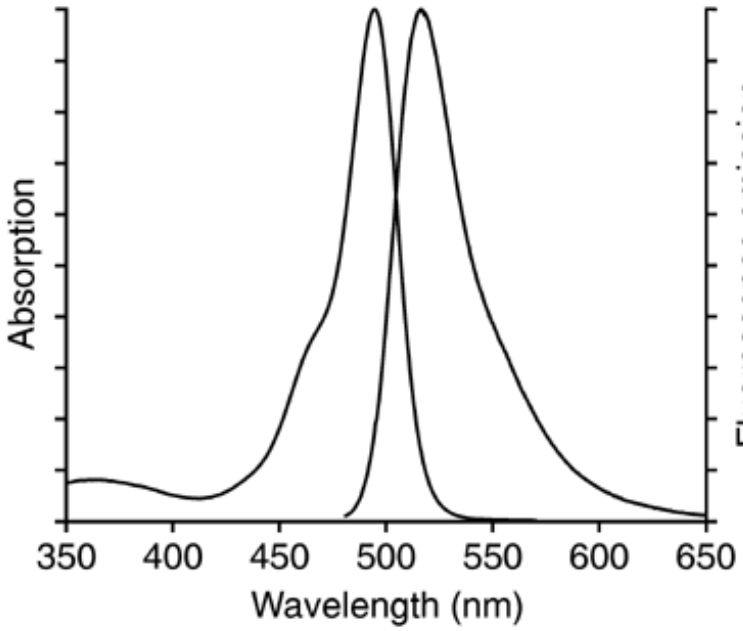

(a) Absorption and fluorescence emission spectra of Ca2+-saturated fluo-4 in pH 7.2 buffer [7].

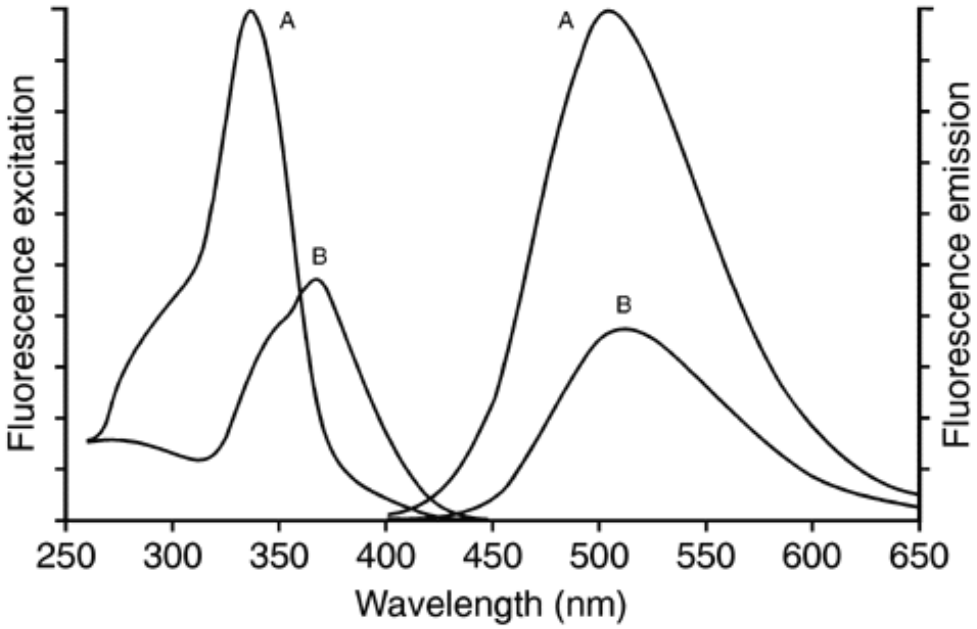

(b) Fluorescence excitation (detected at 510 nm) and emission (excited at 340 nm) spectra of Ca^{2+}-saturated (A) and Ca^{2+}-free (B) fura-2 in pH 7.2 buffer [7]

Figure 2.4 *The excitation and emission spectra of the two dyes most used in this research (a) the non-ratiometric Fluo-4 AM and (b) the ratiometric Fura-2.*

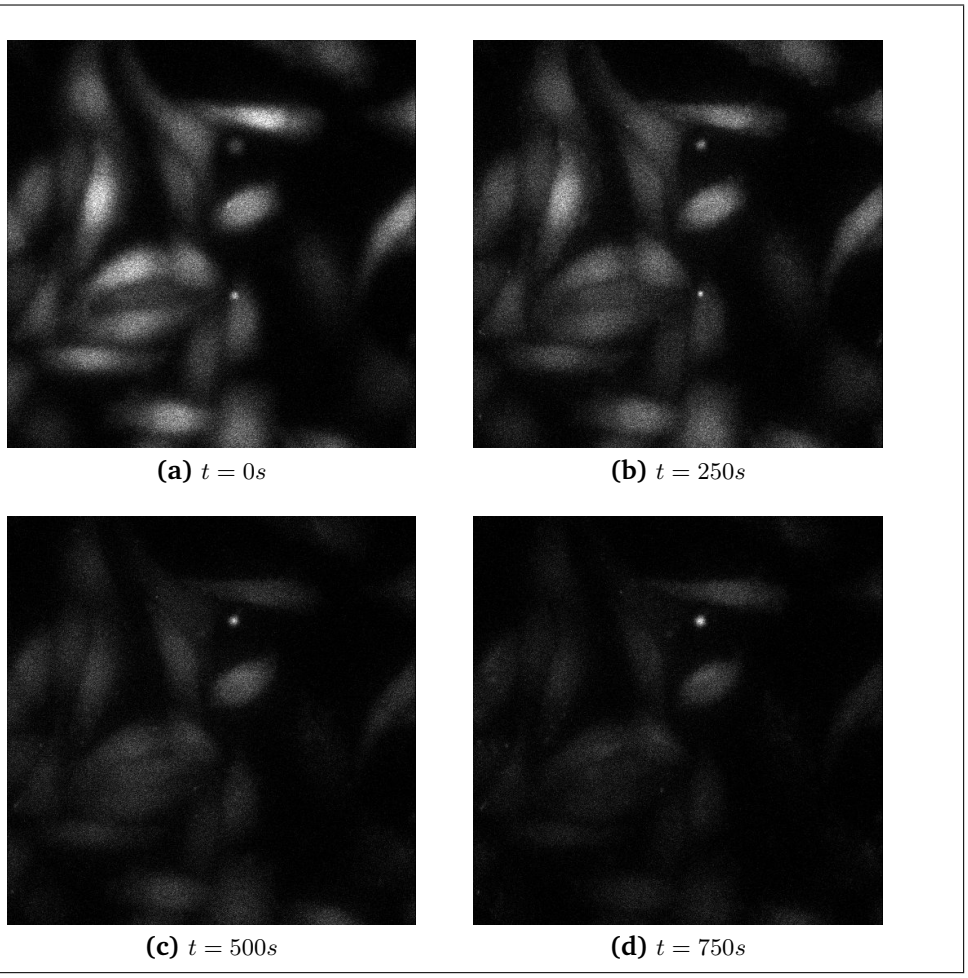

(a) $t = 0s$ **(b)** $t = 250s$

(c) $t = 500s$ **(d)** $t = 750s$

Figure 2.5 *An example of photobleaching in CHO-hOT cells loaded with Fluo-4/AM. Images were taken at 4 frames per second and taken at the times indicated.*

curve. The widest possible range of emission wavelengths that include the emission peak is selected for detection.

Fading, Quenching, and Photobleaching

A wide spectrum of conditions often come into play that ultimately affect the reradiation of fluorescence emission and thus reduce the detectable intensity. The general term for a reduction of fluorescence emission intensity is fading, a catch-all category that is usually further subdivided into quenching and photobleaching phenomena for more precise descriptions. Photobleaching is the irreversible decomposition of the fluorescent molecules in the excited state because of their interaction with molecular oxygen before emission.

Figure 2.5 shows a an example of photobleaching observed in a series of digital images captured at different time points for CHO-hOT cells loaded with Fluo-

4/AM.

Optical Collection Efficiency and Image Detection

In general, only a small number of of photons are available for detection as a consequence of low emission levels. This cannot be improved and thus it is important to maximise the efficiency of detection by improving the optical collection efficiency of the microscope and the detector's quantum efficiency.

The maximum theoretically possible collection efficiency is limited at about 30% by the realisable numerical aperture of the lens. The transmission efficiency of a dichromatic mirror is $\sim 85\%$ and that of the barrier filter is $\sim 80\%$ which further limits the overall collection efficiency to about 20%.

A charge-coupled device is used to receive this signal which has a quantum efficiency of $\sim 50\%$ so the detected signal would be only 10 percent of the emitted fluorescence. Even with a perfect detector, only about 20 percent of the fluorescence emission photons could be detected.

2.2.3 Microscopes

In order to image individual cells in culture, we used both epifluorescence and laser-scanning confocal microscopy in accordance with §2.2.4. The microscopes were equipped with filters, dichroic mirrors objective lenses, to maximise the efficiency of the collection of light from the fluorophore being used. Two microscopes and a micro plate reader were used in the course of this research.

Epifluorescence Microscope Olympus BX51W1

Monochromator Cairn Optoscan-2

Detector Andor Luca S EMCCD 658M-TIL

Perfusion ALA-VM8 controlled by BPS-8 valve control system, Scientifica, UK

Temperature control Heated petri-dish holder and solution warming pencil controlled by TC-20 Thermocontroller, Scientifica, UK

Confocal Microscope Zeiss LSM 510META

Lasers LSM 510 Laser Module, Argon Ion laser

Detector PMT

Perfusion Gilson minipluls 3 perfusion pump

Temperature control "temp control - $37°C$." Zeiss, UK

Microplate reader

The PHERAstar FS is a multidetection microplate reader for HTS and assay development. The compact PHERAstar FS microplate reader can perform all leading non-isotopic detection technologies. The system utilises a modular optical system which appropriate filters, mirrors, beamsplitters, dichroics or polarizers incorporated into one hand-held module. Here we used the HTRF optical module as well as the systems ability to initiate sequential dual excitation, simultaneous dual emission, and ratiometric calculations to perform the Cis-Bio® IP-One HTRF® assay in §4.2.5.

Maintaining physiological conditions

In order to create reliable, replicable results it was necessary to maintain conditions as close to physiological as possible. Therefore, petri dishes in the microscope were warmed to $37°C$ and solutions were perfused with the solution under investigation pre-heated to $37°C$ by a thermostatically controlled warming pencil.

2.2.4 Visualising Ca^{2+}

- Fluorescent Ca^{2+}-indicators are molecules whose optical properties (the excitation spectrum, emission spectrum or both spectra) change when they bind Ca^{2+}
- Several strategies are commonly used to introduce indicators into cells
- Indicators can be classified as ratiometric or non-ratiometric, depending on whether Ca^{2+} changes only the magnitude of their absorption or emission, or whether their spectra shift horizontally along the wavelength axis

Loading Ca^{2+}-Indicators

The plasma membrane acts as the principle barrier to the loading of Ca^{2+}-indicators into the cytosol. This is since Ca^{2+}-indicators are hydrophilically charged (often with $-COO^{-}$ groups) in their Ca^{2+} sensitive states which means they cannot easily cross the lipid membranes. To avoid permeabalising the cells, and thus losing the intracellular milieu, several methods have been developed to

allow the incorporation of Ca^{2+}-indicators into the cytoplasm whilst maintaining cell integrity. The most common solution is to load cells loaded with dyes that have undergone esterification of the charged groups to attempt to 'mask' their negative charge(s). These esterified-indicators have to be diluted in DMSO since they are highly lipophilic. Often, a detergent such as Pluronic acid is added to the stock solution to reduce lipophobicity and thus aid the loading.

Loading ester into cells is highly convenient but there are several potential disadvantages which must be considered:

- One must be careful to avoid overloading the cells with indicator and thus increasing the intracellular buffering and damping the Ca^{2+} signals one is trying to observe
- Ester loading also suffers from compartmenalisation of the indicator into organelles such as the mitochondria or endoplasmic reticulum which can complicate any calibrations performed
- Many cells have an ability to rapidly clear indicator molecules from their cytoplasm
- Incomplete ester hydrolysis: The presence of the ester groups prevents the indicator from chelating Ca^{2+} and makes it Ca^{2+}-insensitive A Ca^{2+}-insensitive, but still fluorescent indicator will contribute to the overall signal resulting in an underestimate of the Ca^{2+} concentration. Incomplete ester hydrolysis occurs in cells with low esterase activity but can often be overcome by extending the deesterification period

Minimal indicator loadings for acceptable signal-noise ratio are preferable to reduce the effect on cellular buffering. Performing ester loading at 21^oC, before adjusting the cells back to the desired experiment temperature, can usually reduce the compartmentalisation and clearance of the indicator from the cells. The use of sulfinpyrazone (100 μM), probenicid $(1\ mM)$ or leakage-resistant indicators (e.g. fura-2/PE; TefLabs) can prevent indicator loss from most cells. The most appropriate incubation times and concentrations may vary between indicators and cell types and was worked through empirically here.

Taking into account the above, Ca^{2+} was successfully visualised in CHO-hOT cells when loaded with the appropriate Ca^{2+}-indicator in accordance with Protocol 4 from a stock solution of indicator which was made using Protocol 2. Cells were either loaded using modified Krebs HEPES (described in Protocol 3) as the extracellular dilute unless cells were to be loaded at 37^oC in a 5%-CO_2/95% humidified air environment, in which case serum-free *F-12* media is used.

Fluorescent Ca^{2+}-Indicators

As discussed in §2.2.4, choosing a suitable Ca^{2+}-indicator is vital for visualising the desired process. The majority of the data in this thesis was collected using two well-established Ca^{2+}-indicators, the non-ratiometric Fluo-4 AM and the radiometric Fura-2.

Fluo-4 AM

Fluo-4 AM is based on the fluo-4 core chemistry and is an improved analog of fluo-3 AM with the two chlorine substituents replaced by fluorines. This minor structural modification results in a dye that loads faster and is brighter at equivalent concentrations, making it the preferred indicator for a variety of applications. It was used here because of its brightness and its proven pharmacology as the most rigorously tested, highly cited and used dye in the industry [3].

Fura-2

Whilst fluo-4 AM gives excellent signal-to-noise, it was important to also validate our results using a radiometric indicator. Measuring by ratio considerably reduces the effects of uneven loading or leakage of the dye as well as the impact upon traces of photobleaching and problems measuring Ca^{2+} in cells of non-uniform thickness. Measurements of fura-2 fluorescence can usually be made over a period of an hour without significant loss of fluorescence resulting from either leakage or bleaching. In addition, fura-2 is bright enough to permit measurements at intracellular concentrations of dye unlikely to cause significant Ca^{2+} buffering or damping of Ca^{2+} transients. In particular, at low concentrations of the indicator, 340/380 nm excitation ratio for fura-2 allows accurate measurements of the intracellular Ca^{2+} concentration (Figure 2.6).

This is because ratiometric readouts are known to minimise the effects of photobleaching, leakage, uneven loading, and varying cell thicknesses in mixed populations, delivering more robust and reproducible results. We chose Fura-2 because, again, it is widely cited in a variety of cell lines, including CHO-K1 [4].

Why use both Fura-2 and Fluo-4?

It was always the intention of this work to use both a radiometric and non-ratiometric indicator to validate any results seen and to eliminate any that may

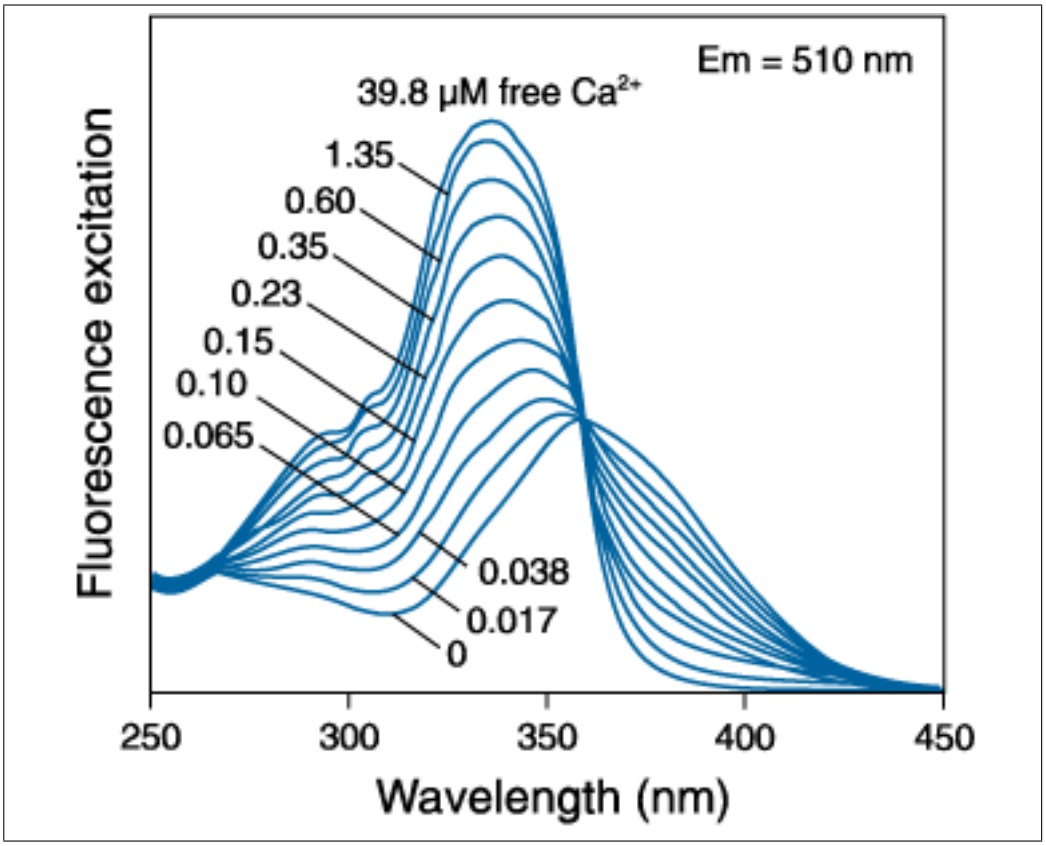

Figure 2.6 *Fluorescence excitation spectra of fura-2 in solutions containing* $0 - 39.8\ \mu M$ *free* Ca^{2+} *[4].*

have been either an artefact of the dye or type of dye used or include any results missed because of the nature of the dye used. As this work progressed, this proved particularly pertinent as strong evidence (in press but not presented here) came to light that Fluo-4 has a light-sensitive excitation process. Therefore, all experiments presented here have been conducted with at least two dishes using Fluo-4 and Fura-2 to establish the discrepancies. Because light intensities were reduced accordingly to reduce the impact of the observed light-sensitivity which resulted in the same qualitative results occurring for all experiments presented here with both Fura-2 and Fluo-4 the distinction between traces is not commented pin further in the rest of this document.

2.2.5 Computer modelling and calculation

MATLAB®

MATLAB®is a high-level language and interactive environment for numerical computation, visualisation, and programming produced by The MathWorks, Inc. (http://www.mathworks.com). MATLAB 2013a was used for data extraction and

modelling computations as well as some statistical analysis.

XPPAUT and AUTO

The XPPAUT package was developed by Bard Ermentrout at the University of Pittsburgh [50] and is freely available free at http://www.math.pitt.edu/ bard/xpp/. It is a mixed GUI-based interactive package for numerically solving and analysing differential equations written in its own $.ode$ language. It also provides a simple GUI to most of the common features of the numerical bifurcation software AUTO (ftp://ftp.cs.concordia.ca/pub/doedel/auto), originally developed by E J Doedel [42].

GraphPad Prism

GraphPad Prism combines scientific graphing, comprehensive curve fitting (non-linear regression), statistics, and data organisation. It is used for some statistical analysis and plotting of data.

2.3 Protocols

Protocol 1 Cell culture of CHO-hOT1 cells

Method

1. $CHO-hOTR$ cells are cultured in $75\ cm^2$ flasks in $F-12$ media containing $50\ ml\ FCS$ and $5\ ml\ Penicillin/streptomycin$ (100IU). All environments should remain sterile and good aseptic technique is necessary.
2. Cells are passaged every $2-3$ days or until 80% confluence is reached. Cells are passaged by rinsing with $10\ ml\ PBS$ and addition of $4\ ml$ TrypLE (3ml 1x concentration) incubated at 37^oC for $2-3$ mins and gentle agitation.
3. Cell suspensions are collected in $30ml$ universals and pelleted by centrifugation ($800\ rpm$, $4\ mins$, RT) and the supernatant discarded.
4. Pellets are re-suspended in supplemented $F-12$ media and counted using a *neuberger haemocytometer*. Cells are counted in $4 \times 1\ mm^2$ regions $(100\ nl)$ and an average taken. The number of cells per ml is calculated as this figure $\times 10,000$. Cells are adjusted to a density of $2.5 \times 10^6\ cells/ml$.
5. A repeating pipette tips is sterilised by dousing in ethanol and thoroughly rinsing in sterile PBS.
6. $20\ \mu l$ of cell suspension at a density of $2.5 \times 10^6\ cells/ml$ is dispensed into appropriate wells on the $384-$well plates. This volume will give a seeding density of $50,000\ cells/well$.
7. Plates are cultured overnight (37^oC, $5\% - CO_2/95\%$ humidified air environment) to allow cells to adhere before assay the next day.

Protocol 2 Making a stock solution of esterified Ca^{2+}-indicator

Equipment and reagents

- Vortex
- Pluronic F-127 (SIGMA)
- Anhydrous DMSO (SIGMA)
- Solid indicator

Method

1. Disolve 20% (w/w) Pluronic F-127 in an appropriate volume of dry DMSO
2. Vortex this until the Pluronic is dissolved while simultaneously gently warming the solution. The temperature should not exceed 40^oC. This takes some time.
3. Add an appropriate volument of the DMSO/Pluronic mixture to the indicator solid to make a stock solution. Likely of $1\ mM$.
4. Ensure the entire indicator has been dissolved in the DMSO/Pluronic mixture by agitating the solution on the vortex.

Protocol 3 Physiological State Solution (PSS)

Equipment and reagents

- 136 $mM\ NaCl$ (SIGMA)
- 5 $mM\ KCl$ (SIGMA)
- 2 $mM\ CaCl_2$ (SIGMA)
- 0.25 $mM\ MgCl_2$ (SIGMA)
- 10 $mM\ Glucose$ (SIGMA)
- 5 $mM\ HEPES\ Na^+$-salt (SIGMA)
- Autoclaved H_2O (SIGMA)
- 32% HCl (for pH adjustment) (SIGMA)

Method

1. Determine the required mass of solute for the quantity of Krebs to be made.
2. Pour over the H_2O into a beaker on a warming mixing plate.
3. Once mixed, bring to $37°C$ and use HCl to bring to pH 7.4.

Protocol 4 Loading of cells with the ester form of Ca^{2+}-indicators

Equipment and reagents

- Vortex
- Petri dish
- Extracellular solution (Molecular Probes)
- Cells
- Protocol 1

Method

1. Make up a $2\mu M$ solution of the indicator by adding $4\mu L$ of the $1\ mM$ stock solutions (see Protocol 1) to $2\ ml$ of an appropriate extracellular solution. Make sure the indicator stock is completely dissolved by vortexing.
2. Was cells thrice to remove serum prior to loading. This is since the constituents of serum can bind to indicators and reduce their free concentration.
3. Put the $2\ ml$ of indicator solution and incubate for 30 minutes, preferably at room temperature and in a dark place.
4. Remove the indicator solution, but keep for additional loadings (can usually be reused 3-5 times, depending on the actual cell density). Replace with indicator-free extracellular solution and incubate the cells for an additional $20 - 30\ mins$ at room temperature in the dark to allow complete de-esterification of the indicator.

Protocol 5 Determining the location of cells using ImageJ

Equipment and reagents

- Cells imported into ImageJ

Method

1. Take an average of all images in the stack
2. Threshold this image by eye to capture the majority of the cells in a recording
3. Segment any multi-cell areas by hand
4. Add all cells to ROI Manager
5. If ratiometric recording, extract data using Ratio ROI Manager
6. If non-ratiometric recording, extract data using MultiMeasure

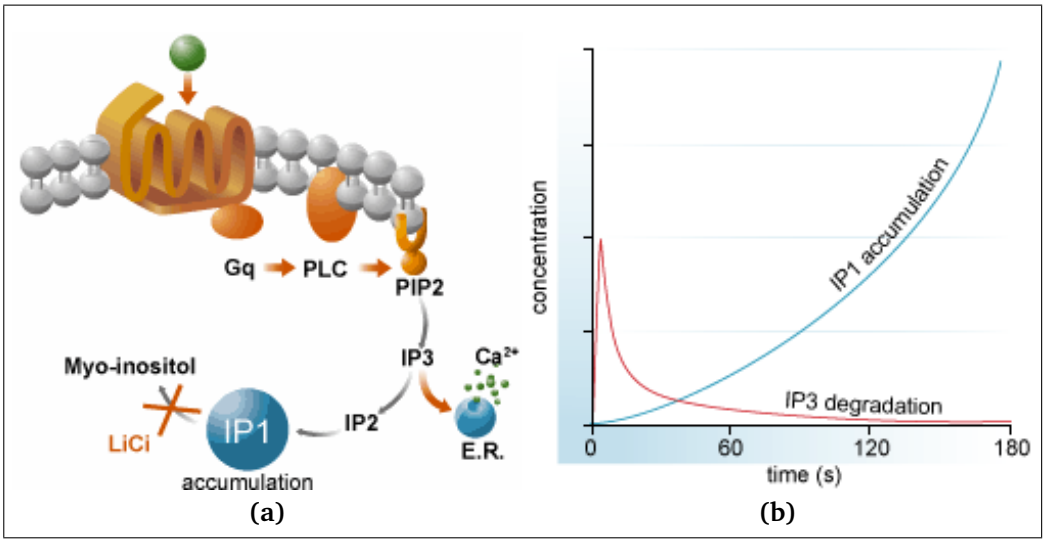

Figure 2.7 *(a) The G_q stimulation pathway to produce IP_3 via PLC and PIP_2 demonstrating how IP_3 triggers release from the ER and how $LiCl^+$ prevents IP_1 from being recycled into myo-inositol. (b) the fast time-scale of $InsP_3$ degradation and the resulting IP_1 accumulation [6].*

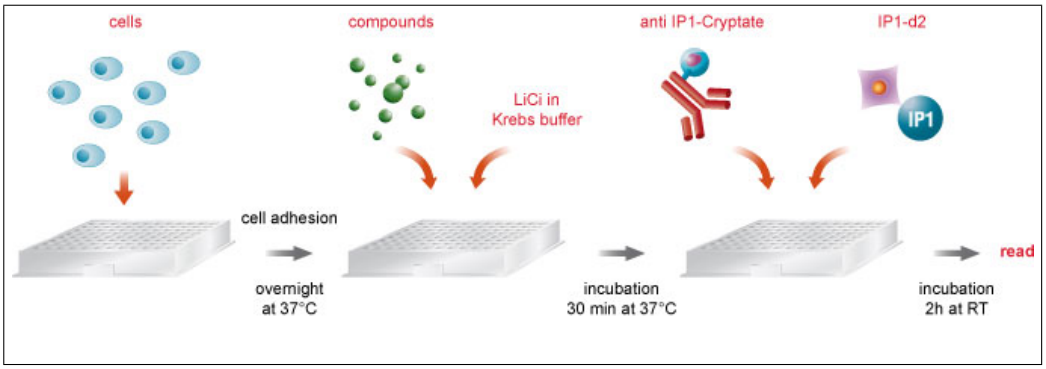

Figure 2.8 *Schematic detailing how the competitive HTRF assay works. The IP-One assays are competitive immunoassays that use terbium cryptate-labeled anti-IP1 MAb and d2-labeled IP1. LiCl is added to the cell stimulation buffer, causing the accumulation of IP1 upon receptor activation. The assay can be run in a single microplate and requires just a single 1 hour incubation following cell stimulation.*

Protocol 6 Extracting the data using MATLAB

Equipment and reagents

- Cell traces extracted from Image J using Protocol 5

Method The below is a pseudo-code description of the protocol used to extract the statistics from the cell.

1. Import the data from ImageJ
2. Scale the time-scale depending on the frames per second the recording was taken
3. Detect minima and maxima. A method of peak detection using a thresholding algorithm was developed for this purpose.
4. Correct for photobleaching. Several methods were tried here. It was empirically established that fitting a line ($y = k \in \mathbb{R}$) through the found minima of radiometric dyes and performing an exponential fit in the case of non-ratiometric dyes resulted in good removal of the effects of photobleaching.
5. Detect minima and maxima for a second time (in case some were undetectable due to photobleacing before correction)
6. Calculate the statistics A_{in}, A_{osc}, t_{in}, t_{osc}, $t_{in}^{1/2}$ and $t_{osc}^{1/2}$ for each (pair) of oscillations.
7. Calculate averages for oscillations statistics
8. Export the statistics for that Ca^{2+} trace

Protocol 7 Inositol-1-phosphate Homogeneous Time Resolved Fluorescence assay

Equipment and reagents This Cis-Bio assay is based on a monoclonal antibody specific for IP_1, labeled with Lumi4-Tb cryptate, a new HTRF technology. This antibody competes with native IP_1 produced by cells and IP_1 coupled to the dye d2 (§2.8).

The specific signal is inversely proportional to the concentration of IP_1 in the the cell lysate. Data reduction using the fluorescence ratio ($665\ nm/620\ nm$) eliminates possible photophysical interference and means the assay is unaffected by buffer conditions and coloured compounds.

Method

1. Stimulation buffer is provided with the assay kits at $5\times$ concentration. This is diluted 1 part $5\times$ stimulation buffer + 4 parts $Milli-Q$ grade H_20).
2. All agonists, vehicle controls and antagonists are diluted in 1x stimulation buffer and laid out in a duplicate assay plate at $2\times$ final concentrations.
   (a) **NB** If for a competitive antagonist assay different concentrations of agonist and antagonist are required, make these up as $4\times$ final concentrations and add equal volumes of each to the agonist plate.
3. 2.3 Aspirate (*do not* bang) cell culture media from each well of the assay plate and wash with $20\ \mu l$ stimulation buffer. Aspirate this wash buffer away and replace with $7\ \mu l$ stimulation buffer.
   (a) **NB** Wash the cells in regions/blocks so as not to allow cells to dry out between washes.
4. Allow both the assay plate and duplicate agonist plate to warm to 37^oC in an incubator (with the lids on to minimise evaporation)
5. The assay is initiated by transfer of $7\ \mu l$ from the agonist plate to the corresponding well on the assay plate. Allow the assay to proceed for the desired time-frame (for time-course analysis, this is performed at the desired time point, for dose-response analysis this is $1\ hr$) at 37^oC.
6. Make up both the $IP1-d2$ and $Ab-Crpt$ reagents by adding $0.5\ ml\ H_20$ to the vial and then $2.5\ ml$ of lysis buffer.
7. Make up the assay control by adding $0.5\ ml$ stimulation buffer.
8. Make up the $IP-1$ standards as per Calibrations Curve.
9. Add $14\ \mu l$ of $IP-1$ standards, negative controls (stimulation buffer) and buffer blanks ($IP-1$ standard 0 from Calibrations Curve) to desired well before assay termination.
10. The assay is terminated by the addition of $3\mu l\ IP1-d2$ to each well using a repeating pipettes. (do not add to negative control well - add $3\ \mu l$ lysis buffer instead)
11. Immediately add $3\ \mu l$ of $Ab-Crpt$ to all wells
12. To ensure through mixing of reagents briefly spin the plates (approx. $300\ rpm$ for $5-10$ seconds) to ensure all reagents are at the bottom of the well and shake the plate using the shake function on a plate reader.
13. Leave the plate in the dark for at least $1\ hr$ and no more than $24\ hrs$ before reading.for an additional 20-30 mins at room temperature in the dark to allow complete de-esterification of the indicator.

2.4 Data Analysis

2.4.1 ImageJ Ca^{2+} Trace Extraction

The most common form of data requiring extraction from Ca^{2+}-imaging were epifluorescence and confocal microscopy recordings of an area in a petri dish. The computer captured a series of time-stamped greyscale images which can be played as a Ca^{2+}-imaging video. In general, the higher the pixel value recorded by the detector, the more light the Ca^{2+}-indicator was emitting and, hence, the higher concentration of Ca^{2+} that was present.

This, of course, was a qualitative measure and so we used the java-based image processing and analysis tool, ImageJ [5] to extract quantitative data from these Ca^{2+}-imaging videos. The first step was to extract the exact location of the cells within a recording. This was done through a combination of automation and human inputs detailed in Protocol 5 and the steps in this process are demonstrated in Figure 2.9.

Once the cells were identified, then they were selected as regions of interest and the average pixel value of each region of interest for each frame in the video was taken and this formed the data for a Ca^{2+}-trace for a given cell within that recording.

2.4.2 MATLAB Data Extraction/Processing

Once the traces were extracted from each cell within the Ca^{2+}-imaging videos, some parameters of Ca^{2+} transients were calculated. Figure 2.10 depicts an idealised trace which demonstrates the pieces of data that were extracted. They were:

- The area underneath the initial transient and between the resting Ca^{2+} fluorescence – A_{in}
- The time taken between the peak of the initial transient and the peak of the second transient – t_{in}
- The average time taken between the peaks of established oscillations (excluding the first transient) – t_{osc}
- The average area underneath established oscillations and between the resting Ca^{2+} fluorescence (excluding the first transient) – A_{osc}
- The full-width half-magnitude of the initial transient – $t_{in}^{1/2}$

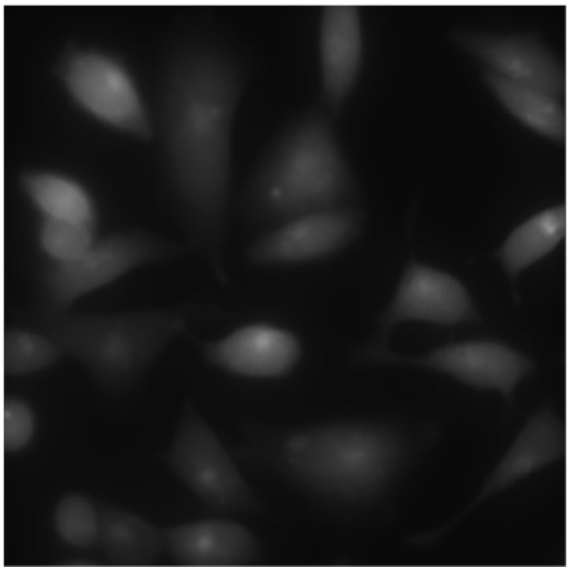

(a)

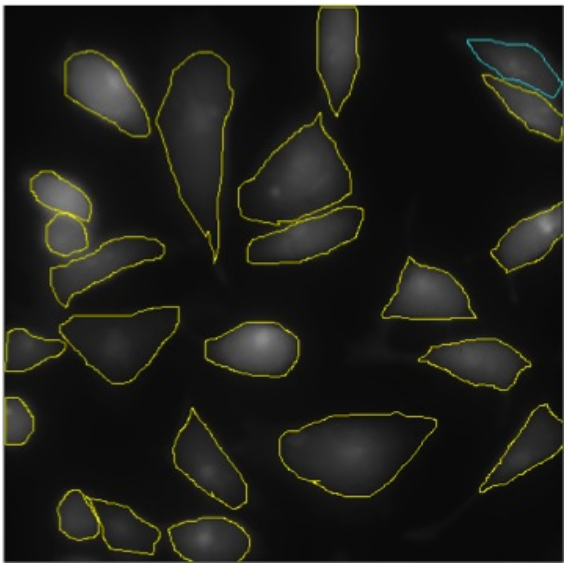

(b)

Figure 2.9 *The process of cell segmentation and average intensity extraction: (a) An maximal intensity of pixel z-projection image is first generated and then (b) the cells outlines are delineated and the average pixel value per frame for each region-of-interest are extracted.*

- The full-width half-magnitude of the average of the peaks of the established oscillations (excluding the first transient) – $t_{osc}^{1/2}$

These parameters were chosen because they have been shown to yield important insights into different aspects of Ca^{2+} signalling in many other papers in the field [22, 129]. The first step in order to extract A_{in}, A_{osc}, t_{in}, t_{osc}, $t_{in}^{1/2}$ and $t_{osc}^{1/2}$ from the Ca^{2+} traces was to identify the minima and maxima.

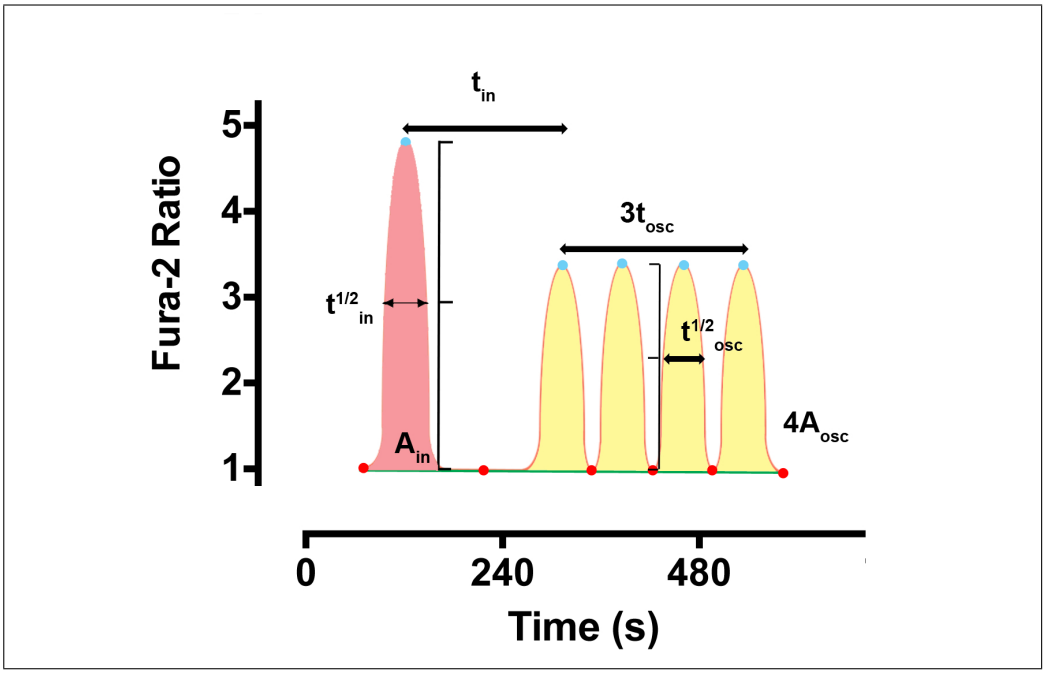

Figure 2.10 *An idealised Ca^{2+} trace demonstrating the pieces of data - A_{in}, A_{osc}, t_{in} and t_{osc} - that are extracted using Protocol 6. A_{osc} and t_{osc} are determined by taking an average of the area underneath, and time between peaks of the established oscillations respectively.*

Determining the minima and maxima proved a non-trivial problem. Due to the always-present noise in real-life signals, any zero-derivative method falls foul of detecting multiple peaks where there are none. Therefore, Protocol 6 used the logic that a peak (or a trough) is surrounded by points that are lower (higher) than it. It found the highest point around which there were points lower by a value, δ, on both sides. In our work δ was set to be one tenth of the maximum amplitude of the Ca^{2+} signal which, in almost all cases resulted in almost all peaks being detected with only the occasional detection of a non-peak. Cases which had incorrectly identified peaks were excluded from the analysis.

Once the peaks had been detected, the statistics were found using the data for the maxima and minima of the system. The same protocol used the trapezium rule to approximate the area under curve and above the resting Ca^{2+} fluorescence.

Once the data were extracted, MATLAB was used to collate and analyse the data and to perform any statistical analysis on it. These statistics were then plotted using GraphPad Prism.

2.4.3 Baseline Artefact and Statistical Significance

Throughout, data are presented as an exemplar trace, post-processing with summary data for each of the statistics investigated. Before analysing the data, All

the traces were normalised to one using the identified minimas to make the data comparable and independent of loading variabilities.

Because the data is noisy, using the current method of minima detection, the lowest point is an undershoot of the actual minima. This results in the fitted straight line through those points having non-zero gradient. Several methods were trialled to avoid introducing analysis-bias, but these often behaved erratically and so the traces here are calculated assuming the line through the minimas should have zero gradient. This sometimes results in an apparent incline of decline in the baseline of the normalised traces. Here, normalised exemplar traces are presented since these were used for data extraction. However, when drawing conclusions, the original traces were compared to ensure this was indeed an artefact of the data extraction. In all cases, except the loading of ER Tracker which is known to photo bleach rapidly and occasional cells within a viewing, any fluctuation in baseline was not consistent throughout cells in a dish.

Furthermore, because of the high n-numbers considered here, statistical significance is easily obtained with potentially little biological motivation. The often hundreds of samples used lead to only a small change in the mean being necessary to suggest they are significantly different from all other conditions considered. Therefore, in order to not clutter the diagrams and reduce their clarity, a dot $(\cdot)$ has been places above any conditions whose mean is not statistically different from all of the other means in the graph under a 99% t-test.

Part B

Results

Chapter 3

General Characteristics of Responses to Oxytocin in *CHO–hOT* Cells

3.1 Introduction

Much is known about the G_q pathway described in §1.1. However, what is not established for certain is the relationship between Ca^{2+} oscillations and the level and nature of $InsP_3$ dynamics. Ca^{2+} oscillations have been reported to

- occur in constant $InsP_3$
- require $InsP_3$-oscillations
- induce $InsP_3$-oscillations

Before investigating the specific behaviours of the *CHO–hOT* cell line, it is first sensible to investigate the system's responsiveness to the agonist of interest, *OT*. Caroppo [29] demonstrates that there is little concentration dependence upon the *OT*-induced Ca^{2+} oscillations seen when *OT* is applied to BHK-21 cells. Upon application of *OT* to cells loaded with Ca^{2+}-indicator, an initial transient response is seen which is followed by oscillations. A typical response for a Fura-2 loaded *CHO–hOT* cell is shown in Figure 3.1 (a) with an explication of how the data analysis protocol from §2.4 was applied in (b).

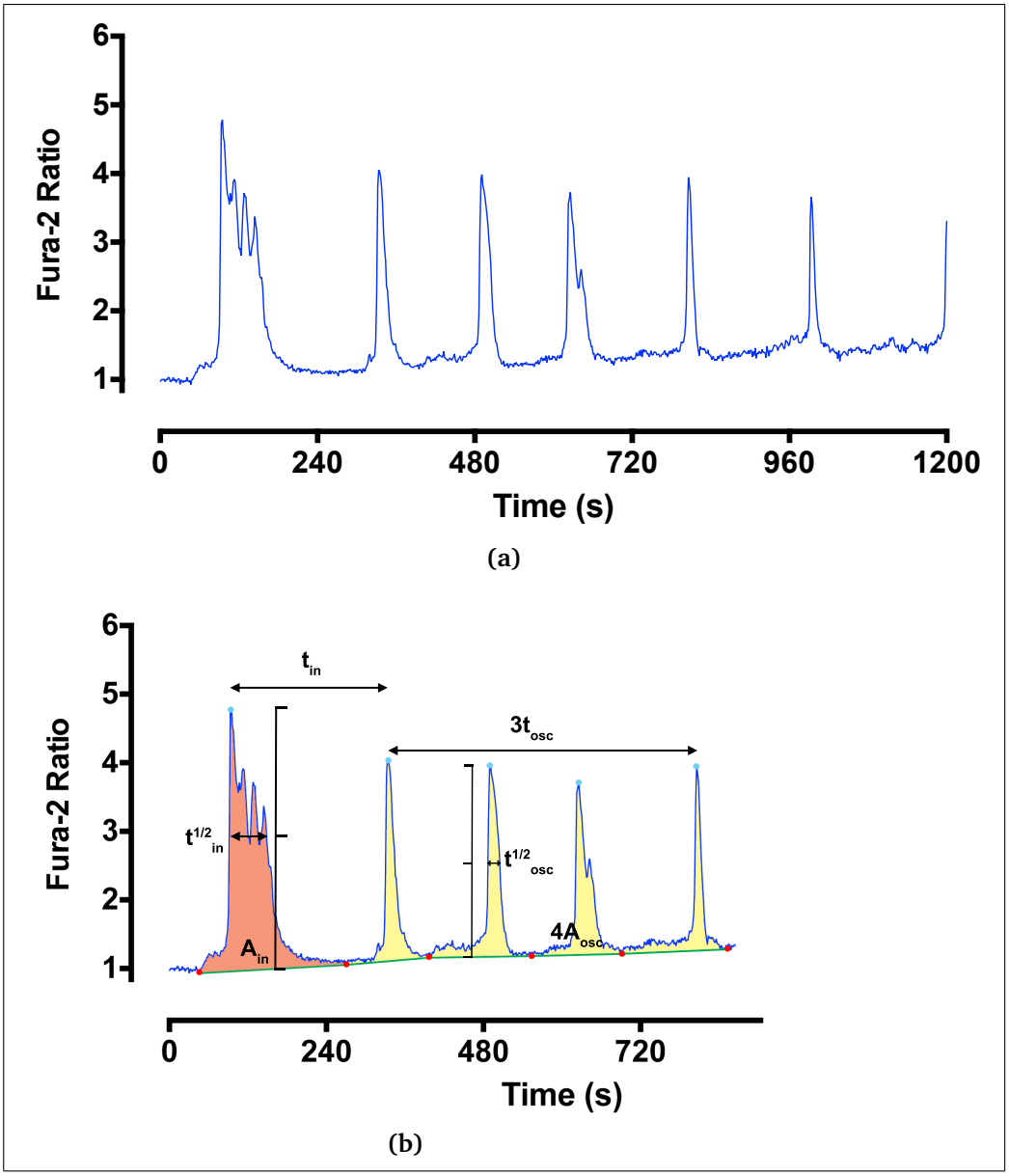

Figure 3.1 *A representative Ca^{2+} trace recording from a Fura-2 loaded* CHO–hOT *cell stimulated at $t = 100\ s$ with 1nM* OT *shown (a) as extracted and (b) with the calculations for the data shown in an idealised trace in Figure 2.10.*

3.2 Results

3.2.1 Lack of Concentration Effect Response of CHO-hOT to Oxytocin

Figure 3.1 (a) and Figure 3.2 show typical traces for each of the four concentrations of *OT* (1, 10, 25 and 75 nM) which were applied to induce oscillations. Their behaviour agrees with the summarative data extracted from three petri dishes under these conditions shown in Figure 3.3. Figure 3.3 shows that

- as *[OT]* increases, both (a) the initial time and (c) the initial area increase
- this pattern does not follow through to (b) the period nor (d) the area of oscillations
- the initial full-width half-magnitude of the *[OT]* $= 75\ nM$ oscillations is significanly larger than the lower concentrations which appear to be similar to one another.
- again, the oscillation full-width half-magnitude does not replicate this pattern

It is also noteworthy that the number of cells responding to *OT* increases in a concentration-dependent manner as per Figure 3.4.

3.2.2 Absence to Extracellular Calcium ($[Ca^{2+}]_{EC} = 0$)

The initial experiments above were conducted with a $[Ca^{2+}]_{EC}$ of $2\ mM$. These were repeated with $[Ca^{2+}]_{EC}$ equal to $0\ mM$ by omitting Ca^{2+} from the PSS and adding $100\ \mu M$ EGTA to eliminate any Ca^{2+} contamination due to impurities of other salts in PSS.

The resulting response was different from the original experiments as can be seen in the typical trace in Figure 3.5. Upon application of *OT*, an initial transient is seen but not the ensuing oscillations seen in the presence of extracellular calcium (for example Figure 3.2). Thereafter, the Ca^{2+} level remains at its basal level even in the presence of *OT*.

3.3 Discussion

The intuitive understanding of signalling presented in §1.1 might lead to an expectation that application of increased *[OT]* might lead to, for instance, an in-

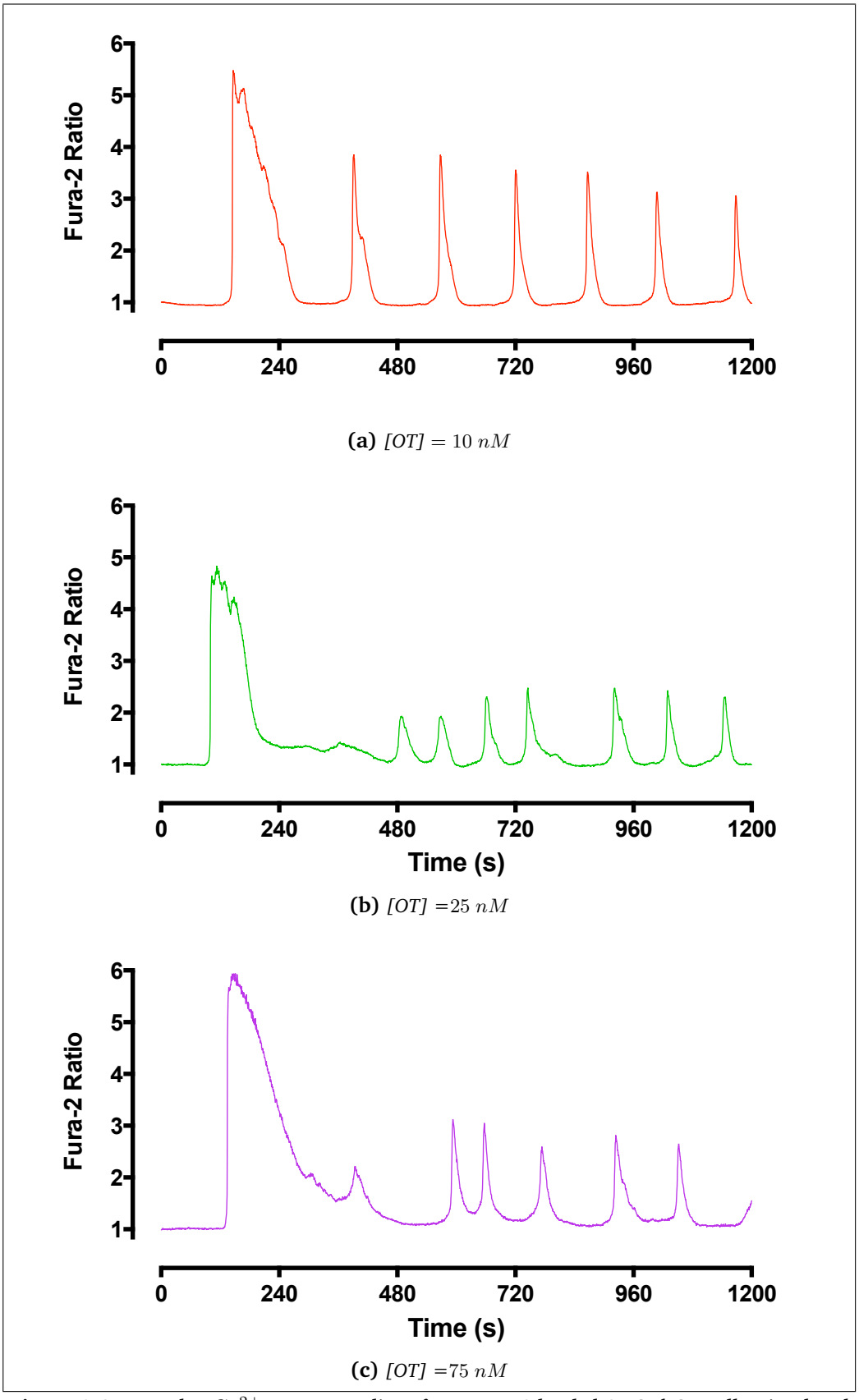

(a) *[OT]* $= 10\ nM$

(b) *[OT]* $=25\ nM$

(c) *[OT]* $=75\ nM$

Figure 3.2 *Exemplar* Ca^{2+} *trace recordings from Fura-2 loaded* CHO–hOT *cells stimulated at* $t = 100\ s$ *with different concentrations of* OT*, shown.*

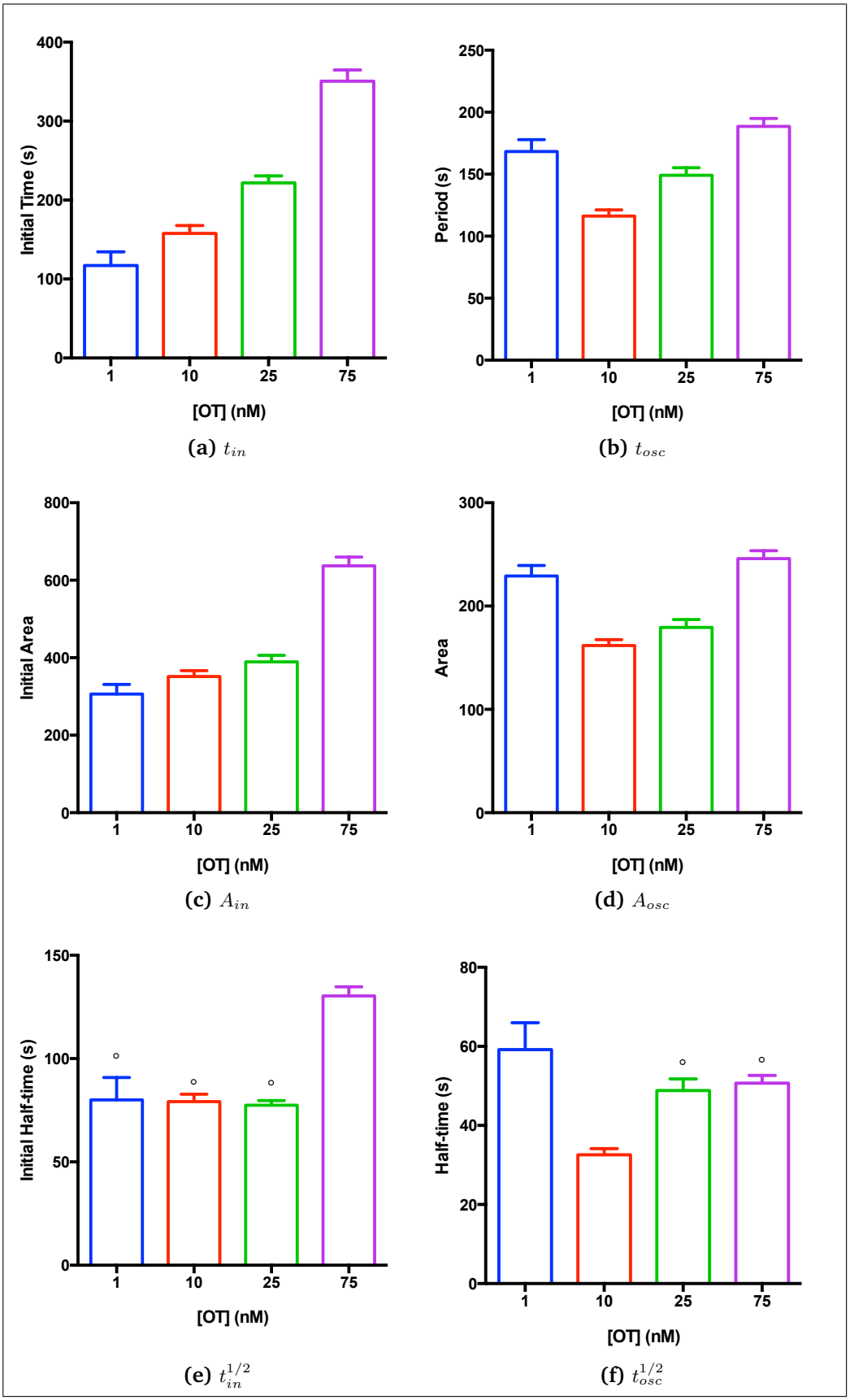

(a) t_{in} (b) t_{osc}

(c) A_{in} (d) A_{osc}

(e) $t_{in}^{1/2}$ (f) $t_{osc}^{1/2}$

Figure 3.3 *Summary data of* Ca^{2+} *trace recordings from at least 3 Fura-2 loaded* CHO–hOT *cells per-concentration of* OT *applied at* $t = 100\ s$ *with 1nM Oxytocin. Data points were taken from all oscillatory cells within at least 3 different petri dishes with cell numbers of* $69, 81, 92$ *and* 92 *for each concentration* $1, 10, 25$ *and* $75\,nM$*, respectively.*

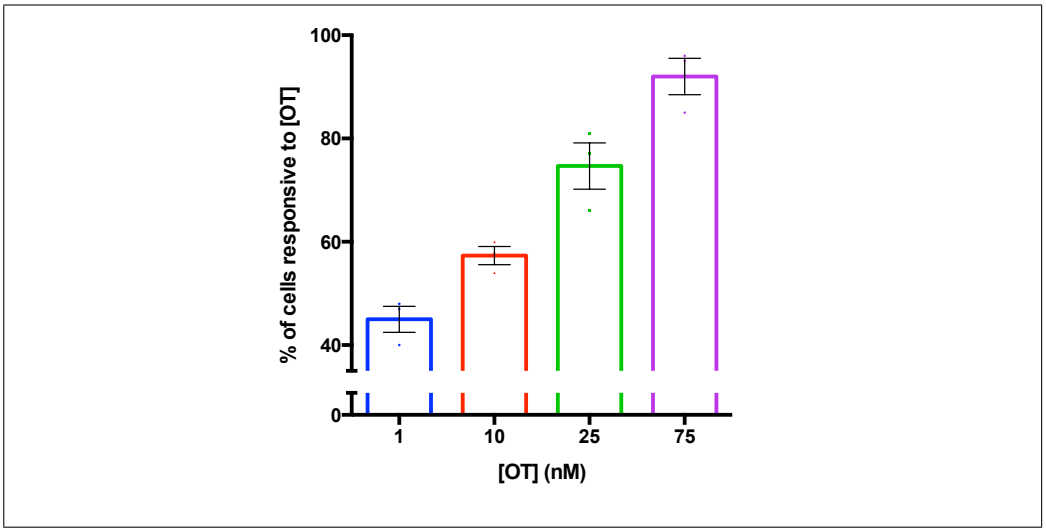

Figure 3.4 *Figure showing the proportion of cells that were responsive to* OT *stimulation at a fixed concentration within a viewing field.*

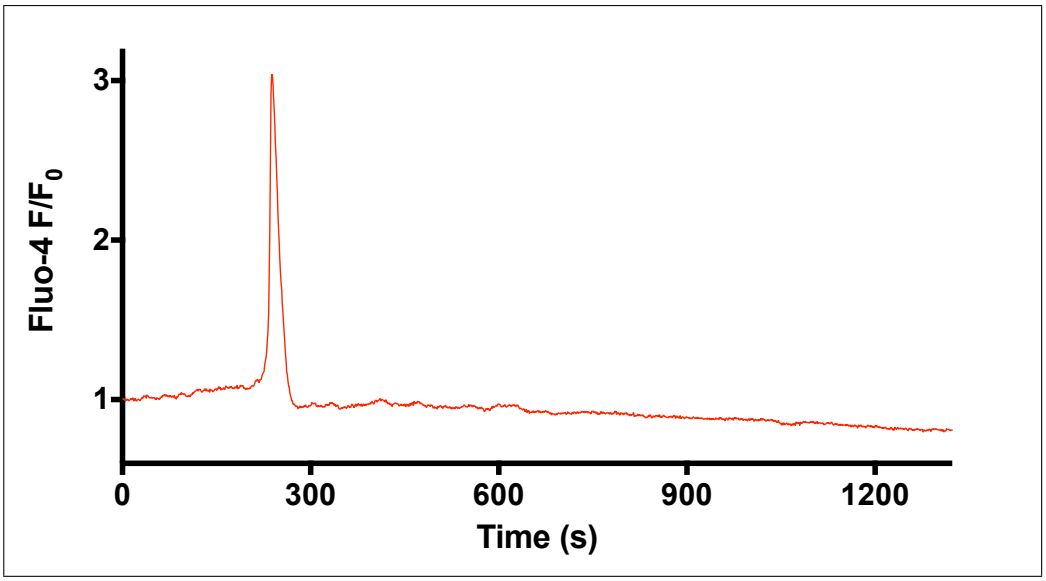

Figure 3.5 *Exemplar data* Ca^{2+} *trace recordings from a Fura-2 loaded* CHO–hOT *cell stimulated at* $t = 100\ s$ *with* $1\ nM$ OT *in the absence of* Ca^{2+}_{EC}*, shown.*

creased frequency in oscillations. That is, that an increased concentration of agonist might result in increased activity of the G_q cascade (as described in Figure 1.7). Such an increase in the production of $InsP_3$ would cause the open probability of the $InsP_3R$ to increase, potentiating release of Ca^{2+} from the ER. Since it is the release from these stores which causes Ca^{2+} oscillations in the cytosol, this potentiation may lead to an expectation that the frequency of oscillations would increase. The same rationale could be used to expect a concomitant increase in the area of those oscillations.

However in contrast to steady-state oscillations, it appears that this intuition is wrong. As far as the established *OT*-induced Ca^{2+} oscillations are concerned, the results above for *CHO–hOT* cells agree with the experiments conducted in BHK-21 cells by [29]. Varying the concentration of *OT* applied has no discernible concentration-dependent effect on the three data points used to assess ensuing oscillations, their period, area and full-width half-magnitude. One possible explanation is that *CHO–hOT* cells have a mechanism to control the dynamics of the ensuing *OT*-induced Ca^{2+} oscillations regardless of the concentration of agonist applied. This might be a useful, or indeed vital, mechanism if, for instance, the extracellular milieu were not well mixed. If oscillations were left unregulated in the case of a muscle fibre, for instance, this might lead to desynchronised *OT*-induced Ca^{2+} oscillations and, thus chaotic muscle contractions.

The 'OFF' mechanisms (§1.1) provide a potential for such mechanism of control. Several of the Ca^{2+}-extrusion process from the cytosol are themselves Ca^{2+}-dependent (see Chapter 4). Thus in a situation where there is high $\left[Ca^{2+}\right]_i$ these 'OFF' mechanisms are more active. This would cause the return to basal Ca^{2+} to be faster in the case where release is higher (high-$InsP_3$) rather than lower (low-$InsP_3$). Thus the regulation of *OT*-induced Ca^{2+} oscillations regardless of concentration may focus around a mechanism for ensuring that oscillations are of a constant duration regardless of the applied agonist concentration.

On the contrary, however, the initial transient response does show concentration-dependent effects. It is possible, therefore that the initial transient may be part of the proposed mechanism of *OT*-induced Ca^{2+} oscillations control. The initial transient has often been seen as a 'setting'-pulse for the system to 'programme' for the regular oscillations which follow it; it is possible that the duration of *OT*-induced Ca^{2+} oscillations and total Ca^{2+} release somehow encodes the information required to do this. This initial transient increases in both area and initial time as *[OT]* increases, but the initial full-width half-magnitude is reasonably constant for all bar the highest concentration of *OT*, $75\ nM$. This might suggest that maintaining a constant full-width half-magnitude is important for establishing *OT*-induced Ca^{2+} oscillations. That application of *OT* in concentra-

tions greater than $100\ nM$ resulted in heightened $\left[Ca^{2+}\right]_i$ rather than oscillations might suggest that the system is reaching its limit of being able to compensate the full-width half-magnitude for variation in *[OT]* at the $75\ nM$ concentration.

The number of cells responding to *OT* increases in a concentration-dependent manner (Figure 3.4) which suggests a potentially binary response to *OT*. The probability of that response resulting in *OT*-induced Ca^{2+} oscillations increases as *[OT]* increases. This might provide the cell's Ca^{2+} signalsome with an addition tool for the regulation of Ca^{2+} signalling (§1.2).

In the case where $\left[Ca^{2+}\right]_{EC}$ is zero, only the initial transient is seen. *OT*-induced Ca^{2+} oscillations are unable to establish suggesting that extracellular Ca^{2+} provides a vital component for them to establish. This follows since extracellular Ca^{2+} entry is vital for, or at least mediates, many of the 'ON' and 'OFF' reactions. It thus seems pertinent to investigate the role of extracellular Ca^{2+} entry in more detail and this is the subject of Chapter 4.

3.4 Conclusion

OT-induced Ca^{2+} oscillations are more likely to establish in higher concentrations of agonist. Such established *OT*-induced Ca^{2+}-oscillations do not show concentration-dependency of their period, area or full-width half-magnitude in agreement with [29]. The initial transient, however, does show concentration-dependent effects on both the area and initial time suggesting a role in 'priming the system'.

The full-width half-magnitude is maintained approximately constant in *[OT]* lower than $75\ nM$ but a concentration of greater than $75\ nM$ leads to a significantly increased full-width half-magnitude. Combined with the fact that at *[OT]* of $100\ nM$ or greater *OT*-induced Ca^{2+} oscillations could not establish, with the system instead reaching a new steady-state $\left[Ca^{2+}\right]_i$, this suggests the system has an ability to control full-width half-magnitude which breaks-down at excessively high *[OT]*.

One a single transient is seen without any *OT*-induced Ca^{2+} oscillations when extracellular Ca^{2+} is removed suggesting the importance of extracellular Ca^{2+} entry for the establishment of Ca^{2+} oscillations.

Chapter 4

The Role of Extracellular Calcium Entry and Extrusion

4.1 Introduction

4.1.1 Background

The plasma membrane is crucial for the maintenance of intracellular calcium concentration, $\left[Ca^{2+}\right]_i$. It is responsible for both the removal of Ca^{2+} from the cell and Ca^{2+} entry if required to form a signal. Extrusion of Ca^{2+} from the cell is handled by two mechanisms which help to maintain the low cytoplasmic basal $\left[Ca^{2+}\right]_i$ by actively discharging Ca^{2+} from the cell [77].

The first sort, the plasma membrane Ca^{2+} ATPase (PMCA) pump uses the energy of one or two molecules of ATP to drive one ion of Ca^{2+} out of the cell. It is called a P-type pump since its pumping cycle uses a phosphorylated intermediate involving the transient transfer of a phosphoric group to an aspartate residue on the polypeptide. This protein phosphorylation causes a conformational change which allows the transport of a single Ca^{2+} ion across the membrane. Dephosphorylation restores the protein back to its initial state, primed for pumping. The net result is the breaking and loss of the high-energy phosphate bond of ATP. The energy is used to drive the Ca^{2+} pumping activity of the ATPase. The structure of the ATPase protein is thought to have 10 transmembrane spanning domains. As is the case with many proteins involved in signalling several tissue-specific isoforms exist in humans. These isoforms arise from four genes as well as alternative splicing of the gene transcripts [109].

$Na^+/Ca^{2+}-$exchangers form the the second type of mechanism for Ca^{2+} extru-

sion. They use the sodium electrochemical gradient across the plasma membrane to facilitate the extrusion of Ca^{2+}. There are two main types:

1. The $Na^+/Ca^{2+}-$exchanger, a simple exchanger, moves one Ca^{2+} out for every three Na^+ ions that move inwards (for more details see §7.1.2)
2. The NCKX co-transports one Ca^{2+} and one K^+ ion with the subsequent movement of four Na^+ ions inwards.

Whilst Ca^{2+}-ATPase are known to have a higher affinity for Ca^{2+} ions than $Na^+/Ca^{2+}-$exchangers, the $Na^+/Ca^{2+}-$exchanger transport Ca^{2+} ions at a much faster rate; a typical Ca^{2+}-ATPase has been shown to pump Ca^{2+} ions at a rate of 30 s^{-1} whereas the $Na^+/Ca^{2+}-$exchangers are able to exchange ions at up to 2000 s^{-1}. Thus after an influx of Ca^{2+}, perhaps caused by a signalling event, the $Na^+/Ca^{2+}-$exchangers are most important in expelling large amounts of Ca^{2+} from the cell until $\left[Ca^{2+}\right]_i$ enters the micromolar range where the slower but higher-affinity ATP-ase is able to continue to decrease the cytoplasmic $\left[Ca^{2+}\right]$ further [72].

As discussed in §1.1, the gap junction network between cells provides a powerful way of calcium entry into a cell with comparatively low $\left[Ca^{2+}\right]_i$ from one with higher $\left[Ca^{2+}\right]_i$. This passive mechanism allows for the propagation of a signal across a tissue. However, in most cells the plasma membrane also acts as the major site of re-entry of Ca^{2+} from the extracellular fluid into the cytosol.

Voltage-Gated Ca^{2+} channels (CaVs) often play an important role in Ca^{2+}-re-entry into the cell. Their structure contains a helix-turn-helix domain which is thought to act as the sensor for a voltage change across the membrane. In response to any change in voltage, they allow very rapid entry into the cell through the channel resulting in changes in $\left[Ca^{2+}\right]$ both within the whole cytoplasm and in the immediate vicinity of the channel.

A second method of Ca^{2+} re-entry is via transient receptor protein (TRP) ion channels. Their proteins are topologically tetrameric structures of six membrane-spanning helices with intracellular N- and C-termini which create a relatively non-selective pore through the membrane. In mammals there numerous isoforms of these channels, split into six classes, grouped into two broad groups. Group 1 includes: TRPC (**C**anonical), TRPV (**V**anilloid), TRPM (**M**elastatin) and TRPA (**A**nkyrin). In group 2 there are TRPP (**P**olycystic) and TRPML (**M**ucolipin) [67, 110, 33].

TRP channels are sensitive to a vast range of stimuli. They are known to be sensitive (in an activating or inhibitory way) to temperature, pH and mechanical stress as well as being sensitive to a host of chemicals, including

- calmodulin,
- phospholipase C,
- S100 proteins,
- annexins,
- reactive oxygen species,
- ADO ribose,
- DAG

Their dysfunction has been noted in kidney disease and it is known that they are influential in development [40].

Recently, a further route of entry triggered the depletion of intracellular stores has been shown to serve as a signal for the re-entry of Ca^{2+} through the plasma membrane. This entry operates by way of a process called capacitative Ca^{2+} entry (CCE), through what is referred to as store-operated channels (SOCs). More on this is covered in Chapter 7.

4.1.2 Experiment

In Chapter 3, oxytocin-induced Ca^{2+} oscillations were shown to be unable to establish in the absence of extracellular Ca^{2+}, Ca^{2+}_{EC}. Indeed in this case (as demonstrated in Figure 3.5) the typical response is to see an initial transient of Ca^{2+} followed by a return to basal levels of Ca^{2+} and no regular oscillations are established.

Thus the role(s) that Ca^{2+}_{EC} has on $1\ nM$ oxytocin-induced Ca^{2+} oscillations are investigated. First by varying $\left[Ca^{2+}\right]_{EC}$ directly by altering the final concentration of Ca^{2+} in the (extracellular) PSS. Then the roles of the $Na^{+}/Ca^{2+}-$exchanger and PMCA are investigated by altering their ability to function. This is achieved by varying $\left[Na^{+}\right]_{EC}$ for the former and inhibition using Caloxin 3A1 in the case of the latter. Finally, another route of receptor-operated entry is investigated using ATP to stimulate purinergic receptors.

4.2 Results

4.2.1 Varying $\left[Ca^{2+}\right]_{EC}$

In order to see the relationship between oscillation frequency and extracellular calcium concentration, three physiologically reasonable concentrations were chosen:

- **Low** $\left[Ca^{2+}\right]_{EC} = 0.5\ mM$

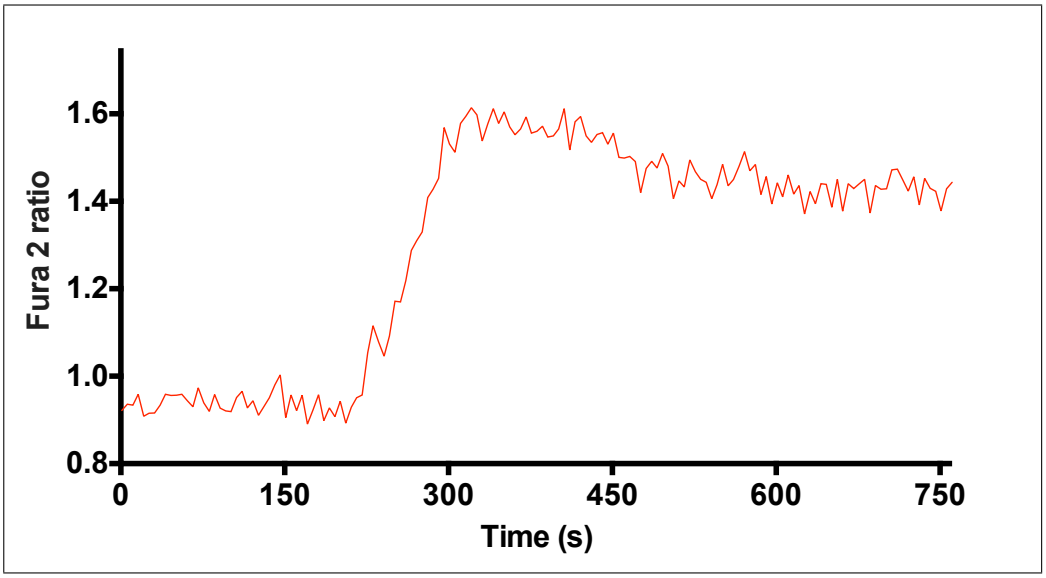

Figure 4.1 *An example trace of the toxic response in CHO-hOT to* $10\ mM\ Ca^{2+}$*-PSS upon application of* $1\ nM$ OT.

- **Physiological** $\left[Ca^{2+}\right]_{EC} = 2\ mM$
- **High**

The **high** concentration was initially taken as $10\ mM$ such that a more broad range of concentrations could be investigated. However, this invariably resulted in an irreversible rise of Ca^{2+} and cell death as illustrated in Figure 4.1. The value was thus reduced to $\left[Ca^{2+}\right]_{EC} = 4\ mM$.

Cells were loaded with Fluo-4/AM as per Protocol 4 and both washed and stored in $2\ mM\ Ca^{2+}$-PSS before experimentation. At the start of a recording a baseline of 30 seconds of $2\ mM\ Ca^{2+}$-PSS perfusion was taken. The PSS concentration under investigation was then perfused in the absence of oxytocin for 60 seconds to test for any impact the change in extracellular calcium alone might have. Then $1\ nM$ oxytocin was introduced to the perfusion line and the resultant oscillations recorded. Representative traces for each of the three PSS concentrations are shown in Figure 4.2 and the statistics data is summarised in Figure 4.4.

It is also interesting to note that, following the same protocol and using the same perfusion apparatus, the onset of oscillations is faster when $\left[Ca^{2+}\right]_{EC}$ is higher; that is, the initial transient occurs more quickly in higher $\left[Ca^{2+}\right]_{EC}$. Figure 4.3 illustrates this initial transient and shows the approximately 10 seconds between the onset of the initial transient. This increase in lag-time before the initial transient occurs as concentration decreases comes with a concomitant decrease in the gradient at which the the transient leaves the basal level and reach its peak.

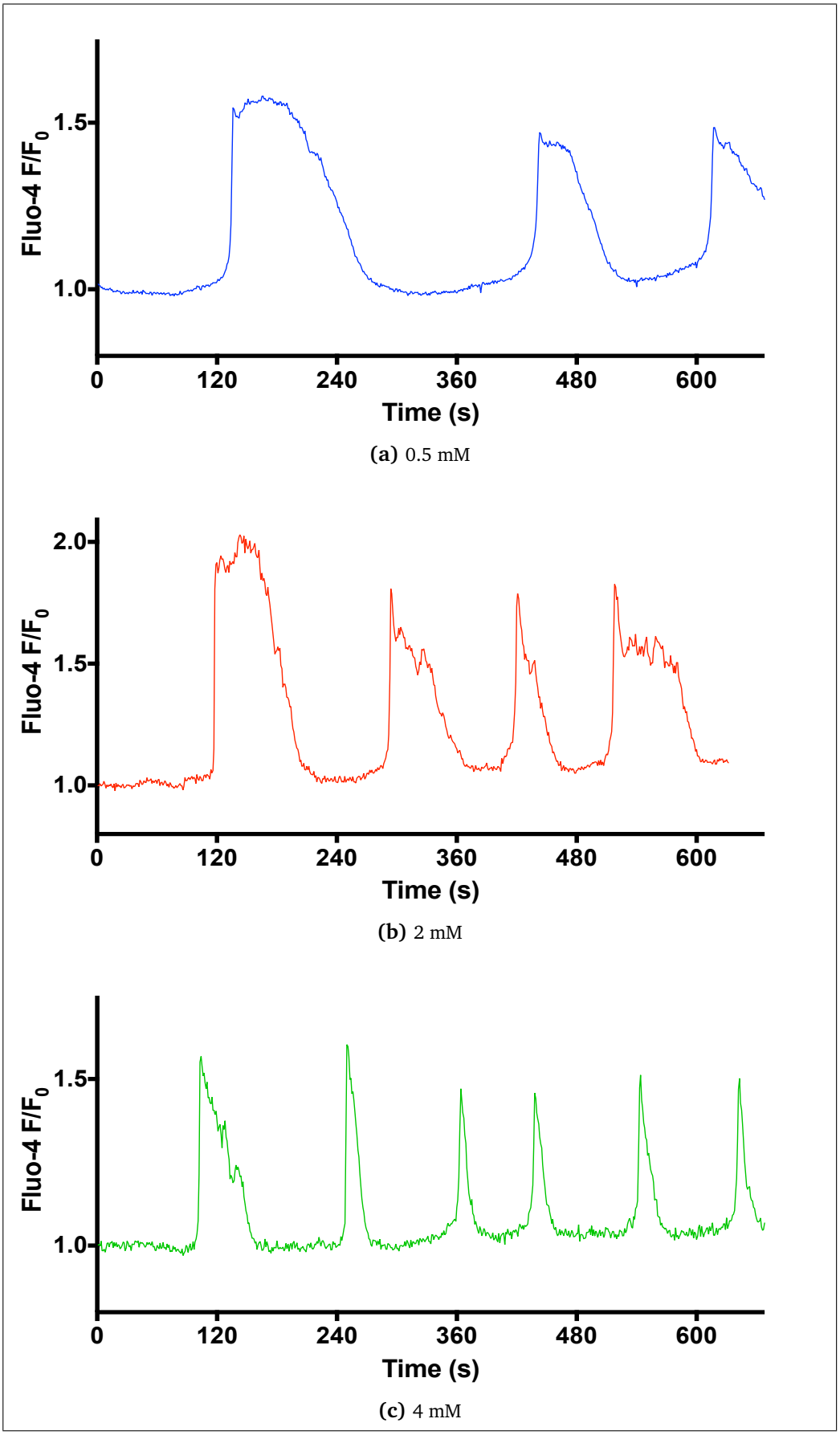

(a) 0.5 mM

(b) 2 mM

(c) 4 mM

Figure 4.2 *Typical oscillations induced by* $1\ nM$ OT *in* CHO–hOT *cells loaded with Fluo-4/AM different* $[Ca^{2+}]_{EC}$*: (a)* $0.5\ mM$*, (b)* $2\ mM$ *and (c)* $4\ mM$*.*

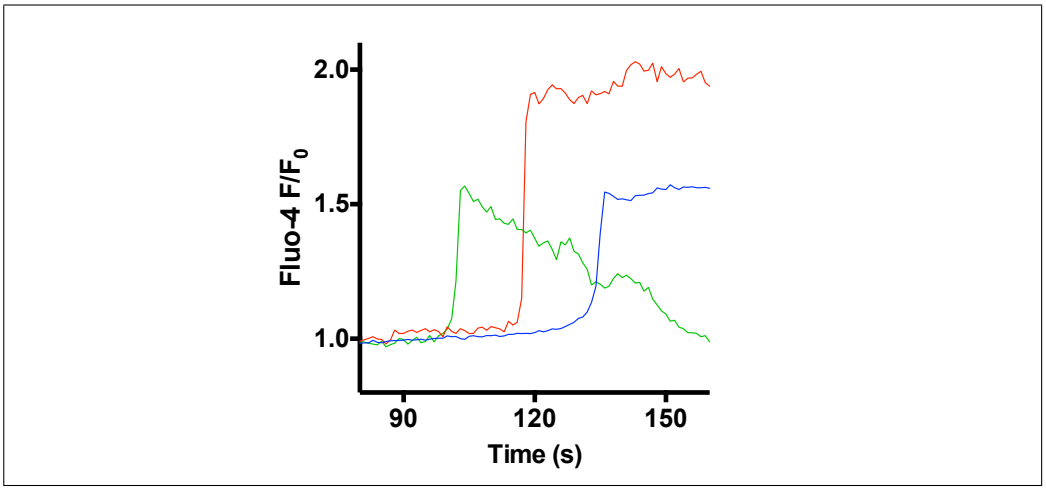

Figure 4.3 *A magnification of the initial transient Ca^{2+} increase seen in Figure 4.2. The gradient of the initial transient and its time of onset are faster with increased $\left[Ca^{2+}\right]_{EC}$.*

Taking Figure 4.2 and Figure 4.4 together reveals the change in the pattern of oscillations as $\left[Ca^{2+}\right]_{EC}$ is changed. Figure 4.2 demonstrates the trend for the period of oscillations to decrease as $\left[Ca^{2+}\right]_{EC}$ is increased which is supported by the analysis of the full data-set shown in Figure 4.4 (c). This decrease in period also appears to come with a decrease in the time, t_{in}, between the initial transient and the second (Figure 4.4 (a)). The shape of the initial transient appears quite different as $\left[Ca^{2+}\right]_{EC}$ is varied: the lowest dose appears to have oscillations of long duration (and, thus, larger area) with the oscillations becoming more pointed as $\left[Ca^{2+}\right]_{EC}$ increases. Whilst this is supported by Figure 4.4 (b), the same is not seen once oscillations have established: Figure 4.4 (d) demonstrates that whilst there is a larger area under the oscillations for the lowest dose the physiological and high doses appear to have a similar average area of oscillations.

Paired Data

The data summarised in Figure 4.4 is taken from recordings from hundreds of cells in viewing fields across several petri dishes over different experimental days and cell passage number. The data is analysed together on the assumption that cultures perform in a similar, predictable way to one another and that the cells within a given dish behave independently of one another. This is a common assumption in the field of calcium imaging and has been performed in numerous other works [129, 22]. However, it was decided to validate the approach by trying a second protocol.

At the start of a recording a baseline of a 30 seconds perfusion of 2 mM PSS was taken. To start, the high concentration was perfused in the absence of oxytocin for 60 seconds to eliminate any impact the change in extracellular calcium might

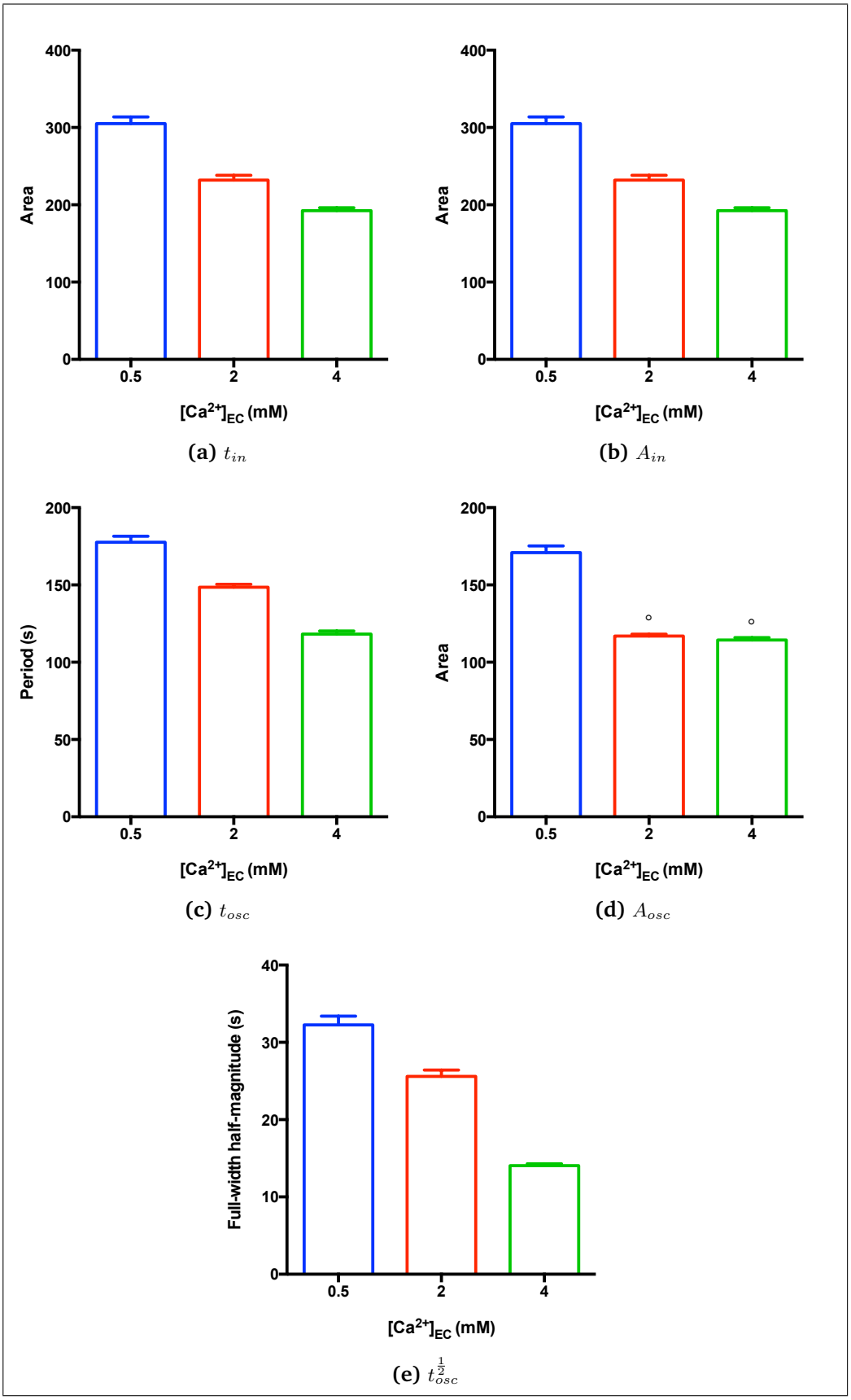

Figure 4.4 *Summary data for Fluo-4/AM loaded* CHO–hOT *cells stimulated with with 1nM Oxytocin in the presence of different* $\left[Ca^{2+}\right]_{EC}$*. Data points were taken from all oscillatory cells within at least 3 different petri dishes with cell numbers of* 156, 187 *and* 152 *for each concentration* 0.5, 2 *and* $4\,mM$*, respectively.*

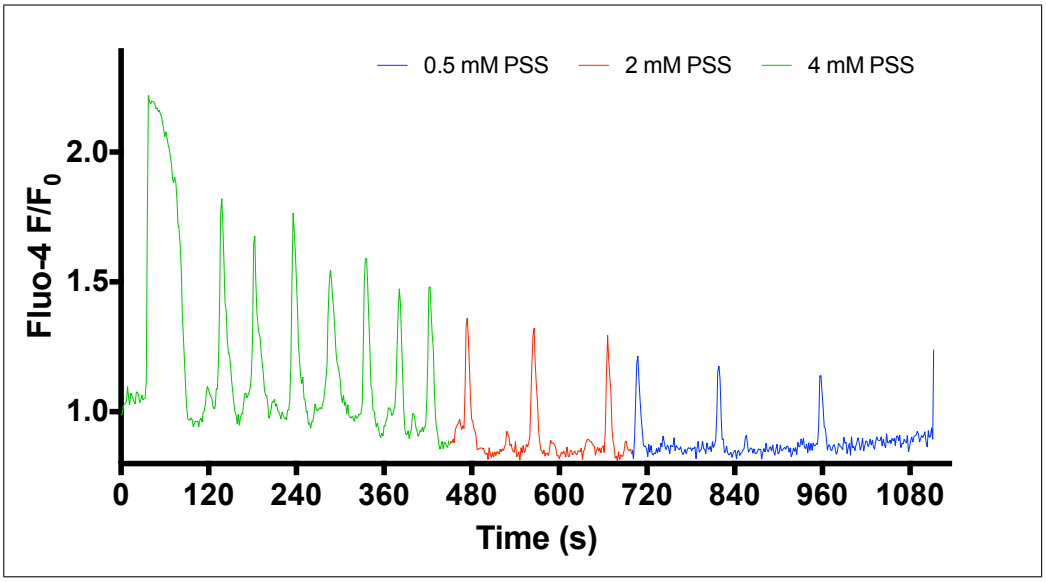

Figure 4.5 *A typical trace of the response in* CHO–hOT *cells when* $\left[Ca^{2+}\right]_{EC}$ *is changed in the presence of* $1\ nM$ OT.

have had. Then 1nM oxytocin was introduced to the perfusion line and the oscillations recorded. The concentration of extracellular calcium was then stepped to the medium concentration *OT*-containing solution at $t = 450\ s$ through the recording. Oscillations were allowed to stabilise and then a further step to the low concentration solution was performed at $t = 650\ s$.

This protocol was employed so that a paired $t-$test could be used to assess whether there is a difference in the mean oscillation frequency of the same cell when the concentration of extracellular calcium is varied. This test has increased statistical power over the previous protocol because it does not need to assume independence of the individual cells as would need to be assumed to perform an unpaired $t-$test on the data in Figure 4.4. However, in this case any information contained in the initial transient is lost, meaning that it is necessary to either perform both sets of experiments or to run the original protocol on the same viewing field for all the concentrations but with a 'reset gap' of, say, 10 minutes between each recording. The former was chosen because photobleaching was deemed too severe in the latter case as well as a concern that the cells might suffer fatigue from being asked to oscillate multiple times and thus introduce that fatigue as experimental bias.

An exemplar trace of one cell using this protocol is shown in Figure 4.5. It shows that the oscillation period increases as $\left[Ca^{2+}\right]_{EC}$ decreases and the area under the oscillations (and their amplitude) decreases. Figure 4.6 (a) and (c) show the same cells in different $\left[Ca^{2+}\right]_{EC}$ connected by dotted lines for t_{osc} and A_{osc}, respectively. In general both of these quantities appears to increase as $\left[Ca^{2+}\right]_{EC}$

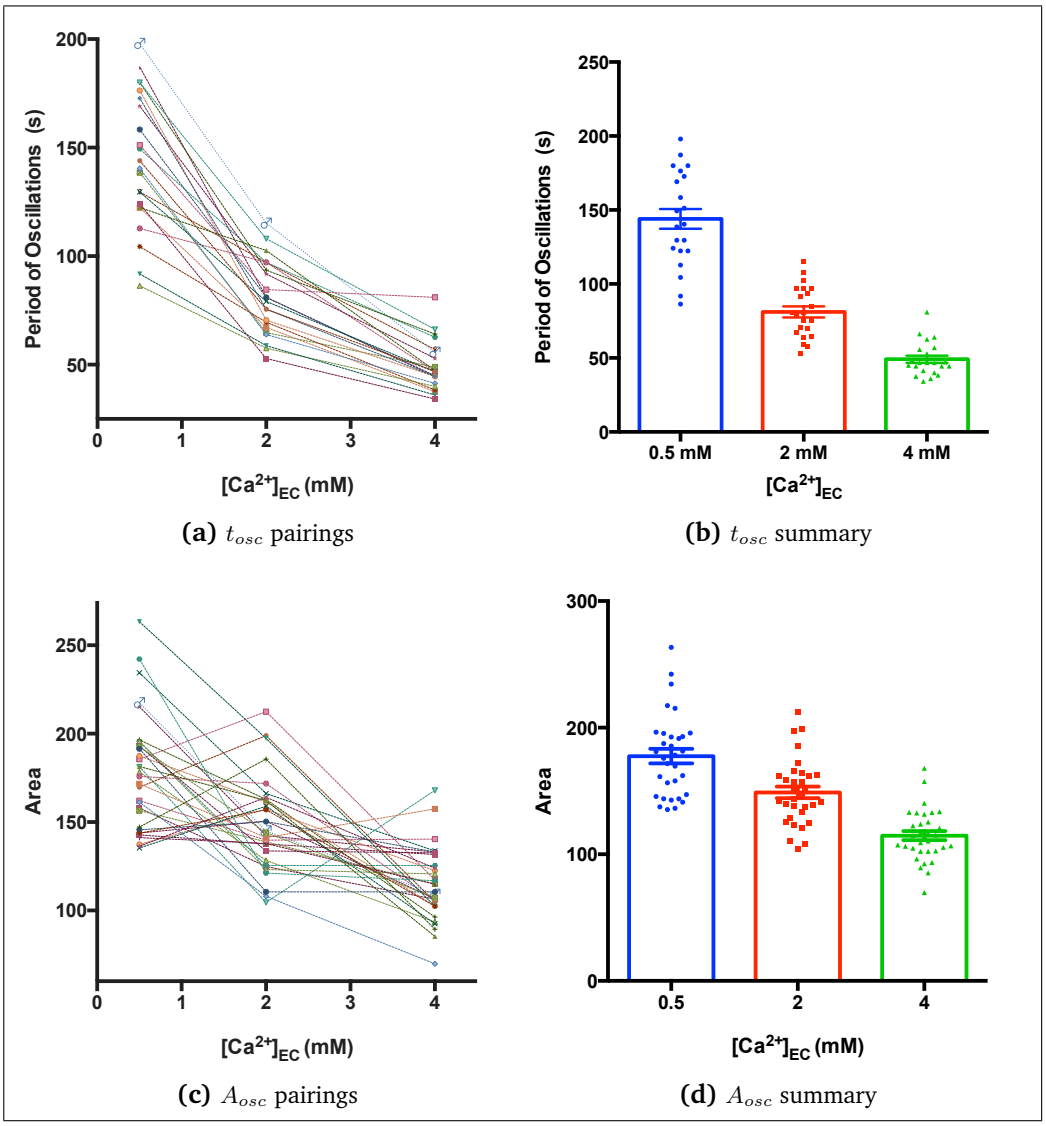

(a) t_{osc} pairings **(b)** t_{osc} summary

(c) A_{osc} pairings **(d)** A_{osc} summary

Figure 4.6 *The oscillation frequencies of cells when different concentrations of $1nM$ OT-containing extracellular calcium are applied. This recording is from one viewing field in one petri dish. Coloured lines connect the readings from the same cell. Here the number of cells which oscillate under all three conditions is 32 and each data point is plotted as a dot to indicate the spread as the dataset is smaller than others presented here.*

decreases which is confirmed by the summary data in Figure 4.6 (b) and (d); each column is significantly different from the others).

4.2.2 Varying PMCA activity

One method for varying Ca^{2+} extrusion from the cell is to vary the activity of the PMCA using the specific PMCA antagonist, Caloxin 3A1. Caloxins were developed by a screening method using phage display. They target the exdoms of the PMCA since they have little homology with the other members of P-type ATPases (such as the SERCA). They are, therefore, able to uniquely target PMCA.

The first number in a Caloxin's name denotes the exdom used as a target for the screening. The letter indicates the screening method employed with A denoting that screening was done with synthetic peptide as a target. The second number denotes a serial number obtained within the same exdom-method category [123].

Since they target the exdoms, Caloxin 3A1 can be added to the extracellular medium to inhibit the PMCA without permeabilisation. Caloxin 3A1 has a relatively low-affinity for the pump with a $K_i = 0.2\ mM$ [31].

The first PMCA selective inhibitor, Caloxin 2A1 ($K_i = 0.4\ mM$) produced 50% inhibition of Ca^{2+} and Mg^{2+}-ATPase activity of PMCA in human erythrocyte ghosts at a concentration of $0.4\ \pm 0.1\ mM$ [31]. Caloxin 3A1 is thus used at $200\ \mu M$ in our experiments with the hope that it will reduce PMCA activity substantially, although may not eliminate it completely. The PMCA isoform known to exist in *CHO–hOT* cells is type three [1].

Figure 4.8 provides a summary of the data from an experiment where cells loaded with Fluo-4 were pre-treated for 10 minutes to allow the system to reach equilibrium with either PSS or containing $200\ \mu M$ Caloxin 3A1. *OT* was then applied and the resultant *OT*-induced Ca^{2+} oscillations recorded in the presence and absence of $200\ \mu M$. Compared to the control, Caloxin 3A1 elicited the following effects on *OT*-induced Ca^{2+} oscillations:

- a reduction in (a) initial time (b) period
- an increase in the area of both the (c) initial transient and (d) ensuing oscillations
- a reduction in the both the (e) initial full-width half-magnitude and (f) oscillations' full-width half-magnitude.

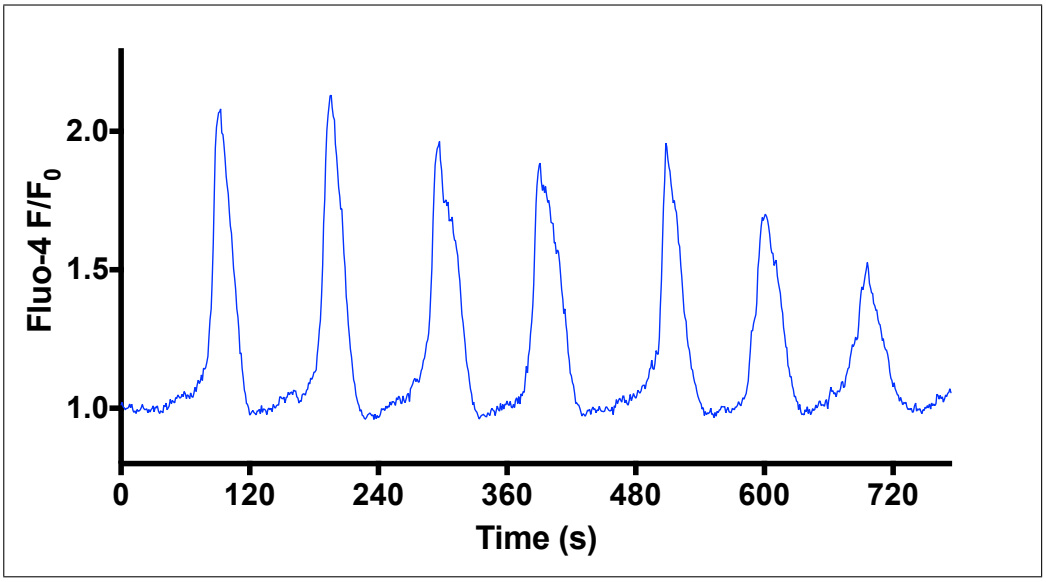

Figure 4.7 *Example Ca^{2+} trace for* OT *induced (at $t = 0$ s) oscillations recording in the presence of Caloxin 3A1 pre-treated for 10 minutes before this recording started. Recording in Fluo-4 loaded* CHO–hOT *cells with* OT *applied at $t = 0$ s*

4.2.3 Varying $[Na^+]_{EC}$

Manipulating the extracellular Na^+ concentration is a second way of altering the removal of Ca^{2+} from the cell.

In the case of normal $[Na^+]_{EC}$, the $Na^+/Ca^{2+}-$exchanger removes one Ca^{2+} ion from the cell at the expense of delivering three Na^+ ions into the cytoplasm. This is called the direct or forward mode of the $Na^+/Ca^{2+}-$exchanger. When the transmembrane Na^+ gradient is reversed, i.e. $[Na^+_{EC}]$ is higher than $[Na^+]_{EC}$, the exchanger delivers Ca^{2+} into the cytoplasm working in reverse mode. Ca^{2+} entry in the reverse mode is only transient unless the $Na^+ /K^+ - ATPase$ is inhibited and $[Na^+_{EC}]$ is maintained at a high level.

Figure 4.9 displays two typical Fluo-4 signal traces for experiments conducted to establish the role of Na^+_{EC} on *OT*-induced Ca^{2+} oscillations. In order to keep the experiments compatible with those with Na^+ present in the PSS, the sodium was isosmotically substituted with sucrose [82]. The first experiment, Figure 4.9 (a), shows a moderate increase in the basal as PSS is replaced with this Na^+ 0-PSS at $t = 100s$. The system then returns to its resting level of fluorescence until *OT* is introduced at $t = 1300s$ which results in the typical initial-transient followed by oscillations. These *OT*-induced Ca^{2+} oscillations were substantially potentiated in the absence of extracellular Na^+ with higher frequency. Activation of $Na^+/Ca^{2+}-$exchanger by re-introducing the sodium ions into extracellular medium markedly decreased the amplitude and frequency of the *OT*-induced Ca^{2+} oscillations as can be seen in the typical trace in Figure 4.9 (b).

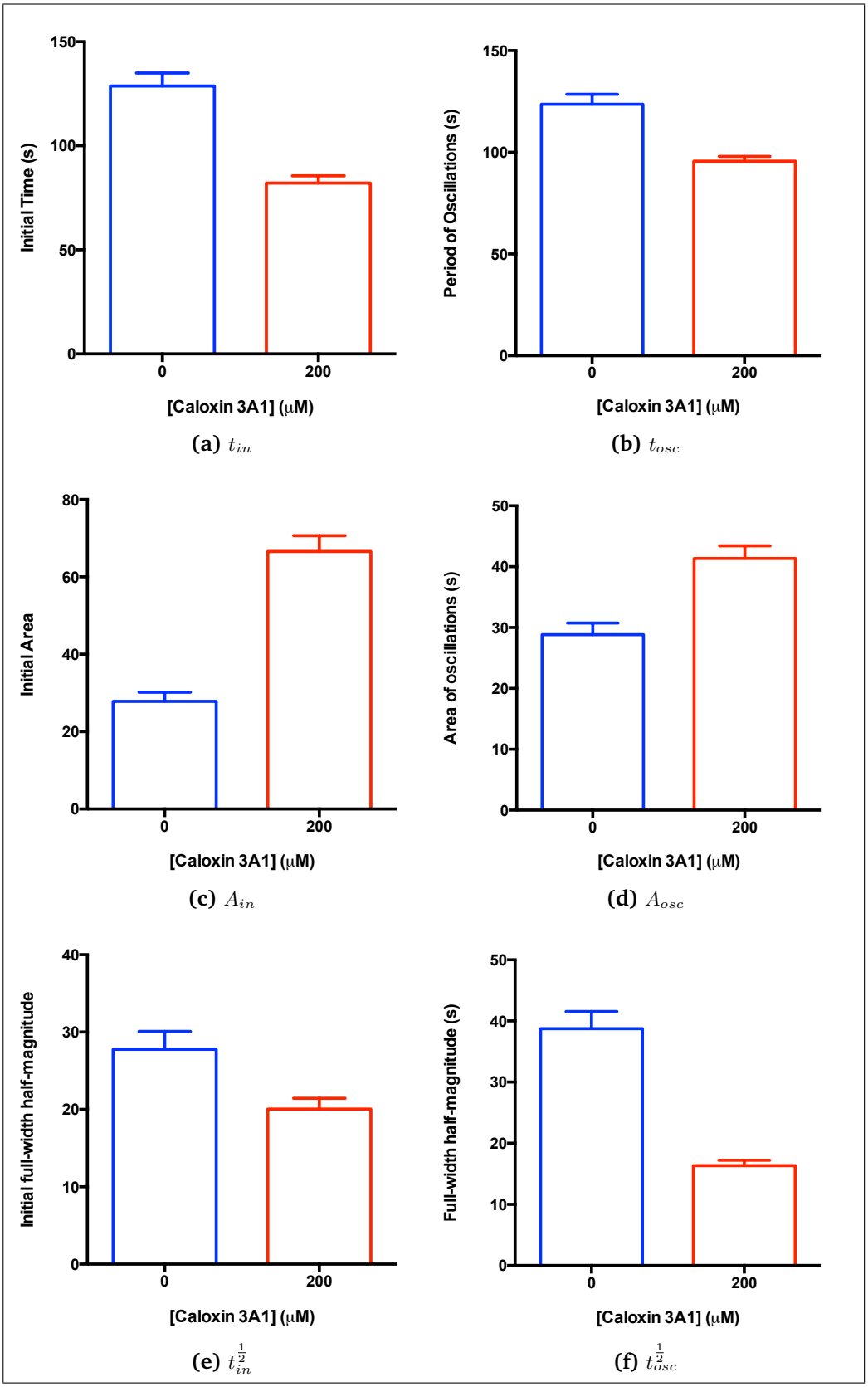

(a) t_{in} **(b)** t_{osc}

(c) A_{in} **(d)** A_{osc}

(e) $t_{in}^{\frac{1}{2}}$ **(f)** $t_{osc}^{\frac{1}{2}}$

Figure 4.8 *Summary data for* OT *induced oscillations with the inhibition of PMCA using Caloxin 3A1 in Fluo-4 loaded* CHO–hOT *cells. Data points were taken from all oscillatory cells within at least 3 different petri dishes with cell numbers of* 77 *in the absence and* 197 *in the presence of* $200\,\mu M$ *Caloxin 3A1.*

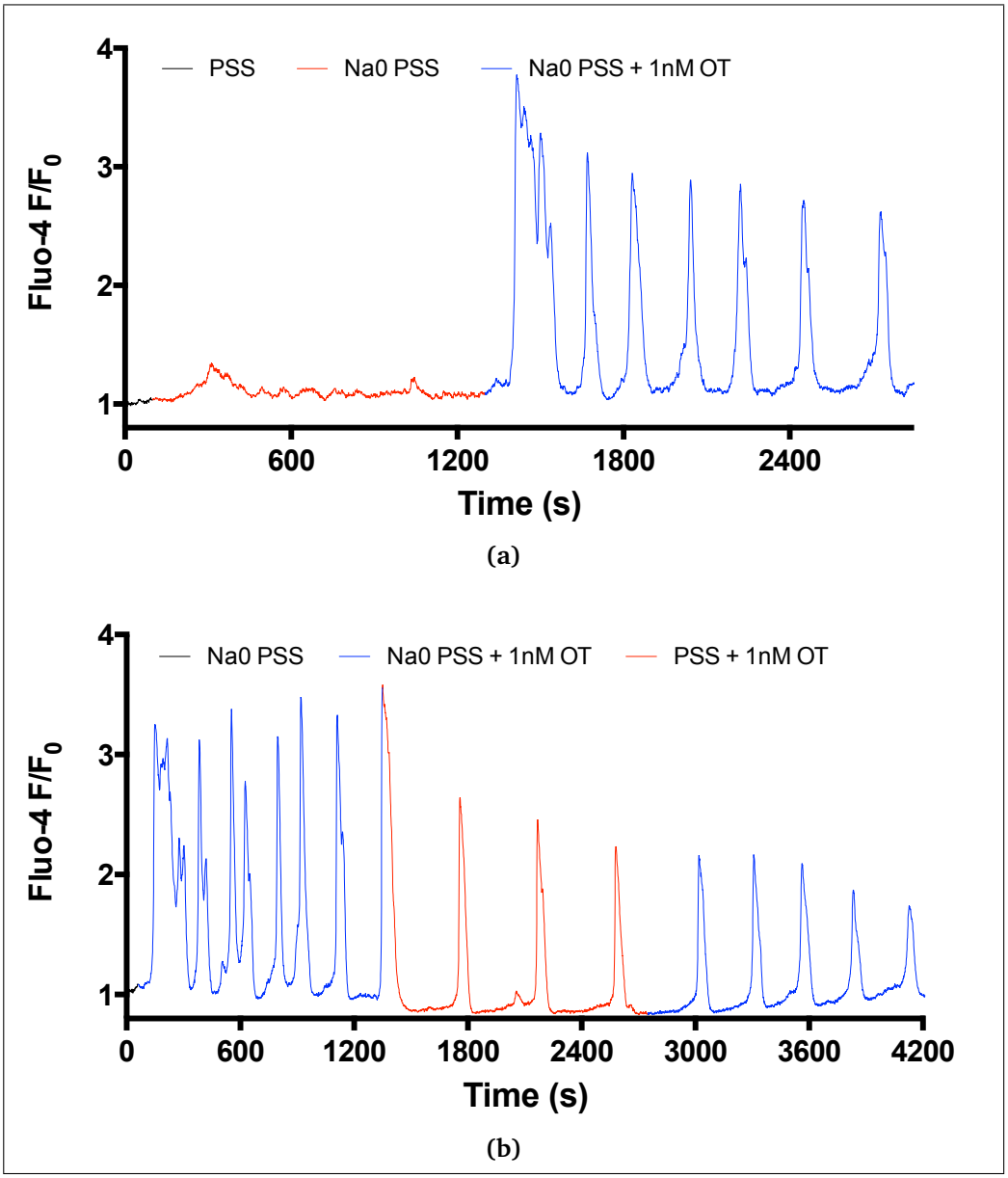

Figure 4.9 *Exemplar data of Ca^{2+} trace recording from Fluo-4 loaded* CHO–hOT *cells showing (a) oscillations in the absence of extracellular Na^{+} and (b) the impact of reintroducing extracellular Na^{+} upon established oscillations.*

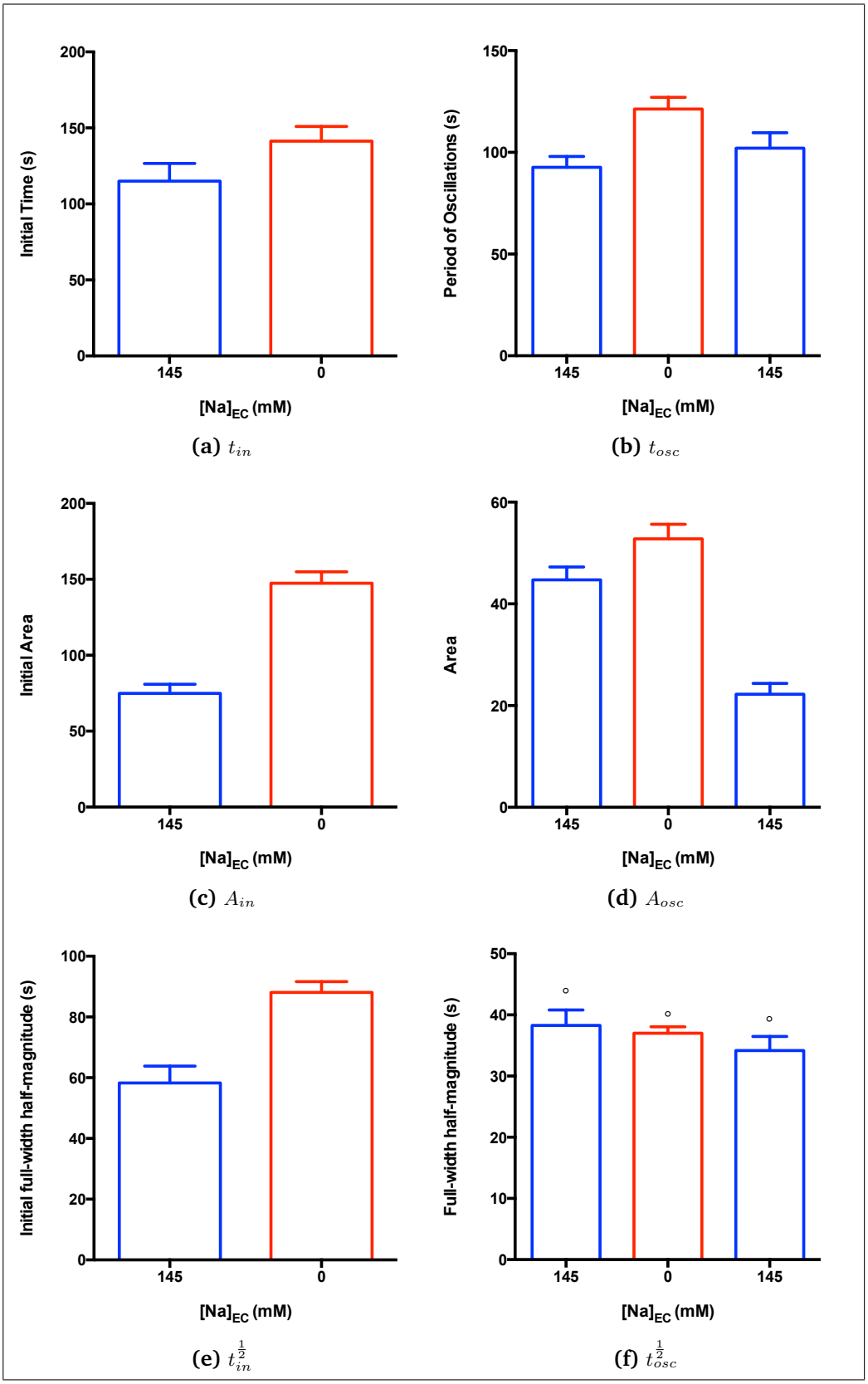

(a) t_{in} **(b)** t_{osc}

(c) A_{in} **(d)** A_{osc}

(e) $t_{in}^{\frac{1}{2}}$ **(f)** $t_{osc}^{\frac{1}{2}}$

Figure 4.10 *Summary data of Ca^{2+} trace recording from Fluo-4 loaded* CHO–hOT *cells showing (a) oscillations in the absence of extracellular Na^+ and (b) the impact of reintroducing extracellular Na^+ upon established oscillations. Data points were taken from all oscillatory cells within at least 2 different petri dishes with cell numbers of over 45 in all cases.*

These results are supported by the summary data shown in Figure 4.10.

- both the initial time (a) and the period of oscillations (e) increase with the removal of Na^+_{EC}
- oscillations return to a reduced period when $[Na^+]_{EC}$ is returned to $145\,mM$ ((b), second blue column)
- the area of the initial transient (c) in the absence of extracellular sodium is double that of the initial transient in $145\,mM$ $[Na^+]_{EC}$.
- the full-width half-magnitude of the initial transient (c) in the absence of extracellular sodium is almost double that of the initial transient in $145\,mM$ Na^+_{EC}.
- the area of the established oscillations (d) increases with removal of Na^+_{EC} and decreases again upon reintroduction
- the full-width half-magnitude of the established oscillations are statistically indistinguishable from one another.

4.2.4 Varying receptor operated calcium entry

ATP as an extracellular signal

ATP is best known as a molecule that acts as a ubiquitous supply of energy within cells. ATP is made in small amounts by the anaerobic metabolism of glycolysis. This is not normally sufficient to sustain an active cell and thus the majority of the cells ATP is produced by mitochondrial aerobic respiration. Whilst ATP is vital for the survival of an individual cell, extracellular releases can happen for example from cells involved in the secretion of neurotransmitters, or through storage granules from cells such as lymphocytes. Cell death and consequent breakup can also lead to the release of intracellular ATP into the extracellular medium and thus the local concentrations of ATP may reach the high nanomolar or even low micromolar region. Whilst there are three different (extracellular) ectonucleotidases responsible for the removal of ATP from the extracellular milieu by the sequential hydrolysis of ATP to adenosine, many cells, including smooth muscle, have been shown to posses purinergic receptors on their surface capable of detecting ATP [49].

Purinergic receptors fall into two families, with $P1$ receptors sensitive to adenosine and $P2$ receptors having the highest affinity for ATP. $P2$ receptors have further been divided into two families with five subclasses the metabotropic family with subclasses $P2_Y$, $P2_U$, and $P2_T$ and the family of ionotropic receptors with

subclasses $P2_X$ and $P2_Z$ [27, 99]. $P1$ and $P2_Y$ receptors are G protein-coupled receptors whereas $P2_X$ receptors are ligand-gated ion channels. The $P2$ isoforms known to exist in *CHO–hOT* cells are $P2_X$ types 1, 2, 3, 5, 6 and 7 and $P2_Y$ types 1, 2, 4, 6, 10, 12, 13 and 14 [1].

These ligand-gated ion channels are non-selective cation channels, pervious to Ca^{2+}, which are responsible for mediating excitatory postsynaptic responses, similar to nicotinic and ionotropic glutamate receptors [71]. $P2_X$ receptors are distinct from the rest of the widely known ligand-gated ion channels, as the genetic encoding of these particular channels indicates the presence of only two transmembrane domains within the channels [96]. $P2_X$ receptors mediate a large variety of responses including contraction of smooth muscle cells, platelet aggregation, and apoptosis [26, 25].

Here, ATP is used as a tool to investigate the impact of introducing additional, non-store operated, Ca^{2+}-entry into the cytosol via $P2_X$ receptors whilst G_q-mediated Ca^{2+} oscillations (via ATP-activated stimulation of $P2_Y$ receptors) trigger the release of $InsP_3$. Thus an investigation into the concentration-depence was conducted. ATP was applied in concentrations of $1,\ 10$ and $100\ \mu M$ to *CHO–hOT* cells loaded with Fluo-4 and the resultant ATP-induced Ca^{2+} oscillations were recorded for analysis. Figure 4.11 summarises the data and demonstrates:

- the initial time, area and full-width half-magnitude all increase with increasing $[ATP]$
- the period of ensuring ATP-induced Ca^{2+} oscillations decreases, showing dose-dependence, unlike *OT*-induced Ca^{2+} oscillations
- the average oscillation period is always less than 80 seconds, compared to over 110 seconds in *OT*-induced Ca^{2+} oscillations
- the area of oscillations and full-width half-magnitude is much larger for $[ATP] = 100\ \mu M$ than for the lower concentrations

Figure 4.12 shows two traces from an experiment designed to investigate the impact that pre-application of ATP in Ca^{2+}-free PSS would have upon *OT*-induced Ca^{2+} oscillations. PSS was switched for Ca^{2+}-free PSS containing $1\ \mu M\ ATP$ at $t = 100\ s$. An initial ATP transient is seen which results in $\left[Ca^{2+}\right]_i$ at a lower level than before the transient but no ensuing oscillations. This matches the response to *OT* in Ca^{2+}-free PSS from Chapter 3. Upon re-introduction of Ca^{2+} and *OT* at $t = 700\ s$ in both traces the $\left[Ca^{2+}\right]_i$ stabilises. In the case of (a) *OT*-induced Ca^{2+} oscillations establish but without the initial larger transient seen when *OT* is applied without pre-dosing with ATP. A return to Ca^{2+}-free PSS containing ATP at $t = 1500\ s$ results in an ATP initial response of similar

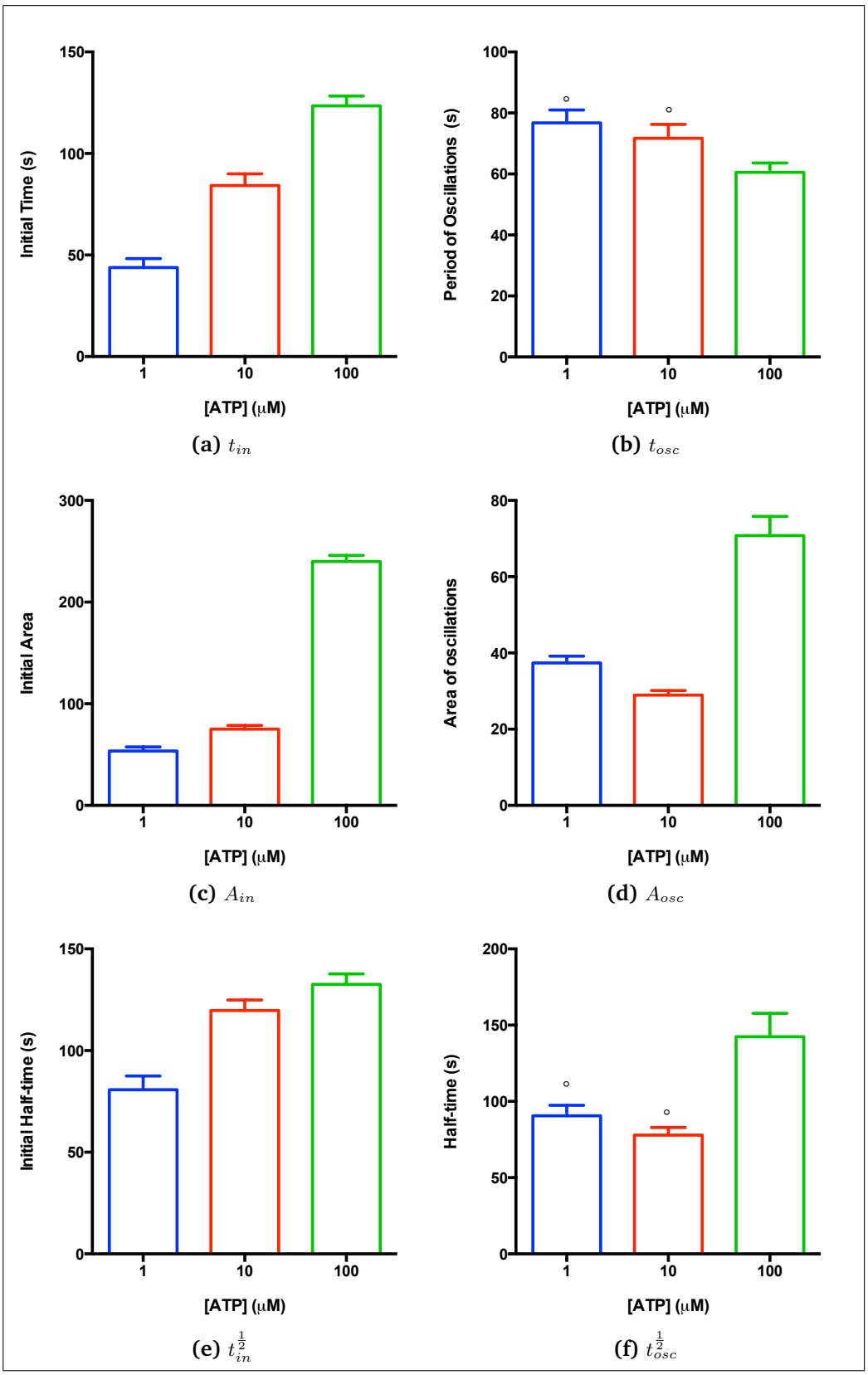

(a) t_{in} **(b)** t_{osc}

(c) A_{in} **(d)** A_{osc}

(e) $t_{in}^{\frac{1}{2}}$ **(f)** $t_{osc}^{\frac{1}{2}}$

Figure 4.11 *Summary data for the application of varying concentrations of* ATP*.Data points were taken from all oscillatory cells within at least 2 different petri dishes with cell numbers of* 60*,* 95 *and* 135 *for each concentration* 1*,* 10 *and* $100\,nM$*, respectively.*

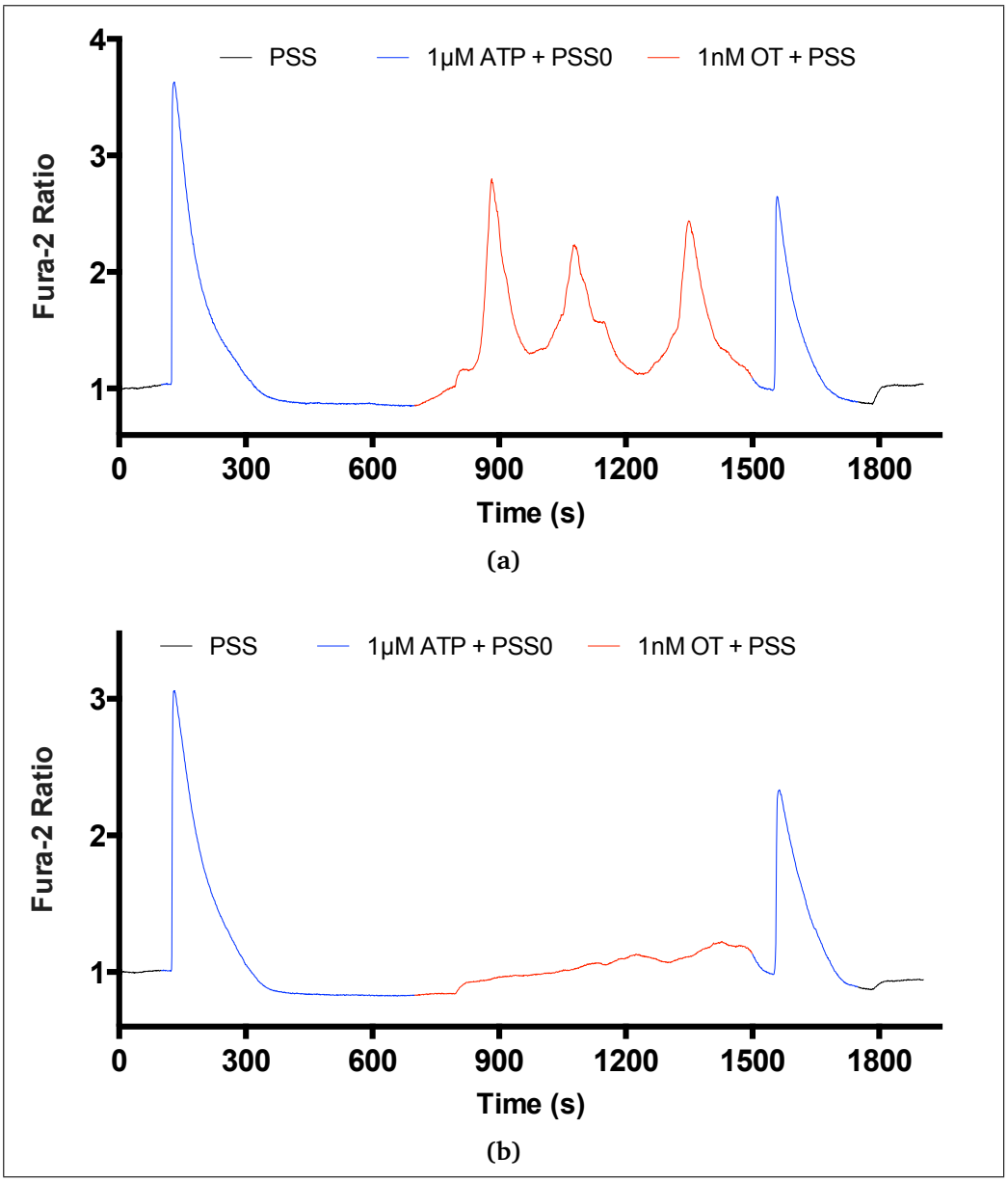

Figure 4.12 *Example traces* OT *oscillations after pre-dosing with* ATP *in the absence of* Ca^{2+}_{EC}. *Upon switching to* OT *with* $\left[Ca^{2+}\right]_{EC}$ *of* $2\ mM$ *oscillations ensue without the initial 'setting' pulse. A second application of* ATP *results in a similar initial transient response to the first application.*

morphology, albeit often with slightly reduced amplitude, to the initial transient seen after the first application of ATP.

4.2.5 IP3

The previous section demonstrated that the period of the oscillations is much shorter in the case of ATP-induced oscillations than in *OT*-mediated oscillations in Chapter 3. One possible explanation for this would be that stimulation by ATP results in more successful stimulation of the PLC pathway than *OT* stimulation (§1.1).

GPCRs carry information within the cell via two major signalling pathways: the activation of G_s or G_i protein coupled receptors results in a variation of the cyclic AMP (cAMP) level, and the activation of G_q protein coupled receptors results in a transient increase of intracellular Ca^{2+}, via the secondary messenger $InsP_3$. After the GPCR G_q activation, however, the lifetime of $InsP_3$ is very short (less than 30 sec) before being degraded into IP_2 and then IP_1. Fortunately, after activation of the GPCR, IP_1 can accumulates in the cell upon addition of $LiCl$ (§2.7). The amount of accumulated IP_1 can be precisely quantified using a CisBio IP-One Tb assay (Protocol 7).

Before commencing measurement, it is first necessary to establish a sensible duration to allow for the biggest dynamic range from the assay. Figure 4.13 shows the time course data for the assay on application of 100 nM OT and 100 μM ATP. The response of the assay to OT appears linear with a linear-regression R^2 value of 0.96 and does not appear to tail off. The ATP response appears to be similar but has much shallower gradient and a linear-regression $R^2 = 0.8838$.

Dose-response data was then collected by applying ligands of different concentrations to the wells and recording their response. Figure 4.14 demonstrates the conventional sigmoidal dose-response and the values for that response are given in curve the data for which are in Table 4.1.

The EC_{50} value of the ATP sensitive component is much higher than the OT sensitive component which is as expected physiologically as much higher concentrations are needed to stimulate Ca^{2+} oscillations.

The maximal IP_1 reading, demonstrated by the top value in the parameterisation (Table 4.1), is much higher for the *OT* response suggesting that much more IP_3 was produced over the time period than in the case of ATP. This result is the opposite than you would have intuitively expected given that the ATP-induced oscillations are of much higher frequency than those induced by OT.

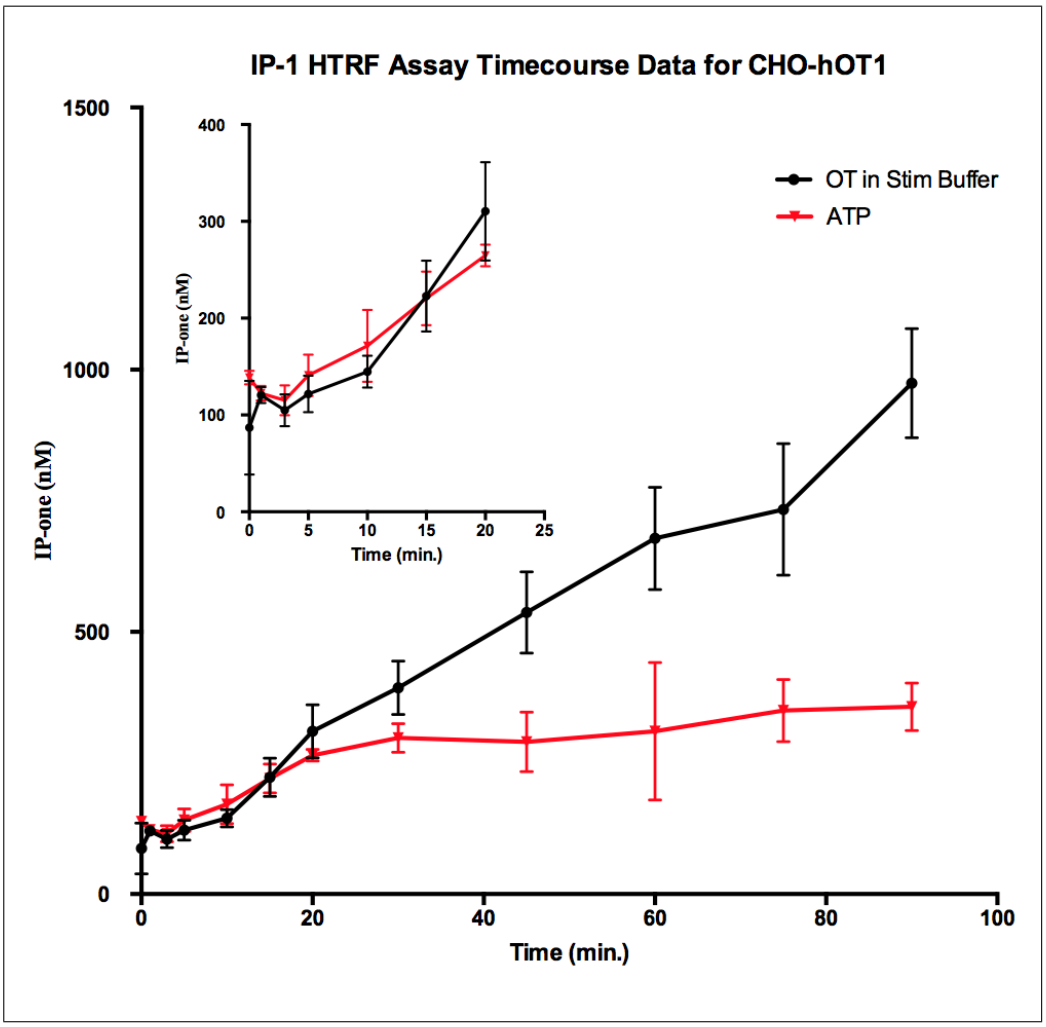

Figure 4.13 *IP1-1 HTRF Assay Timecourse Data for CHO-hOT1 cells*

Ligand	OT	ATP
Bottom	106.7	112.7
Top	961.2	272.2
EC_{50}	$102.4\,nM$	$8.748\,\mu M$

Table 4.1 *Sigmoidal dose-response parameters*

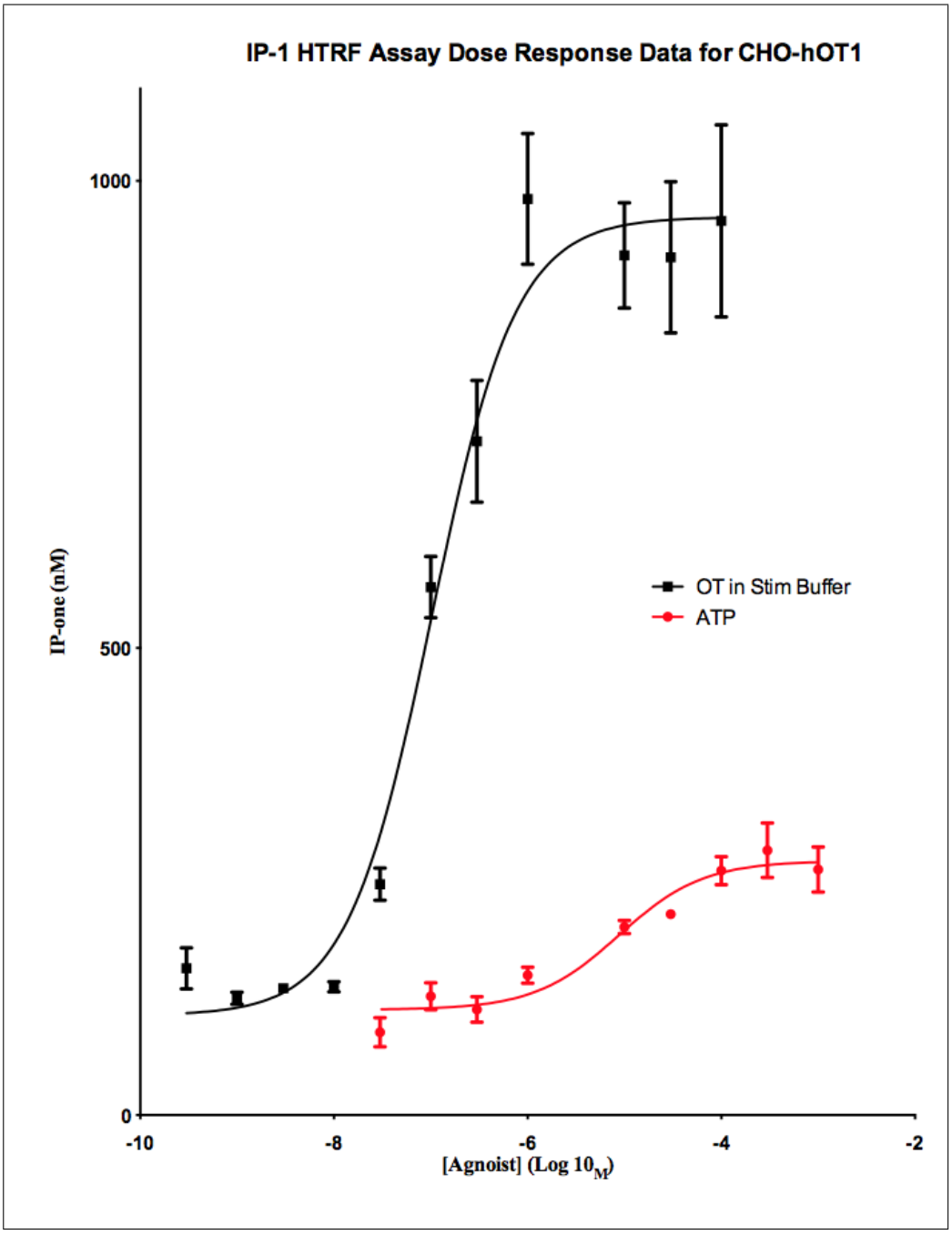

Figure 4.14 *IP1-1 HTRF Assay Dose Response Data for* CHO–hOT *cells.*

4.3 Discussion

Chapter 3 revealed the importance of Ca^{2+}_{EC} in establishing *OT*-induced Ca^{2+} oscillations. When extracellular Ca^{2+} was removed, an initial transient was seen but *OT*-induced Ca^{2+} oscillations did not commence. This chapter initially investigated both the role of $\left[Ca^{2+}\right]_{EC}$ in *OT*-induced Ca^{2+} oscillations. *OT*-induced Ca^{2+} oscillations were present when $1\ nM$ *OT* was applied in the presence of

$\left[Ca^{2+}\right]_{EC} = 0.5,\ 2$ and $4\ mM$. When $\left[Ca^{2+}\right]_{EC}$ was increased beyond $4\ mM$, the cells were unable to handle this level of increased entry of Ca^{2+} through the plasma membrane. This raises questions about the role of Ca^{2+} storage within the cytosol and, in particular the role of the ER Ca^{2+} pump and ER buffering which are addressed in Chapter 5.

The period, area and full-width half-magnitude of *OT*-induced Ca^{2+} oscillations was shown to decrease with increasing $\left[Ca^{2+}\right]_{EC}$. This was thought to be due to the potentiation, by Ca^{2+}, of calcium extrusion processes through the plasma membrane, such as the PMCA and the $Na^{+}/Ca^{2+}-$exchanger. This lead to an investigation into the role of these two mechanisms.

The action of the $Na^{+}/Ca^{2+}-$exchanger is known to require Na^{+}_{EC} to export Ca^{2+} from the cell. Iso-osmotically substituting Na^{+} for sucrose in the PSS resulted in an effectively Na^{+}-free PSS. In the absence of Na^{+}_{EC}, *OT*-induced Ca^{2+} oscillations were potentiated in terms of their frequency and their area, presumably due to the reduced function of $Na^{+}/Ca^{2+}-$exchanger. This probably means other modes of Ca^{2+} removal were employed. These process operate most efficiently at different $\left[Ca^{2+}\right]_{i}$ and indeed are able to extrude Ca^{2+} at a different rate. The $Na^{+}/Ca^{2+}-$exchanger works best at high $\left[Ca^{2+}\right]_{i}$ and has a very high rate of exchange as described above and thus both the increased frequency and area of oscillations are to be expected when the efficacy of this process is removed.

Inhibiting Ca^{2+} extrusion from the cell by inhibiting the PMCA using $200\ \mu M$ Caloxin 3A1 resulted in a significant reduction in the period of oscillations. Previous studies using Caloxin 2a, for instance [38], had shown that the PMCA was essential for Ca^{2+} oscillations to establish. However, the normal response was for an initial transient to occur but not return to basal $\left[Ca^{2+}\right]_{i}$, instead remaining at a new, higher than basal, 'steady-state' $\left[Ca^{2+}\right]_{i}$. Here this pattern is not seen, most likely because, rather than complete inhibition of PMCA the aim here was to reduce its function to see the role it has in modulating *OT*-induced Ca^{2+} oscillations. Given that this is the case, the same argument holds for PMCA-blocking as for the $Na^{+}/Ca^{2+}-$exchanger since the role of the PMCA is similar to that of the $Na^{+}/Ca^{2+}-$exchanger. Both the efficient range and the rate of extrusion by the PMCA are lower than that of the $Na^{+}/Ca^{2+}-$exchanger but one would expect reducing its efficacy to increase the frequency of oscillations since $\left[Ca^{2+}\right]_{i}$ is forced to remain artificially high for longer than normal. This argument applies to understanding why the area of those oscillations is increased. The full-width half-magnitude is significantly attenuated in the presence of Caloxin 3A1 which matches the corresponding data for Caloxin 2A1 inhibition of PMCA in [38].

ATP was employed as further way of manipulating Ca^{2+} entry into the cell. ATP was used to provide an additional Ca^{2+} entry mechanism through its activation of Ca^{2+}-permeable $P2_x$ receptors. The initial transient showed a similar dose-dependence to *OT*-induced Ca^{2+} oscillations. The established ATP-induced Ca^{2+} oscillations show dose dependence. Critically, ATP-induced Ca^{2+} oscillations are at much higher frequency than *OT*-induced Ca^{2+} oscillations.

The possibility that ATP acting on $P2_x$ receptors resulted in more $InsP_3$ production than *OT* acting on *OT* receptors was eliminated by using the CisBio IP-One assay to determine the amount of $InsP_3$ being produced. This technique was not sensitive enough to $InsP_3$ to have its dynamic range in the concentration ranges *OT*-induced Ca^{2+} oscillations and ATP were seen in imaging experiments. However, the dynamic range of the EC_{50} curve shown in Figure 4.14 was almost ten-fold that of ATP than in the case of *OT*. This is precisely the opposite from what would have been the case had $1\ \mu M\ ATP$ better stimulated the G_q cascade via $P2_x$ receptors than $1\ nM$ *OT* could via *OT* receptor. It is thus likely that increased influx of Ca^{2+} into the cell through $P2_y$ receptors resulted in the increase in ATP-induced Ca^{2+} oscillations period and area over *OT*-induced Ca^{2+} oscillations.

Moreover, application of $1\ \mu M\ ATP$ in the absence of extracellular Ca^{2+} resulted in an initial transient much the same as for *OT*-induced Ca^{2+} oscillations. The $\left[Ca^{2+}\right]_i$ is lower after the transient and ATP-induced Ca^{2+} oscillations cannot establish, perhaps, since the ER has emptied. However, upon switching ATP in Ca^{2+}-free PSS to Ca^{2+}-containing PSS with $1\ nM$ *OT*, *OT*-induced Ca^{2+} oscillations establish but without the initial 'setting' transient for virtually all other initial application experiments. When ATP in Ca^{2+}-free PSS was reapplied after these oscillations established, a transient Ca^{2+}-response was seen with the same morphology as the original ATP-induced transient. Taken together, the likely explanation for this is that in the absence of extracellular Ca^{2+}, an application of ATP causes the Ca^{2+}-stores, in particular the ER to empty. Reintroduction of Ca^{2+} and *OT* resulted in oscillations which started with a reduced component of Ca^{2+} release from the ER. These oscillations were sufficient to refill the store enough for an ATP-induced transient to occur.

4.4 Conclusion

Extracellular Ca^{2+} has a vital role in *OT*-induced Ca^{2+} oscillations in *CHO–hOT*. Removing Ca^{2+}_{EC} entirely prevents *OT*-induced Ca^{2+} oscillations from establishing at all whilst varying its concentration from $0.5\ mM\ Ca^{2+}$ upwards leads to

ever more frequent *OT*-induced Ca^{2+} oscillations until concentrations in excess of $5\ mM$ which cause a catastrophic Ca^{2+} release and no *OT*-induced Ca^{2+} oscillations.

Varying the cell's ability to extrude Ca^{2+} impacts on *OT*-induced Ca^{2+} oscillations. Partial inhibition of the PMCA by Caloxin 3A1 and removal of Na^{+}_{EC} to remove Ca^{2+} extrusion via the $Na^{+}/Ca^{2+}-$exchanger results in a potentiation of the frequency of *OT*-induced Ca^{2+} oscillations when compared with control samples.

Introducing an additional method of Ca^{2+} entry via $P2_x$ receptors using ATP significantly increased the activity of *OT*-induced Ca^{2+} oscillations. In particular, when a cell is pre-treated with ATP in the absence of Ca^{2+}_{EC}, *OT*-induced Ca^{2+} oscillations oscillations begin without the initial 'setting' transient when *OT* and Ca^{2+} is reintroduced simultaneously. When ATP is reapplied in Ca^{2+}-free PSS, an identical initial transient to its first application is seen. This suggests the cell's store had become depleted in the absence of Ca^{2+}_{EC} but was able to refill itself whilst *OT* and Ca^{2+} were present. This motivates the investigation into the role that the ER and its buffering mechanisms have in *OT*-induced Ca^{2+} oscillations in the following chapter.

Chapter 5

Manipulating ER Ca^{2+} Uptake and Buffering

5.1 Introduction

As identified in §1.2, a vital aspect of Ca^{2+} signalling is a cell's ability to maintain a very low cytoplasmic Ca^{2+} concentration whilst also having the capacity to allow $\left[Ca^{2+}\right]_i$ to suddenly rise and then restore to its original low level. These processes are facilitated by the intracellular stores of calcium which allow cyclic sequestering and releasing Ca^{2+} as needed for signalling. The cell's major store for this purpose is the lumen of the endoplasmic reticulum, which is also referred to as the sarcoplasmic reticulum in the case of muscle cells.

5.1.1 Rapid Ca^{2+} Release from the ER

As introduced in Figure 1.7, one of the products of phosphatidylinositol 4,5-bisphosphate ($PtdInsP_2$) breakdown is $InsP_3$ which is responsible for the release of Ca^{2+} from the ER via the $InsP_3$-sensitive $InsP_3R$ on the ER membrane [32].

Originally termed $P400$, when discovered as glyco-proteins involved in the development in mutant mice, there are three paralogs of the $InsP_3R$ expressed differently between different tissue types. The receptors are tetrameric in conformation with a C-terminal domain. Each subunit has a molecular weight of $313kDa$ and contains a relatively unselective cationic pore which allows the transport of Ca^{2+} through the membrane. Each subunit of the $InsP_3R$ also contains an arginine and lysine rich region at the N-terminal end which acts as a ligand binding

site for the protein in a similar way to that described for plasma membrane receptors in Chapter 4. $InsP_3$ acts as a ligand binding to the $InsP_3R$, opening the channel to allow Ca^{2+} through. The N-terminal region is on the cytoplasmic side of the membrane and has binding sites for two ATP molecules and at least two Ca^{2+} ions [97].

Importantly, $InsP_3$ is not the only regulator of the $InsP_3R$: their activation is also controlled by $\left[Ca^{2+}\right]_i$ and $\left[Ca^{2+}\right]_{ER}$ [57]. This way, Ca^{2+} acts not only as a co-activator of the $InsP_3R$ but also allows modulation of $InsP_3$ mediated Ca^{2+} release by current levels of cytoplasmic and intraluminal $\left[Ca^{2+}\right]$. This results in a 'bell-shaped' response as demonstrated in [15] and discussed further in Chapter 4.

This feed-forward style control mechanism is vitally important since it means that relatively low Ca^{2+} rises gain a control on Ca^{2+} release meaning that small changes in $\left[Ca^{2+}\right]$ can be rapidly converted into large changes. Inhibition at high $\left[Ca^{2+}\right]_i$ adds a level of moderation which might attempt to avoid extreme $\left[Ca^{2+}\right]_i$ such as those seen in Figure 4.1.

5.1.2 Ca^{2+} Uptake into the ER

As with the plasma membrane, Ca^{2+} needs to be actively pumped through the membrane of the ER and then released from it as required. The membrane of the ER thus contains calcium pumps which pump cytoplasmic Ca^{2+} into the lumen of the ER. These pumps, commonly referred to as Sarco/Endoplasmic Reticulum Calcium ATPase (SERCA) pumps, can make up to 80% of the protein component of the membrane in the case of smooth muscle at a density of up to 25,000 per μm^2 and, as such their importance to the cell's signalling activity becomes clear [93].

Similarly to their plasma-membrane cousins, the pumps use the breakdown of ATP to extract the energy to actively transport Ca^{2+} from the region of very low Ca^{2+} concentration to the relatively high Ca^{2+} concentration of the lumen of the ER. Another similarity to the plasma membrane equivalent is that they are also P-type ATPases due to the involvement of a phsophoryl intermediate in the pumping step. That is, a phosphatase group is added to an aspartate residue on the polypeptide causing a conformational change which results in the movement of Ca^{2+} ions across the membrane where they are then released. Once this phosphate group is removed, the enzyme is restored to its original conformation, allowing further cycles of ATP hydrolysis which thus results in Ca^{2+} being pumped. It is thought that two Ca^{2+} ions are transported for each

molecule of ATP which is hydrolysed [35].

Like the PMCA, a SERCA pump also has ten transmembrane spanning regions defined in its polypeptide. There is, however, very little sequence homology between the two types of Ca^{2+} pumps despite their topological and functional similarity. The ER protein contains two main domains with a third, smaller one, on the luminal side of the membrane. The calcium channel is one of these domains and is thus buried in the membrane with Ca^{2+} ions binding near the centre line of the membrane. The other domain contains the ATPase activity on the cytoplasmic side of the membrane and the site of phosphorylation.

In experiments where a functional Ca^{2+}-ATPase was reconstituted into a phospholipid membrane, it was shown to pump Ca^{2+} ions at a rate of about 30 s^{-1}. Another result demonstrated an ability of these reconstituted pumps to work in reverse mode, pumping Ca^{2+} in the opposite direction if the $\left[Ca^{2+}\right]$ was artificially reversed. This situation seems unlikely in vivo but has helped to elucidate the exact molecular mechanism involved in the pumping behaviour of Ca^{2+}-ATPases [34].

SERCA pumps arise from three genes in a tissue-specific manner; the genes SERCA1 and SERCA2 are expressed in different types of muscle tissue and SERCA3 is expressed in non-muscle. A lactone, thapsigargin is a highly specific inhibitor of SERCA activity which does not inhibit the activity of plasma membrane pumps. Thapsigargin, however, irreversibly blocks the activity of the SERCA and thus CPA a reversible SERCA inhibitor is used here so the restorative effects (or otherwise) after wash-out can be seen.

The action of the SERCA pump is controlled, rather than continuous, since such regulation would allow Ca^{2+} to be rapidly removed, or more slowly if an elongated response were required. High $\left[Ca^{2+}\right]$ increases the activity of the pump whilst high $\left[Ca^{2+}\right]_{EC}$ decreases activity [28] .

5.2 Results

5.2.1 Manipulating intrastore $[Ca^{2+}]$ with SERCA Inhibitor CPA

Figure 5.1 shows an exemplar trace when a relatively high dose — 5 μM — of the SERCA blocker CyPA is applied to cells oscillating in the presence of 1 nM *OT*.

Immediately upon application, a transient response is seen which appears wider than the ordinary oscillations. Rather than returning to basal Ca^{2+} levels, the system then appears to reach a steady state plateau at a significantly increased

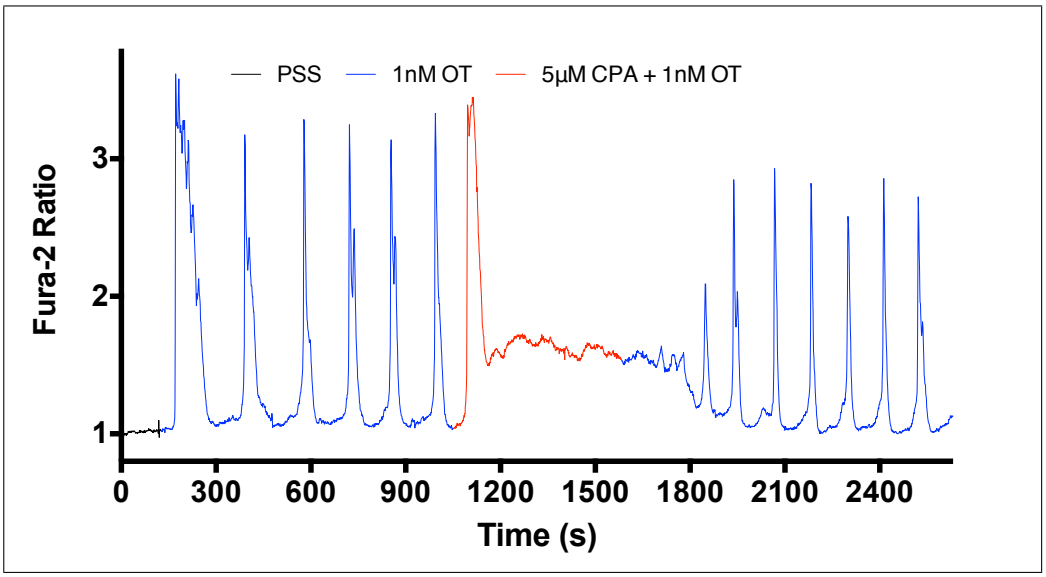

Figure 5.1 *Example trace of the effect on oscillations of the application of* $5\ \mu M$ *CPA*

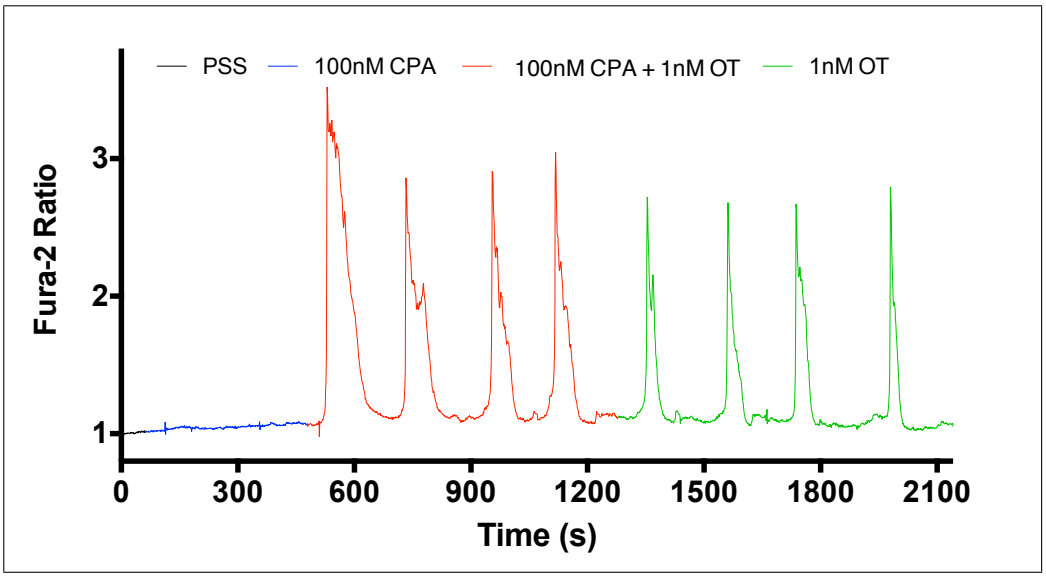

Figure 5.2 *Example trace of the effect on oscillations of the application of* $100\ nM$ *CPA*

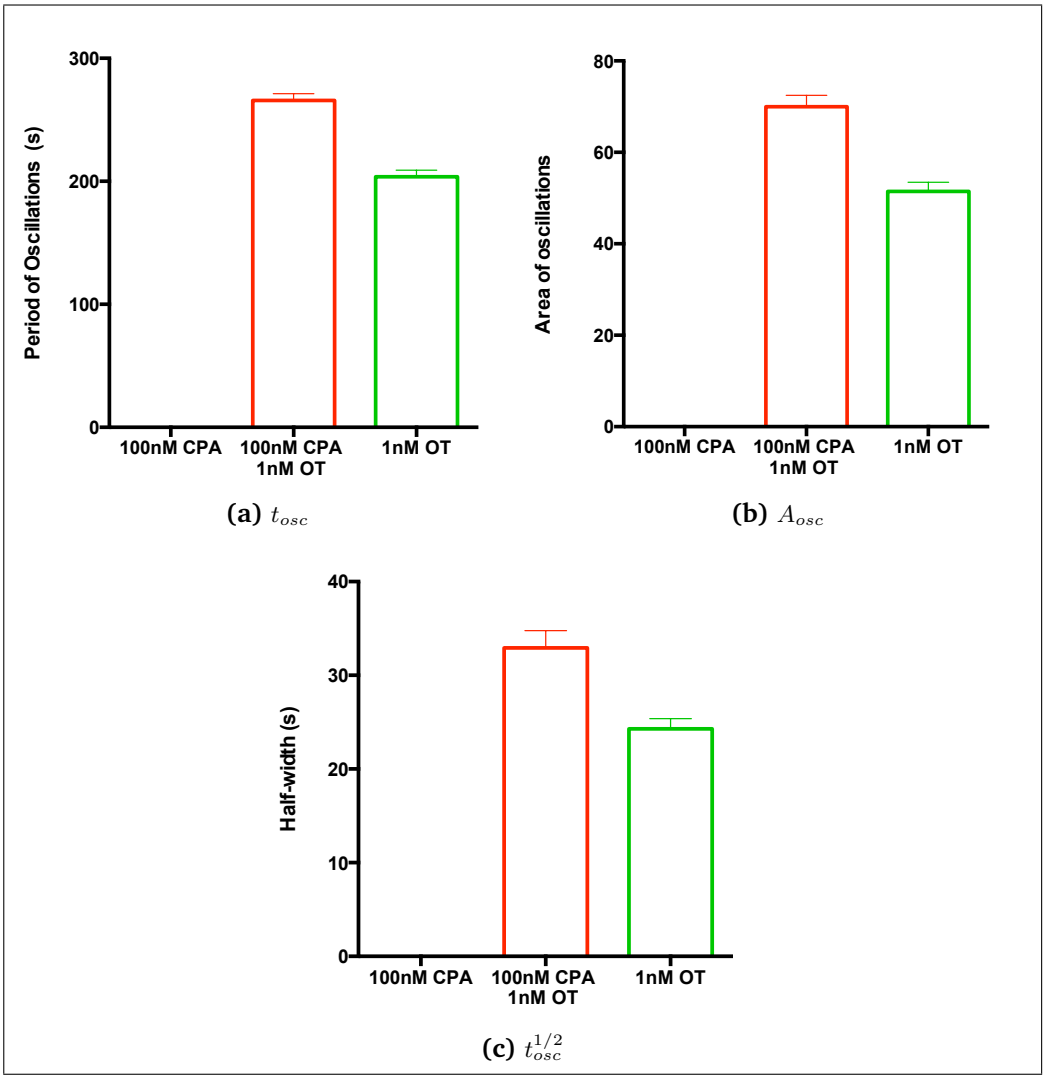

(a) t_{osc} **(b)** A_{osc} **(c)** $t_{osc}^{1/2}$

Figure 5.3 *Summary data for the effect on oscillations of the application of* $100\ nM$ *CPA. Data points were taken from all oscillatory cells within at least 3 different petri dishes with oscillatory cell numbers of* 59 *and* 67*, in the presence and absence of CPA, respectively.*

level, here with a ratio of approximately 1.5. On removal of CPA, oscillations are restored and the trough of oscillations returns to its original level.

Pre-treatment with a lower dose — $100\ nM$ — of CPA in the absence of *OT* resulted in no distinguishable change to basal $[Ca^{2+}]$, nor did any Ca^{2+} oscillations occur. Following this priming, an application of 1 nM *OT* induced oscillations which were broader, had increased area and had longer period than those after the CPA wash out. A typical trace of such an experiment is shown in Figure 5.2 and the summary data in Figure 5.3 confirms this.

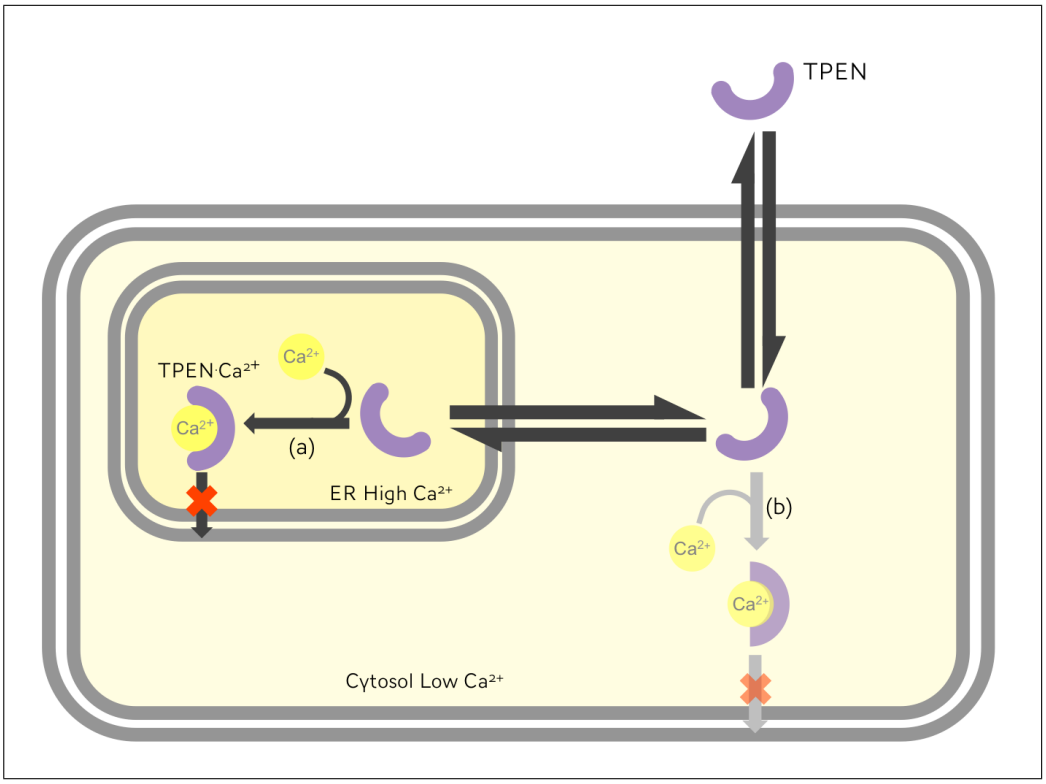

Figure 5.4 *The action of TPEN in increasing luminal buffering: Membrane-permeant, Ca^{2+} free TPEN becomes trapped in a compartment (red crossed arrows) upon chelation with Ca^{2+}. Because of the higher concentration of Ca^{2+} in the ER much more TPEN becomes trapped there (process (a)) rather than in the lower concentration cytosol (process (b)). the stores.*

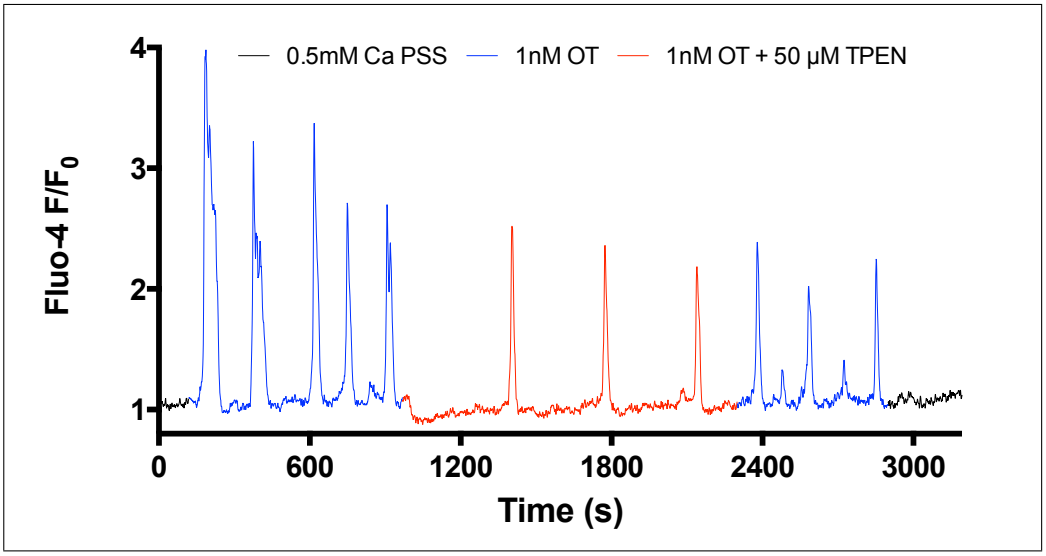

Figure 5.5 *Example trace of the effect on oscillations of the application of $50\ \mu M$ TPEN.*

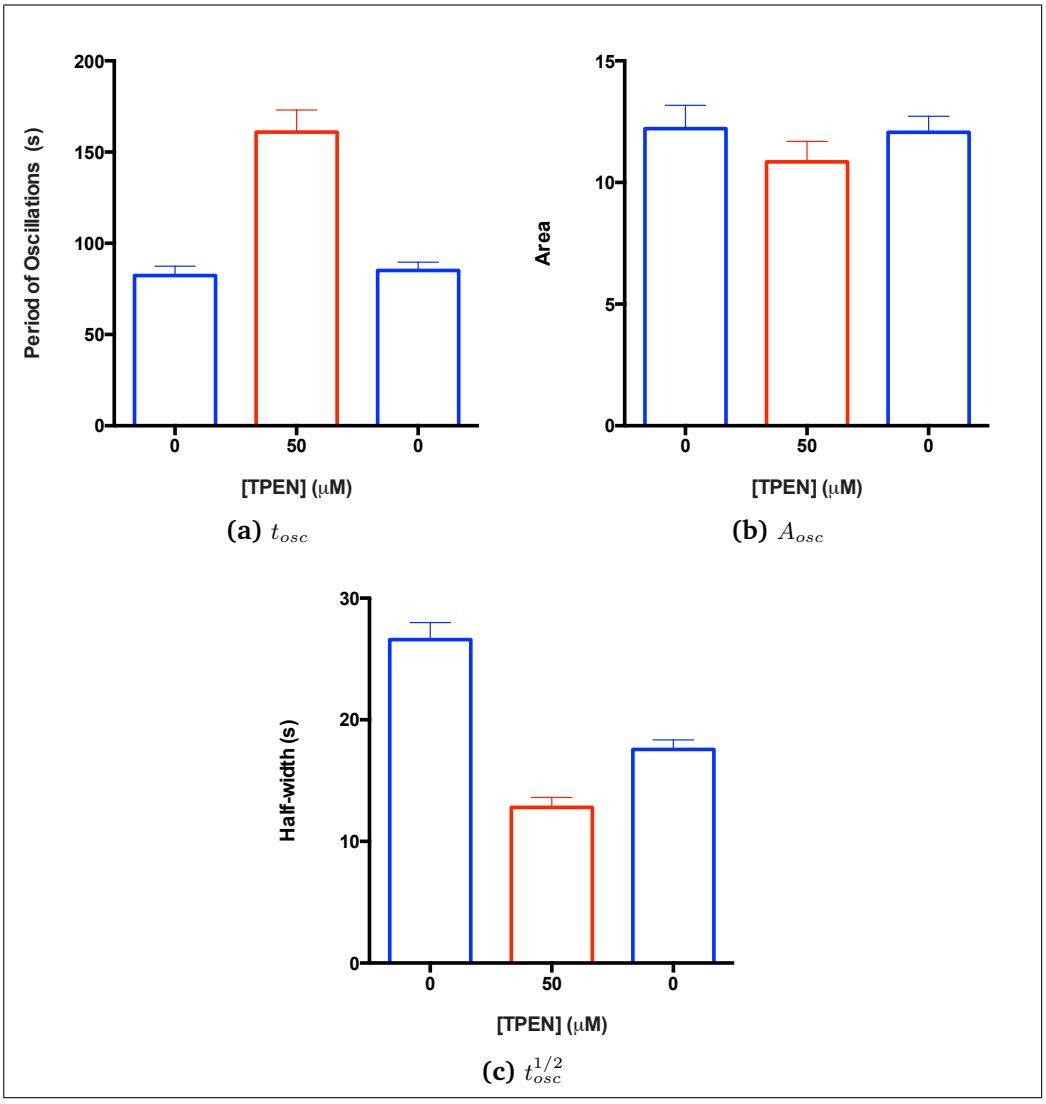

(a) t_{osc} **(b)** A_{osc} **(c)** $t_{osc}^{1/2}$

Figure 5.6 *Summary data for the effect on oscillations of the application of* $50\ \mu M$ *TPEN. Data points were taken from all oscillatory cells within at least 3 different petri dishes with cell numbers of* 165, 125 *and* 127 *for the three stepped concentrations of TPEN, respectively.*

5.2.2 Manipulating intrastore $[Ca^{2+}]$ with a membrane permeant Ca^{2+}-chelator, $TPEN$

Physiologists have long used the 'ammonium pre-pulse' technique to study intracellular pH regulation [19]. When exposed to ammonia/ammonium $\left(NH_3/N_4^+\right)$, cells initially alkalise but then continued exposure to the weak base allows protons (originating from endogenous acid loading processes) to accumulate in the cell. This is because they are rapidly picked up by NH_3 (a weak base capable of penetrating the cell membrane) to form the cell impermeant protonated NH_4^+. On removal of NH_3/N_4^+ from the extracellular media, NH_3 rapidly exits the cell, causing the dissociation of NH_4^+ and H^+ leaving its interior 'loaded' with protons

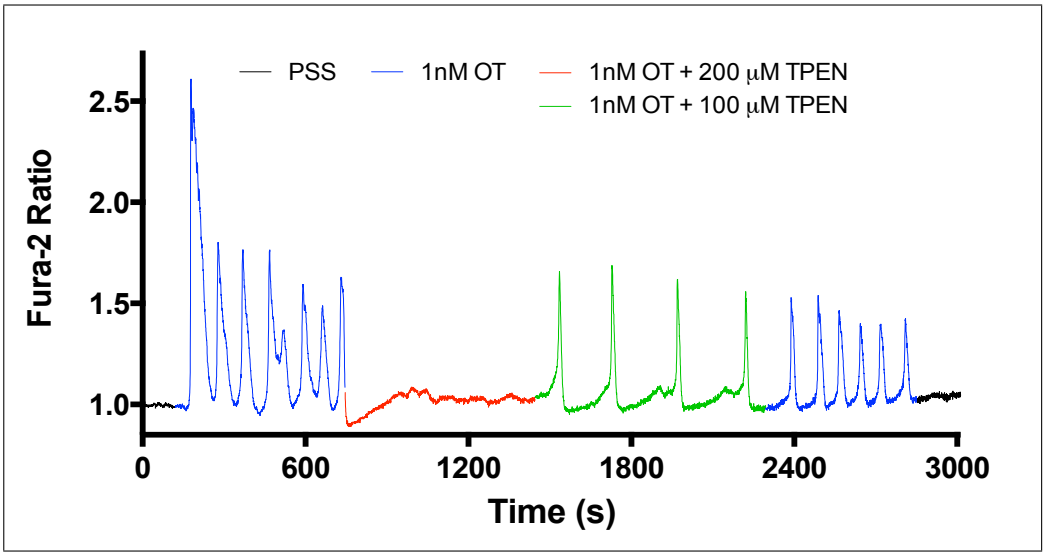

Figure 5.7 *Example trace of the cessation of oscillations in the presence of* $200\ \mu M$ *TPEN and their restart, with reduced period, when reduced to* $100\ \mu M$*. Oscillations return to normal period upon TPEN wash-out.*

and thus significantly acidified.

TPEN is used here in an analogous way to control the free $[Ca^{2+}]$. Originally described as a scavenger of heavy metals [9], it has a K_d of $40-130\mu M$ for Ca^{2+} making it ideally suited for manipulating the intraluminal $[Ca^{2+}]$. Like ammonia/ammonium, TPEN's neutral, uncomplexed form is membrane-permeant and becomes charged and membrane-impermeant when bound to Ca^{2+} [29]; thus when free TPEN partitions into compartments of high $[Ca^{2+}]$, it chelates Ca^{2+}, lowering the free $[Ca^{2+}]$ and becomes trapped in the process (Figure 5.5).

Figure 5.5 shows a typical trace from experiment where 1nM-oxytocin was applied at $t = 100s$ and followed by the introduction of 50 μM TPEN at $t = 1000s$ which was kept in place until it was washed out at $t = 2300s$. The following effects were observed:

- Prior to the application of TPEN, oxytocin-induced oscillations establish themselves.
- These oscillations halt upon application of TPEN and the basal level of $[Ca^{2+}]_i$ is reduced significantly.
- The $[Ca^{2+}]_i$ slowly recovers over a period of approximately five minutes
- Oscillations then resume at a lower frequency
- Upon the removal of TPEN, higher frequency oscillations reinstate themselves.
- Oscillations cease when *OT* is washed out.

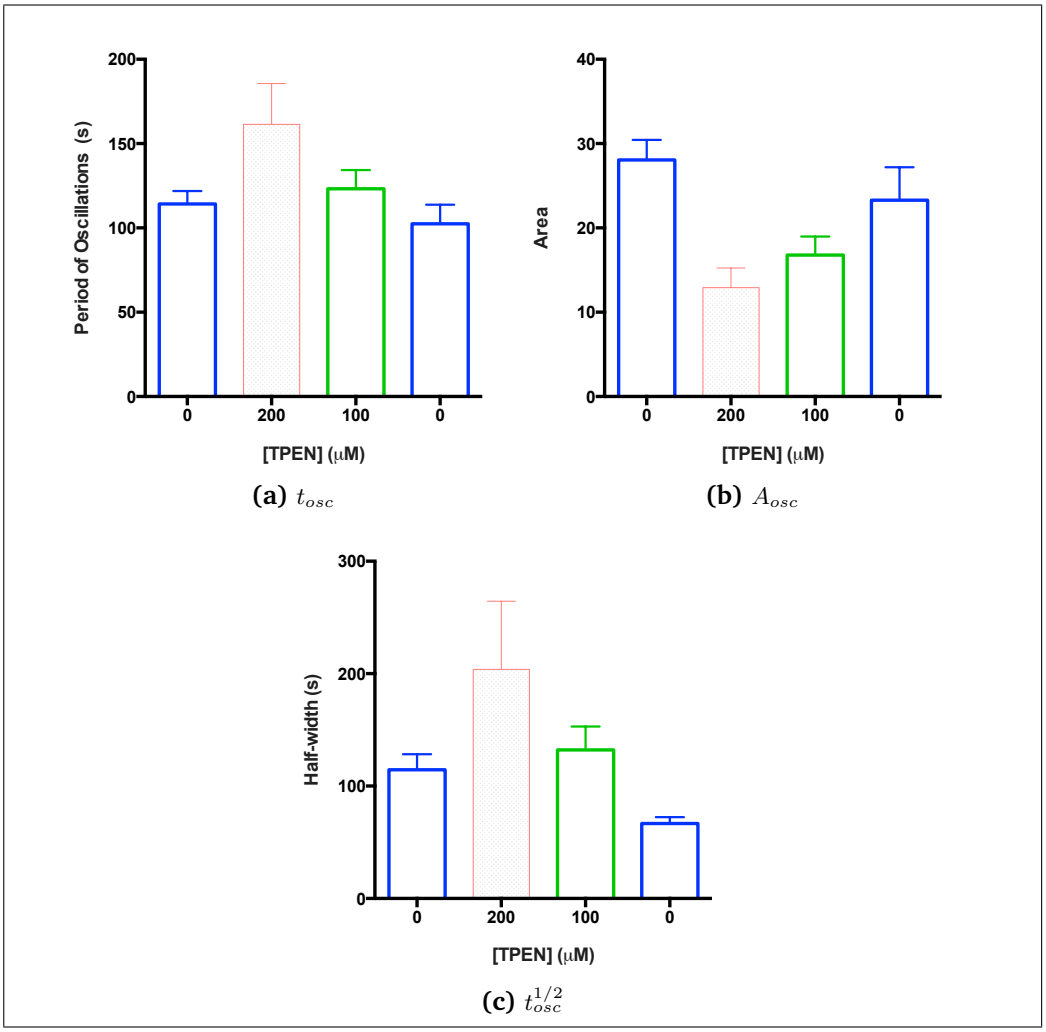

Figure 5.8 *Summary data of the effect on oscillations of the application of higher concentrations of TPEN. Data points were taken from all oscillatory cells within a petri dish with cell numbers of* 48 *with only* 6 *cells remaining oscillatory in the presence of* $200\ \mu M$ *TPEN.*

This is supported by summary data in Figure 5.6 which shows a distinct increase in period of established oscillations in the presence of 50 μM TPEN compared with the oscillations which establish before its application and once it was washed out. The area of the *OT*-induced Ca^{2+} oscillations remains unchanged in the presence of 50 μM TPEN but the half-width of those oscillations is significantly decreased. The half-width partially recovers when TPEN is washed out.

Higher concentrations of TPEN abolished oscillations completely, as demonstrated, for instance, in Figure 5.7. Similar behaviour to Figure 5.5 is seen:

- Oscillations establish on application of 1nM *OT*
- When 200 μM TPEN is added, the basal level of $\left[Ca^{2+}\right]_i$ decreases and recovers, again over a period of approximately 5 minutes

- In this higher concentration, however, oscillations do not restart but some variation in the baseline is seen
- When the concentration on TPEN is reduced to 100 μM, oscillations restart, at a reduced frequency than in the absence of TPEN
- Upon washout of TPEN, oscillations return to their original, increased frequency.
- Oscillations cease when *OT* is removed

The summative data for this experiment, shown in Figure 5.8, supports the above observations. Oscillations were seen in the presence of 1nM OT, but were abolished in all bar 6 out of 48 cells when 200 μM TPEN was introduced. The oscillations restarted in all bar 3 cells when $[TPEN]$ was reduced to 100 μM with increased period from the TPEN-free oscillations which preceded the application of TPEN and those which follow once TPEN was washed out. The area of oscillations was decreased and half-width increased in 100 μM TPEN. Both measures recovered upon removal of TPEN. The 200 μM TPEN data for the 6 cells which remained oscillating is shown for completeness with a thin border and grey colouring in Figure 5.8.

Those cells that remained able to oscillate in 200 μM TPEN exhibit the same pattern of increased period, decreased area and increased half-width of oscillations as for 100 μM TPEN only with a more extreme effect.

5.3 Discussion

Elucidating the role of the lumen of the ER is vital for understanding Ca^{2+} signalling.

CPA is known to block the SERCA pump when applied in high doses, here 5 μM. Therefore, it is used here to manipulate the re-uptake of Ca^{2+} into the ER after release through $InsP_3R$. Blocking all SERCA pump activity yielded an initial transient with wider halfwidth than the preceding oscillations. This fits with the hypothesis proposed in §1.1 that the SERCA acts as an 'OFF' reaction, responding to the initial rise of Ca^{2+} by working to restore the level of Ca^{2+} to the basal level. Whilst the action of other mechanisms (such as those controlling Ca^{2+} extrusion through the plasma membrane discussed in the pervious chapter) do manage to return the cytosolic Ca^{2+} most of the way to the basal $\left[Ca^{2+}\right]$, the system cannot return to the steady-state plateau in the absence of SERCA pump activity and oscillations do not establish. This suggests that the SERCA pump, and thus, $\left[Ca^{2+}\right]_{ER}$ is vital for *OT*-induced Ca^{2+} oscillations to occur.

In low doses, here 100 nM, CPA is expected to block only a proportion of SERCA pumps rather than stop all passage of Ca^{2+} through the pumps. It is applied here to establish the impact of manipulating, rather than removing, uptake of Ca^{2+} into the lumen of the ER. Rather than inhibiting *OT*-induced Ca^{2+} oscillations and resulting in an increased steady-state $\left[Ca^{2+}\right]$, a modulation of the oscillations is seen. On pre-treatment, we see no change in basal $\left[Ca^{2+}\right]_i$ suggesting that the system was at steady-state or was able to compensate for any $\left[Ca^{2+}\right]_i$ in and out of cytoplasm. *OT*-induced Ca^{2+} oscillations establish in 100 nM CPA, but when it is removed, the oscillations increase in frequency and decrease in both area and half-time. This suggests that uptake of Ca^{2+} back into the ER via the SERCA pump is vital in maintaing both the frequency and the duration of *OT*-induced Ca^{2+} oscillations.

In addition to investigating re-uptake of Ca^{2+} into the ER, TPEN was used to investigate the impact of varying the concentration of Ca^{2+} in the ER upon *OT*-induced Ca^{2+} oscillations. In vivo, the concentration of free Ca^{2+} ions is buffered by proteins such as calsequestrin and calreticulin. As yet there is no clear evidence of a direct role for this buffering in the ER other than as an easy-to release store. It is clear, however, that the ER would not be able to function normally if the free $\left[Ca^{2+}\right]$ were allowed to vary too much, as it would be in an ER without buffering. The role of the ER is not just as a store of Ca^{2+}— it has other roles in protein folding and trafficking, for instance — and it is possible that the excess free Ca^{2+} ions might hinder this additional functionality. However, it has been suggested that the activity of the SERCA pump is $\left[Ca^{2+}\right]_{ER}$ dependent and it was recently discovered that release of Ca^{2+} from the ER via $InsP_3R$ is known to be modulated by $\left[Ca^{2+}\right]_{ER}$. [57]

Once the TPEN levels have reached equilibrium the vast majority of the TPEN gets trapped in the ER rather than in the cytosol because of the comparatively high $\left[Ca^{2+}\right]_{ER}$. This causes the buffering capacity in the ER to rise and the available $\left[Ca^{2+}\right]_{ER}$ to decrease. 200 μM of TPEN resulted in the cessation of in a vast majority of *OT*-induced Ca^{2+} oscillations whilst lower doses, 50-100 μM resulted in oscillations of reduced frequency. That some cells continue to oscillate in the highest dose of TPEN whilst the majority stop could be explained by the assumption that luminal $\left[Ca^{2+}\right]$ varies to some extent between different cells as does the $InsP_3R$ sensitivity to luminal Ca^{2+}. The initial drop below basal $\left[Ca^{2+}\right]_i$ on application of TPEN can be attributed to an initial influx of TPEN being trapped in the cytosol or to a decrease in Ca^{2+} leak from the ER due to TPEN accumulation in the ER resulting in a decreased $\left[Ca^{2+}\right]_{EC}$.

Once this new Ca^{2+} level within the ER level has stabilised, with lower doses of TPEN, oscillations are able to establish but at a much lower frequency. A possible

rationale here is that the impact of the reduced $\left[Ca^{2+}\right]_{ER}$ reduces the ability of the $InsP_3R$ to release Ca^{2+} into the cytosol. One must be careful of such this conclusion, however, since non-specific effects on the SERCA have been described in [124].

5.4 Conclusion

The ER is a vital moderator of *OT*-induced Ca^{2+} oscillations and, in particular, the concentration therein has a significant impact upon those *OT*-induced Ca^{2+} oscillations. Too low and oscillations are terminated entirely. If Ca^{2+} uptake into the ER is eliminated then not only do oscillations cease but a new steady state of $\left[Ca^{2+}\right]_i$ is reached reflecting a balance between Store-operated Ca^{2+} entry (Chapter 7) and Ca^{2+} removal by the plasma membrane Ca^{2+} pump and $Na^+/Ca^{2+}-$exchanger. Partial inhibition of SERCA pumps provides a way of moderating *OT*-induced Ca^{2+} oscillations.

Chapter 6

Formulating a Model

In order to inform the approach for the thesis, an initial model was needed. This model was based on the work described in §1.4 and was constructed by combining this with an understanding of our model system — the *CHO–hOT* cell line — both from the literature and our experiments.

6.1 Evidence for Utilising a Compartmental Modelling Approach

6.1.1 Homogeneity

Spatial aspects have been shown to be important when considering Ca^{2+} signalling . In particular the distribution of the Endoplasmic Reticulum and mitochondria have proven to be important in models.

Hence the approach taken was to investigate whether such heterogeneity applied in the proposed system model. *CHO–hOT* cells were loaded variously with indicators for the ER (ER-Tracker^{TM} Blue-White DPX), nucleus (Hoechst 33342), plasma membrane (di-3-ANEPPDHQ) and mitochondria (MitoTracker® Green) as per Protocol 1.

This resulted in the images in Figures 6.1 and 6.2. In Figure 6.1 we see a DIC image of the cells in (a) and in (b) the homogeneity of the ER (green) throughout the cytosol right to the plasma membrane of the cell (red). In Figure 6.2 it can be seen that the ER appears almost homogeneously throughout the cytosol of the cell. The distribution of the mitochondria was also homogeneous — i.e. they were regularly spaced throughout the cell. Figure 6.2 shows an overlay of

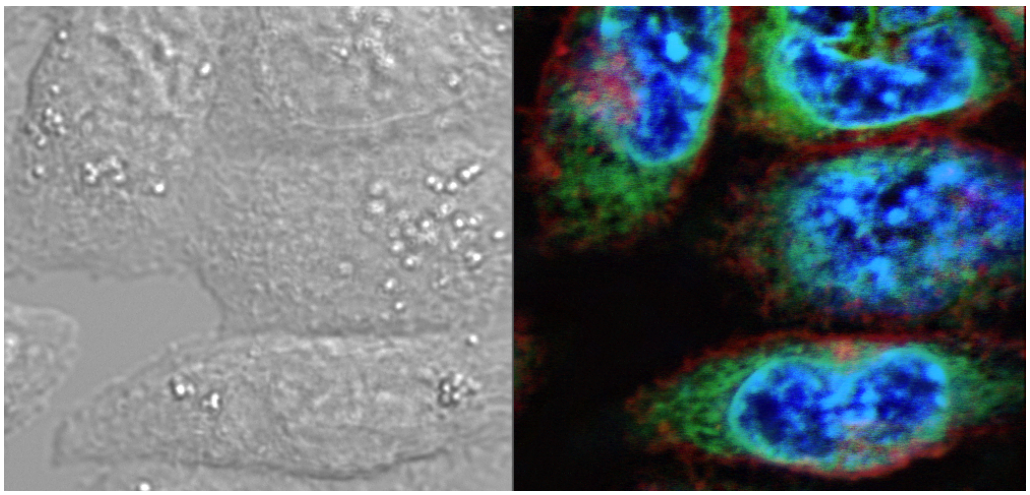

(a) (b)

Figure 6.1 *Images of CHO h-OT cells in (a) DIC and in (b) showing the nucleus (shown in blue, stained using Hoechst 33342), endoplasmic reticulum distribution (shown in green, stained using ER-Tracker^{TM} Blue-White DPX) and the plasma membrane (shown in red, stained using di-3-ANEPPDHQ).*

recordings from both dyes within one cell to demonstrate the co-localisation of the mitochondria with the ER.

6.1.2 Lack of Resolvability of Microdomains

Localised events have been shown to lead to global Ca^{2+} events. Puffs or sparks are coordinated elemental releases from small clusters of RYR and $InsP_3R$. In coronary smooth muscle cells in which both puffs and sparks as well as their resultant calcium waves have been demonstrated to play an important role in Ca^{2+} signalling [18]. Despite the best efforts made it was not possible to resolve either these elementary calcium events nor calcium waves in the *CHO–hOT* cell line.

Visualising such elementary events had previously been performed in coronary smooth muscle [18] using line-scan confocal microscopy. The protocol laid out there was followed exactly in order to attempt to visualise elementary events in *CHO–hOT* cells. The protocol allowed the successful visualisation of elementary events in Human Myometrial Smooth Muscle, recorded at 25 frames per second, which is shown in Figure 6.3. However, when applied to CHO cells the protocol failed to resolve any such events even at 50 frames per second for full cell recordings and just under 75 frames per second using confocal line scanning mode. Several different attempts were made to improve the protocol, including adding slow buffers to the cell to quench global cytosolic Ca^{2+} transients such

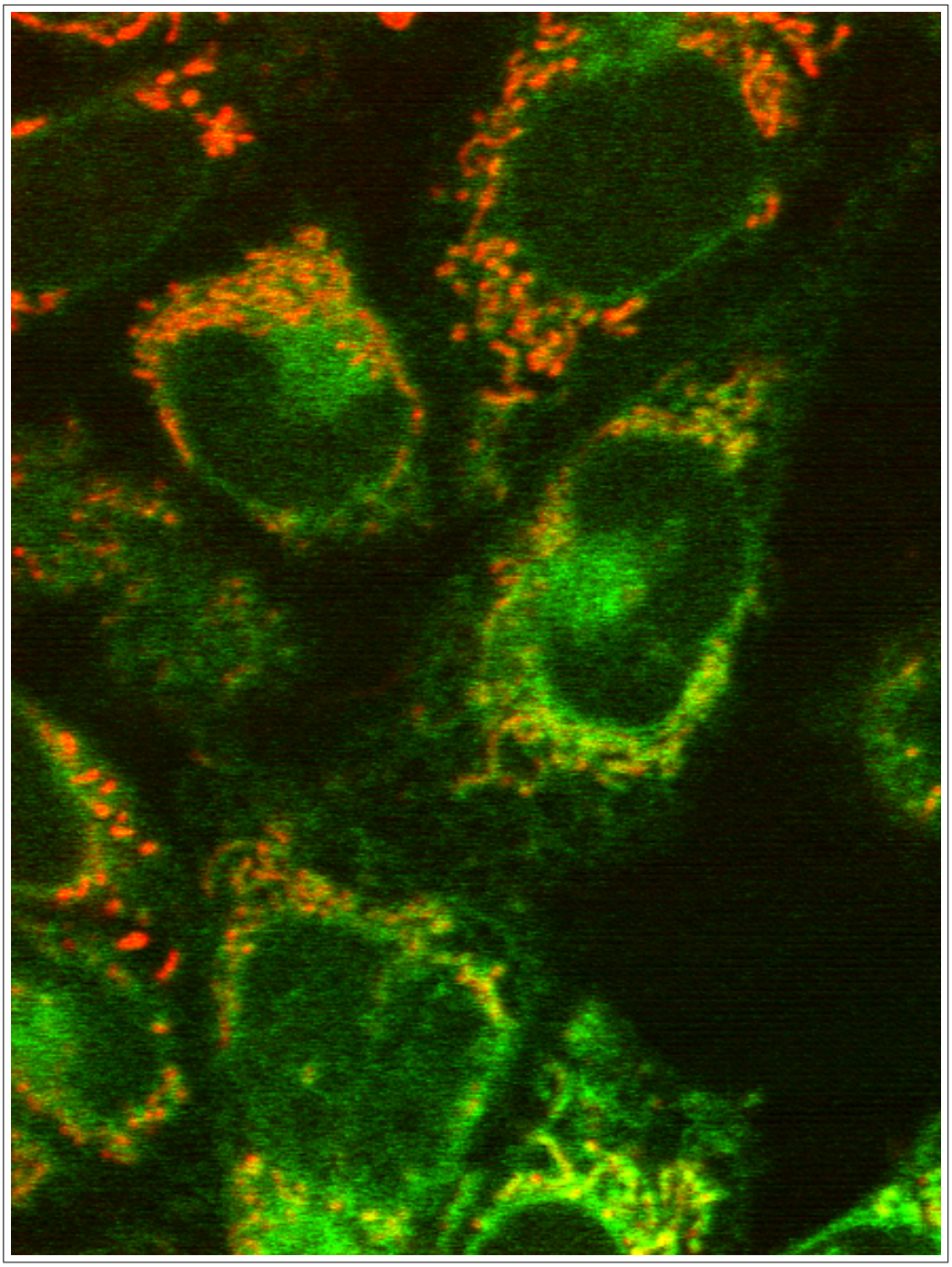

Figure 6.2 *Overlay of mitochondrial image (red) and the Endoplasmic Reticulum (green) in CHO-hOT cells loaded with ER-Tracker^{TM} Blue-White DPX and MitoTracker® Green.*

that the elementary (local) Ca^{2+} releases might be seen but no such events could be observed.

Absence of a phenomenon is not proof that it is not there, of course, but it does suggest that a localised approach in these cells would prove fruitless. In particular, it suggests that any micro-domains of unusually high or low $[Ca^{2+}]$ produced when Ca^{2+} release is triggered are below the resolution of the microscope used in both time and spatial dimensions. The experiments were conducted at $1\ pixel = 0.167\ \mu m$ and 25 frames per second. Thus any localised events relevant to signalling must have been happening on a scale smaller than this or they have been too closely positioned for the individual elementary events to be resolved. Close apposition of elementary Ca^{2+} release events would lead to a smooth appearance of global Ca^{2+} transients as observed in our experiments. Similar 'sparkless' Ca^{2+} release has been previously described in CHO cells overexpressing the cardiac type of ryanodine receptors, for instance in [17]. Because of the homogeneous distribution of the ER and the lack of well-defined localised Ca^{2+} release events, *OT*-induced Ca^{2+} oscillations were modelled here using a whole-cell compartmental modelling approach.

6.1.3 Notation

Throughout the notation $c_i = [Ca^{2+}]_i$, $c_e = [Ca^{2+}]_{ER}$ and $c_o = [Ca^{2+}]_{EC}$ is adopted.

6.2 Two-Pool Model

The two-pool model - so named because of the assumption of the existence of two distinct internal Ca^{2+} stores, one that is sensitive to $InsP_3$ and the other to Ca^{2+}- established itself as one of the first ways to model the $InsP_3$-dependent Ca^{2+} release described in §1.1 [61, 62, 81].

Whilst this model is able to produce an excellent mathematical approximation of the calcium dynamics of the whole-cell, it is typical of early mathematical modelling attempts in that it proposes a new physiological mechanism which gives insight, without necessarily having the physiological evidence for it.

This whole-cell model, a schematic of which is depicted in Figure 6.5, is based upon the assumption that agonist stimulation leads directly to the production of $InsP_3$ which, in turn, causes the release of Ca^{2+} through $InsP_3Rs$ from the $InsP_3$-sensitive store. This released Ca^{2+} then stimulates release of Ca^{2+} from a Ca^{2+} sensitive store.

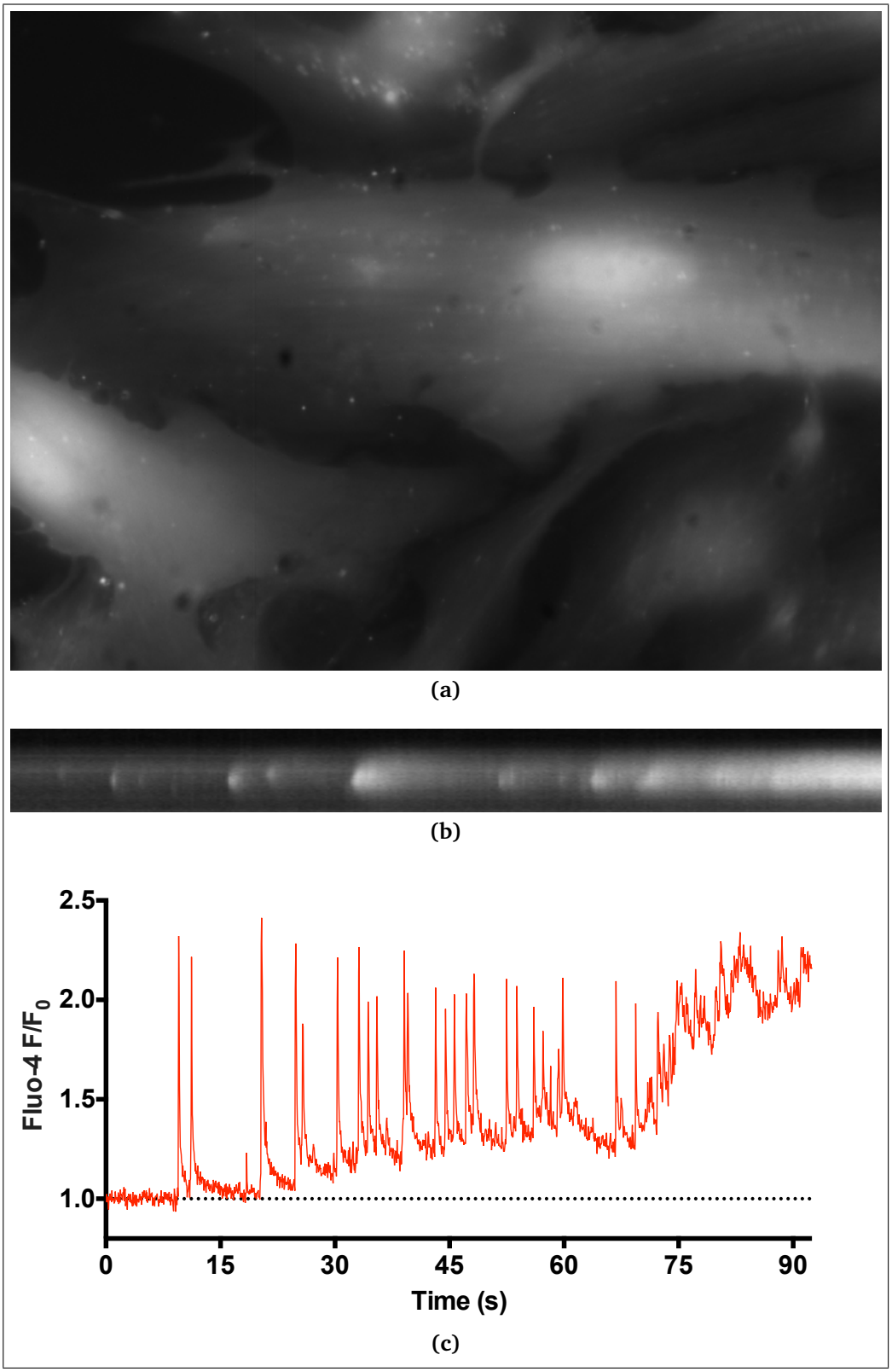

Figure 6.3 *Puffs in myometrial smooth muscle recorded at 25fps. (a) Average recording of stack showing lack of homogeneity of Ca^{2+}, (b) a pseudo line-scan showing that increases in Ca^{2+} start from a localised point and spread out spatially over time and (c) a region of interest analysis of a small area showing fast releases as the local baseline increases from rest to $\sim 90\ s$*

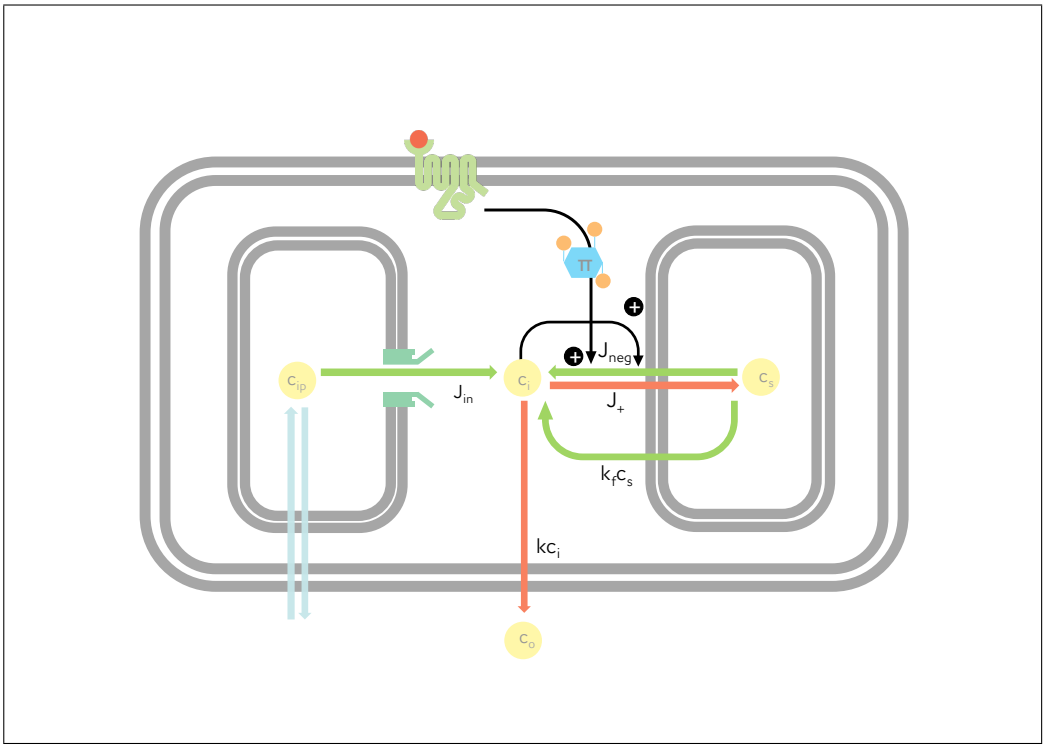

Figure 6.4 *Schematic diagram of the Two-Pool model*

6.2.1 Assumption

This model assumes that the $InsP_3$-sensitive store is close to the membrane and thus the Ca^{2+} concentration in the $InsP_3$ sensitive store is constant as the store is quickly refilled from the extracellular medium as depicted in Figure 6.5.

The model assumes that the calcium concentration in the $InsP_3$ sensitive store is constant, and hence the initial stimulus produces a constant release rate of calcium. Thus the system can be written, using the original notation of Goldbeter and Dupont [47], as:

$$\frac{dc_i}{d\tau} = J_{in} - kc_i - \hat{f}(c_i, c_e), \tag{6.2.1}$$

$$\frac{dc_e}{d\tau} = \hat{f}(c_i, c_e) \tag{6.2.2}$$

with

$$\hat{f}(c_i, c_s) = J_+ - J_{neg} - k_f c_s, \tag{6.2.3}$$

$$J_{in} = v_0 + v_1\pi, \tag{6.2.4}$$

$$J_+ = V_1 \frac{c_i^n}{K_1^n + c_i^n}, \tag{6.2.5}$$

$$J_{neg} = V_2 \frac{c_e^m}{K_2^m + c_e^m} \frac{c_i^p}{K_3^p + c_i^p}. \tag{6.2.6}$$

In this system

- π is the degree of saturation of the $InsP_3R$.
- J_{in} represents the total (constant) entry of Ca^{2+} into the cytosol and consists of
  - the influx v_0 from the extracellular medium and
  - the $InsP_3$ stimulated Ca^{2+} negease $v_1\pi$.
- J_+ and J_{neg} are (respectively) the rates of pumping into a release from the Ca^{2+} sensitive store with
  - V_1 and V_2 demoting their maximum rates.
  - K_1, K_2 and K_3 are the threshold for pumping, release and activation
  - n, m and p are the Hill coefficients characterising that pumping, release and activation
- $k_f c_e$ and kc_i refer to passive efflux from the Ca^{2+}-sensitive store and from the cytosol (respectively)
- all concentrations are relative to the total cellular volume.

6.2.2 Transforming the Two-Pool Model into a One-Pool Model

Whilst there exists evidence of cells with separate Ca^{2+}-sensitive and $InsP_3$-sensitive stores , this is not known for *CHO–hOT* cells. Dupont and Goldbetter went on to investigate whether Ca^{2+} oscillations were possible in a model containing a single pool sensitive to $InsP_3$ and Ca^{2+}- the so-called One-pool model.

Equation (6.2.2) still represents the global behaviour of the system but that the 'detailed nature of some of the processes had to be modified.' In particular, whilst pumping in the $InsP_3$- and Ca^{2+}-sensitive store is still given by Equation (6.2.5), the release of Ca^{2+} into the cytosol now takes the form

$$J_- \;=\; \pi J_{neg} \;\;=\;\; \pi V_2 \frac{c_e^m}{K_2^m + c_e^m} \frac{c_i^p}{K_3^p + c_i^p}, \tag{6.2.7}$$

where π represents the degree of saturation by $InsP_3$ of this 'bi-activated' receptor.

In the two-pool model, the term $v_1\pi$ denotes the constant influx of Ca^{2+} from the $InsP_3$-sensitive pool. If this term is suppressed in the one-pool model (because the effect of $InsP_3$ on Ca^{2+} release is then expressed by J_-) and one only considered a constant Ca^{2+} influx, v_0, from the extracellular medium, this model

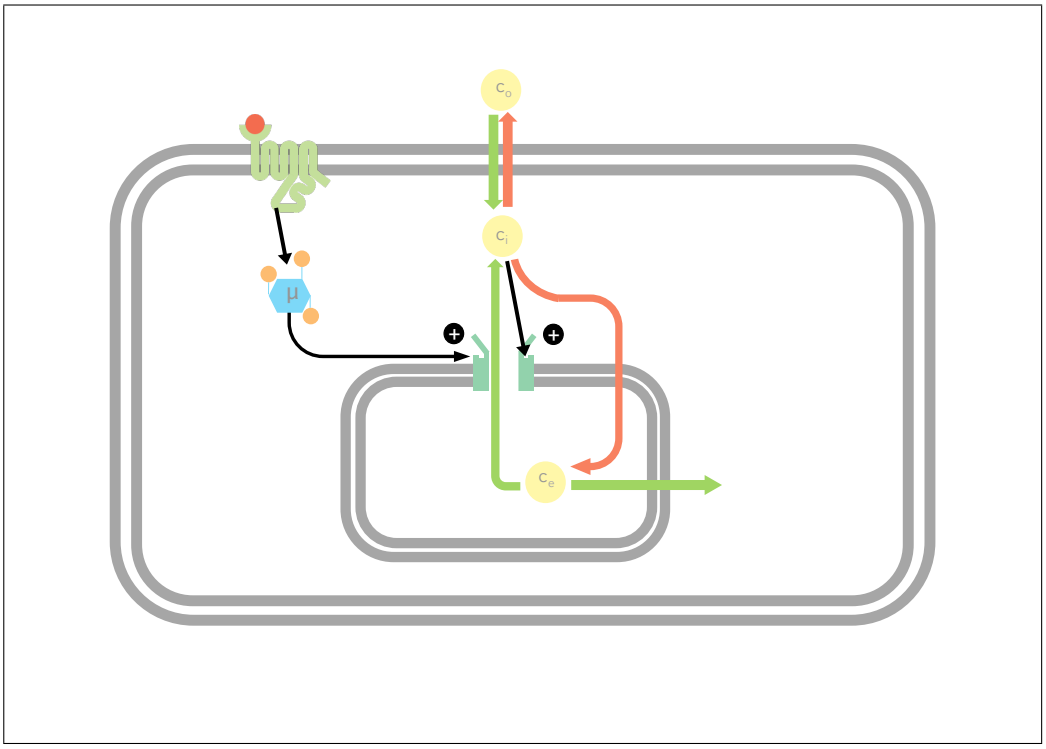

Figure 6.5 *Schematic diagram of the One-Pool model*

loses an important property of the Ca^{2+}-induced Ca^{2+}-release (CICR) model: that the mean cytosolic Ca^{2+} concentration rises with the stimulation level.

In most cell types [13, 68, 127, 128] a low (high) concentration of agonist generates a constant low (high) level of cytosolic Ca^{2+}, when the stimulus is outside the range leading to sustained oscillations. This shortcoming is obviated by assuming that stimulation not only causes $InsP_3$ synthesis, but also leads to direct activation of Ca^{2+} entry from the extracellular medium into the cytosol. Such a stimulus-activated Ca^{2+} entry has been reported [65, 43, 126] in some cell types and could be triggered by depletion of the intracellular stores, a discussion of which is in Chapter 7.

Dupont and Goldbeter [47] adopted the simplest possible assumption - that the influx of Ca^{2+} from the extracelluar medium triggered by external stimulation is proportional to the parameter π, much as the $InsP_3$-regulated release from the Ca^{2+} pool. And thus, the expression for J_{in} was replaced with the mathematically identical but differently motivated statement

$$J_{in} = v_0 + v_1\pi \tag{6.2.8}$$

where v_0 still denotes the constant rate of Ca^{2+} influx in the absence of stimulation while v_1 is now the maximum rate of stimulus-induced influx of Ca^{2+} from

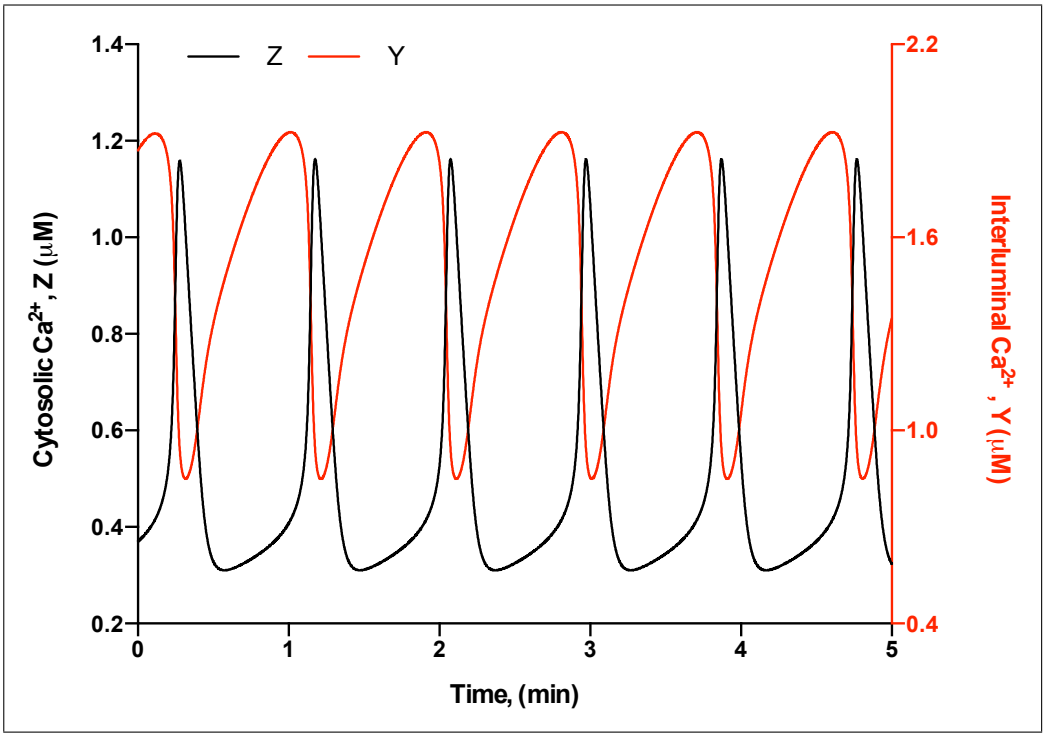

Figure 6.6 *Typical Ca^{2+} oscillations generated by the one-pool model based on $InsP_3$-sensitive Ca^{2+}-induced Ca^{2+} release. The black and red lines represent the evolution of cytosolic and intraluminal Ca^{2+}, respectively. $\pi = 0.4$, $v_0 = v_1 = 3.4\ \mu M.min^{-1}$, $V_1 = 50\ \mu M.min^{-1}$, $V_2 = 650\ \mu M.min^{-1}$, $K_1 = 1\ \mu M$, $K_2 = 2\ \mu M$, $K_3 = 0.9\ \mu M$, $k = 10\ min^{-1}$, $k_f = 1\ min^{-1}$, $n = m = 2$ and $p = 4$. Initial conditions are $c_s = 1.87\ \mu M$ and $c_i = 0.37\ \mu M$.*

the extracellular medium into the cytosol.

Thus, although based on distinct assumptions, the one-pool model, where Ca^{2+} and $InsP_3$ behave as co-agonists, is mathematically similar to the two-pool model with the only difference being the replacement of J_{neg} with $J_- = \pi J_{neg}$. The necessary stability for Ca^{2+}-oscillations to occur is consequently inherited in one-pool model from its two-pool grandparent. This is demonstrated in Figure 6.6 where cytosolic Ca^{2+} oscillations obtained by a numerical simulation mirroring that demonstrated in the original paper are shown together with the obtained variation in intraluminal Ca^{2+}, that is to say Ca^{2+} concentration within the $InsP_3$- and Ca^{2+}-sensitive one-pool.

6.2.3 Non-dimensionalisation

For simplicity of analysis, it is sensible to non-dimensionalise this system of equations. Some thought allows one to rewrite the components thus

$$\frac{\hat{f}\left(c_i, c_s\right)}{\pi V_2} = \frac{V_1}{\pi V_2}\left[\frac{\left(\frac{c_i}{K_1}\right)^n}{1+\left(\frac{c_i}{K_1}\right)^n}\right] - \left[\frac{\left(\frac{c_s}{K_2}\right)^m}{1+\left(\frac{c_s}{K_2}\right)^m}\right]\left[\frac{\left(\frac{c_i}{K_1}\right)^p}{\left(\frac{K_3}{K_1}\right)^p+\left(\frac{c_i}{K_1}\right)^p}\right] - \frac{k_f K_2}{\pi V_2}\left(\frac{c_s}{K_2}\right) \tag{6.2.9}$$

which can be written

$$f\left(u,v\right) = \frac{\hat{f}\left(c_i, c_s\right)}{\pi V_2} = \beta\left[\frac{u^n}{1+u^n}\right] - \left[\frac{v^m}{1+v^m}\right]\left[\frac{u^p}{\alpha^p+u^p}\right] - \delta v \tag{6.2.10}$$

using the new parameters $\beta = V_1/\pi V_2,\ u = c_i/K_1,\ v = c_s/K_2,\ \alpha = K_3/K_1$ and $\delta = k_f K_2/\pi V_2$. The system thus becomes

$$\frac{du}{d\tau} = \frac{1}{K_1}\frac{dZ}{d\tau} = \frac{J_{in}}{K_1} - ku - \frac{\pi V_2}{K_1} f\left(u,v\right), \tag{6.2.11}$$

$$\frac{dv}{d\tau} = \frac{1}{K_2}\frac{dY}{d\tau} = \frac{\pi V_2}{K_2} f\left(u,v\right), \tag{6.2.12}$$

which by rescaling time to simplify the system using $t = \tau k$ becomes:

$$\frac{du}{dt} = \frac{J_{in}}{kK_1} - u - \frac{\pi V_2}{kK_1} f\left(u,v\right), \tag{6.2.13}$$

$$\frac{dv}{dt} = \frac{\pi V_2}{kK_2} f\left(u,v\right), \tag{6.2.14}$$

and thus

$$\frac{du}{dt} = \mu - u - \frac{\gamma}{\varepsilon} f\left(u,v\right), \tag{6.2.15}$$

$$\frac{dv}{dt} = \frac{1}{\varepsilon} f\left(u,v\right), \tag{6.2.16}$$

with $\mu = J_{in}/kK_1,\ \varepsilon = kK_2/\pi V_2$ and $\gamma = K_2/K_1$.

6.2.4 Stability

Steady states, with starred coordinates $(u^\star, v^\star)$, occur when both $du/dt = 0$ and $dv/dt = 0$. In general, for this system, this happens when

$$f(u^\star, v^\star) = 0, \tag{6.2.17}$$

$$u^\star = \mu. \tag{6.2.18}$$

As the (general) form of $f(u, v)$ is cubic, there are two possible cases: that of either one or three real roots. Before looking in general, it is informative to note that in the case for the variables in Figure 6.6, the requirement is that

$$u = 0.476, \tag{6.2.19}$$

$$0 = v^3 + 4.82v^2 + v - 4.62. \tag{6.2.20}$$

This form has the solutions $v \in \{-4.34, -1.30, 0.82\}$ which leaves $(u^\star, v^\star)$ as $(0.47, 0.82)$ since $v \geq 0$ and, on translation to concentrations

$$(c_i^\star, c_s^\star) = (K_1 u^\star, K_2 v^\star) = (0.48, 1.64), \tag{6.2.21}$$

which is a reasonable level for the cytosolic and endoplasmic reticulum Ca^{2+} level, respectively.

6.2.5 Linear stability Analysis

A simple change of variables, $w = u + \gamma v$ allows the system to become

$$\frac{dw}{dt} = \frac{du}{dt} + \gamma \frac{dv}{dt} \qquad = \mu - u, \tag{6.2.22}$$

$$\frac{dv}{dt} = \frac{1}{\varepsilon} f\left(w - \gamma v, v\right) = \frac{1}{\varepsilon} F\left(w, v\right). \tag{6.2.23}$$

The nullclines of the transformed Equations (6.2.22 - 6.2.23) can be seen in Figure 6.7 and show the characteristic N-shaped and straight line nature of a generalised Fitz-Hugh Nagumo model [56].

It is here that the power of this seemingly simple model becomes clear - in that the system, reduced to its two equations and non-dimensionalised cleverly can be rewritten as, and thus adopt the behaviour of, an analytically soluble model. The actual stability analysis follows but from this reduction we know that the model will exhibit the same temporal behaviour as the Fitz-Hugh Nagumo model. That is, it is an excitable system which shows oscillatory behaviour which is accessed via a Hopf bifurcation. The system also inherits the property of the Fitz-Hugh

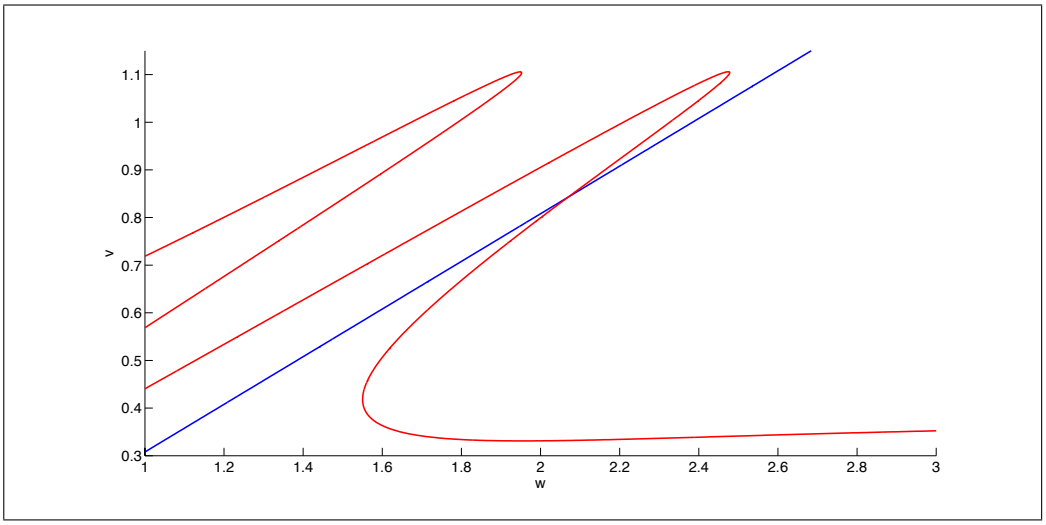

Figure 6.7 *Nullclines and a sample trajectory of the one-pool model transformed to w, v coordinates and using the parameters from Figure 6.6.*

Nagumo model that if something is slightly below the lower Hopf bifurcation point, a sub-threshold addition of Ca^{2+} gives a small response, while a super-threshold addition causes a large transient before the return to the steady state typical of Ca^{2+} oscillations.

Whilst this model cannot, in its original formulation, replicate all recent experimental results (for instance the slow inhibitory effect that Ca^{2+} is known to have on $InsP_3$-mediated release [103]) it is this analytical tractability and simple translation into a generalised Fitz-Hugh Nagumo system which makes it an important tool to consider in studying Ca^{2+}-oscialltions to this day.

The stability of the general steady state is determined by first determining the Jacobian Matrix, J of the system

$$J := \left(\begin{array}{cc} \dfrac{\partial a(u,v)}{\partial u} & \dfrac{\partial a(u,v)}{\partial v} \\ \dfrac{\partial b(u,v)}{\partial u} & \dfrac{\partial b(u,v)}{\partial v} \end{array} \right) \Bigg|_{(u^\star,v^\star)} \tag{6.2.24}$$

$$= \left(\begin{array}{cc} -1 - \dfrac{\gamma}{\varepsilon} f_u & \dfrac{\gamma}{\varepsilon} f_v \\ \dfrac{1}{\varepsilon} f_u & \dfrac{1}{\varepsilon} f_v \end{array} \right) \Bigg|_{(u^\star,v^\star)}, \tag{6.2.25}$$

where $a(u,v) = \mu - u - \frac{\gamma}{\varepsilon} f(u,v)$ and $b(u,v) = \frac{1}{\varepsilon} f(u,v)$ and then using this to

find the characteristic equation

$$|J - \lambda I_2| = \det \begin{pmatrix} -1 - \frac{\gamma}{\varepsilon} f_u - \lambda & \frac{\gamma}{\varepsilon} f_v \\ \frac{1}{\varepsilon} f_u & \frac{1}{\varepsilon} f_v - \lambda \end{pmatrix} \tag{6.2.26}$$

$$= \left(-1 - \frac{\gamma}{\varepsilon} f_u - \lambda\right)\left(\frac{1}{\varepsilon} f_v - \lambda\right) - \frac{\gamma}{\varepsilon} f_v \frac{1}{\varepsilon} f_u \tag{6.2.27}$$

$$= \lambda^2 + H\lambda - \frac{f_v}{\varepsilon}, \tag{6.2.28}$$

where

$$H = \frac{1}{\varepsilon}\left(\gamma f_u(u^\star, v^\star) - f_v(u^\star, v^\star) + \varepsilon\right), \tag{6.2.29}$$

the roots of which can be used in order to determine the stability of the system.

Since we know $f_v < 0$, the roots of the characteristic equation (6.2.28) have negative real part (and the steady state is thus stable) if $H > 0$. They have positive real part if $H < 0$. When H=0 the steady state changes stability through a Hopf bifurcation, and at these points a period orbit branch appears.

This oscillatory behaviour is most clearly seen in a bifurcation diagram such as the one seen in Figure 6.8 which was constructed numerically using the XPPAUT implementation of the software package AUTO [42]. As the bifurcation parameter, μ, is increased it can be seen that oscillations appear and later disappear at a supercritical Hopf bifurcation. These two bifurcation points, connected by a branch of stable periodic orbits, show that oscillations can occur with constant μ, demonstrating that the elements of the CICR mechanism is sufficient to produce oscillations without the need for oscillations in the concentration of $InsP_3$.

In the two- and one-pool model, Ca^{2+} stimulates its own release, while the flow of Ca^{2+} from the internal store is terminated when the concentration of Ca^{2+} in the internal store becomes too low. However, more recent experimental evidence suggests that, in addition to this stimulatory role, Ca^{2+} also inhibits its release from the store, but on a slower timescale[103]. It is believed that this activation and inactivation of the $InsP_3R$ by Ca^{2+} is the fundamental mechanism underlying $InsP_3$-dependent Ca^{2+} oscillations.

A number of models which incorporate this hypothesis have appeared and been reviewed, for example, in [120, 125], however, this enables the introduction of a model which uses a more physiologically informed impetus for its design: the Wagner-Keizer Model approach which considers fluxes into and out from the compartments of the system with fluxes written as biologically-informed functions of the physiological state of the system rather than mathematical constructs.

The initial investigation here is of a Wagner-Keizer model with the famous ap-

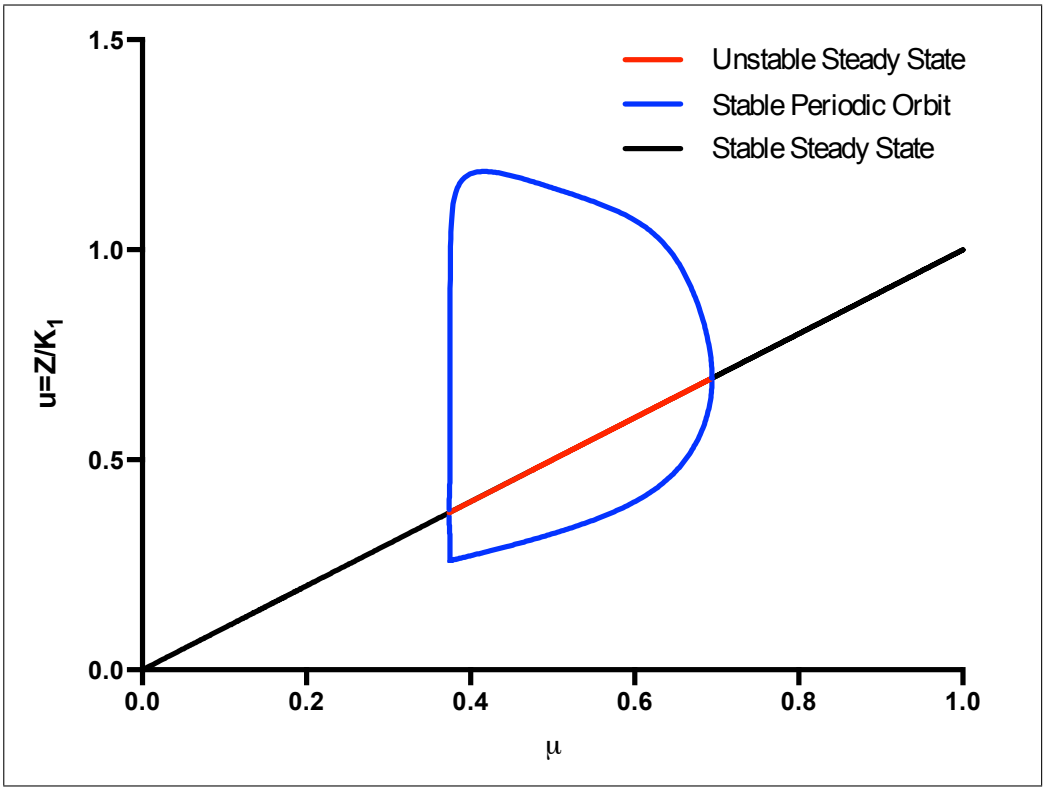

Figure 6.8 *A bifurcation diagram for the parameter μ in the u, v-non-dimensionalised one-pool model showing the steady state calcium level and its stability whilst it is initially a stable steady state for low values of μ (black) then goes through a supercritical Hopf bifurcation (shown) and becomes an unstable steady state (red) displaying stable periodic orbits whose amplitude minima and maxima are shown (blue). The steady state then returns to a stable steady state (black) through another supercritical Hopf-bifurcation point. Standard parameters as per Figure 6.6.*

proach to modelling the $InsP_3R$ developed by De Young and Keizer[39] which mimics the molecular subunit configuration of the $InsP_3R$ to reflect the sequences of activation and inactivation of the channel that result from the binding of $InsP_3$ and Ca^{2+}- to both the activating and inactivating site of - the $InsP_3R$.

6.3 Wagner-Keizer Two-Compartment Approach

Combining the above, the approach taken here is to use the Wagner-Keizer two-compartment approach introduced in §1.4. The reason Ca^{2+} is so dynamic a signalling molecule is the combination of ON and OFF reactions, summarised in Figure 1.9 on page 26, which control its flux into the organelles as well as across the plasma membrane. In order to successfully model this system, therefore, it is necessary to develop a biologically informed mathematical model of each of the fluxes relevant to the system.

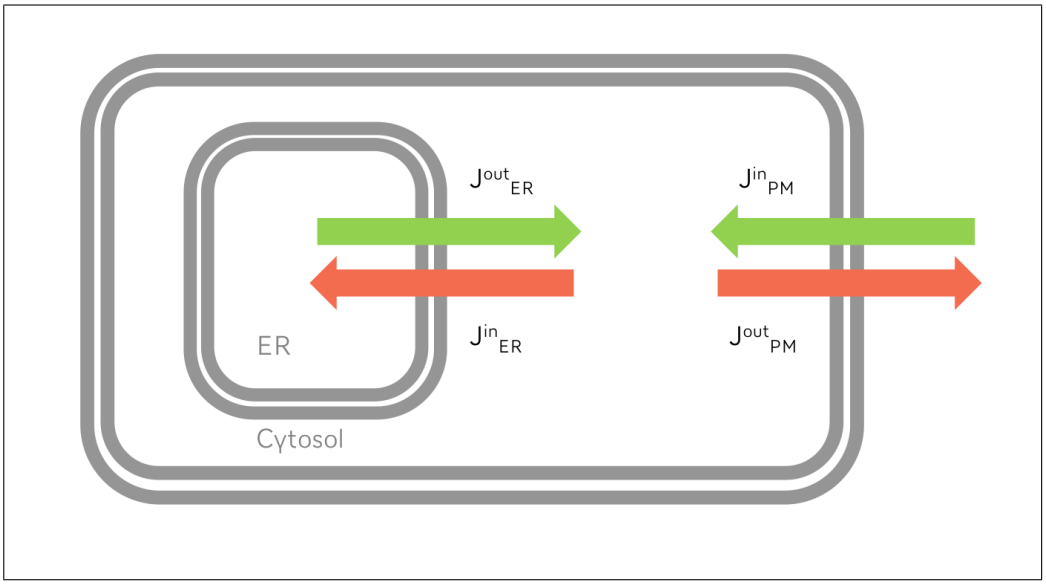

Figure 6.9 *Schematic of Wagner Keizer flux model*

Thus, it is necessary to identify mathematical expressions for the fluxes identified in Figure 1.9 in order to express the fluxes to understand the schematic in Figure 6.9. To implement this approach it is necessary to identify the nature of the Ca^{2+} fluxes through the membrane (identified in Figure 1.9), determine which of these is important to the signalling process and then manipulate the parameters such that the resultant output is biologically informed, as well as replicating the observed data.

An approach to modelling the system which relies only upon biologically known information was proposed by Wagner and Keizer in their 1994 paper, *Effects of rapid buffers on* [132]. This model, now referred to as the Wagner-Keizer Model, is widely used as a whole-cell model because it is based on constructing a mathematical description of understood fluxes in and out of known compartments within the cell as described by the schematic in Figure 6.9.

Throughout, $k \in \{i, e\}$ is used to indicate the intracellular medium or the Sarcoplasmic Reticulum, respectively. Thus N_i and N_e are the total number of Ca^{2+} ions - bound and free - in the cytosol and the ER, respectively. Therefore,

$$c_k^{total} = \frac{N_k}{V_k}, \tag{6.3.1}$$

where V_k is the volumes of each compartment. The change in N_k from each

compartment is used to write out the system of equations:

$$\frac{dN_i}{dt} = J_{pm}^{in} - J_{pm}^{out} - J_e^{in} + J_e^{out}, \tag{6.3.2}$$

$$\frac{dN_e}{dt} = J_e^{in} - J_e^{out}, \tag{6.3.3}$$

where J have units μmoles/s. Converting these to concentrations gives

$$\frac{dc_i^{total}}{dt} = j_{pm}^{in} - j_{pm}^{out} - j_e^{in} + j_e^{out}, \tag{6.3.4}$$

$$\frac{dc_e^{total}}{dt} = \frac{V_i}{V_e}\left(j_e^{in} - j_e^{out}\right), \tag{6.3.5}$$

where volumes are absorbed into the j terms giving them units of concentration/time, μM/s.

Assuming Rapid Buffering

There is a full investigation into the dynamic relationship,

$$Ca^{2+} + B \underset{k_2}{\overset{k_1}{\rightleftharpoons}} Ca^{2+} \cdot B \tag{6.3.6}$$

between Ca^{2+} meeting its buffer, B, and forming a complex, $c_i \cdot B$ in Chapter 7. However the rapid rapid buffering assumption, which presumes that the buffering system is constantly in its equilibrium state,

$$c_k = \frac{K_k \left[Ca^{2+} \cdot B\right]_k}{[B]_k}, \tag{6.3.7}$$

is required as a tool to extract the amount of 'free', that is to say unbuffered, Ca^{2+} available in each compartment of the model.

Differentiating Equation (6.3.7) and using the chain rule gives an expression for dc_k/dt, i.e. what is of essential interest and which can be measured:

$$\begin{aligned}\frac{dc_k}{dt} &= \frac{dc_k}{dc_k^{total}} \times \frac{dc_k^{total}}{dt} \\ &= \left(1 + \frac{K_k \left[B\right]_k^{total}}{\left(K_k + c_k\right)^2}\right)\end{aligned} \tag{6.3.8}$$

which, when Equation (6.3.8) is combined with Equations (6.3.4) and (6.3.5)

generates

$$\frac{dc_i}{dt} = f_i \left(j_{pm}^{in} - j_{pm}^{out} - j_e^{in} + j_e^{out} \right), \tag{6.3.9}$$

$$\frac{dc_e}{dt} = \frac{f_e V_i}{V_e} \left(j_e^{in} - j_e^{out} \right), \tag{6.3.10}$$

which can have the number of parameters reduced by taking a new parameter

$$\sigma = \frac{V_e f_i}{V_i f_e}. \tag{6.3.11}$$

6.3.1 $InsP_3$ Receptor Modelling

Before dealing with the other fluxes, it is necessary to first consider how to model the $InsP_3R$ as part of j_e^{out}. The $InsP_3R$ is a Ca^{2+} channel located on the ER. For a long time, the two-pool model of $InsP_3$ dependent release had been used and it matched experimental data well. Work in the early 1990's suggested, however, that the role of Ca^{2+} is more complex than just a stimulatory Ca^{2+} step. Ca^{2+} also, on a slower time scale, causes inhibition of its own release [103, 16]. It is understood that this dual stimulatory and inhibitory role that Ca^{2+} plays is the fundamental mechanism underlying $InsP_3$-dependent Ca^{2+} oscillations and waves [121, 125]. There have been many attempts at modelling this receptor to include various experimental findings but none captures all of its dynamics without being overly complex.

6.3.2 Fluxes out from the ER - j_e^{out}: an $InsP_3R$ Model

Bezprozvanny *et al* [16] had shown that the open-probability of the $InsP_3R$'fit well' the functional form

$$\left[\frac{c_i k}{(c_i + K)(c_i + k)} \right]^m, \tag{6.3.12}$$

with $K = k = 0.2\mu M$ and $m = 2.7$. In 1992, Keizer and DeYoung constructed a simplified model of the $InsP_3R$ which took into account all possible states and the transitions between them (based on above evidence).

They made the assumption that the $InsP_3R$ consists of three identical subunits. To agree with the experimental evidence above, each subunit has a single 'potentiating' $InsP_3$ binding site and two Ca^{2+} biding sites, one activating and one inactivating. Labelling the sites 1,2 and 3 for $InsP_3$, Ca^{2+}-activating and Ca^{2+}-activating, respectively as S_{ijk} (where $i,\ j$ and $k \in \{0, 1\}$ corresponds to whether

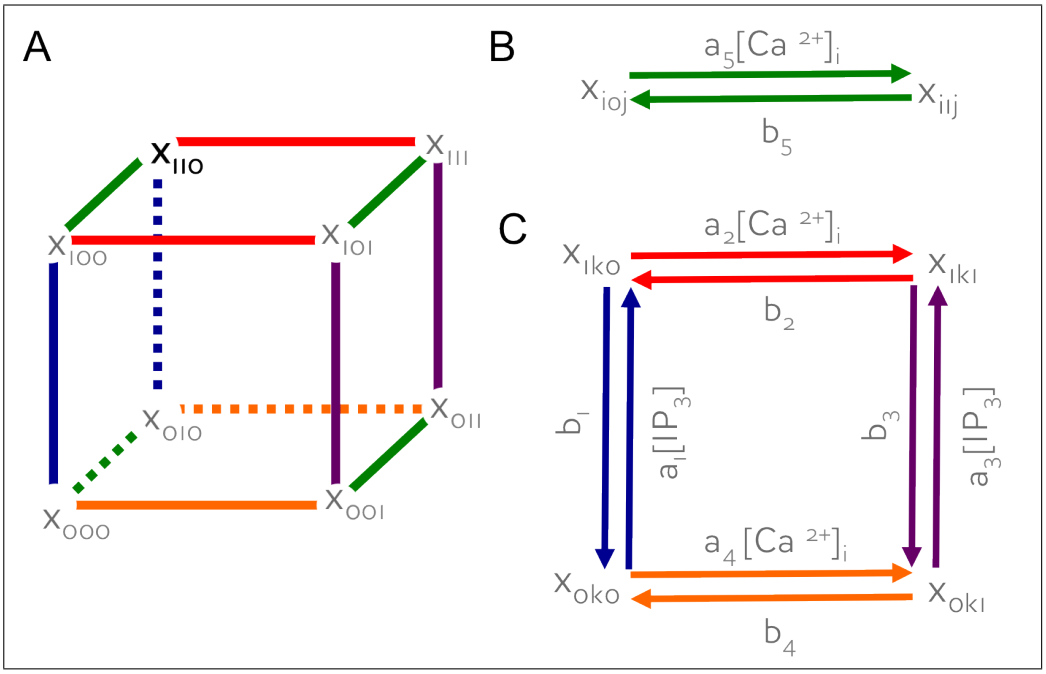

Figure 6.10 *States of the $InsP_3R$ in the De Young Keizer model*

a site is occupied (1) or not (0)) as the state a receptor is in and x_{ijk} as the fraction of receptors in that state.

For Ca^{2+} to flow through the receptor, each of the three subunits must be in their open state (S_{110}) - that is, $InsP_3$-potentiated and with activating Ca^{2+} site bound and the inactivating Ca^{2+} site unbound. Thus, the open probability of the receptor given by this model is proportional to $(x_{110})^3$.

Mass action

The schematic in Figure 6.10 may be used to describe the system. Three simplifications are made:

- Rate constants are independent of whether or not Ca^{2+} is bound or not
- Ca^{2+} binding to the activation site is assumed independent of $InsP_3$-binding and Ca^{2+}-inactivation
- Mass action kinetics

The first two assumptions lead to the planar diagrams shown in B and C for $i, j, k \in \{0, 1\}$ resulting in a reduced system with 10 parameters, rather than 24. The final assumption leads to a series of 7 differential equations for each of the fractions, x_{ijk} except for one (since $\sum_{i,j,k} x_{ijk} = 1$ removes linear independence).

An exemplar equations would be

$$\frac{dx_{000}}{dt} = -\left((a_1[IP_3]x_{000} - b_1x_{100}) + (a_4c_ix_{000} - b_4x_{001}) + (a_5c_ix_{000} - b_5x_{010}).\right) \tag{6.3.13}$$

j_e^{out} has two components, the Ca^{2+} flux through the $InsP_3R$/channel and a constant leak flux. Thus, the outward Ca^{2+} flux from the ER is given by

$$j_e^{out} = c_1\left(v_1x_{110}^3 + v_2\right)(c_e - c_i), \tag{6.3.14}$$

where v_1 and v_2 set the maximal Ca^{2+} fluxes and $c_1 = 0.185$ is the ratio of the volume of the $InsP_3$-sensitive Ca^{2+} pool (the ER) to the cytosolic volume [75].

6.3.3 Fluxes into and out from the cytosol - j_{pm}^{in} and j_{pm}^{out}

Flux of Ca^{2+} into the cytosol from outside the cell are grouped together as j_{pm}^{in} and consist of

- Current
- Leak

Current Most Ca^{2+} entry into the cell occurs through ion channels with ionic currents. I_{Ca} for instance, are measured in pA and so a factor, often called α, is needed to covert to μ moles. In this case

$$\alpha = (2FV_i) \tag{6.3.15}$$

where $F = 96480\,C/mol$ is Faraday's constant (the magnitude of electric charge per mole of electrons $= eN_A =$ elementary charge $\times$ Avogadro's number); the 2 corresponds to the valency of Ca^{2+} and V_i is the volume of the cytosol. Thus, the current is modelled as

$$-\alpha I_{Ca} \tag{6.3.16}$$

Leak Constant, unregulated leak conductance is modelled thermodynamically using the form

$$j_{pml} = v_{pml}(c_o - c_i) \tag{6.3.17}$$

where $v_{pml}$is the leak permeability ($\mu M/s$) and $(c_e - c_i)$ is the thermodynamic driving force for a symmetric channel.

Taken together, gives the expression for the entrance of Ca^{2+} through the plasma membrane,

$$j_{pm}^{in} = v_{pml}(c_o - c_i) - \alpha I_{Ca} \tag{6.3.18}$$

In the original formulation the flux of Ca^{2+} out from the cytosol into the extracellular medium consists of consist only PMCA pumps (as opposed to including other extrusion methods such as the $Na^{+}/Ca^{2+}-$exchanger). The action of which is given the name j_{pm}^{out}.

PMCA Similar in action to Sarco-Endoplasmic Reticulum Ca^{2+} ATPase, the Plasma Membrane Ca^{2+} ATPase (or PMCA) removes calcium from the cell (in all eukaryotes). There are 4 isoforms of PMCA and the pump has stoichiometry of $1Ca^{2+} : 1ATP$ for the PMCA pump. It has a high affinity, with a K_m of 100 to 200 nM [75]. Thus

$$j_{pm}^{out} = \frac{v_{pmca}c_i^2}{K_{pmca}^2 + c_i^2} \tag{6.3.19}$$

6.3.4 Determining the parameters

In their model of whole-cell Ca^{2+}-oscillations, De Young and set j_e^{in} as 0 and $\left[Ca^{2+}\right]_{EC}$ is taken as a constant (even though j_e^{out} is non-zero) thus removing one ODE from the Wagner-Keizer formulation. The model utilises the $\left[Ca_i^{2+}\right]^2$ conservation condition, $c_0 = c_1 c_e + c_i$, to determine the constant c_e. Taking c_0 to be 2.0 μM leads to maximum values of $\left[Ca^{2+}\right]_i$ and $\left[Ca^{2+}\right]_{ER}$ of approximately 1.7 μM and 10 μM, respectively.

The remaining parameters, a_i, v_i and k_3, were determined so that

1. c_i oscillations occur within a reasonable range of $InsP_3$, (350-800 nM);
2. the equilibrium $\left[Ca_i^{2+}\right]$ in the absence of $InsP_3$ is approximately 50 nM [75]
3. the qualitative nature of inhibition of Ca^{2+} release by Ca^{2+}, as experimentally found by Parker and Ivorra [103] could be reproduced [75]and
4. the mean open time of the $InsP_3R$ is the order of a few milliseconds [75].

Following the derivation laid out in [39] , the model initially generates a cube of transition states (identical to that of the original model). Combining equation (6.3.13) and the assumptions and the Mass-action assumption, it can be seen that the original system can be written as a matrix equation as in figure 6.11 and solved at steady state as the figures given there.

a_1	400	$\mu M/s$	b_1	52	$/s$	r_1	6	$/s$
a_2	0.2	$\mu M/s$	b_2	0.21	$/s$	r_2	0.108	$/s$
a_3	400	$\mu M/s$	b_3	377.36	$/s$	r_3	0.76	$\mu M/s$
a_4	0.2	$\mu M/s$	b_4	0.029	$/s$	k_p	0.1	μM
a_5	20	$\mu M/s$	b_5	1.65	$/s$	c_e	1.69	μM

Table 6.1 *Constants used in DeYoung Keizer's original formulation of the model*

Table 6.1 shows the binding rate constants, a_i, and the dissociation constants d_i that De Young and Keizer used in their original work. Note that only 4 of the 5 dissociation constants are independent due to the thermodynamic constraint of detailed balance, i.e. $d_1 d_2 = d_3 d_4$ [64]. The constants in table 6.1 were obtained by fitting steady state data by Bezprozvanny et al. [15].

The $InsP_3R$ is an integral part of the $InsP_3R$ channel, through which Ca^{2+} is released from the endoplasmic reticulum. Biochemical experiments and electron microscopy revealed that the $InsP_3R$ channel consists of 4 subunits and that it is conducting when at least 3 of the 4 subunits are activated [70, 15, 134]. In the De Young-Keizer model, the configuration with $InsP_3$ and Ca^{2+} bound to the activating binding sites, but with an unoccupied Ca^{2+} inhibiting binding site is the activated state of the receptor. Consequently, the open probability of an $InsP_3R$ channel is given by

$$P_{open} = 4\left(x^{\star}_{110}\right)^3 - 3\left(x^{\star}_{110}\right)^4 \tag{6.3.30}$$

where

$$x^{\star}_{110} = \frac{d_2[IP_3]^{\star} c_i^{\star}}{\left(c_i^{\star} + d_5\right)\left(d_1 d_2 c_i^{\star} + d_3 c_i^{\star} + c_i^{\star}[IP_3]^{\star} + d_2[IP_3]^{\star}\right)} \tag{6.3.31}$$

Exemplars of the calculated equilibrium open probability of the $InsP_3R$ as a function of cytosolic Ca^{2+} concentration for the parameters given in Table 6.1 is given in Figure 6.12. The function is bell-shaped and decreases physiologically for lower $[InsP_3]$.

$$
\begin{bmatrix}
-a_1 - a_4 - a_5 c_i & b_4 & b_5 & b_1 & 0 & 0 & 0 \\
a_4 c_i & -a_3 p - b_4 - a_5 c_i & 0 & 0 & b_5 & b_3 & 0 & 0 \\
a_5 c_i & 0 & -b_5 - a_4 c_i - a_1 p & 0 & b_4 & 0 & b_1 & 0 \\
a_1 p & 0 & 0 & -b_1 - a_2 c_i - a_5 c_i & 0 & a_2 & b_5 & 0 \\
0 & a_5 c_i & a_4 c_i & 0 & -a_5 - b_4 - a_3 p & 0 & 0 & b_3 \\
0 & a_3 p & 0 & a_2 c_i & 0 & -a_3 - a_2 - a_5 c_i & 0 & b_5 \\
0 & 0 & a_1 p & a_5 c_i & 0 & 0 & -b_1 - a_2 c_i - b_5 & b_2 \\
1 & 1 & 1 & 1 & 1 & 1 & 1 & 1
\end{bmatrix}
\begin{pmatrix} x_{000} \\ x_{001} \\ x_{010} \\ x_{100} \\ x_{011} \\ x_{101} \\ x_{110} \\ x_{111} \end{pmatrix}
=
\begin{pmatrix} 0 \\ 0 \\ 0 \\ 0 \\ 0 \\ 0 \\ 0 \\ 1 \end{pmatrix}
\tag{6.3.20}
$$

$$x^*_{000} = d_1 d_2 d_5 \delta \tag{6.3.21}$$

$$x^*_{010} = d_1 d_2 c^\star_i \delta \tag{6.3.22}$$

$$x^*_{011} = d_3 \left(c^\star_i\right)^2 \delta \tag{6.3.23}$$

$$x^*_{110} = d_2 \left[IP_3\right]^\star c^\star_i \delta \tag{6.3.24}$$

$$x^*_{100} = d_2 d_5 \left[IP_3\right]^\star \delta \tag{6.3.25}$$

$$x^*_{001} = d_3 d_5 c^\star_i \delta \tag{6.3.26}$$

$$x^*_{101} = d_5 c^\star_i \left[IP_3\right]^\star \delta \tag{6.3.27}$$

$$x^*_{111} = \left(c^\star_i\right)^2 \left[IP_3\right]^\star \delta \tag{6.3.28}$$

$$\delta^{-1} = \left(c^\star_i + d_5\right)\left(d_1 d_2 + d_3 c^\star_i + c^\star_i \left[IP_3\right]^\star + d_2 \left[IP_3\right]^\star\right) \tag{6.3.29}$$

Figure 6.11 *Steady-state matrix equation for the original DeYoung Keizer model and its solutions.*

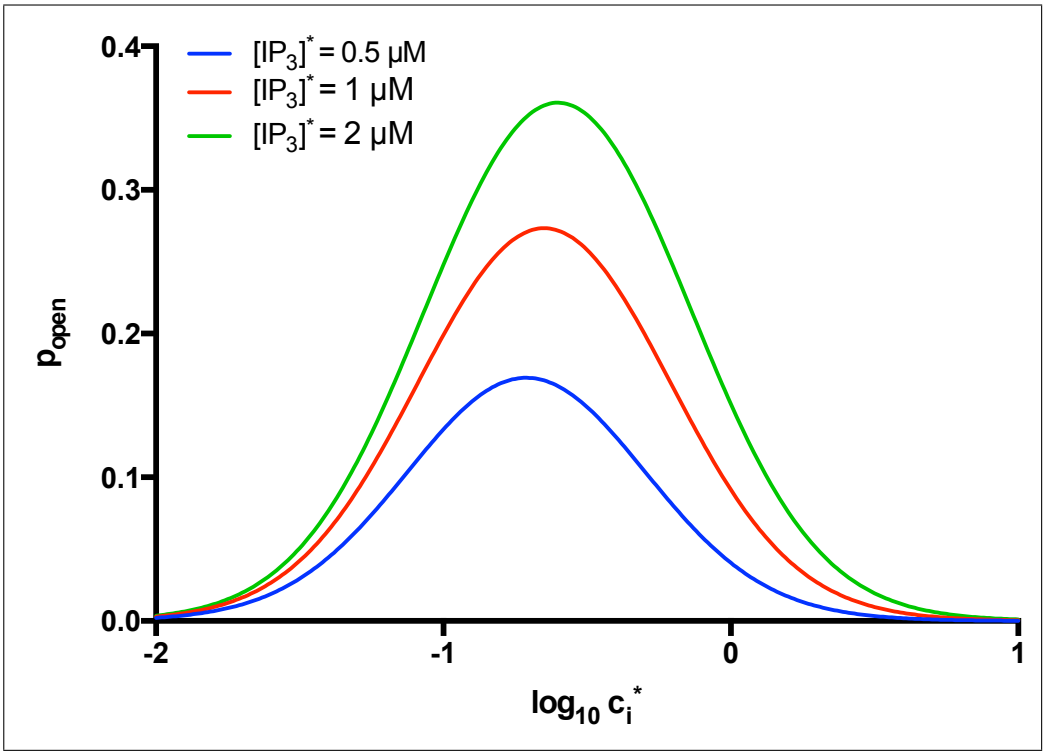

Figure 6.12 *Stationary value of the open probability P_{open} of an $InsP_3R$ channel. Parameter values as in table 6.1 and $[IP_3] = 0.5\,\mu M$*

6.3.5 Wagner-Keizer Model with DeYoung-Keizer $InsP_3R$ Model

Combining the fluxes from the above section with the Wagner-Keizer approach results in the system of equations:

$$\frac{dc}{dt} = j_{pm}^{in} - j_{pm}^{out} - j_e^{in} + j_e^{out}, \tag{6.3.32}$$

$$\frac{dc_e}{dt} = 0, \tag{6.3.33}$$

$$\tag{6.3.34}$$

where

$$j_{pm}^{in} = v_{pml133}(c_o - c_i) - \alpha I_{Ca} \tag{6.3.35}$$

$$j_{pm}^{out} = \frac{(v_{pmca})\left(c_i^2\right)}{K_{pmca}^2 + c_i^2} \tag{6.3.36}$$

$$j_e^{in} = 0 \tag{6.3.37}$$

$$j_e^{out} = c_1\left(v_1 x_{110}^3 + v_2\right)(c_e - c_i) \tag{6.3.38}$$

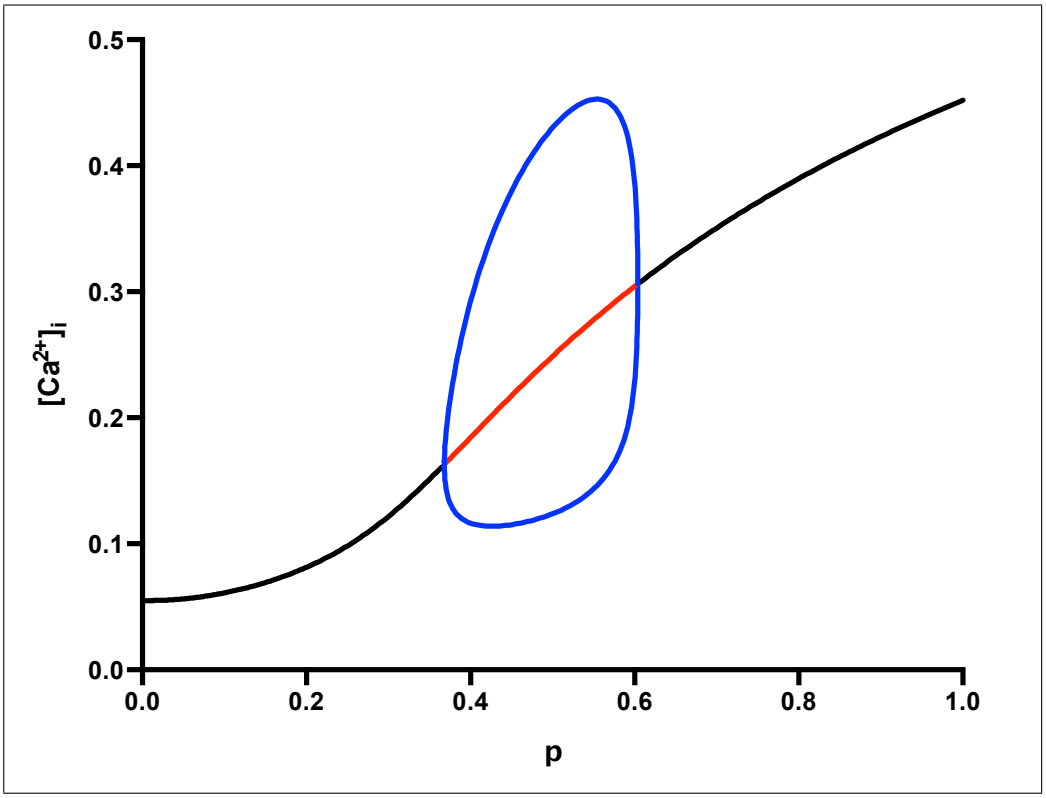

Figure 6.13 *DeYoung Keizer standard parameter bifurcation diagram*

and the parameters are taken as those in Table 6.1 and the initial conditions are

$$c_i(0) = 0.1\ \mu M, \tag{6.3.39}$$
$$c_e(t) = 1.60\ \mu M, \tag{6.3.40}$$
$$x_{ijk} = 0.1\ \ \forall i,j,k \in \{0,1\}. \tag{6.3.41}$$

6.3.6 Stability

For the parameters in the physiological range (shown in Table 6.1) the model shows a bifurcation structure similar to that seen in the two- and one-pool model. This structure is shown in the bifurcation diagram of the model as a function of the main bifurcation parameter, p, in Figure 6.13. Here, an increase in $InsP_3$ periodic orbits appear via a supercritical Hopf bifurcation which is connected to a second similar Hopf bifurcation by connected by a branch of stable periodic orbits.

The model can be shown to behave with very different bifurcation structure with a change of parameters, r_1 to 20 s^{-1}, r_2 to 0.004 s^{-1} , r_3 to 1.2 $\mu s^{-1} M^{-1}$ and $c_e r$ to 1 μM as shown in Figure 6.14. This diagram shows a 'folding-up' of the curve of steady states which forms two limit points. For a small window of values of p,

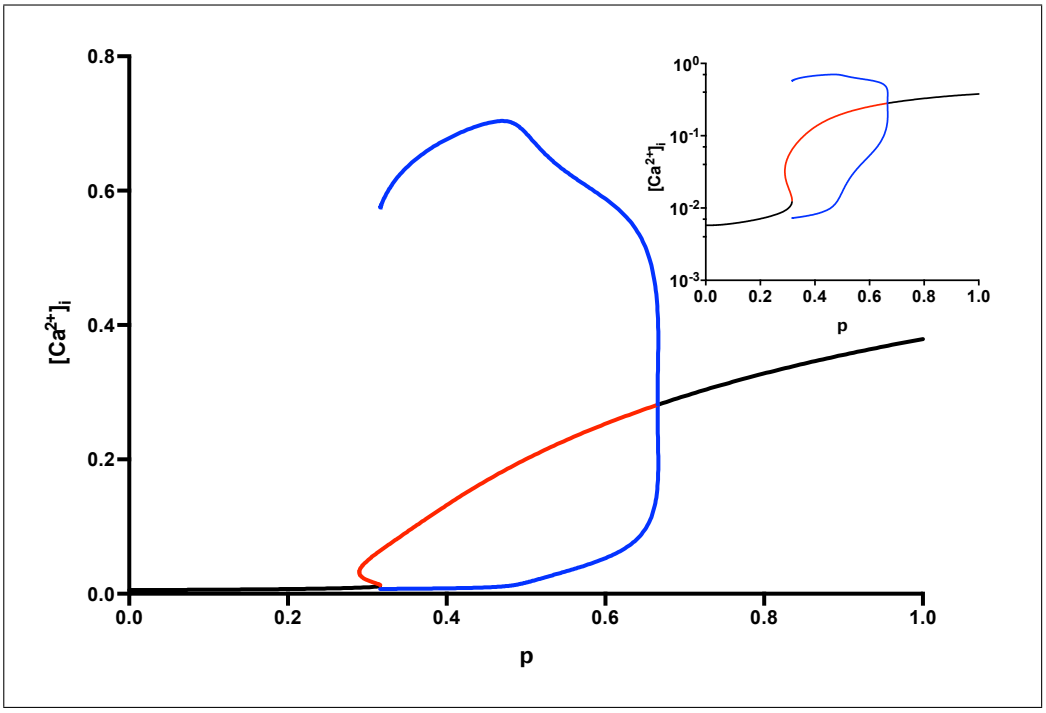

Figure 6.14 *DeYoung Keizer modified parameter bifurcation diagram (see text)*

three steady-state solutions exist between these two limit points whereas for low and high $InsP_3$ concentrations there is only one stable fixed point.

For the parameter values of p where the system has an unstable steady state, periodic oscillations occur. The branch of stable periodic orbits is broken into two different branches, both of which arise in a homoclinic bifurcation and end in a supercritical Hopf bifurcation.

6.4 Discussion and Conclusion

The two models introduced in this chapter represent two approaches to compartmental modelling of Ca^{2+} oscillations. In many ways their approaches appear quite similar. However, the impetus for the equations of the two-pool model were to reproduce the output of the system, that is the Ca^{2+} oscillations, by using mathematically motivated functions for fluxes. There was little evidence for separate $InsP_3$-sensitive and Ca^{2+}-sensitive store of Ca^{2+} and so the one-pool model rationalisation was developed. This resulted in the same system of equations — with differing motivation — being applicable and the Ca^{2+}-store was recued to a single pool which was $InsP_3$ and Ca^{2+} sensitive.

One of the original motivations of the two-pool model was to keep the system in two-dimensions, that is two equations, such that the Poincaré-Bendixson The-

orem could be applied to gain an understanding of the oscillations. Further, non-dimensionalisation of this system resulted in a Fitz-Hugh Nagumo-like system. This excellent piece of modelling thus took a simplification of the system and reduced its equations to ones that are not only mathematically tractable but the dynamic behaviour of which is well understood.

Whilst the tractability of this model is both desirable and useful and lead to a number of insights into Ca^{2+} oscillations, there is also a need for a physiologically motivated approach to modelling. This approach, first taken by Wagner and Keizer results in a similar equations for $\left[Ca^{2+}\right]_i$ and $\left[Ca^{2+}\right]_{ER}$ but uses realistic expressions for the fluxes through the relevant channels. The system is, in essence still a two-dimensional model but because of the use of the De-Young Keizer model for the flux throughout the $InsP_3R$ it becomes a nine dimensional system. The power of this approach is that the results are rooted in the physiology and, indeed, are consequently different from those provided by the one-pool model. Some power of the results is lost since the model cannot be addressed in the same level of analytical completeness.

Chapter 7

Towards a Physiologically-informed Model

The previous chapters have demonstrated the importance of extracellular calcium entry into the cell (Chapter 4) and luminal $[Ca^{2+}]$ (Chapter 5) on *OT*-induced Ca^{2+} oscillations. The mathematical models presented in the above chapter, however, are unable to replicate these facets of results:

- Whilst the one-pool reduction of the two-pool model has a luminally-sensitive $InsP_3R$ model, it assumes constant entry of Ca^{2+} into the cell with a component which is $InsP_3$-dependent.
- The Wagner-Keizer model, on the other hand, can be chosen to consider Ca^{2+}-entry (although in its original formulation it only considers a contribution from the PMCA and by passive leak) its DeYoung-Keizer model of the $InsP_3R$ does not have a luminally sensitive component.

Furthermore, neither of these modelling approaches considers Store-Operated Calcium Entry (SOCE) a common and ubiquitous mechanism of regulating Ca^{2+} influx into cells [8, 40, 101, 102].

It thus seems pertinent to investigate possible mechanisms for the three modelling facets that fail to be replicated by the models introduced in Chapter 6:

1. Ca^{2+}-entry
2. Ca^{2+}-buffering
3. Store-operated Ca^{2+}-entry.

7.1 Ca^{2+}-entry

In the one-pool model the term J_{in} represents the Ca^{2+} entry. This is a function of p, the proportion of $InsP_3R$'s that are in an activated state. Therefore, in order to investigate a more physicological form of Ca^{2+} it is first sensible to investigate the role V_in as a plays in the system by replacing it with a constant parameter. Once its role is established, the form of the fluxes needed to represent the physiology can be contracted to match the understanding gained from this investigation.

7.1.1 Replacing J_{in} with a constant

The motivation and derivation of the one-pool model (see §6.2.2) hold when setting J_{in}, the Ca^{2+}-entry into the cell through the plasma membrane, as a constant. Thus we investigate the fixed points of the system. The fixed points of the system, $(c_i^\star, c_e^\star)$, occurs when

$$0 = J_{in} - J_+ + J_- + k_f c_e^\star - k c_i^\star \tag{7.1.1}$$

$$0 = J_- - V_+ - k_f c_e^\star \tag{7.1.2}$$

and thus (by summing)

$$c_i^\star = \frac{J_{in}}{k} \tag{7.1.3}$$

is the unique fixed point of the system.

Equation 7.1.3 shows that in the original one-pool model the steady-state value of $\left[Ca^{2+}\right]_i$ is only dependent on the ratio of J_{in} and the constant k, which moderates the flux out of the cell. This suggests that the steady-state level of $\left[Ca^{2+}\right]_i$ depends entirely (and only) on extracellular entry into the cell.

The original model considers the expression for J_{in} as a constant (ligand-independent) entry, v_0, along with an (ligand-dependent) $InsP_3$-generated, $v_1\pi$, component of Ca^{2+} entry into the cell.

Thus, it is informative to reformulate the model, considering J_{in} to be a constant of the same magnitude as in the original formulation. Thus J_{in} is set as equal to the constant $3.4 + 0.4 \times 3.4$ and this results in the bifurcation structure as shown in Figure 7.1.

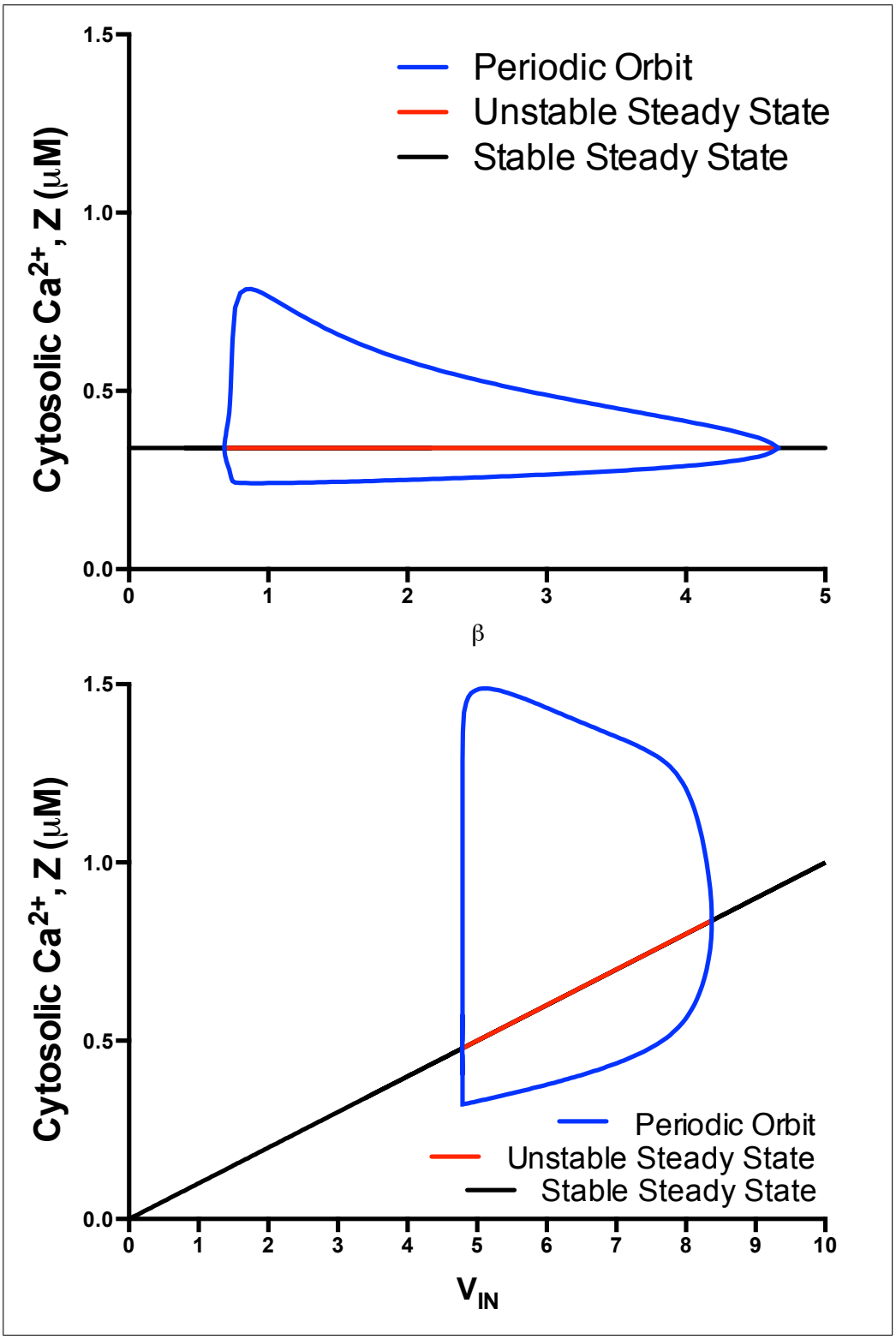

Figure 7.1 *Bifurcation diagrams of one-pool model with constant Ca^{2+} entry, $v_in \in \mathbb{R}$ (a) on β and (b) on J_{in}*

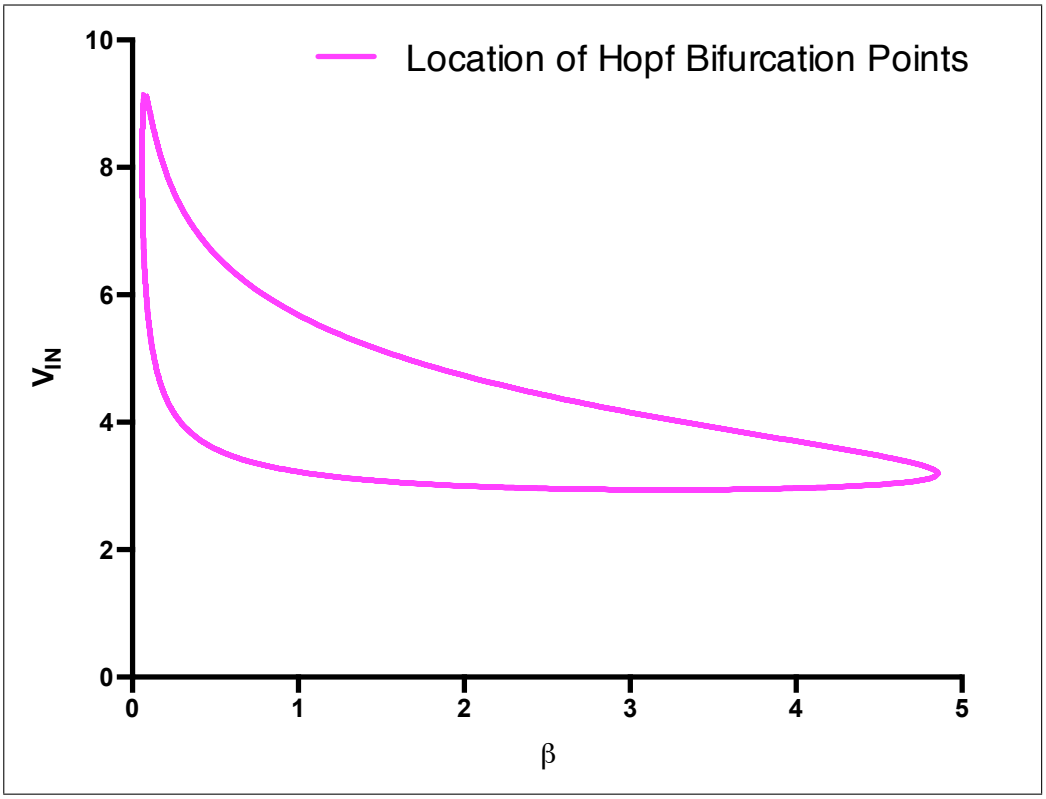

Figure 7.2 *Two parameter bifurcation analysis showing the location of the Hopf bifurcation points on varying J_{in} and β*

7.1.2 Modelling J_{in}

In trying to match the model's behaviour with the suggestion that extracellular Ca^{2+} entry is vital for oscillations (§ 4) as well as attempting to ensure that the term J_{in} represents something more physiological than merely constant Ca^{2+} influx (v_0) with an $InsP_3$-sensitive Ca^{2+}-entry state ($v_1\pi$)), the impact of varying the two key parameters, π and J_{in} is investigated. The two-parameter bifurcation analysis shown in Figure 7.2 shows the location of the Hopf Bifurcation points upon varying those parameters. That is, how the 'window' of parameters which leads to oscillations changes as those parameters vary.

Treating extracellular Ca^{2+} entry as constant yields the same bifurcation structure as the original model. Replacing this constant with a more physiologically informed expression is important. The Ca^{2+}-flux across the plasma membrane consists of the three elements introduced in Chapter 6

- current,
- leak, and
- PMCA.

The $Na^+/Ca^{2+}-$exchanger was revealed as an important modulator of *OT*-induced Ca^{2+} oscillations and so an expression for its flux must be derived and included in the model. The biology of the $Na^+/Ca^{2+}-$exchanger is introduced in §4.2.3 and it is from this biology that a number of mathematical models of the flux of Ca^{2+} through the $Na^+/Ca^{2+}-$exchanger have been formed. The simplified [74] four-state model constructed by Kang *et al* [72] is often used in compartmental models and is thus employed here.

Flux through $Na^+/Ca^{2+}-$exchanger

Letting E_i and E_0 denote the conformation of an exchanger whose binging sites are exposed to the interior and exterior of a cell, respectively. Starting at $E_i 3Na^+$ (the exchanger bound with three Na^+), the exchanger can bind Ca^{2+} inside the cell, simultaneously releasing three Na^+ to the interior. A change of conformation to E_0 then allows the exchanger to release its Ca^{2+} to the extracellular medium and bind three external Na^+. The Na^+ then returns to the E_i state which completely the cycle. This can best be described in the following reaction scheme:

$$E_i 3Na_i^+ + Ca_i^{2+} \underset{k_{-1}}{\overset{k_1}{\rightleftharpoons}} E_i Ca_i^{2+} + 3Na_i^+ \tag{7.1.4}$$

$$E_i Ca_i^{2+} \underset{k_{-2}}{\overset{k_2}{\rightleftharpoons}} E_o Ca_o^{2+} \tag{7.1.5}$$

$$E_o Ca_i^{2+} + 3Na_o^+ \underset{k_{-3}}{\overset{k_3}{\rightleftharpoons}} E_o 3Na_o^+ + Ca_o^{2+} \tag{7.1.6}$$

$$E_o 3Na_o^+ \underset{k_{-4}}{\overset{k_4}{\rightleftharpoons}} E_o 3Na_i^+. \tag{7.1.7}$$

Letting x_1, x_2, x_3, and x_4 be the fraction of the $Na^+/Ca^{2+}-$exchanger in the state $E_i 3Na_i^+$, $E_i Ca_i^{2+}$, $E_o Ca_o^{2+}$, $E_o 3Na_o^+$, respectively it follows directly that the equations governing the flux through the $Na^+/Ca^{2+}-$exchanger are

$$\frac{dx_1}{dt} = k_{-1}x_2 n a_i^3 + k_4 x_4 - x_1(k_1 c_i + k_{-4}) \tag{7.1.8}$$

$$\frac{dx_2}{dt} = k_{-2}x_3 + k_1 c_i x_1 - x_2(k_2 + k_{-1} n a_i^3) \tag{7.1.9}$$

$$\frac{dx_1}{dt} = k_2 x_2 + k_{-3} c_o x_4 - x_3(k_3 n a_o^3 + k_{-3}) \tag{7.1.10}$$

$$1 = x_1 + x_2 + x_3 + x_4 \tag{7.1.11}$$

Calculating the study state (using MATLAB) calcium leads to

$$J_{NAX} = k_4 x_4^* - k_{-4} x_1^* = \frac{k_1 k_2 k_3 k_4 c_i n a_o^3 - k_{-1} k_{-2} k_{-3} k_{-4} n a_i^3 c_o}{16 \text{ positive terms}}, \tag{7.1.12}$$

where the denominator is given by the expression

$$\begin{aligned} & n a_i^3 k_4 k_{-1} k_{-2} + c_i k_1 k_2 k_4 + n a_i^3 k_{-1} k_{-2} k_{-4} \\ & + c_i k_1 k_4 k_{-2} + n a_o^3 k_2 k_3 k_4 + n a_o^3 k_2 k_3 k_{-4} \\ & + c_o k_2 k_{-3} k_{-4} + c_o k_{-2} k_{-3} k_{-4} + n a_i^3 n a_o^3 k_3 k_4 k_{-1} \\ & + n a_i^3 n a_o^3 k_3 k_{-1} k_{-4} + c_i n a_o^3 k_1 k_2 k_3 + c_i n a_o^3 k_1 k_3 k_4 \\ & + n a_i^3 c_o k_{-1} k_{-2} k_{-3} + n a_i^3 c_o k_{-1} k_{-3} k_{-4} + c_i c_o k_1 k_2 k_{-3} \\ & + c_i c_o k_1 k_{-2} k_{-3} \end{aligned} \tag{7.1.13}$$

Combining this expression for the flux through the $Na^+/Ca^{2+}-$exchanger with those derived for current, leak and the PMCA we get the total flux across the plasma membrane, J_{pm} (positive into the cell) as:

$$J_{pm} = J_{pml} + J_{current} - J_{pmca} - J_{nax} \tag{7.1.14}$$

$$= v_{pml}(c_e - c_i) - \alpha I_{Ca} - \frac{v_{pmca} c_i^2}{K_{pmca}^2 + c_i^2} - J_{nax} \tag{7.1.15}$$

This expression replaces directly J_{in} from the De-Young Keizer formulation and so requires no further work to analyse the stability of the two models. Figure 7.3 shows the bifurcation diagram for the model when the extracellular Na^+ parameter, Na_{EC}^+, is varied in the case of (a) the one-pool and (b) the DeYoung Keizer Model.

7.2 Including Luminal-Ca^{2+} sensitivity of $InsP_3R$

In the One-Pool model Ca^{2+} stimulates its own release from the ER, while the flow of Ca^{2+} from the internal store is terminated when the concentration of Ca^{2+} in the internal store becomes too low since the flux through the IPR is given by

$$J_{ipr} \quad = \quad \pi V_2 \frac{c_s^m}{K_2^m + c_s^m} \frac{c_i^p}{K_3^p + c_i^p} \tag{7.2.1}$$

However, more recent experimental evidence indicates that not only does Ca^{2+} stimulate its own release, it also inhibits it, but on a slower timescale[103]. It is

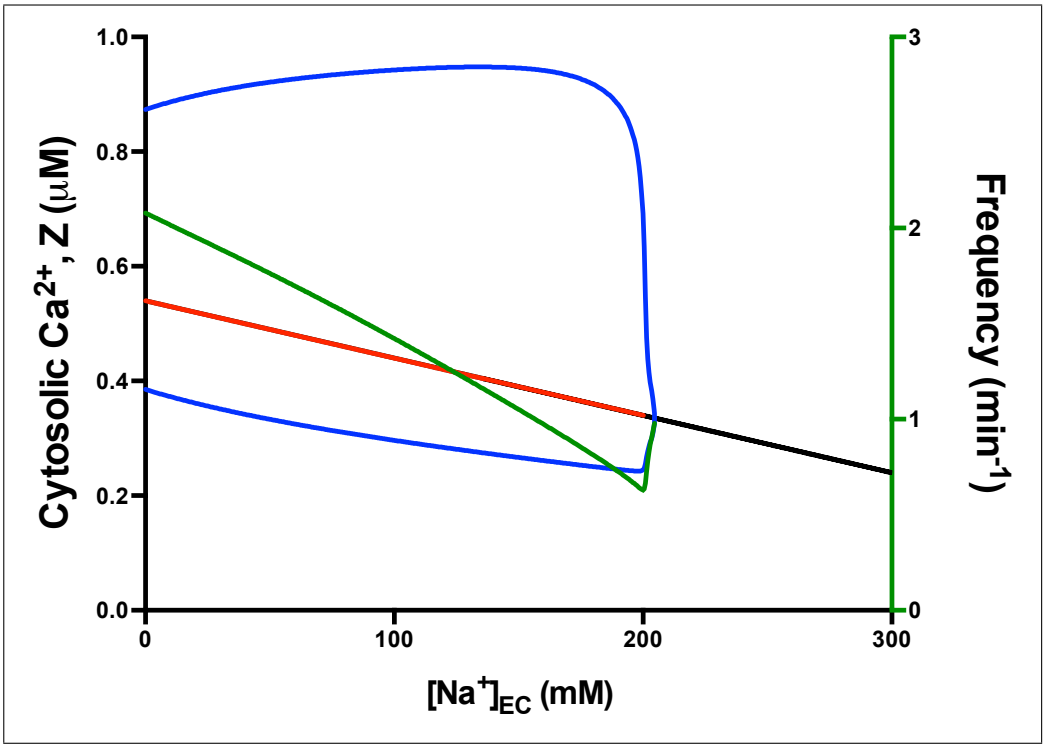

Figure 7.3 *Na^+/Ca^{2+}−exchanger model firurcation diagram on varying $[Na^+]_{EC}$ the One-pool model with physiological J_{PM}*

believed that this sequential activation and inactivation of the $InsP_3R$ by Ca^{2+} is the fundamental mechanism underlying $InsP_3$-dependent Ca^{2+} oscillations and waves. A number of models which incorporate this hypothesis have appeared and been reviewed, for example, in [120, 125].

One approach to modelling the physiological understanding of the $InsP_3R$ was developed by De Young and Keizer [39], and it mimics the molecular subunit configuration of the $InsP_3R$ to reflect the activation/inactivation sequence of the channel that results from the binding of $\left[Ca^{2+}\right]_i$ and $InsP_3$ to the $InsP_3R$.

This model, however, does not consider the impact of luminal $\left[Ca^{2+}\right]$ identified both in §5.2.2 and in the literature, for instance, [57].

7.2.1 Adding $[Ca^{2+}]_{ER}$ sensitivity to the DeYoung Keizer IP_3-Receptor Model

To introduce luminal sensitivity to the model, we replace a_j from the original formulation with $a_j := a_j\left(\left[Ca^{2+}\right]_{ER}\right)$. This is initially taken to be

$$a_j \frac{c_e}{c_e^\star} \qquad j \in \{1,3\} \tag{7.2.2}$$

where $c_e^\star$ is the equilibrium value of the luminal calcium concentration.

The derivation of the steady states remains the same as for Figure 6.11, and in the special case chosen above such that

$$a_j\left(c_e^\star\right) = a_j \tag{7.2.3}$$

the model inherits the steady state open probability as before. Of course it is possible vary the function $a_j\left(c_e\right)$ to make the receptor more or less sensitive to $\left[Ca^{2+}\right]_{ER}$ as suggested by the data.

7.3 Buffering

When considering sensitivity to luminal $\left[Ca^{2+}\right]$ it is vital to understand the dynamics of buffering and to make an informed decision whether to include buffering, dynamic or rapid, when modelling a system.

7.3.1 1-Compartment Model

In order to investigate the impact and importance of buffering in the system it is first necessary to develop and interrogate a simplified model. This allows for an investigation into the importance of elements in the buffering system such as luminal Ca^{2+} buffering and to make an informed choice as to whether to employ dynamic buffering, rapid buffering or, indeed, to neglect buffering altogether.

An initial one-compartment model that looks at the interaction of Ca^{2+} with its buffer given by the reaction system

$$C + B \underset{k_2}{\overset{k_1}{\rightleftharpoons}} S \tag{7.3.1}$$

where free Ca^{2+}, its buffer(s) and its buffered-complex $Ca \cdot B$ are given by C, B and S, respectively. Assuming the reactions occur with probability proportional to the concentrations of C, B and S (the mean-field assumption) results in the system of equations,

$$\frac{dC}{dt} = -k_1 CB + k_2 S \tag{7.3.2}$$

$$\frac{dB}{dt} = -k_1 CB + k_2 S \tag{7.3.3}$$

$$\frac{dS}{dt} = k_1 CB - k_2 S \tag{7.3.4}$$

with initial conditions $B(0) = B_0$ and $C(0) = C_0$.

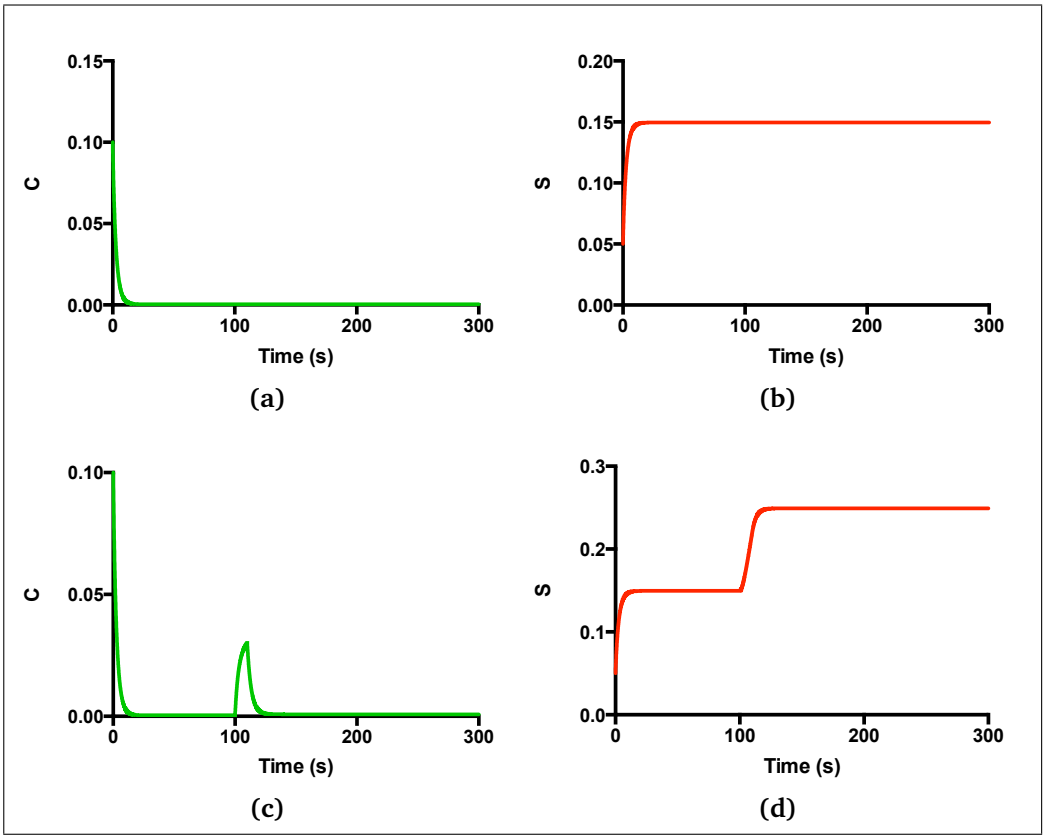

Figure 7.4 *Buffering model runs for (a, c) C and (b,d) S with varying values of a; (a, b) $a = 0$, (c, d) $a = 0.01$*

A perturbing injection of free (unbuffered) Ca^{2+} into the system is considered by adding a function, $\mu(t)$, which describes the rate of that injection, to the dC/dt equation. $\int_0^t \mu(u)du$ can be thought of as the total amount of Ca^{2+} injected into the system after time t.

Examples of the system are depicted in Figure 7.4 where $\mu(t)$ is considered as a step function,

$$\mu(t) = \begin{cases} 0 & t < 100 \\ a \in \mathbb{R}_{\geq 0} & t \in [100, 110] \\ 0 & t > 110 \end{cases} \tag{7.3.5}$$

Reducing the system to one equation

Solving the the system in Equations (7.3.2 -7.3.4) for the equilibrium (which occur at values of t, $t^\star$, where $dC/dt = dB/dt = dS/dt = 0$) give $\mu(t^\star) \equiv 0$ and

$$S^\star = \frac{k_1 C^\star B^\star}{k_2}. \tag{7.3.6}$$

Also from Equations (7.3.2 -7.3.4) both

$$\frac{dS}{dt} = -\frac{dB}{dt} \tag{7.3.7}$$

$$\frac{dC}{dt} = \frac{dB}{dt} + \mu(t) = \mu(t) - \frac{dC}{dt} \tag{7.3.8}$$

which gives $B(t) = B_0 - S(t)$ and $C(t) = C_0 - S(t) + \int_0^t \mu(u)du$.

Thus the system collapses to one equation

$$\frac{dS}{dt} = k_1 \left(C_0 - S + \int_0^t \mu(u)du \right) (B_0 - S) - k_2 S \tag{7.3.9}$$

$$= k_1 S^2 - \left(k_2 + k_1 C_0 + k_1 B_0 + k_1 \int_0^t \mu(u)du \right) S + k_1 B_0 \left(C_0 + \int_0^t \mu(u)du \right) \tag{7.3.10}$$

with fixed points

$$S_\pm = \frac{-b \pm \sqrt{b^2 - 4ac}}{2a} \tag{7.3.11}$$

where

$$a = k_1 \tag{7.3.12}$$

$$b = -\left(k_2 + k_1 \left(\int_0^t \mu(u)du + C_0 + B_0 \right) \right) \tag{7.3.13}$$

$$c = k_1 B_0 \left(C_0 + \int_0^t \mu(u)du \right) \tag{7.3.14}$$

Behaviour around the equilibria

To consider the behaviour immediately about the equilibria, the system is linearised using Taylor's Theorem by taking the Taylor expansion about $S_\pm$ at the point S. This is the equivalent of taking the Jacobian introduced in §1.4 but allows higher order terms to be considered since the system is in one dimension and yields:

$$\frac{dS}{dt} = f(S_\pm) + f'(S_\pm)(S - S_\pm) + \frac{f''(S_\pm)}{2!}(S - S_\pm)^2 + \cdots + \frac{f^{(k)}(S_\pm)}{(k)!}(S - S_\pm)^k + \ldots \tag{7.3.15}$$

restricting this to the first term approximation and changing variables by setting $s = S - S_{\pm}$ (and noting $\frac{ds}{dt} = \frac{dS}{dt}$) gives

$$\begin{aligned} \frac{ds}{dt} &\approx sf'(S_{\pm}) && (7.3.16) \\ &= s\left(2aS_{\pm} + b\right) && (7.3.17) \end{aligned}$$

where a and b are given in Equation 7.3.12 and 7.3.13, respectively. This linearisation, reveals two pieces of additional information:

1. It is clear from equation (7.3.17) that S_+ is (globally) unstable whilst S_- is (globally) stable since

$$\frac{ds}{dt} \approx s\left(\pm\sqrt{b^2 - 4ac}\right) \tag{7.3.18}$$

   is positive for the positive root and vice versa for the negative root giving the required eigenvalue conditions for (in-)stability. Changing focus to consider the physiological behaviour about S_-.

2. The solution of equation (7.3.17),

$$s(t) = (S_0 - S_{\pm})\, e^{(2aS_{\pm}+b)t} \tag{7.3.19}$$

   gives us (if $S_0 \neq S_{\pm}$ and S_0 is in the vicinity of $S_{\pm}$) exponential decay to the equilibrium.

Homogeneous Full Taylor

In fact, because the expression is polynomial (of order two), it is possible to use the Taylor expansion to describe exactly what the solution curve looks like about the equilibria. Assuming a, b and c are independent of time we can take the full Taylor expansion, we have,

$$\begin{aligned} \frac{ds}{dt} &= sf'(S_{\pm}) + s^2 f''(S_{\pm}) && (7.3.20) \\ &= as^2 + (2aS_{\pm} + b)s && (7.3.21) \end{aligned}$$

which, by separation of variables, solves to give the inelegant

$$s(t) = \frac{(2aS_{\pm} + b)\exp\left((t-d)\left(2aS_{\pm} + b\right)\right)}{1 - a\exp\left((t-d)\left(2aS_{\pm} + b\right)\right)} \tag{7.3.22}$$

where d can be determined from the initial conditions. This represents a full solution (with changed coordinates about the equilibria) in the homogeneous

case.

Non-Homogeneous Full Taylor

Further, the solution can be given explicitly when the coefficients are functions of time as Equation 7.3.21 can be seen as a Bernoulli equation of the form

$$\frac{ds}{dt} + p(t)s = q(t)s^n \tag{7.3.23}$$

with $p(t) = -(2a(t)S_{\pm} + b(t))$, $q(t) = a(t)$ and $n = 2$ which solves to give a full solution in the non-homogeneous case

$$s(t) = \frac{e^{-\int p(t)dt}}{-\int e^{-\int p(t)dt} q\,(t)\,dt + D}. \tag{7.3.24}$$

Once we include luminal sensitivity to the $InsP_3R$ we must consider SOCE. etc.

7.4 Store-operated Ca^{2+}-entry (SOCE)

First introduced by Putney in 1986 [107], under the name of capacitative calcium entry (CCE), SOCE describes the process by which depletion of intraluminal Ca^{2+} activates store-operated channels (SOCs) for Ca^{2+} century across the plasma membrane. The best studied SOC is the Ca^{2+}-activated Ca^{2+}-channel (CRAC) [21, 55, 54, 87, 102, 106, 136]. Depletion of the $\left[Ca^{2+}\right]_{EC}$ causes STIM1 to move to the SR-PM junctions, bind to Orai1, and activate SOCs for Ca^{2+}-entry from the extracellular space [85].

Two major components of SOCE have been discovered

- Stromal interaction molecule 1 (STIM1) is a transmembrane protein residing primarily in the ER. STIM1 contains an EF-hand, an N-terminius directed towards the lumen of the SR, and a C-terminus facing the cytoplasmic side. STIM1 functions as an $\left[Ca^{2+}\right]_{EC}$ sensor. And
- Orai1 is a transmembrane protein present in the plasma membrane with intracellular N- and C-termini and is an essential component of the store-operated channel [83, 105, 107].

It was not until the late 2000s that the mechanism that STIM1 uses to sense and communicate ER $\left[Ca^{2+}\right]$ to Orai1 was discovered [41, 53, 58, 73, 83, 95, 102, 105, 108, 139].

Emptying of Ca^{2+} from the ER causes a conformational change of STIM1 and leads to oligomerisation, which enables the polybasic region to target STIM1 to target STIM1 to SR-PM junctions, and causes a conformational change in STIM1 to expose its CRAC-activation domain (CAD, amino-acids 342-448 [102]). In the junctions, the exposed CAD binds to Orai1. Stim1-Orai1 interactions change the conformation of Orai1, which drives the opening of CRAC channels and triggers Ca^{2+} entry.

Moreover, the channel opening is optimised β phosphatidylinositol 4-phosphate ($PI4P$ [79, 133]) while the channel opening is disrupted by a large cell volume increase [86]. On the other hand, the CRAC channel is inactivated by calmodulin [95], annexing 6 [94] and protein kinase C [92]. Inhibition of mitochondrial Ca^{2+} uptake decreases SOCE [51, 114].

7.4.1 Modelling SOCE

Only a few attempts [135, 80, 98, 85, 63] have been made to model this phenomenon and the models have varied wildly as biological understanding of this process has increased. The first two of these, [135, 80] were published before a molecular basis for SOCE was established and were informative when published and led to some of the biological discoveries described above. [85, 98] include more physiological expressions for SOCE but neither accounts for the slow translocation of oilgermerised STIM1 to the plasma membrane - a process which is known as the rate-limiting step for SOCE activation [84]. Indeed, in [98], a slow diffusion of Ca^{2+} between two distinctly modelled SR components (SR since they consider muscle), the internal SR and the superficial SR is hypothetically introduced to help replicate experimental results. SOCE is then activated when the superficial SR is depleted rather than due to the slow translocation.

Design of a SOCE Output Feedback Controller

[85] explicitly models both luminal Ca^{2+} dissociation from STIM and binding of STIM to Orai and deciding an output feedback controller to return the system to basal Ca^{2+}. Their methodology is introduced here.

The dynamic binding of and dissociation of $\left[Ca^{2+}\right]_{ER}$ and STIM1 can be modelled by the differential equation

$$\frac{d[STIM1]}{dt} = -f_s[STIM1][Ca^{2+}]_{SR}^{n_s} + b_s([TS] - [STIM1]), \tag{7.4.1}$$

where f_s is the binding rate, b_s is the dissociation rate, n_s is a positive expo-

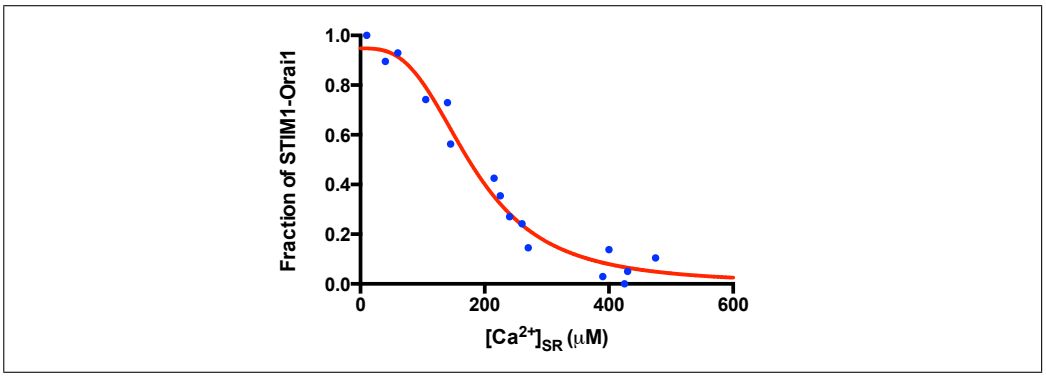

Figure 7.5 *Steady-state* $[SO]$ *fit-data*

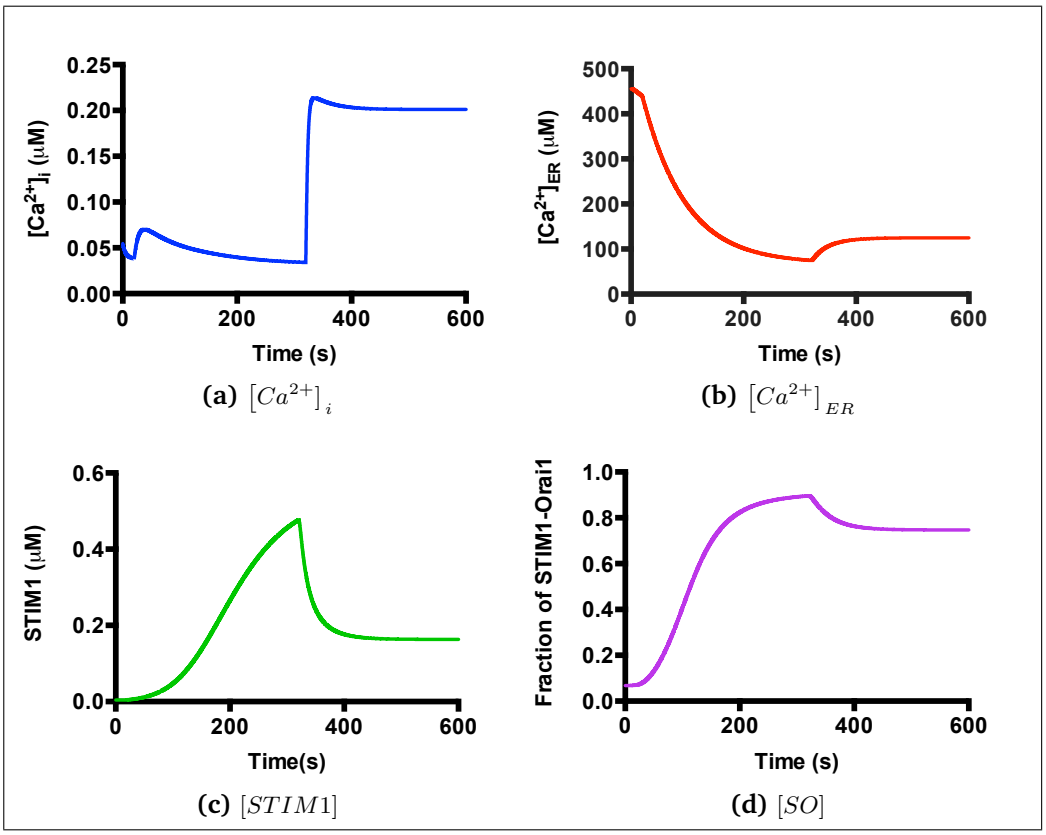

(a) $[Ca^{2+}]_i$ **(b)** $[Ca^{2+}]_{ER}$

(c) $[STIM1]$ **(d)** $[SO]$

Figure 7.6 *SOCE simulations from the model by [85] with parameters from that work. This simulation shows the behaviour of the mode, first when the function of the SERCA is reduced to mimic the addition of thapsigargin. Then, at* $t = 320$ sc_0 *is suddenly increased from* $10\ \mu M$ *to* $2000\ \mu M$ *to observe the response of the system to this.*

nent, $[TS$ is the concentration of total STIM1. Here we assume that as soon as the $\left[Ca^{2+}\right]_{ER}$ is released from the luminal EF-hand of STIM1, the STIM1 is immediately in the ER-PM junctions. Thus $[STIM1]$ can be regarded as the concentration of the active cytosolic part of STIM1 in the ER-PM junctions. The net rate of Ca^{2+} binding to and release from STIM1 is given by

$$r_{stim} = -f_s[STIM1][Ca^{2+}]_{SR}^{n_s} + b_s([TS] - [STIM1]). \tag{7.4.2}$$

The dynamic binding of the active cytosolic part of STIM1 to Orai1 (the region of amino acids 70-91 [102]) and the dissociation from Orai1 can be described by

$$STIM1 + Orai1 \underset{b_0}{\overset{f_0}{\rightleftharpoons}} SO, \tag{7.4.3}$$

where SO denotes the complex of STIM1 and Orai1. It then follows that

$$\frac{d[SO]}{dt} = f_0(1 - [SO])[STIM1] - b_0[SO], \tag{7.4.4}$$

where f_0 is a binding rate, b_0 is a dissociation rate, and $[SO]$ is the fraction of STIM1-Orai1 complex among the total Orai1, that is, $[SO]$ is the ration of the concentration of STIM1-Orai1 and the total concentration of Orai1. The term $b_0[SO]-f_0(1-[SO])[STIM1]$ isn't included in Equation 7.4.1 because the binding of the cytosolic part of STIM1 to Orai does not affect the luminal part of STIM1. The Equations 7.4.1 and 7.4.4 constitute a dynamical output feedback controller:

$$p_{soce} = [SO]. \tag{7.4.5}$$

Experimental data about the dependence of the SOCE current on the SR Ca^{2+} concentrations as obtained by Luik et al [87] (figure 1c). Theses data can be used to determine the values of parameters in the Equations 7.4.1 and 7.4.4. The data were obtained at equilibrium of the system which, for Equations 7.4.1 and 7.4.4 is given by

$$\overline{SO} = \frac{f_0 b_s[TS]}{b_0 b_s + f_0 b_s[TS] + b_0 f_s[Ca^{2+}]_{sr}^{n_s}}. \tag{7.4.6}$$

Since no data about the total STIM1 concentration are available, $[TS]$, is taken to be 1 μM. The parameters n_s, f_s, b_s, f_0, b_0 are determined by fitting the steady $\overline{SO}$ defined by Equation 7.4.6 into the data of Luik et al [87]. R_{soce} and I_{serca} are selected to result in the equilibrium calcium levels of $= 0.05$ μM [138] and 450 μM [59, 138] when $\left[Ca^{2+}\right]_{EC}$ =1500 μM [48]. The parameters R_{ipr} and R_{leak} are adjusted in simulation to match runs to experimental observations.

7.5 Discussion

The two models investigated in the previous chapter are powerful tools for looking at whole-cell Ca^{2+} dynamics. They have been the basis of several hypotheses and informative studies into Ca^{2+}-signalling. They both come from different philosophies of modelling. The one-pool model sought to be phenomenological, attempting to replicate the outcome of the system, choosing convenient mathematical The Wagner Keizer model with the physiologically-informed De-Young Keizer $InsP_3R$ model attempts to model the states and flux of the receptor as exactly as possible.

Adding an expression for the flux through the $Na^+/Ca^{2+}-$exchanger removes the simplicity of the system that made the one-pool model's simple formulation in two-dimensions useful. Therefore, henceforth the Wagner-Keizer approach alone will be adopted.

An investigation into buffering revealed expressions for the binding and unbinding of Ca^{2+} and its buffers taking a single-compartment view. This rationale is often used to justify assuming rapid buffering but the work herein provides a useful exact expression for the buffering dynamics in this case, from which an informed decision can be made as to its (non-)inclusion when choosing to model each compartment.

This is important when considering SOCE since the ER's ability to release Ca^{2+} may impact upon the cell's need for the, relatively slow, activation of SOCE. [85] present a physiologically informed model of SOCE via a feedback control mechanism.

There are two problems with their approach which the following chapter seeks to address. The first is that the whole-cell model is a non-oscillatory one. An injection of $InsP_3$ is required to initiate each transient whereas physiologically $InsP_3$ is known either to oscillate or remain at a constant level for constant agonist stimulation. This is addressed by implementing this model into a Wagner-Keizer approach in Chapter 8.

Further, in generating a feedback-control mechanism, it was assumed that as soon as luminal Ca^{2+} is released from the luminal EF-hand of STIM1, the STIM1 is instantaneously present in the ERÐPM junctions. This is not only known not to be true, but it is also known to be the rate limiting process for SOCE and thus its inclusion seems essential to a model which can inform us about the role of SOCE in *OT*-induced Ca^{2+} oscillations. This refinement is introduced in Chapter 8.

Chapter 8

A Two-Compartment Physiologically-informed *CHO–hOT* Ca^{2+}-Oscillation Model with SOCE and Luminally-sensitive $InsP_3R$

8.1 Formulating the Model

In accordance with the introduction to modelling in Chapter 6 and the fluxes derived to improve the physiological relevance of the model in Chapter 7, the whole-cell Ca^{2+} dynamics are modelled by the stem of ODEs [74]:

$$\frac{dc_i}{dt} = J_{pm}^{in} - J_{pm}^{out} + J_e^{in} - J_e^{out}, \tag{8.1.1}$$

$$\frac{dc_e}{dt} = \gamma \left(J_e^{out} - J_e^{in} \right). \tag{8.1.2}$$

The other fluxes are defined as

- J_{pm}^{in}, the Ca^{2+} flux into the cytosol through the plasma membrane. It consists of expressions for the three fluxes
  - receptor operated Ca^{2+} entry, J_{roce}, which is modelled as

$$J_{roce} = v_0 \pi \tag{8.1.3}$$

  - leak through the plasma membrane, J_{pml}, which is modelled as

$$J_{pml} = v_1, \tag{8.1.4}$$

    and

  - store-operated Ca^{2+} entry, J_{soce} the expressions for which are discussed below

- J_{pm}^{out}, the Ca^{2+} flux out from cytosol, through the plasma membrane consists of the flux through
  - the Plasma membrane Ca^{2+}-ATPase, J_{pmca}, which is modelled as in Chapter 6 as

$$J_{pmca} = \frac{V_p c_i^2}{K_p^2 + c_i^2}, \tag{8.1.5}$$

    and

  - the $Na^+/Ca^{2+}-$exchanger, J_{nax} which is modelled as in §4.2.3,

$$J_{nax} = \frac{k_1 k_2 k_3 k_4 c_i n a_o^3 - k_{-1} k_{-2} k_{-3} k_{-4} n a_i^3 c a_o}{16 \text{ positive terms}}, \tag{8.1.6}$$

    from §1.4

- J_e^{in}, the flux of Ca^{2+} from the cytosol into the ER, via the
  - Sarco/Endoplasmic Reticulum Ca^{2+}-ATPase, J_{serca}, which is modelled as in Chapter 6 as

$$J_{serca} = \frac{V_s c_i^2}{K_s^2 + c_i^2}, \tag{8.1.7}$$

- J_e^{out}, the flux of Ca^{2+} from the cytosol into the ER, and consists of
  - Ca^{2+} release via $InsP_3R$, J_{ipr}, the modelling of which is discussed below and
  - leak from the ER, J_{erl} which is modelled as a constant

$$J_{erl} = v_{erl}, \tag{8.1.8}$$

8.1.1 Modelling $InsP_3R$

As explained in §6.3.1 the choice of $InsP_3R$ release model is highly sensitive and, depending on the choice made can lead to very different results. It is generally accepted that, since $\left[Ca^{2+}\right]_{ER}$ is much higher than $\left[Ca^{2+}\right]_i$ that Ca^{2+} transport

through the receptor is driven by that Ca^{2+} concentration gradient and thus flux through the $InsP_3R$ is of the general form

$$J_{ipr} = V_{ipr} p_{ipr} \left(c_e - c_i\right). \tag{8.1.9}$$

Here

- V_{ipr} represents the maximal rate through the $InsP_3R$,
- p_{ipr} is the $InsP_3R$ channel open probability and

Here the simplest luminally-sensitive $InsP_3R$ model is employed as per the Goldbeter-Dupont Model

$$p_{ipr} = \frac{c_e^m}{K_2^m + c_e^m} \frac{c_i^p}{K_3^p + c_i^p} \tag{8.1.10}$$

8.1.2 Modelling the Mitochondria

Inhibition of the mitochondria is known to have an inhibitory effect on SOCE [51, 114]. The dynamics of mitochondrial uniporters is complex, however and it can be assumed that a proportion of the PMCA extrusion term accounts for the mitochondrial sequestering of Ca^{2+} as per [113].

8.1.3 Model Equations

Thus, taking into account all of the above the following system of ODEs was proposed to model the system illustrated in Figure 8.1 and with equations:

$$\frac{dc}{dt} = v_1\pi + v_0 - J_{nax} - \frac{V_p c_i^2}{K_p^2 + c_i^2} + \left(J_{ipr}(c_i, c_e) + J_{erl}\right)\left(c_e - c_i\right) - \frac{V_s c_i^2}{K_s^2 + c_i^2}, \tag{8.1.11}$$

$$\frac{dc_e}{dt} = \gamma\left(\left(J_{ipr}(c_i, c_e) + J_{erl}\right)\left(c_e - c_i\right) - \frac{V_s c_i^2}{K_s^2 + c_i^2}\right) + \frac{V_{soce} c_o}{K_{soce} + c_o}[so], \tag{8.1.12}$$

$$\frac{d[so]}{dt} = f_0\left(1 - [so]\right)[stim] - b_0[so], \tag{8.1.13}$$

$$\frac{d[stim]}{dt} = -f_s[stim]c_s^{n_s} + b_s\left([ts] - [stim]\right). \tag{8.1.14}$$

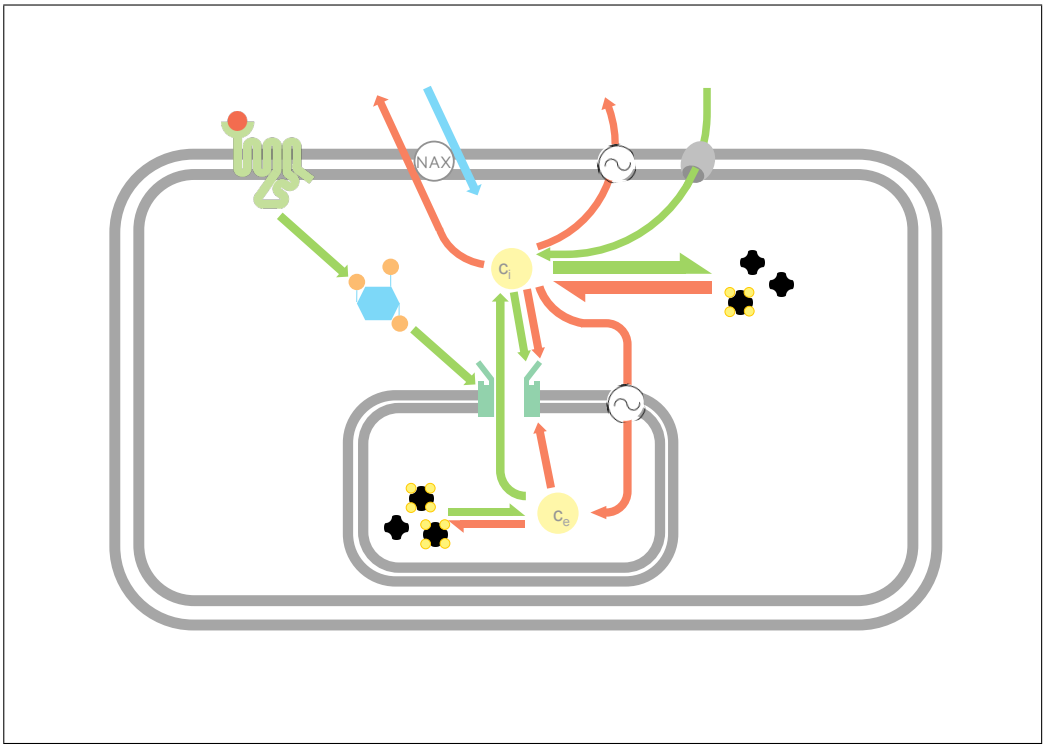

Figure 8.1 *Schematic of Two-Compartment Physiologically-informed* CHO–hOT Ca^{2+}*-Oscillation Model with SOCE and Luminally-sensitive* $InsP_3R$

8.2 Results

8.2.1 Varying $InsP_3$

Figure 8.2 shows the bifurcation diagram for the model with respect to the parameter π. In Chapter 3 it was established that there was little dose-dependency of the oscillations. The bifurcation diagram in (a) is very similar to those for the original one-pool model (Figure 6.8 in §6.2). For this parameter choice, the frequency of oscillations, shown in (b), varies between one and three oscillation every two minutes. The parameters used have been chosen such that frequency of model oscillations when $\pi = 1$ is ~ 0.6 oscillations per minute in order to agree with the average period of $100\ s$ for *CHO–hOT* cells in Chapter 3. Our model here inherits frequency and amplitude dose-dependence from the one-pool formulation but only within a relatively small range of frequencies and amplitude.

Figure 8.3 puts this bifurcation into context and allows a replication of Figure 3.2 in (a). As with the experiments that lead to this figure, our model was run to equilibrium, then at three 5 minute intervals, the parameter π was stepped down by 0.2 from 1.4 to 1 to represent the transition from the high dose of *OT* to the low dose. Figure 8.3 (b) demonstrates what happens when π is increased further,

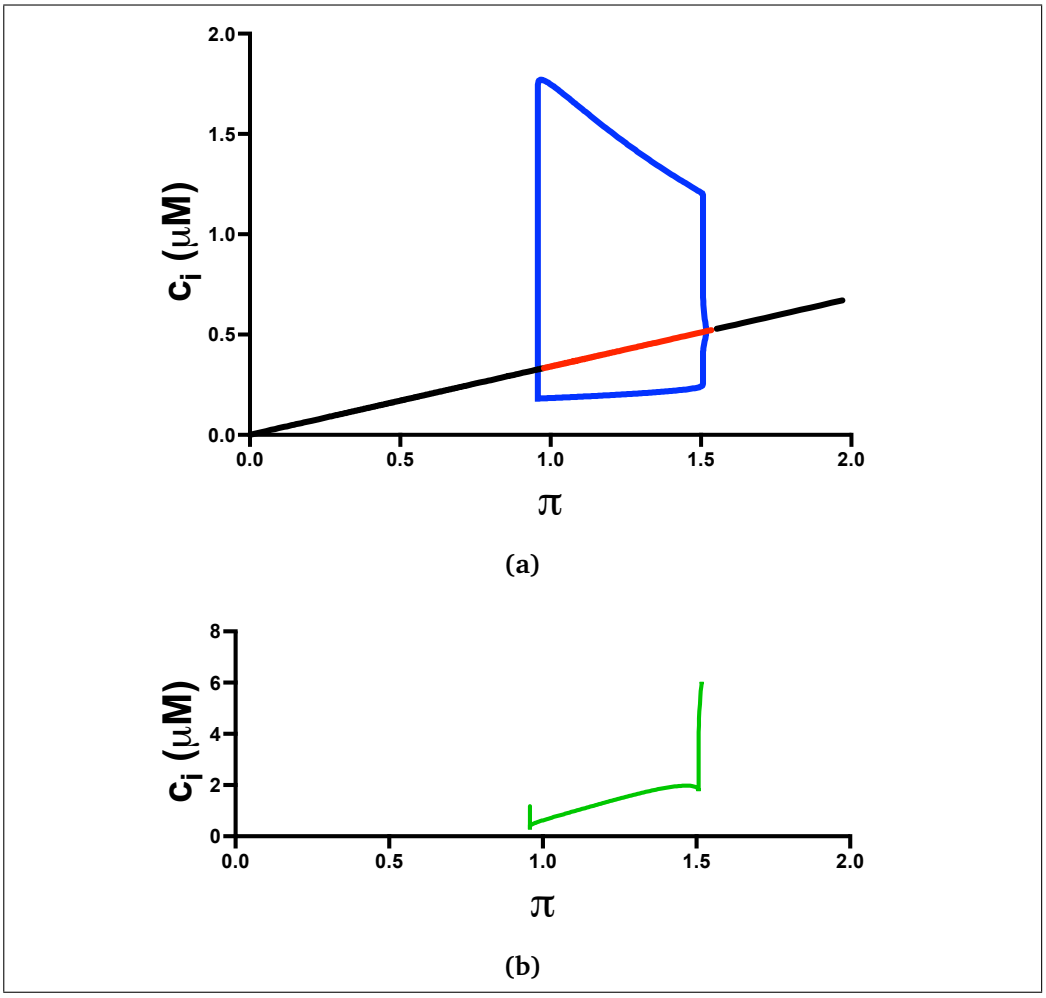

Figure 8.2 *(a) Bifurcation diagram and (b) frequency of oscillations on varying π*

here to 4. As in the experimental case, the model gives one transient and then comes back to rest at an increased $\left[Ca^{2+}\right]_i$ steady-state.

8.2.2 The Role of Extracellular Calcium, Ca^{2+}_{EC}

Varying $\left[Ca^{2+}\right]_{EC}$

The bifurcation diagram for varying c_o, the parameter which represents Ca^{2+}_{EC}, is shown in Figure 8.4 (a) along with a description of the change in frequency of oscillation in (b). Figure 8.4 (c) shows a two-parameter bifurcation diagram. Such a diagram shows the locations of the Hopf-Bifurcations when the two parameters are varied, the space between them represents the range of parameters for which oscillations can occur.

Figure 8.5 shows exemplar traces of the model to imitate Figure 4.5 in (a) and Figure 4.1 in (b). For (a) the model was brought to equilibrium with c_o set at

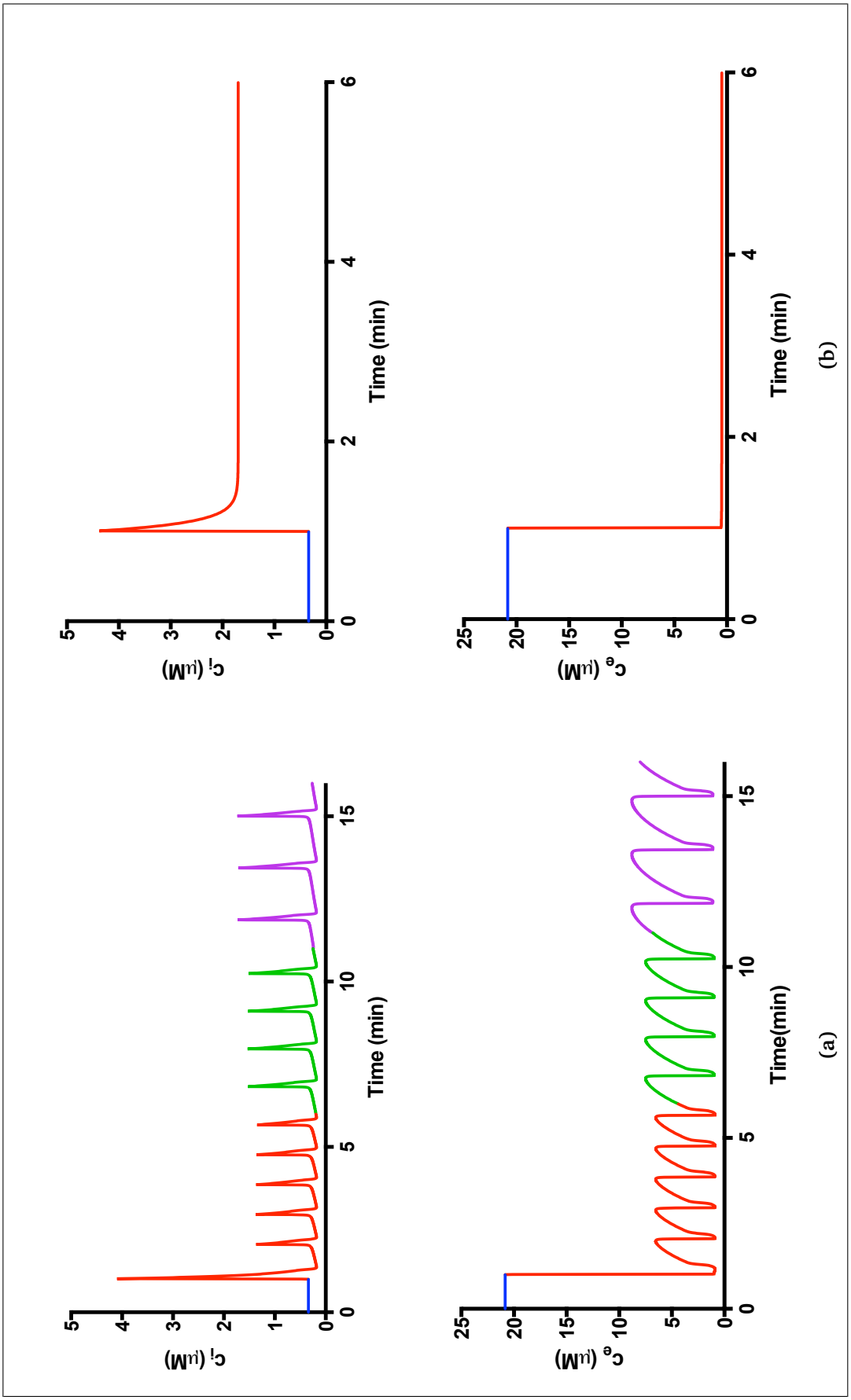

Figure 8.3 *Example runs of the model (a) varying* π *(b)* $\pi = 4$

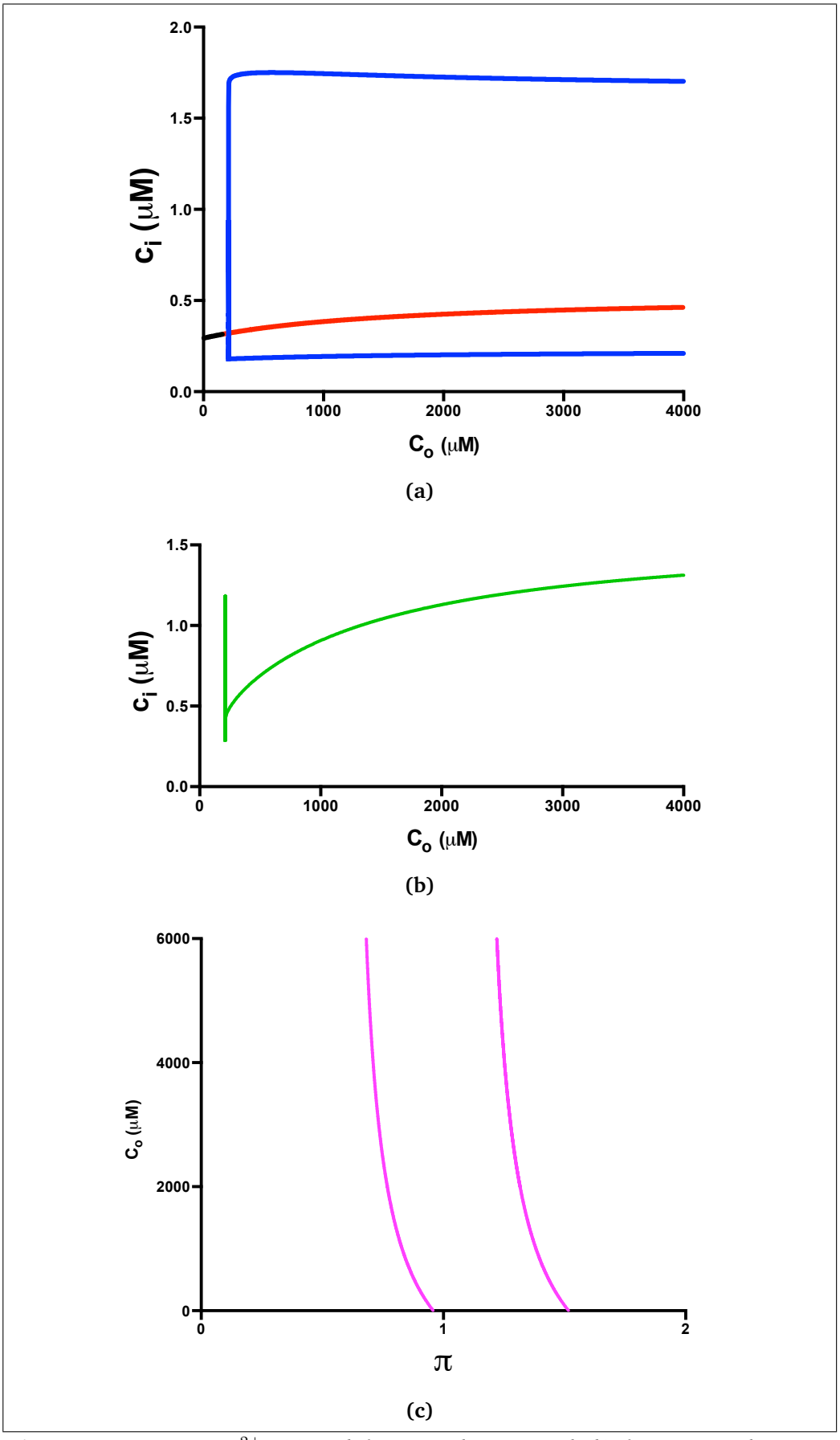

Figure 8.4 *Vareying Ca^{2+}_{EC} (a) c_o bifurcation diagram and (b) frequency with a two-parameter bifurcation plot on varying π and c_o simultaneously.*

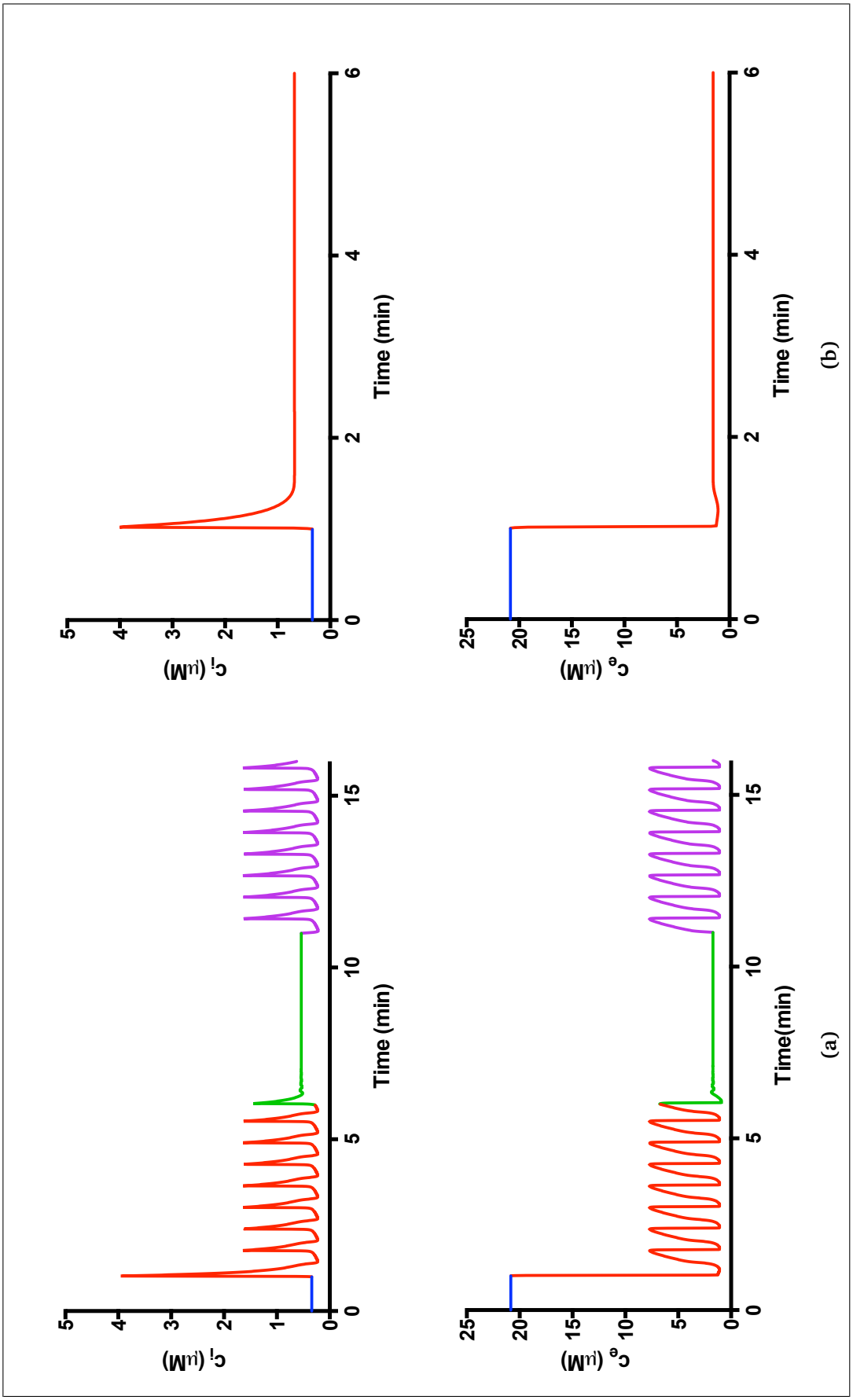

Figure 8.5 *Ca^{2+}_{EC} model runs to duplicate (a) varying Ca^{2+}_{EC} and (b) removing it.*

$500\ \mu M$, it was then left for 60 seconds before switching π to equal 1. After 5 minutes, c_0 was stepped up to $2000\ \mu M$ and then again to $4000\ \mu M$ after a further 5 minutes. The period of the oscillations quickened at each step with little variation in the amplitude. For (b) the model was brought to equilibrium with c_o set at $500\ \mu M$, it was then left for 60 seconds before switching π to equal 1. This resulted in a single 'initial' transient followed by an increased steady-state value of $c_i = \left[Ca^{2+}\right]_i$.

Varying PMCA activity

Figure 8.6 shows (a) the bifurcation diagram and (b) the frequencies associated with varying the parameter V_{PMCA} which represents the maximum flux available to the system through the PMCA. TheRsteady-state solution increases linearly with increase in V_{PMCA}, within the range of parameters that allow for oscillations the amplitude is approximately constant but the frequency of those oscillations increases with V_{PMCA}. Figure 8.6 (c) shows the impact on the ranges of π for which oscillations occur for a given V_{PMCA}.

Varying $[Na^+]_{EC}$

Figure 8.7 shows traces which replicate the experiments in Figure 4.9 (a) and (b). In (a) the model is run to equilibrium with $[Na^+]_{EC} = 145\ mM$ and then allowed to run for one minute. was then set to $0\ mM$ and, after a small rise from basal $\left[Ca^{2+}\right]_i$ the system returns to rest. After a further 5 minutes π is switched to 1 and oscillations occurred as in Figure 4.9. In (b) the system is run to equilibrium with $[Na^+]_{EC} = 0\ mM$ and then allowed to run for one minute before π is switched to 1. After 5 minutes $[Na^+]_{EC}$ is returned to $145\ mM$ and the period of oscillations decreases markedly. On return of $[Na^+]_{EC}$ to $145\ mM$ oscillations return to their original frequency.

Varying ROCE

Chapter 4 reveals that in ATP can be used as a way of increasing receptor-activated entry via direct Ca^{2+} entry though $P2_y$ receptors as well as by stimulating the release of Ca^{2+} from the lumen of the ER through the stimulation of $P2_x$ receptors and thus the G_q signalling pathway. The final section in that chapter identified that the increase in frequency of oscillations was not due to increased production of $InsP_3$ (modelled as π). Indeed quite the opposite; the

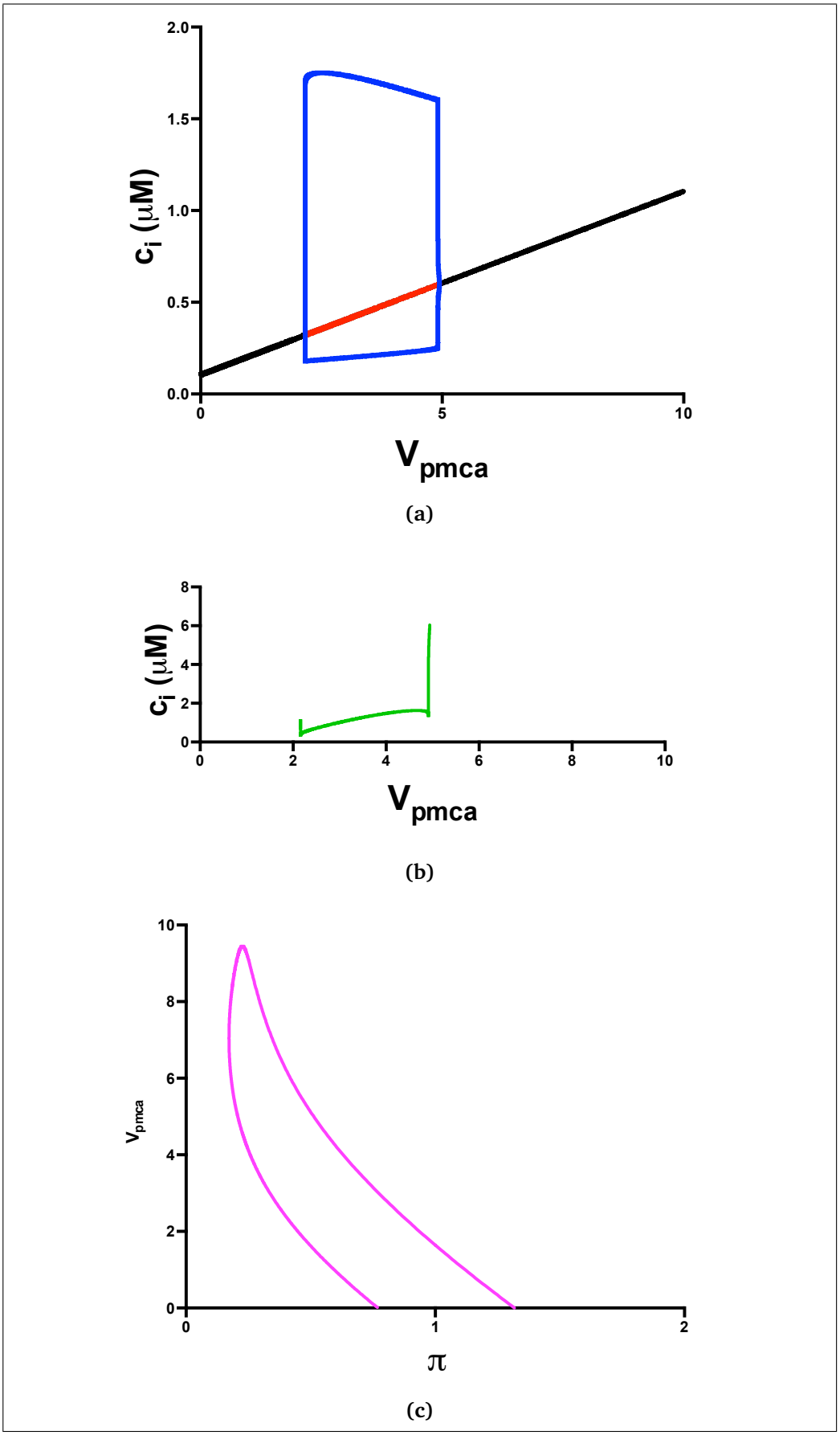

Figure 8.6 *(a) Bifurcation diagram and frequency for v_{pmca} and a two-parameter bifurcation diagram for π and v_{pmca}.*

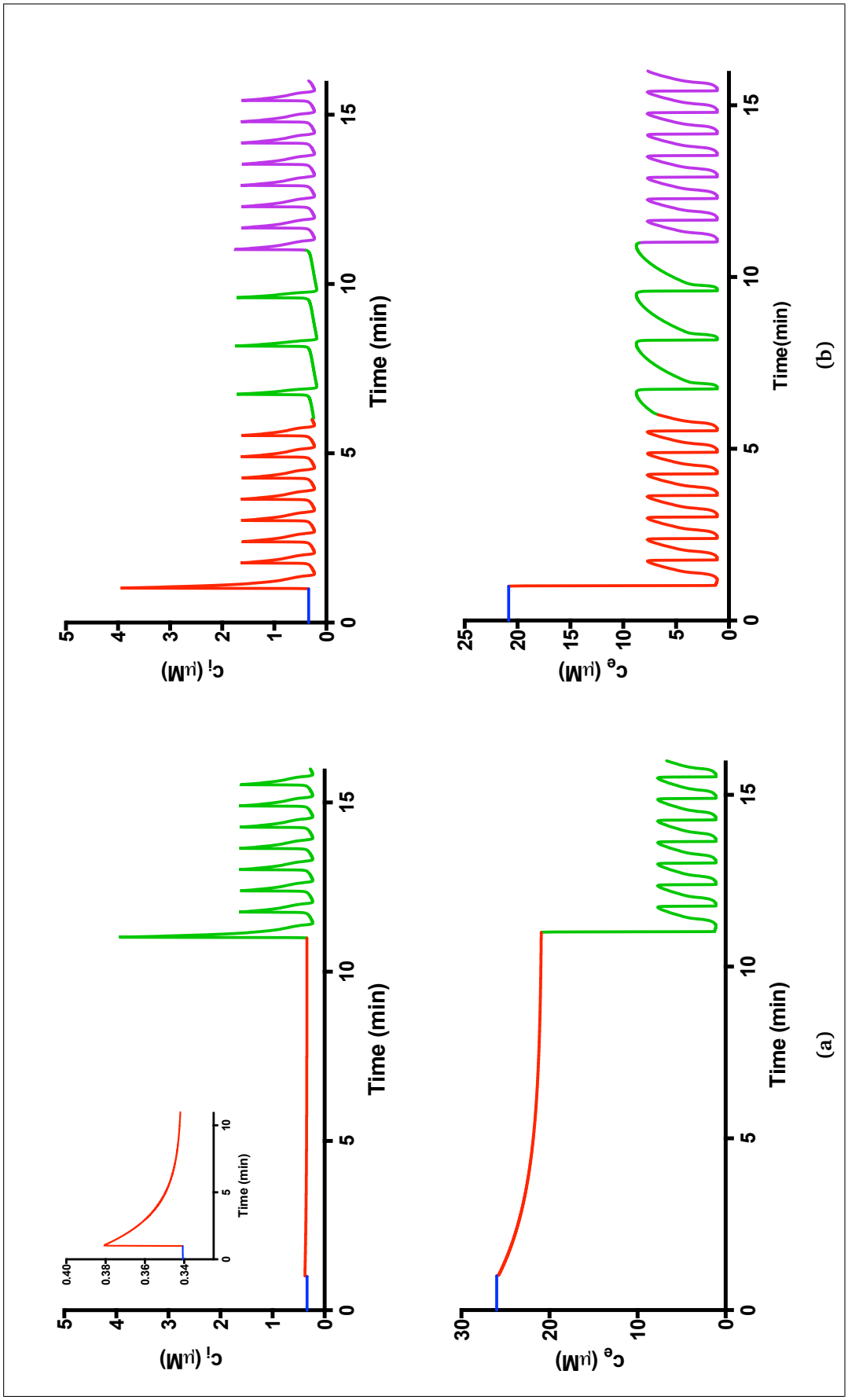

Figure 8.7 *Modelling runs to duplicate experiments for varying* $[Na^+]_{EC}$.

amount of $InsP_3$ was lower in the case of ATP-induced Ca^{2+} oscillations when compared to *OT*-induced Ca^{2+} oscillations.

Stimulation by *OT* has thus far been modelled by setting the parameter $\pi = 1$. In order to model stimulation by ATP π is reduced to 0.75 (to account for the reduced production of $InsP_3$) In the absence of a physiologically informed modely for Ca^{2+} entry through $P2_y$ receptor, the constant influx of Ca^{2+} through the plasma membrane, modelled as the constant, v_0 is increased from 0.01 to $5.5\ \mu M\ min^{-1}$.

Figure 8.8 replicates experimental Figure 4.12. The model is run to equilibrium in the absence of Ca^{2+}_{EC}, that is $c_0 = 0$. After one minute, π is set to 0.75 and v_1 is increased to 5.5 to represent the addition of ATP to the system. We see an initial transient but no ensuing oscillations. This differs from the experiment since the steady state level of after this initial transient is higher than the original equilibrium. When, after five minutes, the parameter values for ATP application were instantaneously switched to those for *OT* and calcium restored to the extracellular medium ($\pi = 1,\ v_0 = 0.01$ and $c_o = 2000$). Oscillations occur but without an initial (larger) transient (in agreement with the experimental result). When the parameters are returned to those for ATP stimulation in the absence of after a further five minutes the response is identical to that of the original application of ATP.

8.2.3 The Role of Luminal Calcium, $[Ca^{2+}]_{ER}$

Varying SERCA activity

As discussed in Chapter 5, the SERCA inhibitor CPA is known to reduce the number of available SERCA pumps to transport Ca^{2+} into the ER. This is modelled using the parameter V_s which represents the maximum rate a Ca^{2+} transport by the SERCA. The bifurcation diagrams can be seen in Figure 8.9 (a) with (b) showing the frequency of those oscillations and (c) shows the relationship between the oscillations and the two SERCA parameters V_s and K_s.

Figure 8.10 replicates the experiments in Figure 5.1 in (a) and Figure 5.2 in (b). In (a) after running the model to equilibrium, it is run for a further minute before π is increased to 1. After 5 minutes, V_s is reduced to 100 and after one transient, the system reaches a new steady state, higher than the original one. When V_s is returned to its original value after a further 5 minutes oscillations restart. In (b) after running the model to equilibrium, it is run for a further minute before V_s is reduced to 175. After a small increase in $\left[Ca^{2+}\right]_i$, the system returns to its previous equilibrium. After 5 minutes π is increased to 1. After 5 minutes

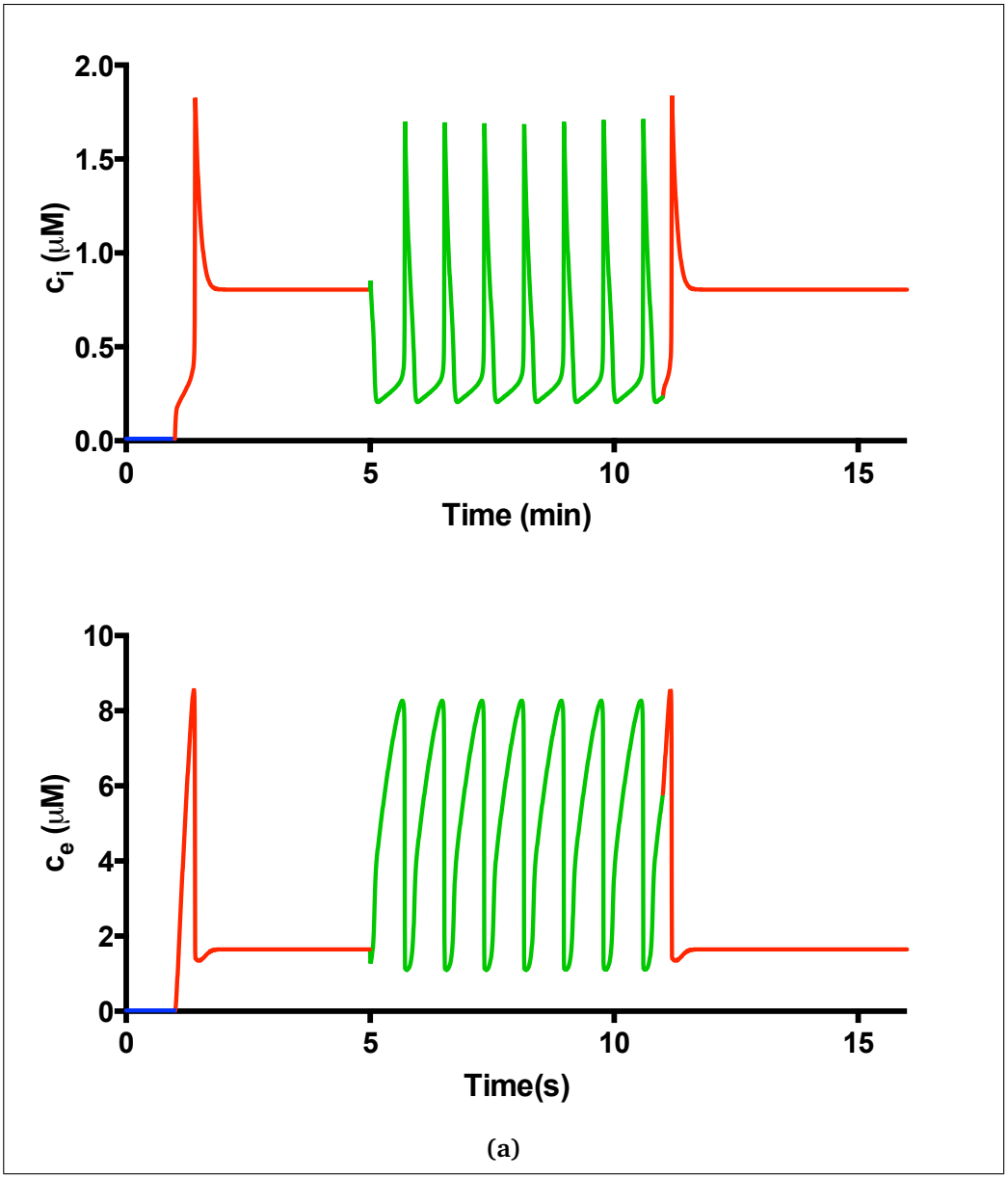

(a)

Figure 8.8 *Modelling runs to mimic the impact of varying J_{rOce} using ATP pre-dosing.*

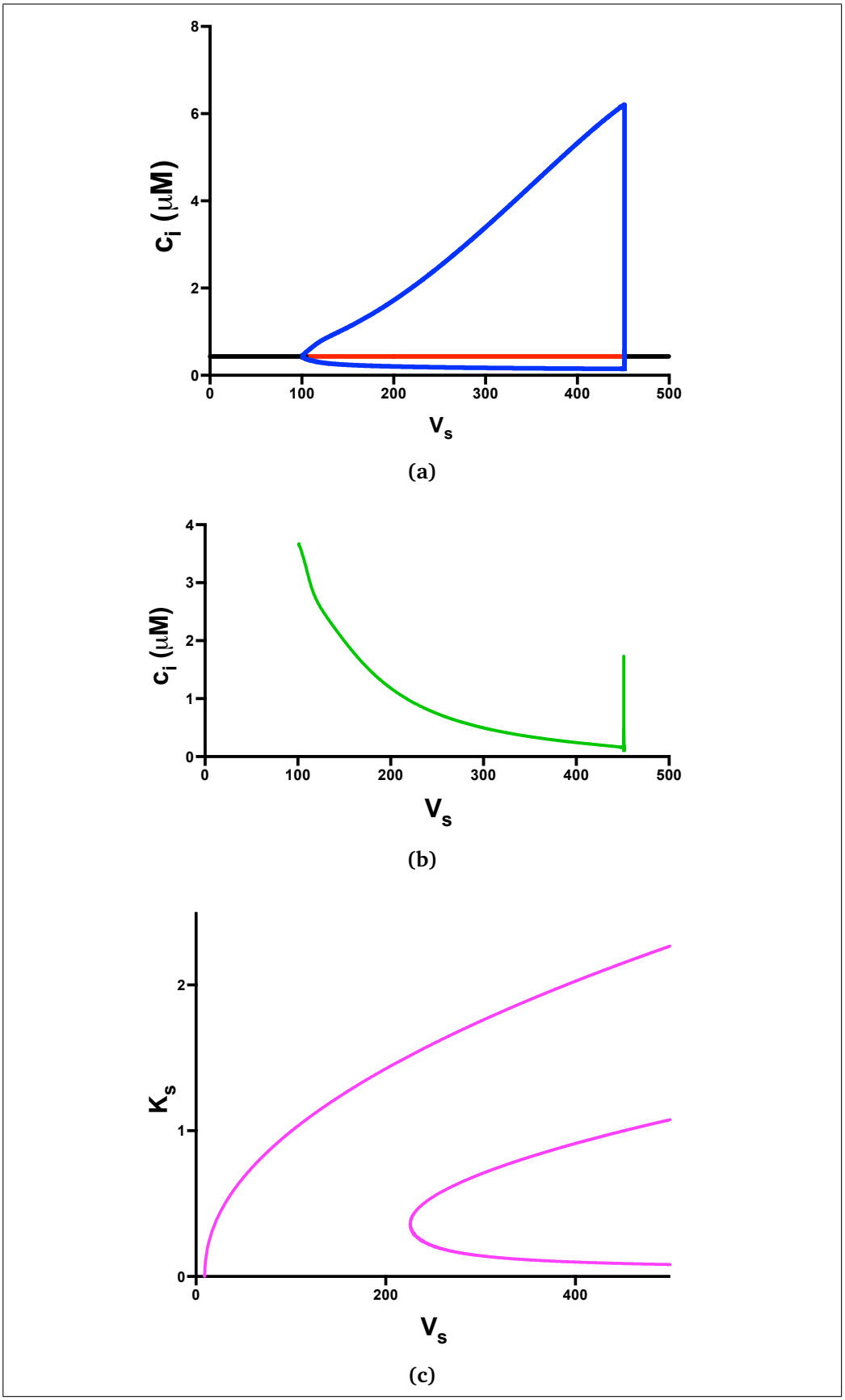

Figure 8.9 *(a) Bifurcation diagram for SERCA activity via v_s and the ensuing frequency. (c) the relationship between the two SERCA parameters, V_s and K_s and the location of the Hopf bifurcations.*

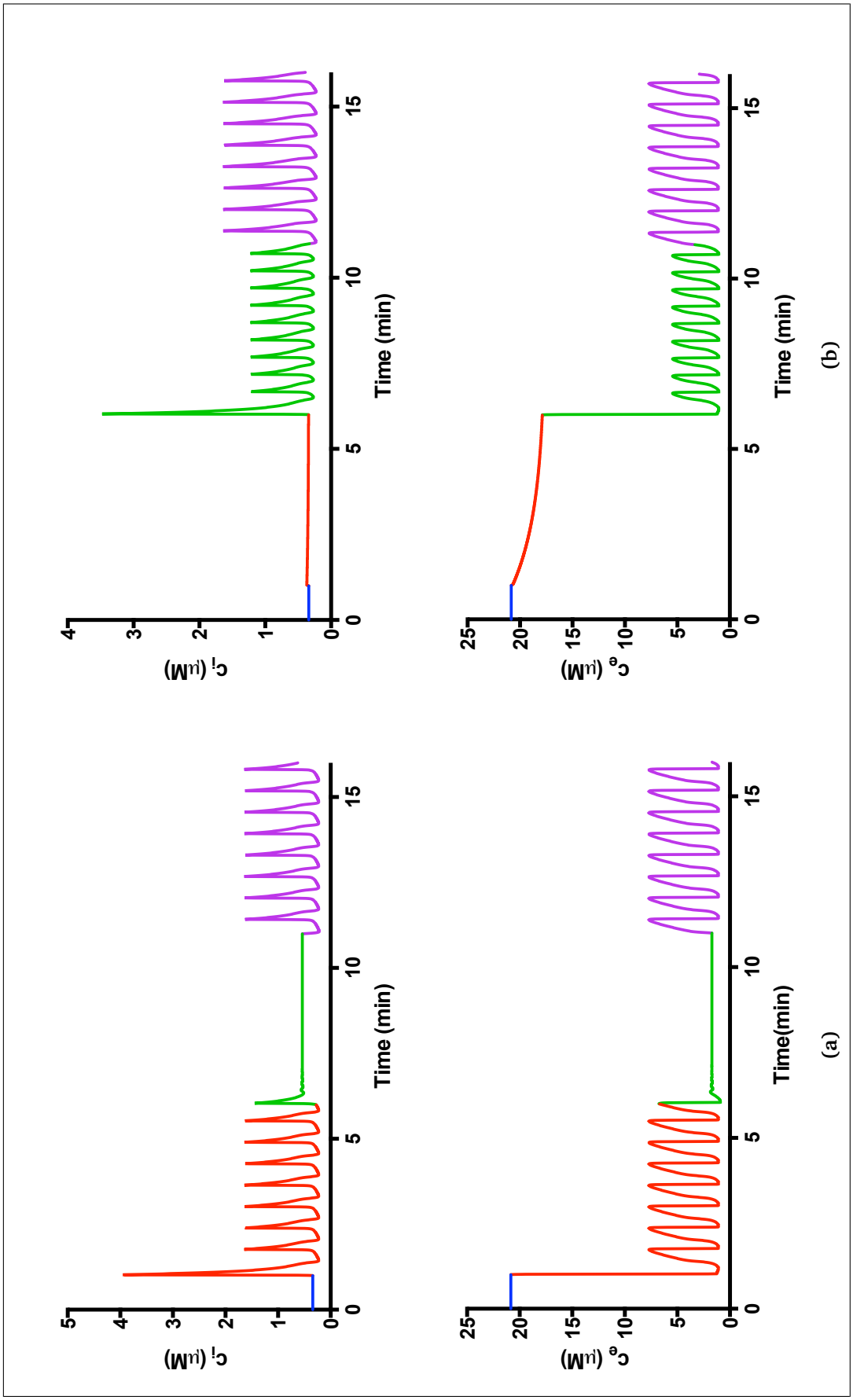

Figure 8.10 *The effect of (a) knocking out the SERCA pump and (b) reducing its effectiveness*

of oscillations, V_s is returned to its original value, slowing the oscillations and increasing their period.

8.3 Discussion and Conclusion

The motivation for all of the modelling in this chapter came from the experimental data obtained in Chapters 3-5. The tools with which to create a physiological model were introduced in Chapters 6 and 7 and were combined here to create as physiologically informed a model as possible.

To the author's knowledge, this represents the first time a physiologically-informed model of SOCE has been included in an oscillatory model and thus addresses the main failing of the SOCE model produced by Liu et. al. [86]. Physiological models for Ca^{2+}_{EC} entry into and out from the cytosol were also included in order to probe the behaviour using physiological models.

The one observed phenomenon that the model does not replicate is that *OT*-induced Ca^{2+} oscillations are not concentration dependent in experiments but they are in the model. The model presented here was to enable the system to behave physiologically. However, most physiologically informed $InsP_3R$ models result in increased flux in the presence of higher concentration of ligand, represented by an increased proportion of the available receptors being bound. It is possible to remove this concentration-dependence from the model easily using a physiologically uninformed approach, namely assuming that it is only the absence or presence of *OT* in a particular concentration band that impacts the results. However, this goes against the approach presented here. The most simple physiological explanation is a question of detailed balance; that the system is kept in an un-excited state regardless of the concentration of *OT* present by an unknown mechanism (possibly the network of mitochondria). This would be a question for further work.

This model was created in order to tie together and inform an understanding of the role of intraluminal calcium in *OT*-induced Ca^{2+} oscillations. Therefore, the model was used to replicate as closely as possible the experimental results contained herein. The current formulation of the model is capable of replicating, qualitatively at least, the behaviour seen in the experiments. In particular the model is able to replicate all the results concerning Ca^{2+} entry and extrusion from the cell.

Part C

Conclusion and Future Work

Chapter 9

Conclusion and Future Work

9.1 Conclusion

The ubiquity of Ca^{2+} signalling makes understanding its underlying processes vitally important. This thesis probes one part of that system — the regulation of agonist-induced Ca^{2+} oscillations — using both a theoretical and experimental approaches. *CHO–hOT* cells transfected with human *OT* receptor are used as the vehicle to assess the mechanisms underlying the oxytocin-induced $\left[Ca^{2+}\right]_i$ oscillations.

The aims of this project was to investigate the regulatory role of intraluminal $\left[Ca^{2+}\right]$ on oxytocin-induced Ca^{2+} oscillations. The three aims were met as follows:

9.1.1 Varying the Plasmalemmal Ca^{2+} Entry and Removal

At the beginning, general properties of *OT* responses were investigated. The ensuing oscillations were shown to be dose independent in accordance with [29]. The initial transient of these oscillations, however showed dose-dependence. The removal of extracellular Ca^{2+} resulted in an initial transient but no established oscillations.

This inability to establish oscillations in the absence of Ca^{2+}_{EC} prompted an investigation into the role that Ca^{2+}_{EC} plays in *OT*-induced Ca^{2+} oscillations. An initial investigation into the impact of directly varying extracellular Ca^{2+} impacted upon *OT*-induced Ca^{2+} oscillations in a dose-dependent way the *OT*-induced Ca^{2+} oscillations in the range $0.5 - 4\ mM\ Ca^{2+}_{EC}$. Concentrations of $> 5mM$ Ca^{2+}_{EC} resulted in a single transient followed by a raised steady-state $\left[Ca^{2+}\right]_i$.

This study into the impact of changing Ca^{2+}_{EC} motivated an investigation into the role that the two Ca^{2+} extrusion systems present in *CHO–hOT* cells — the PMCA and $Na^{+}/Ca^{2+}-$exchanger— have in *OT*-induced Ca^{2+} oscillations. Decreasing the activity of these, using the specific PMCA inhibitor Caloxin 3A1 and by lowering $Na^{+}/Ca^{2+}-$exchanger activity by reducing Na^{+}_{EC}, resulted in potentiated *OT*-induced Ca^{2+} oscillations.

ATP was then used as a tool to increase Ca^{2+} entry through the plasma membrane via receptor operated Ca^{2+} entry (ROCE) through the activation of both $P2_x$ (ROCE) and $P2_y$ (G_q stimulation of $InsP_3$) receptors. This had a significant impact on the Ca^{2+} oscillations seen — in particular the oscillation frequency was much higher than was able to be realised by stimulation of the G_q cascade alone via *OT* receptors by *OT*.

9.1.2 Manipulating Ca^{2+} Buffering Within the ER and Ca^{2+} Uptake into the ER Lumen

The work with ATP motivated the investigation into the role that the ER and its buffering mechanisms have in *OT*-induced Ca^{2+} oscillations. ER buffering was altered using TPEN and Ca^{2+} uptake into the ER was modified by reducing the activity of the SERCA pump using the SERCA-inhibitor CPA.

9.1.3 Constructing a Mathematical Model that Replicates the Experimentally Observed Phenomena

Taken together these experimental results have elucidated the role that Ca^{2+} entry and the ER have in the regulation of agonist-induced Ca^{2+} oscillations. Supplied with this biological insight into the system, the validity of existing compartmental models was investigated. Modelling of biological systems can provide a bridge between what has been observed and the processes which underly those observations. After an initial investigation into implementing the experimental results using mathematics, the more realistic and physiologically relevant model was produced. This model is the first physiologically motivated compartmental model to simultaneously include luminally-Ca^{2+}-sensitive $InsP_3R$ and store-operated Ca^{2+} entry.

9.2 Future Work

Throughout this work the *CHO–hOT* cell line has been used. An initial motivation for the use of this cell line was that the $InsP_3R$ form the major source of Ca^{2+} release from the lumen of the ER. Indeed, stimulation of RYR using caffeine did not induce oscillations in these cells. A natural extension of this work would be to integrate the understanding obtained here in a system in which release from both $InsP_3R$ and RYR moderate the regulation of agonist-induced Ca^{2+} oscillations. Comparing, for instance, an investigation into the regulation of agonist-induced Ca^{2+} oscillations in primary human myometrial smooth muscle cells, in which both release channels are important, might aid an understanding of the roles of the individual release mechanisms in these cells. This in turn might lead to insight into a way to moderate these oscillations and quell or induce contractions in patients with premature or dysfunctional labour, respectively.

This might first be investigated by extending the model contained herein to include release from RYR. This might yield predictions which could be tested experimentally to build up a more effective understanding of the system and improve the model and yield further insights. In *CHO–hOT* cells spatial effects of signalling were not resolvable. They are, however, known to be important in other cell types, including human myometrial smooth muscle [137]. Integrating a spatial element to the model could lead to new insights into the role of increased local concentrations of Ca^{2+}, often called Ca^{2+} microdomains, might have upon the system. This is especially pertinent since no such model exists which includes luminally-Ca^{2+}-sensitive $InsP_3R$, physiological models of entry through the plasma membrane and store-operated Ca^{2+} entry.

Part D

References

Bibliography

[1] Chinese Hamster Genome Database. http://www.chogenome.org. Accessed: 15/06/13.

[2] CHO Consortium. http://www.aiche.org/sbe/community/cho-consortium. Accessed: 03/09/13.

[3] Fluo-4 AM and Fluo-4 NW Calcium Indicators. http://www.invitrogen.com/site/us/en/home/Products-and-Services/Applications/Drug-Discovery/Target-and-Lead-Identification-and-Validation/g-protein_coupled_html/cell-based-second-messenger-assays/fluo-4-am-fluo-4-nw-calcium-indicators.html. Accessed: 08/07/13.

[4] Fura-2 Calcium Indicator. http://www.invitrogen.com/site/us/en/home/Products-and-Services/Applications/Drug-Discovery/Target-and-Lead-Identification-and-Validation/g-protein_coupled_html/cell-based-second-messenger-assays/Fura-2-calcium-indicator.html. Accessed: 11/07/13.

[5] Image J. Image Processing and Analysis in Java. http://rsb.info.nih.gov/ij/. Accessed: 03/08/13.

[6] IP-One HTRF assay. http://www.htrf.com/ip-one-htrf-assay. Accessed: 17/10/12.

[7] Spectra Data. http://www.invitrogen.com/site/us/en/home/support/Product-Technical-Resources/Product-Spectra.1200ca.html. Accessed: 15/07/13.

[8] I F Abdullaev, J M Bisaillon, M Potier, J C Gonzalez, R K Motiani, and M Trebak. Stim1 and Orai1 mediate CRAC currents and store-operated calcium entry important for endothelial cell proliferation. *Circulation Research*, 103(11):1289–1299, November 2008.

[9] P Arslan, F Di Virgilio, M Beltrame, R Y Tsien, and T Pozzan. Cytosolic Ca2+ homeostasis in Ehrlich and Yoshida carcinomas. A new, membrane-permeant chelator of heavy metals reveals that these ascites tumor cell lines have normal cytosolic free Ca2+. *Journal of Biological Chemistry*, 260(5):2719–2727, 1985.

[10] S Batra. Effect of oxytocin on calcium influx and efflux in the rat myometrium. *European Journal of Pharmacology*, 1986.

[11] I I Ben-Shlomo, S Y Hsu, R Rauch, H W Kowalski, and A J W Hsueh. Signaling receptome: a genomic and evolutionary perspective of plasma membrane receptors involved in signal transduction. *Signal Transduction Knowledge Environment (STKE)*, 2003(187):RE9–RE9, June 2003.

[12] M J Berridge, M D Bootman, and H L Roderick. Calcium signalling: dynamics,

homeostasis and remodelling. *Nature Reviews: Molecular Cell Biology*, 4(7):517–529, June 2003.

[13] M J Berridge and R F Irvine. Inositol phosphates and cell signalling. *Nature*, 1989.

[14] M J Berridge, P Lipp, and M Bootman. Primer: Calcium Signalling. *Current Biology*, 9(5):R157–R159, 1999.

[15] I Bezprozvanny and B E Ehrlich. Inositol (1,4,5)-trisphosphate InsP2- gated Ca channels from cerebellum: conduction properties for divalent cations and regulation by intraluminal calcium. *Journal of General Physiology*, (104):821–885, 1994.

[16] l Bezprozvanny, J Watras, and B E Ehrlich. Bell-shaped calcium-response curves of lns(l,4,5)P3- and calcium-gated channels from endoplasmic reticulum of cerebellum. *Nature*, 351(6329):751–754, June 1991.

[17] M B Bhat, S M Hayek, J J Zhao, W Zang, H Takeshima, W G Wier, and J J Ma. Expression and functional characterization of the cardiac muscle ryanodine receptor Ca^{2+} release channel in chinese hamster ovary cells. *Biophysical Journal*, 77(2):9–9, July 1999.

[18] M D Bootman, M J Berridge, and P Lipp. Cooking with calcium. *Cell*, 91:367–373, 1997.

[19] W F Boron, A Roos, and P de Weer. NH4Cl and other weak bases in the activation of sea urchin eggs. *Nature*, 274(5667):190–190, July 1978.

[20] G E P Box and N R Draper. *Empirical model-building and response surfaces*. Wiley series in probability and mathematical statistics, 1987.

[21] O Brandman, J Liou, W S Park, and T Meyer. STIM2 Is a feedback regulator that stabilizes basal cytosolic and endoplasmic reticulum Ca^{2+} levels. *Cell*, 131(7):13–13, December 2007.

[22] I Brust-Mascher and W W Webb. Calcium waves induced by large voltage pulses in fish keratocytes. *Biophysical Journal*, 75:1669–1678, September 1998.

[23] J P H Burbach, R A H Adan, and F M Bree. Regulation of Oxytocin Gene Expression and Forms of Oxytocin in the Brain. *Annals of the New York Academy of Sciences*, 652(1):1–13, 1992.

[24] T Burdyga, A Shmygol, D A Eisner, and S Wray. A new technique for simultaneous and in situ measurements of Ca^{2+} signals in arteriolar smooth muscle and endothelial cells. *Cell Calcium*, 34(1):27–33, July 2003.

[25] G Burnstock. Introduction to purinergic signalling in the brain. *Glioma Signaling*, 2013.

[26] G Burnstock, B B Fredholm, R A North, and A Verkhratsky. The birth and postnatal development of purinergic signalling. *Acta Physiologica*, 199(2):93–147, May 2010.

[27] G Burnstock and M Williams. P2 purinergic receptors: modulation of cell function and therapeutic potential. *Journal of Pharmacology and Experimental Therapeutics*, 2000.

[28] Ernesto Carafoli and Claude B Klee. *Calcium As a Cellular Regulator*. Oxford University Press, 1999.

[29] R Caroppo. A reassessment of the effects of luminal [Ca^{2+}] on Inositol 1,4,5-Trisphosphate-induced Ca^{2+} release from internal stores. *Journal of Biological Chemistry*, 278(41):39503–39508, July 2003.

[30] M E Carsten and J D Miller. A new look at uterine muscle contraction. *American Journal of Obstetrics and Gynecology*, 1987.

[31] J Chaudhary, M Walia, J Matharu, E Escher, and A Grover. Caloxin: a novel plasma membrane Ca^{2+} pump inhibitor. *American Journal of Cell Physiology*, 280:1027–1030, February 2001.

[32] C-U Choe and B E Ehrlich. The inositol 1,4,5-trisphosphate receptor (IP3R) and its regulators: sometimes good and sometimes bad teamwork. *Signal Transduction Knowledge Environment (STKE)*, 2006(363):re15–re15, November 2006.

[33] D E Clapham. TRP channels as cellular sensors. *Nature*, 426(6966):517–524, December 2003.

[34] D E Clapham. Calcium Signaling. *Cell*, 131(6):12–12, December 2007.

[35] L Combettes, P Champeil, E A Finch, and S M Goldin. Calcium and Inositol 1,4,5-Trisphosphate-Induced Ca^{2+} Release. *Science*, 265:813–815, August 1994.

[36] H Dale. On some physiological actions of ergot. *The Journal of Physiology*, 1906.

[37] C K W De Dreu, L Greer, G A Van Kleef, S Shalvi, and M J Handgraaf. Oxytocin promotes human ethnocentrism. *PNAS*, 108(4):1262–1266, January 2011.

[38] Annunziata A De Luisi and Aldebaran M AM Hofer. Evidence that Ca(2+) cycling by the plasma membrane Ca(2+)-ATPase increases the 'excitability' of the extracellular Ca(2+)-sensing receptor. *Journal of Cell Science*, 116(Pt 8):1527–1538, April 2003.

[39] G W De Young and J Keizer. A single-pool inositol 1,4,5-trisphosphate-receptor-based model for agonist-stimulated oscillations in Ca^{2+} concentration. *PNAS*, 89(20):9895–9899, October 1992.

[40] W I DeHaven, B F Jones, J G Petranka, J T Smyth, T Tomita, G S Bird, and J W Putney. TRPC channels function independently of STIM1 and Orai1. *Journal of Physiology*, 587(Pt 10):2275–2298, May 2009.

[41] I Derler, M Fahrner, O Carugo, M Muik, J Bergsmann, R Schindl, I Frischauf, S Eshaghi, and C Romanin. Increased Hydrophobicity at the N Terminus/Membrane Interface Impairs Gating of the Severe Combined Immunodeficiency-related ORAI1 Mutant. *Journal of Biological Chemistry*, 284(23):15903–15915, May 2009.

[42] E Doedel. AUTO, 1986.

[43] R J Dolor, L M Hurwitz, Z Mirza, H C Strauss, and A R Whorton. Regulation of extracellular calcium entry in endothelial cells: role of intracellular calcium pool. *American Journal of Physiology - Cell Physiology*, 262(1):171–181, January 1992.

[44] V du Vigneaud, C Ressler, and C J M Swan. The synthesis of an octapeptide amide with the hormonal activity of oxytocin. *Journal of the American Chemical Society*, 1953.

[45] V du Vigneaud, C Ressler, and J M Swan. The synthesis of oxytocin1. *Journal of the American Chemical Society*, 1954.

[46] V du Vigneaud, C Ressler, and S Trippett. The sequence of amino acids in oxytocin, with a proposal for the structure of oxytocin. *Journal of Biological Chemistry*, 205(2):949–957, December 1953.

[47] G G Dupont and A Goldbeter. One-pool model for Ca^{2+} oscillations involving Ca^{2+} and inositol 1,4,5-trisphosphate as co-agonists for Ca^{2+} release. *Cell Calcium*, 14(4):311–322, March 1993.

[48] M M Dvorak, A Siddiqua, D T Ward, D H Carter, S L Dallas, E F Nemeth, and D Riccardi. Physiological changes in extracellular calcium concentration directly control osteoblast function in the absence of calciotropic hormones. *PNAS*, 101(14):5140–5145, April 2004.

[49] C el Moatassim, J Dornand, and J C Mani. Extracellular ATP and cell signalling. *Biochimica et Biophysica Acta (BBA) - Bioenergetics*, 1134(1):31–45, February 1992.

[50] B Ermentrout. *Simulating, Analyzing, and Animating Dynamical Systems*. A Guide to XPPAUT for Researchers and Students. SIAM, 2002.

[51] B Feldman, S Fedida-Metula, J Nita, I Sekler, and D Fishman. Coupling of mitochondria to store-operated Ca^{2+}-signaling sustains constitutive activation of protein kinase B/Akt and augments survival of malignant melanoma cells. *Cell Calcium*, 47(6):13–13, May 2010.

[52] J E Ferrell. Self-perpetuating states in signal transduction: positive feedback, double-negative feedback and bistability. *Current Opinion in Cell Biology*, 14(2):140–148, March 2002.

[53] S Feske. ORAI1 and STIM1 deficiency in human and mice: roles of store-operated Ca^{2+} entry in the immune system and beyond. *Immunological Reviews*, 231(1):189–209, August 2009.

[54] S Feske, Y Gwack, M Prakriya, S Srikanth, S-H Puppel, B Tanasa, P G Hogan, R S Lewis, M Daly, and A Rao. A mutation in Orai1 causes immune deficiency by abrogating CRAC channel function. *Nature*, 441(7090):179–185, May 2006.

[55] S Feske, M Prakriya, A Rao, and R S Lewis. A severe defect in CRAC Ca^{2+} channel activation and altered K^{2+} channel gating in T cells from immunodeficient patients. *Journal of Experimental Medicine*, 202(5):651–662, September 2005.

[56] R FitzHugh. Mathematical models of threshold phenomena in the nerve membrane. *The Bulletin of Mathematical Biophysics*, 1955.

[57] Fraiman and Dawson. A Model of the IP$_3$ receptor with a luminal calcium binding site: stochastic simulations and analysis. *Cell Calcium*, 2005.

[58] I Frischauf, M Muik, I Derler, J Bergsmann, M Fahrner, R Schindl, K Groschner, and C Romanin. Molecular determinants of the coupling between STIM1 and Orai channels: differential activation of Orai1-3 channels by a STIM1 coiled-coil mutant. *Journal of Biological Chemistry*, 284(32):21696–21706, August 2009.

[59] I Frischauf, R Schindl, I Derler, J Bergsmann, M Fahrner, and C Romanin. The STIM/Orai coupling machinery. *Channels*, 2(4):261–268, June 2008.

[60] G Gimpl and F Fahrenholz. The oxytocin receptor system: structure, function, and regulation. *Physiological Reviews*, 81:1–55, March 2001.

[61] A Goldbeter. *Biochemical oscillations and cellular rhythms*. The Molecular Bases of Periodic and Chaotic Behaviour. Cambridge University Press, April 1997.

[62] A Goldbeter and G G Dupont. Minimal model for signal-induced Ca^{2+} oscillations and for their frequency encoding through protein phosphorylation. *PNAS*, 1990.

[63] T Haberichter, E Roux, M Marhl, and J-P Mazat. The influence of different InsP(3) receptor isoforms on Ca^{2+} signaling in tracheal smooth muscle cells. *Bioelectrochemistry*, 57(2):129–138, August 2002.

[64] T L Hill. *Free Energy Transduction in Biology*. Academic Press, 1977.

[65] M Hoth and R Penner. Depletion of intracellular calcium stores activates a calcium current in mast cells. *Nature*, 355(6358):353–356, January 1992.

[66] Y Inoue, K Shimamura, and N Sperelakis. Oxytocin actions on voltage-dependent ionic channels in pregnant rat uterine smooth muscle cells. *Canadian Journal of Physiology and Pharmacology/Revue Canadienne de Physiologie et Pharmacologie*, 70(12):1597–1603, December 1992.

[67] M S Islam. *Transient receptor potential channels*. Springer, 2011.

[68] R Jacob. Calcium oscillations in endothelial cells. *Cell Calcium*, 12(2-3):127–134, February 1991.

[69] K P Jayapal, K F Wlaschin, W-S Hu, and M G S Yap. Recombinant Protein Therapeutics from CHO Cells. *Society for Biological Engineering*, (CHO Consortium):1–8, October 2007.

[70] Qiu-Xing Jiang, Edwin C Thrower, David W Chester, Barbara E Ehrlich, and Fred J Sigworth. Three-dimensional structure of the type 1 inositol 1,4,5-trisphosphate receptor at 24 A resolution. *EMBO J*, 21(14):3575–3581, July 2002.

[71] K Kaczmarek-Hájek, E Lörinczi, R Hausmann, and A Nicke. Molecular and functional properties of P2X receptors–recent progress and persisting challenges. *Purinergic Signalling*, 8(3):375–417, August 2012.

[72] T M Kang and D W Hilgemann. Multiple transport modes of the cardiac Na^{2+}/Ca^{2+} exchanger. *Nature*, 427(6974):544–548, February 2004.

[73] T Kawasaki, I Lange, and S Feske. A minimal regulatory domain in the C terminus of STIM1 binds to and activates ORAI1 CRAC channels. *Biochemical and Biophysical Research Communications*, 385(1):6–6, July 2009.

[74] J P Keener and J Sneyd. *Mathematical Physiology*. II: Systems Physiology. Springer, January 2009.

[75] J Keizer and G W De Young. Simplification of a realistic model of IP3-induced Ca^{2+} oscillations. *Journal of Theoretical Biology*, 1994.

[76] T Kimura, C Azuma, M Takemura, T Inoue, and T Kikuchi. Molecular cloning of a human oxytocin receptor. *Regulatory Peptides*, 1993.

[77] K Kiselyov and S Muallem. Fatty acids, diacylglycerol, Ins(1,4,5)P3 receptors and Ca^{2+} influx. *Trends in Neurosciences*, 22(8):334–337, July 1999.

[78] E Klipp, W Liebermeister, C Wierling, A Kowald, H Lehrach, and R Herwig. *Systems Biology*. John Wiley & Sons, June 2013.

[79] M K Korzeniowski, M A Popovic, Z Szentpetery, P Varnai, S S Stojilkovic, and T Balla. Dependence of STIM1/Orai1-mediated calcium entry on plasma membrane phosphoinositides. *Journal of Biological Chemistry*, 284(31):21027–21035, July 2009.

[80] J M Kowalewski, P Uhlén, H Kitano, and H Brismar. Modeling the impact of store-operated Ca^{2+} entry on intracellular Ca^{2+} oscillations. *Mathematical Biosciences*, 204(2):18–18, December 2006.

[81] K Kuba and S Takeshita. Simulation of intracellular Ca^{2+} oscillation in a sympathetic neurone. *Journal of Theoretical Biology*, 93(4):1009–1031, December 1981.

[82] H Kuriyama, K Ohshima, and Y Sakamoto. The membrane properties of the smooth muscle of the guinea-pig portal vein in isotonic and hyertonic solutions. *Journal of Physiology*, 217:179–199, March 1971.

[83] R S Lewis. The molecular choreography of a store-operated calcium channel. *Nature*, 446(7133):284–287, March 2007.

[84] J Liou, M Fivaz, T Inoue, and T Meyer. Live-cell imaging reveals sequential oligomerization and local plasma membrane targeting of stromal interaction molecule 1 after Ca^{2+} store depletion. *PNAS*, 104(22):9301–9306, May 2007.

[85] W Liu, F Tang, and J Chen. Designing dynamical output feedback controllers for store-operated Ca^{2+} entry. *Mathematical Biosciences*, 228(1):9–9, November 2010.

[86] X Liu, H L Ong, B Pani, K Johnson, W B Swaim, B Singh, and I I Ambudkar. Effect of cell swelling on ER/PM junctional interactions and channel assembly involved in SOCE. *Cell Calcium*, 47(6):491–499, May 2010.

[87] R M Luik, B Wang, M Prakriya, M M Wu, and R S Lewis. Oligomerization of STIM1 couples ER calcium depletion to CRAC channel activation. *Nature*, 454(7203):538–542, July 2008.

[88] L M Luttrell. Transmembrane signaling by G protein-coupled receptors. *Methods in Molecular Biology*, 332:3–49, January 2006.

[89] A I Malik, C C Zai, Z Abu, and B Nowrouzi. The role of oxytocin and oxytocin receptor gene variants in childhood-onset aggression. *Genes*, 2012.

[90] S Marc, D Leiber, and S Harbon. Carbachol and oxytocin stimulate the generation of inositol phosphates in the guinea pig myometrium. *FEBS letters*, 1986.

[91] E N Marieb and K N Hoehn. *Human Anatomy and Physiology*. Pearson Higher Ed, February 2012.

[92] S P McElroy, R M Drummond, and A M Gurney. Regulation of store-operated Ca^{2+} entry in pulmonary artery smooth muscle cells. *Cell Calcium*, 46(2):8–8, July 2009.

[93] K Mikoshiba. IP3 receptor/Ca^{2+} channel: from discovery to new signaling concepts. *Journal of Neurochemistry*, 102(5):1426–1446, August 2007.

[94] K Monastyrskaya, E B Babiychuk, A Hostettler, P Wood, T Grewal, and A Draeger. Plasma membrane-associated annexin A6 reduces Ca^{2+} entry by stabilizing the cortical actin cytoskeleton. *Journal of Biological Chemistry*, 284(25):17227–17242, June 2009.

[95] F M Mullins, C Y Park, R E Dolmetsch, and R S Lewis. STIM1 and calmodulin interact with Orai1 to induce Ca^{2+}-dependent inactivation of CRAC channels. *PNAS*, 106(36):15495–15500, September 2009.

[96] R A North. Molecular physiology of P2X receptors. *Physiological Reviews*, 2002.

[97] M Oh-hora and A Rao. Calcium signaling in lymphocytes. *Current Opinion in Immunology*, 20(3):9–9, May 2008.

[98] H L Ong, X Liu, K Tsaneva-Atanasova, B Singh, B C Bandyopadhyay, W D Swaim, J T Russell, R S Hegde, A Sherman, and I I Ambudkar. Relocalization of STIM1 for activation of store-operated Ca^{2+} entry is determined by the depletion of subplasma membrane endoplasmic reticulum Ca^{2+} store. *Journal of Biological Chemistry*, 282(16):12176–12185, April 2007.

[99] M N Pangalos and C H Davies. *Understanding G Protein-Coupled Receptors and Their Role in the Cns*. (Molecular and Cellular Neurobiology). Oxford University Press, USA, 2002.

[100] J A Papin, T Hunter, B O Palsson, and S Subramaniam. Reconstruction of cellular signalling networks and analysis of their properties. *Nature Reviews: Molecular Cell Biology*, 6(2):99–111, February 2005.

[101] A B Parekh and J W Putney. Store-operated calcium channels. *Physiological Reviews*, 85(2):757–810, March 2005.

[102] C Y Park, P J Hoover, F M Mullins, P Bachhawat, E D Covington, S Raunser, T Walz, K C Garcia, R E Dolmetsch, and R S Lewis. STIM1 Clusters and Activates CRAC Channels via Direct Binding of a Cytosolic Domain to Orai1. *Cell*, 136(5):15–15, March 2009.

[103] I Parker and I Ivorra. Inhibition by Ca^{2+} of inositol trisphosphate-mediated Ca^{2+} liberation: a possible mechanism for oscillatory release of Ca^{2+}. *PNAS*, 87(1):260–264, January 1990.

[104] A Pires-daSilva and R J Sommer. The evolution of signalling pathways in animal development. *Nature Reviews: Genetics*, 4(1):39–49, January 2003.

[105] M Potier and M Trebak. New developments in the signaling mechanisms of the store-operated calcium entry pathway. *Pfluegers Archiv/European Journal of Physiology*, 457(2):405–415, November 2008.

[106] M Prakriya and R S Lewis. Regulation of CRAC channel activity by recruitment of silent channels to a high open-probability gating mode. *Journal of General Physiology*, 128(3):373–386, August 2006.

[107] J W Putney. A model for receptor-regulated calcium entry. *Cell Calcium*, 7(1):1–12, February 1986.

[108] J W Putney. Recent breakthroughs in the molecular mechanism of capacitative calcium entry (with thoughts on how we got here). *Cell Calcium*, 42(2):8–8, July 2007.

[109] J W Putney and R R McKay. Capacitative calcium entry channels. *Bioessays*, 21(1):38–46, January 1999.

[110] I S Ramsey, M Delling, and D E Clapham. An introduction to TRP channels. *Physiology*, 68(1):619–647, January 2006.

[111] S G Rhee. Regulation of phosphoinositide-specific phospholipase C. *Biochemistry*, 70:281–312, January 2001.

[112] J Rivera, A L Bernal, M Varney, and S P Watson. Inositol 1, 4, 5-trisphosphate and oxytocin binding in human myometrium. *Endocrinology*, 1990.

[113] E Roux and M Marhl. Role of sarcoplasmic reticulum and mitochondria in Ca^{2+} removal in airway myocytes. *Biophysical Journal*, 86(4):13–13, March 2004.

[114] S-Y Ryu, P M Peixoto, J H Won, D I Yule, and K W Kinnally. Extracellular ATP and P2Y2 receptors mediate intercellular Ca^{2+} waves induced by mechanical stimu-

lation in submandibular gland cells: Role of mitochondrial regulation of store operated Ca^{2+} entry. *Cell Calcium*, 47(1):65–76, January 2010.

[115] A Sandow. Excitation-contraction coupling in muscular response. *The Yale Journal of Biology and Medicine*, 1952.

[116] R P Shearman. Clinical Reproductive Endocrinology, 1985.

[117] K Shimamura and M Kusaka. Oxytocin induces an inward current in pregnant rat myometrial cells. *Canadian Journal of Physiology and Pharmacology/Revue Canadienne de Physiologie et Pharmacologie*, 1994.

[118] A V Shmigol, D A Eisner, and S Wray. Simultaneous measurements of changes in sarcoplasmic reticulum and cytosolic $[Ca^{2+}]$ in rat uterine smooth muscle cells. *The Journal of Physiology*, 531(3):707–713, March 2001.

[119] A Shmygol and S Wray. Modulation of agonist-induced Ca^{2+} release by SR Ca^{2+} load: direct SR and cytosolic Ca^{2+} measurements in rat uterine myocytes. *Cell Calcium*, 37(3):215–223, 2005.

[120] J Sneyd, J Keizer, and M J Sanderson. Mechanisms of calcium oscillations and waves: a quantitative analysis. *FASEB Journal*, 9(14):1463–1472, November 1995.

[121] J Sneyd, B T Wetton, A C Charles, and M J Sanderson. Intercellular calcium waves mediated by diffusion of inositol trisphosphate: a two-dimensional model. *American Journal of Physiology - Cell Physiology*, 268(6 Pt 1):C1537–C1545, May 1995.

[122] N Sperelakis, Y Inoue, and Y Ohya. Fast Na^{2+} channels and slow Ca^{2+} current in smooth muscle from pregnant rat uterus. *Molecular and Cellular Biochemistry*, 114(1-2):79–89, September 1992.

[123] M M Szewczyk. Biotechnological invention of caloxins – a novel class of allosteri inhibitors specific for plasma membrane calcium pump isoforms . *Open Access Dissertation and Theses*, pages 1–171, January 2011.

[124] Manika Sztretye, Janos Almassy, Tamas Deli, Pacter Szentesi, Carole Jung, Beatrix Dienes, Cecilia A Simut, Ernst Niggli, Istvan Jona, and Laszla Csernoch. Altered sarcoplasmic reticulum calcium transport in the presence of the heavy metal chelator TPEN. *Cell Calcium*, 46(56):347–355, 2009.

[125] Y Tang, J L Stephenson, and H G Othmer. Simplification and analysis of models of calcium dynamics based on IP3-sensitive calcium channel kinetics. *Biophysical Journal*, 70(1):18–18, January 1996.

[126] K Törnquist. Evidence for receptor-mediated calcium entry and refilling of intracellular calcium stores in FRTL-5 rat thyroid cells. *Journal of Cellular Physiology*, 1992.

[127] R W Tsien and R Y Tsien. Calcium channels, stores, and oscillations. *Annual Review of Cell Biology*, 1990.

[128] Y Tsunoda. Oscillatory Ca^{2+} signaling and its cellular function. *The New Biologist*, 3(1):3–17, January 1991.

[129] G Ullah and P Jung. Modeling the statistics of elementary calcium release events. *Biophysical Journal*, 90(10):3485–3495, May 2006.

[130] A Ulloa, A L Gonzales, M Zhong, Y-S Kim, J Cantlon, C Clay, C-Y Ku, S Earley, and B M Sanborn. Reduction in TRPC4 expression specifically attenuates G-protein

coupled receptor-stimulated increases in intracellular calcium in human myometrial cells. *Cell Calcium*, 46(1):73–84, July 2009.

[131] D van Bockstaele. *Mathematical Models of Biological Systems*. OUP Oxford, November 2010.

[132] J Wagner and J Keizer. Effects of rapid buffers on Ca^{2+} diffusion and Ca^{2+} oscillations. *Biophysical Journal*, 67(1):10–10, June 1994.

[133] C M Walsh, M Chvanov, L P Haynes, O H Petersen, A V Tepikin, and R D Burgoyne. Role of phosphoinositides in STIM1 dynamics and store-operated calcium entry. *Biochemical Journal*, 425(1):159–168, January 2010.

[134] J Watras, I Bezprozvanny, and B E Ehrlich. Inositol 1,4,5-trisphosphate-gated channels in cerebellum: presence of multiple conductance states. *The Journal of Neuroscience*, 11(10):3239–3245, 1991.

[135] T F Wiesner, B C Berk, and R M Nerem. A mathematical model of cytosolic calcium dynamics in human umbilical vein endothelial cells. *American Journal of Physiology - Cell Physiology*, 270(5 Pt 1):C1556–C1569, April 1996.

[136] M M Wu, J Buchanan, R M Luik, and R S Lewis. Ca^{2+} store depletion causes STIM1 to accumulate in ER regions closely associated with the plasma membrane. *Journal of Cell Biology*, 174(6):803–813, September 2006.

[137] Roger C Young and Rory O Hession. Intra-and intercellular calcium waves in cultured human myometrium. *Journal of Muscle Research & Cell Motility*, 17(3):349–355, June 1996.

[138] R Yu and P M Hinkle. Rapid turnover of calcium in the endoplasmic reticulum during signaling. Studies with cameleon calcium indicators. *Journal of Biological Chemistry*, 275(31):23648–23653, August 2000.

[139] J P Yuan, W Zeng, M R Dorwart, Y-J Choi, P F Worley, and S Muallem. SOAR and the polybasic STIM1 domains gate and regulate Orai channels. *Channels*, 11(3):337–343, March 2009.